Does antiretroviral therapy accelerate the speed of physiological ageing through the clonal expansion of mitochondrial DNA mutations?

Carla Roca Bayerri

MRes

Thesis submitted to Newcastle University for the Degree of Doctor of Philosophy

Wellcome Trust Centre for Mitochondrial Research

Institute of Neuroscience

September 2019

Abstract

The accumulation of mitochondrial DNA (mtDNA) mutations is well described in normal human ageing as well as in several diseases of older age. It has been suggested that the accumulation of mtDNA mutations within tissues with ageing is likely to be predominantly due to the clonal expansion of existing mutations within cells, rather than high levels of mutagenesis. Antiretroviral treated HIV-infected persons achieve good immune reconstitution, but nevertheless experience an increase in many of the common diseases and physiological changes of older age. Given the known links between mitochondria and ageing, and mitochondria and HIV infection, it is plausible that increased mitochondrial damage may be a biological mediator of ageing in HIV.

MtDNA damage in human brain was investigated in a cohort of HIV+ individuals and HIV-uninfected controls. HIV+ cases showed an increase in mtDNA deletions and a decrease in mtDNA content. In both cases these accentuated the changes seen with age.

A novel derivative from the *PolgA* 'mutator' mouse model was developed to test the role of clonal expansion. The mouse model ('WtN+') contained multiple germline heteroplasmic mtDNA point mutations on a wild-type inbred nuclear background. Mice were aged to different time points, and a subset was dosed with zidovudine, a nucleoside analogue antiretroviral drug, known to inhibit mtDNA replication. Clonal expansion of mtDNA mutations were analysed in post-mitotic (skeletal muscle) and mitotic (colonic crypts) tissues using a combination of molecular and immunohistochemical assays. This novel mouse model showed evidence of clonal expansion of mtDNA mutations, and a mild frailty phenotype.

In summary, these experiments increase our understanding of the natural history of mtDNA mutations in ageing and antiretroviral therapy.

This thesis is dedicated to my grandmother, la meva àvia Montserrat, named after our beautiful mountain in Catalonia. I only wish you could have stayed here longer to see me accomplish becoming a Doctor. Et trobo molt a faltar.

Dolça Catalunya,

pàtria del meu cor,

quan de tu s'allunya

d'enyorança es mor.

Acknowledgements

First and foremost, I owe my deepest sincere gratitude to my supervisor Brendan Payne for the constant support, guidance and patience during these four years. The opportunity you gave me to undertake this PhD has changed my life for the better. Your encouragement and motivation kept me going during setbacks and challenging science times, allowing me the space to become a (quite) independent scientist. I will always thank you.

I thank my second supervisors, first Rita Horvath and then Joanna Elson, for your input during this project.

Thanks to Gavin Hudson for putting up with me and my thousand questions about genetics, sequencing and dilutions; I really appreciate it. To the magician behind a smooth running lab and basically my lab mom Angela, I'm grateful for your constant support. I need to thank Jennifer Duff and Laura Boyd for their technical support in IGM and ION, respectively.

Thanks to Fiona Robertson, I honestly do not know what I would have done without your bioinformatics help, lifesaver! I am infinitely thankful to Carla Bradshaw, who helped me for hours on end with all things mouse related, I really can't thank you enough. Thanks to Brigid Griffin for your valuable help at the CAV. Obviously, a massive shout out to my mice, I hope your heaven is full of treats!

I am tremendously grateful for all the amazing humans I have met throughout the course of my PhD. I started this journey with my dearest Hannah, thanks for always being there for me and for holding my hand and wiping my tears when needed, you're a star.

To my Kretins, Adam, Shane, Yasmin, Pavandeep, Nishani, Charlotte and Matt; I'm so glad I met you all, you brought so much joy into my life. An extra mention to Shane, cheers for teaching me Geordie, bringing me unrequested cuppas and basically never failing at making me smile; and to Pav and Nish, words fall short but I feel like I now have two brown sisters from another mister. To my office VIP members: Ruth, Megan, Jack, Ro and Matthew, thanks for providing fun times as well as sympathising with madness during this write up.

I could not have learned and mastered the art of quadruple immunofluorescence without Tasnim, who went above and beyond to patiently teach me and help at all times. Lizzie, I feel so fortunate to have been part of your special celebrations and hence the India adventure which I will forever cherish in my memory.

I want to thank Amy Vincent for her support with my technique-related enquiries about muscle work and in general all the WTCMR lab on the fourth floor Cookson Building for helping out when I was optimising protocols. Dave H, thanks for showing me how to use the Fiji software and showing me the basics of confocal microscopy. I have to thank Dave B from the Bioimaging Unit, who was so helpful every time the confocal microscope was playing up and taught me the ways around the CD7 system.

Thank you Beth and Nunzia, for being there throughout the ups and downs. To those who somehow have been there along the way, thanks for guiding me. Merci to my amigues and amics back home, although the PhD process is often isolating, I have been lucky enough that my long-time friends always had my back.

Last but not least, I owe everything to my beloved amazing parents Mercè and Xavier, my maezinha and painho. You are the light of my life and I am so lucky to be your daughter. I made it here because of your unconditional love; I hope this makes you proud. Gràcies per tot, us estimo molt.

Author’s declaration

This thesis is submitted for the degree of Doctor of Philosophy at Newcastle University. The research was conducted in the Wellcome Trust Centre for Mitochondrial Research, partly in the Institute of Genetic Medicine and the Institute of Neuroscience, and is my own work if not stated otherwise. The research was completed under the supervision of Dr Brendan Payne and Dr Joanna Elson from September 2015 to September 2019.

I certify that none of the material offered in this thesis has been previously submitted by me for a degree or any other qualification at any other university.

Publications

Ryan Samuels, **Carla Roca Bayerri**, John A Sayer, D Ashley Price and Brendan AI Payne: *Tenofovir disoproxil fumarate-associated renal tubular dysfunction: noninvasive assessment of mitochondrial injury*. AIDS 06/2017; 31(9). DOI:10.1097/QAD.0000000000001466

Courses and conferences attended

Introduction to Linux computing for Bioinformatics – Training course. Newcastle upon Tyne, UK (2016).

7th International Workshop on HIV & Aging – Abstract-driven presentation and poster. Washington DC, USA (2016).

Abbreviations

3TC	Lamivudine
ABC	Abacavir
ADP	Adenosine Diphosphate
AIDS	Acquired Immune Deficiency Syndrome
ANI	Subclinical neuropsychological impairment
ARV	Antiretroviral
ART	Antiretroviral treatment or therapy
ATP	Adenosine Triphosphate
AZT (or ZDV)	Zidovudine
β2M	Beta-2-microglobulin
β-Actin	Beta-actin
BER	Base excision repair
bp	base pair/position
cART	combination antiretroviral treatment or therapy
CCR	Chemokine receptor
CD	Common deletion
CD4	Cluster of differentiation 4
CD8	Cluster of differentiation 8
Cm	centimetre
CN	Copy number
CNS	Central nervous system

CO_2	Carbon dioxide
COX	Cytochrome c Oxidase
CPEO	Chronic progressive external ophthalmoplegia
CSF	Cerebrospinal Fluid
Cq	Threshold cycle of quantification
D4T	Stavudine
DDC	Di-deoxycytidine (zalcitabine)
DDI	Di-deoxyinosine (didanosine)
dH_2O	Distilled water
D-Loop	Displacement loop
DNA	Deoxyribonucleic Acid
dNTP	Deoxyribonucleotide triphosphate
EDTA	Ethylenediaminetetraacetic acid
ETC	Electron transport chain
EtOH	Ethanol
FFPE	Formalin-fixed paraffin-embedded
FTC	emtricitabine
gp120	Glycoprotein 120
H^+	Proton
H_2O	Water
H_2O_2	Hydrogen peroxide
HAART	Highly active antiretroviral therapy

HAD	HIV-associated dementia
HAND	HIV-associated neurocognitive disorder
HCl	Hydrochloric acid
HIV	Human immunodeficiency virus
HIV-RT	HIV reverse transcriptase
H-strand	Heavy strand
IF	Immunofluorescence
IFI16	Interferon-γ-inducible protein 16
IL-1β	Interleukin-1 β
IMM	Inner mitochondrial membrane
IMS	Intermembrane space
Kb	Kilobase
kDa	Kilo-Daltons
KSS	Kearns-Sayre syndrome
L-strand	Light strand
Leu	Leucine
LHON	Leber's hereditary optic neuropathy
LMD	Laser microdissection
Log_{10}(CD)	Logarithm with base 10 of common deletion
LR-PCR	Long-range polymerase chain reaction
Lys	Lysine
M	Molar

MCI (or MCMD)	Mild cognitive motor disorder
MELAS	Mitochondrial myopathy, encephalopathy, lactic acidosis, and stroke-like episodes
MERRF	Myoclonic epilepsy with ragged red fibres
$MgCl_2$	Magnesium Chloride
ml	millilitre
mM	millimolar
M.O.M	mouse on mouse
mRNA	messenger Ribonucleic Acid
mtDNA	Mitochondrial DNA
mtDNA CN	Mitochondrial DNA Copy Number
MT-ND1	Mitochondrial NADH-ubiquinone Oxidoreductase Core subunit 1 gene
MT-ND2	Mitochondrial NADH-ubiquinone Oxidoreductase Core subunit 2 gene
MT-ND4	Mitochondrial NADH-ubiquinone Oxidoreductase Core subunit 4 gene
MT-ND5	Mitochondrial NADH-ubiquinone Oxidoreductase Core subunit 5 gene
mtSSB	Mitochondrial Single Strand Binding protein
NCBI	National Centre for Biotechnology Information
NCI	Neurocognitive impairment
nDNA	nuclear DNA
NER	Nucleotide excision repair

NGS	Normal goat serum or Next generation sequencing
NI	subclinical neuropsychological impairment
nm	nanometer
nM	nanomolar
NN	neurocognitively normal
NNRTI	Non-nucleoside reverse transcriptase inhibitor
NPC	No Primary Control
NRTI	Nucleoside reverse transcriptase inhibitor
NuMT	Nuclear Mitochondrial DNA sequence
O_2	Oxygen
O_2^-	Superoxide
O_D	Optical density
O_H	Origin of heavy strand replication
O_L	Origin of light strand replication
OMM	Outer mitochondrial membrane
OXPHOS	Oxidative phosphorylation
PBMCs	Peripheral blood mononuclear cells
PBS	Phosphate buffered saline
PCR	Polymerase chain reaction
PI	Protease inhibitor
PLWH	People living with HIV
POLG	DNA Polymerase Gamma encoding gene

PolgA	DNA Polymerase Gamma subunit A
Pol γ	Polymerase gamma
QC	Quality Control
qPCR	Quantitative Real-time Polymerase Chain Reaction
rCRS	Revised Cambridge reference sequence
ROS	Reactive oxygen species
RNA	Ribonucleic Acid
rpm	revolutions per minute
rRNA	Ribosomal ribonucleic acid
RT	Reverse transcriptase
SD	Standard Deviation
SDH	Succinate Dehydrogenase
SE	Standard Error
SKM	Skeletal Muscle
SQ	Starting quantity
ssRNA	Single-stranded ribonucleic acid
TAE	Tris-Acetate EDTA
Tat	Trans-activator of transcription
TBST	Tris Buffered Saline with Tween
TCA	Tricarboxylic acid
TDF	Tenofovir disoproxil fumarate
TFAM	Transcription factor A, mitochondrial

TIM	Translocase of inner membrane
TK2	Mitochondrial Thymidine Kinase 2
TOM	Translocase of outer membrane
TOMM20	Translocase of outer mitochondrial membrane 20
tRNA	Transfer ribonucleic acid
Tm	Melting temperature
VCF	Variant calling format
VDAC	Voltage Dependent Anion-Selective Channel
VL	Viral load
wt	wild-type
ZDV (or AZT)	Zidovudine
µm	micromolar
µl	microliter

Contents

List of Figures

List of Tables

Chapter 1. Introduction

1.1 Mitochondrial origins and evolution

Mitochondria are unique extra-nuclear autonomous organelles present in almost all eukaryotic cells which contain their own genome. Mitochondria populate the majority of eukaryotic cells and they are the so-called powerhouses of the cell.

The endosymbiotic theory of mitochondrial origins was proposed by Lynn Margulis (Sagan, 1967; Margulis, 1971). The original theory posited that an anaerobic nucleated cell ingested a free-living aerobic bacterium, i.e. the protomitochondrion (later called mitochondrion). In this way, mammalian mitochondria were thought to originate from an endosymbiotic relationship with an ancient α-proteobacterium more than 2 billion years ago.

The majority of mitochondrial proteins are encoded in the nucleus, suggesting there was a gradual endosymbiotic gene transfer from the mitochondrial endosymbiont to the host nuclear genome, followed by integration into the host genomic DNA.

Phylogenetic gene analysis from the α-proteobacterium *Rickettsia prowazekii* confirmed the Rickettsiaceae family to be the evolutionary ancestors of the mitochondrion (Sicheritz-Ponten *et al.*, 1998).

1.2 Mitochondrial structure and dynamics

Mitochondria are double-membrane-bound organelles, with an outer mitochondrial membrane (OMM) and a lipid bilayer known as the inner mitochondrial membrane (IMM) where respiratory chain complexes are found (Figure 1.1).

The OMM harbours protein channels and transporters that allow movement of metabolites between the cytoplasm and mitochondria such as the voltage-dependent anion channel (VDAC), also known as mitochondrial porin. Translocase of the outer membrane (TOM) together with inner mitochondrial translocase (TIM) form a protein complex aiding entry of nuclear encoded proteins.

The intermembrane space (IMS) is found between these permeable membranes. The IMM encloses the mitochondrial matrix. The matrix contains mitochondrial DNA

molecules along with transcription and translation enzymes, and it is where the TCA cycle occurs. Figure 1.1 shows a schematic depiction of the mitochondrial ultrastructure.

The first model of the mitochondrial structure, the baffle model of cristae, suggested that the IMM folded as invaginations called *cristae mitochondriales* (Palade, 1953). This model was later rendered inexact, as it was found that cristae organised in tubular connections that made mitochondria highly dynamic networks (Daems and Wisse, 1966).

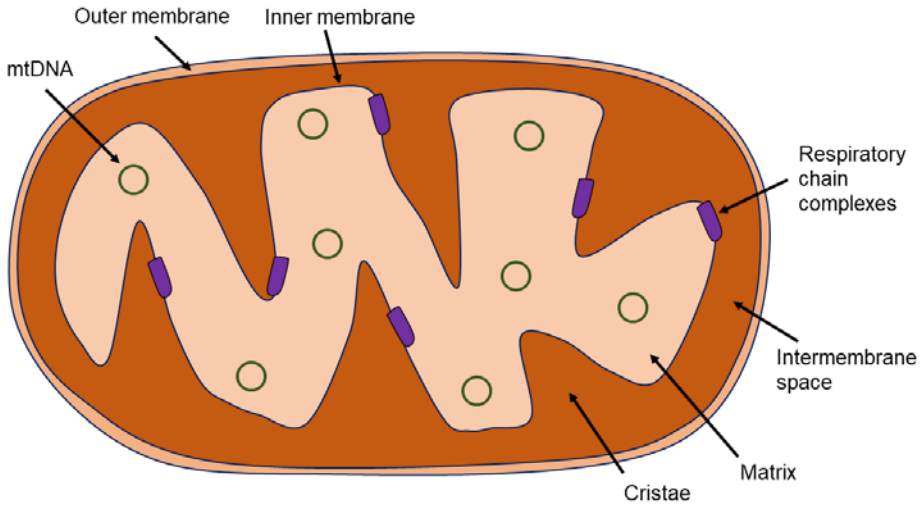

Figure 1.1. Mitochondrial structure. Schematic showing normal structure of mitochondria.

The branching structure of the cytoskeleton forms a network used by mitochondria to move and to constantly undergo fusion and division (fission). These two processes are quality control responses to environmental stresses (Youle and van der Bliek, 2012). Mitochondrial fusion occurs when two mitochondria unite the OMM and IMM forming one mitochondrion. Mitofusin proteins Mfn1 and Mfn2 control mitochondrial fusion of the OMM, and depend on Opa1 for fusion of the IMM. Mitochondrial fission happens when one mitochondrion divides to form two mitochondria. Fission occurs in order to degrade damaged mitochondria, a mechanism leading to mitophagy (autophagy of mitochondria), and is controlled by protein Drp1 helped by Fis1.

Mitochondrial dynamics vary in different cell types, for instance, mitochondria in skeletal muscle are less mobile than in neurons, where they need highly dynamic

mitochondria to be able to travel across the cell body to axonal and dendritic synapses in order to provide ATP and regulate energy homeostasis. Neurons transport mitochondria using neuronal microtubules. Further detail on neuronal mitochondria (in the context of HIV) can be found in Section 1.12.

1.3 Oxidative phosphorylation and ATP synthesis

The majority of adenosine triphosphate (ATP) generation is met by a chain of reactions that start outside the mitochondria and end with oxidative phosphorylation (OXPHOS). Mitochondria are major producers of ATP. ATP synthesis begins in the cytosol of the cell, where anaerobic glycolysis breaks down glucose into pyruvate. Pyruvate is imported into the mitochondrial matrix, where pyruvate dehydrogenase converts it into acetyl Coenzyme A. Acetyl CoA can also be sourced from oxidation of fatty acids. Acetyl CoA is a substrate in the tricarboxylic acid (TCA) or Krebs cycle (Krebs and Johnson, 1937) which occurs in the matrix, whereby a series of enzymatic reactions release by-products and reducing agents NADH and $FADH_2$ which will be further needed in the electron transport chain (ETC) of the OXPHOS system. NADH donates electrons to complex I and $FADH_2$ to complex II.

The ETC is composed of transmembrane respiratory complexes I-IV which are embedded in the inner mitochondrial membrane and shuttle electrons across the respiratory chain complexes, which coupled with proton translocation, is used to generate ATP by complex V (Figure 1.2).

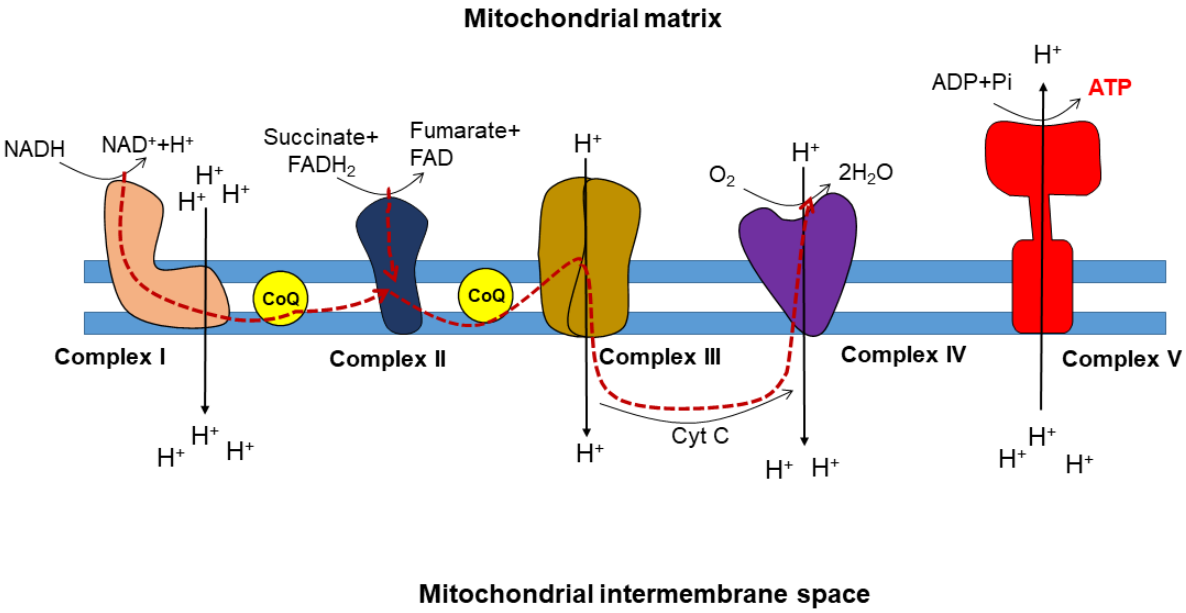

Figure 1.2. Oxidative phosphorylation. Electrons enter the ETC via complex I and II and are shuttled until complex IV (shown by red dotted lines), providing the energy required to translocate protons (H^+) from the matrix into the intermembrane space creating a proton gradient that is used by complex V to synthesize ATP. CoQ is coenzyme Q. Cyt c is cytochrome c, acting as an electron carrier.

Complex I, also known as NADH dehydrogenase, is the largest complex of the ETC, composed of 45 different subunits (Zhu *et al.*, 2016), seven of which are mitochondrially encoded and located in the membrane part of the complex. The remainder are nuclear encoded. It oxidises NADH. Complex I dysfunction is the most frequently observed OXPHOS defect. Nuclear encoded NDUFB8 subunit has been found to be essential to complex I enzymatic activity (Perales-Clemente *et al.*, 2010) therefore is very commonly used for investigations of complex I levels using immunofluorescence (Rocha *et al.*, 2015; Ahmed *et al.*, 2017).

Complex II, also known as succinate ubiquinone oxidoreductase, is only comprised of four subunits and it is the only OXPHOS complex that is entirely nuclear encoded and does not translocate protons to the intermembrane space. The catalytic part is called succinate dehydrogenase (SDH). It oxidises succinate to fumarate. Complex II deficiency is very rare, in fact the rarest of all OXPHOS complexes, accounting for around 2% of reported mitochondrial disease cases (Alston *et al.*, 2012). SDH genes are involved with tumour suppressor activity and mutations have been linked with

some forms of cancer. Coenzyme Q (ubiquinone) is a mobile electron carrier shuttling electrons from complex II to III and thus it is reduced to ubiquinol.

Complex III, or ubiquinol cytochrome c oxidoreductase, is composed of 11 subunits, only one of which – cytochrome b - is mitochondrially encoded. Similarly to complex II, complex III deficiency is rare in humans. Electrons are shuttled from complex III to complex IV via a mobile electron carrier – cytochrome c.

Complex IV, or cytochrome c oxidase (COX), is the last complex of the ETC translocating protons into the intermembrane space and is in charge of the reduction of oxygen to water. Complex IV is comprised of 13 subunits, of which three – MTCOI, MTCOII and MTCOIII - are encoded by the mitochondrial genome (Tsukihara *et al.*, 1996). Complex IV is also commonly affected in human mitochondrial diseases (Johnson *et al.*, 1983; Muller-Hocker *et al.*, 1983; Sciacco *et al.*, 1994). Anti-MTCOI antibodies or COX activity are common assay targets for immunofluorescence or histochemistry protocols of complex IV (Rocha *et al.*, 2015).

Complex V, known as ATP synthase, is the final step of the OXPHOS pathway and it uses the electrochemical gradient created by the electron transfer and proton translocation to phosphorylate ADP into ATP.

Respiratory chain complexes have been found to assemble into supramolecular entities named supercomplexes, namely complexes I, III and IV assemble to form respirasomes. Some advantages of these supercomplexes have been proposed, including improved efficiency in electron shuttling and better stabilisation of the complexes.

1.4 Other mitochondrial functions

The main role of mitochondria is the supply of intracellular energy by ATP production through OXPHOS. However, they are also involved in a myriad of functions including calcium signalling, cellular metabolism, stress responses, haem synthesis and apoptotic cell death (Spinelli and Haigis, 2018).

Mitochondria are also implicated in the formation of iron sulphur clusters (Stehling and Lill, 2013), which are essential in the electron transport of the OXPHOS process. The OXPHOS system is responsible for the majority of production of reactive oxygen species (ROS) when electron leakage from the ETC reduces oxygen to form superoxide (O_2^-). Superoxide anions are a precursor of peroxide (H_2O_2) (Murphy, 2009). Although ROS are potentially a toxic insult to the cell, they are also thought to play an important role in cellular signalling pathways. The debated role of ROS in ageing is discussed below in Section 1.6. Mitochondrial dysfunction has been linked to cancer, neurodegeneration, metabolic diseases and ageing to name but a few (Trifunovic and Larsson, 2008; de Moura *et al.*, 2010; Payne and Chinnery, 2015; Pinto and Moraes, 2015).

Recent evidence suggests mitochondria function as a hub in the mammalian innate immune system. The involvement of mitochondria in innate immune signalling pathways related to microbial infections as well as endogenous stress or injury, has been thoroughly reviewed by *West and colleagues* (West *et al.*, 2011; West and Shadel, 2017).

1.5 Mitochondrial genetics

1.5.1 Mitochondrial genome

In human cells, mitochondrial DNA (mtDNA) is a circular, 16,596-bp, double-stranded DNA molecule. The heavy strand (H-strand) is rich in guanine and the light strand (L-strand) is rich in cytosine. MtDNA codes for 37 genes, out of which 13 encode protein subunits of the mitochondrial electron transport chain, the site of OXPHOS, 22 code for mitochondrial transfer RNAs (tRNAs) and two for ribosomal RNAs (rRNAs) (Anderson *et al.*, 1981). Specifically, these aforementioned 13 mtDNA encoded polypeptides of the OXPHOS are genes ND1-6 and ND4L of complex I; cytochrome b gene of complex III; genes COI, COII and COIII of complex IV; and genes ATP6 and ATP8 of complex V (Figure 1.3). The remaining mitochondrial proteins are encoded in the nuclear genome, estimated to be ~1,500 (Calvo and Mootha, 2010).

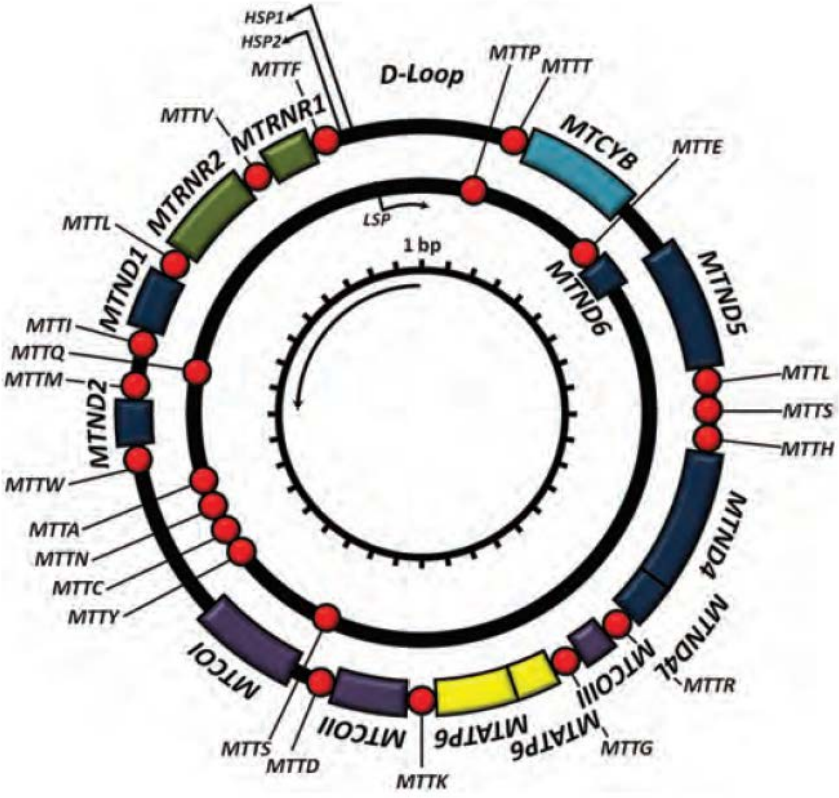

Figure 1.3. Human mitochondrial genome. Schematic representation of the mitochondrial DNA molecule. Genes encoding the mitochondrial respiratory chain complexes are shown in coloured boxes; green boxes are rRNAs; red circles are tRNAs. Image taken from (Chinnery and Hudson, 2013).

The mitochondrial genome is highly efficient, it lacks introns and is almost entirely composed of coding regions except for one ~1 kb noncoding region, called the displacement loop (D-loop). The D-loop contains elements which regulate mtDNA replication and transcription (Arnberg *et al.*, 1971).

Despite mtDNA accounting for only 1% of the total cellular DNA, each cell contains from a few hundreds to thousands of copies of the mitochondrial genome, depending on cellular energy requirements. This is known as mitochondrial DNA copy number (CN) and its molecular analyses are widely used in the study of mitochondrial diseases (Kollberg *et al.*, 2009; Poulton *et al.*, 2009; Martin-Hernandez *et al.*, 2017). MtDNA CN is highly variable and it is believed to be specific to the energy requirements of the tissue (Clay Montier *et al.*, 2009), however the exact mechanisms regulating mtDNA CN have not been elucidated.

In this multi-copy state of the mtDNA, when the copies have the same sequence it is known as homoplasmy. However, when a mutation occurs, these mutant molecules co-exist with wild-type molecules at different levels, a term named heteroplasmy.

It is believed that mtDNA is packaged into DNA-protein complexes called nucleoids and their function has not been fully clarified yet, but they are thought to help with replication and transcription (Kukat *et al.*, 2011).

1.5.2 Mitochondrial DNA replication, transcription and translation

MtDNA replication is independent of cell cycle (Bogenhagen and Clayton, 1977) and is carried out by the sole mtDNA polymerase, the polymerase gamma (pol γ), encoded by the nuclear genes *POLG* and *POLG2* (which codes for a 55 kDa accessory subunit) (Kaguni, 2004).

Mitochondrial DNA polymerase γ has a 3'-5' exonuclease proofreading activity and in conjunction with an mtDNA hexameric twinkle helicase and mtSSB (mitochondrial single strand binding protein) forms the machinery for the replication process, called the mtDNA replisome (Hudson and Chinnery, 2006).

The mtDNA molecules are constantly turned over throughout life in mitotic and also post-mitotic tissues, a process called 'relaxed replication' (Chinnery and Samuels, 1999).

The exact mechanism of mtDNA replication has not been fully determined but two mtDNA replication models have been proposed; asynchronous (strand displacement) and synchronous. In the asynchronous model, transcription with the mtDNA D-loop initiates replication at the origin of heavy-strand replication (O_H) 'unidirectionally' until origin of light-strand replication (O_L) is exposed and then replicated, synthesising the lagging-strand in an anticlock-wise direction (Clayton, 1982). The synchronous model suggested that heavy-strand replication is originated at O_H 'bi-directionally', simultaneously with multiple initiation sites for the lagging-strand (Holt *et al.*, 2000).

The transcription of mtDNA is initiated by mitochondrial transcription factor A (TFAM) through the recruitment of mitochondrial RNA polymerase (POLRMT) and mitochondrial transcription factor B2 (TFB2M) (Hillen *et al.*, 2018). In the elongation step, TEFM increases POLRMT processivity along the DNA strand (Posse *et al.*, 2015). Mitochondrial termination factor (mTERF1) terminates transcription of mature mtDNA transcripts downstream of the 16sRNA gene (Asin-Cayuela *et al.*, 2005).

Mitochondrial translation is carried out by the mitoribosome in three stages: initiation, elongation and termination (Greber *et al.*, 2015). The mitoribosome is a large multi-subunit complex formed of both RNA (coded by mtDNA genes MTRNR1, MTRNR2 and $tRNA^{Val/Phe}$) and protein subunits all encoded within the nuclear DNA (nDNA). Elongation of synthesising peptides is promoted by three elongation factors: mtEFTu, mtEFTs and mtEFG1 (Mai *et al.*, 2017). Translation termination is performed by two

release factors mtRF1a and C12orf65, and ribosome recycling is facilitated by mtEFG2 (Lightowlers and Chrzanowska-Lightowlers, 2010).

1.5.3 Mitochondrial DNA repair mechanisms

The endogenous oxidative environment of the mitochondria leaves mtDNA vulnerable to damage. The constant mtDNA turnover also leads to replication errors. Repair mechanisms in mtDNA are not as robust and extensive as the ones described for nuclear DNA, for instance mtDNA lacks nucleotide excision repair (NER). The main mitochondrial repair pathways include base excision repair (BER) and single strand break repair (SSB) (Prakash and Doublie, 2015).

1.5.4 Heteroplasmy and threshold effect

Heteroplasmy is expressed as a percentage, between 1-99%, and refers to the proportion of mutant mtDNA molecules in relation to the wild-type, in a single cell or tissue. This co-existence of mutant mtDNA species with wild-type is the main driver of the phenotypic expression of mtDNA mutations.

When mutant mtDNA is found above a certain threshold, typically between 70-80 % heteroplasmy level, respiratory chain deficiency in a tissue can arise leading to mitochondrial dysfunction and potentially organ dysfunction. It is thought that for mtDNA deletions a lower threshold of around 60% is enough to produce a biochemical defect, whereas for single point mutations a higher level of heteroplasmy is required since at low heteroplasmy levels wild-type mtDNA compensates for the mutant mtDNA species. This is known as the mitochondrial threshold effect, which is believed to vary between tissues and between different mutations types.

Due to the recessive nature of heteroplasmic mtDNA mutations, cells with low level mutated mtDNA molecules can still be respiratory functional but when increased it can create a mosaic pattern of cellular mitochondrial deficiency within a tissue.

1.5.5 Clonal expansion of mtDNA mutations

Initially, a single somatic mutation will be present among many other wild-type copies of the mitochondrial genome. How can it therefore reach the level required to produce a defective phenotype? Two mechanisms could be responsible: either by accumulation of *de novo* mutations or by clonal expansion of pre-existing mutations.

De novo mutagenesis can happen when different new mutations occur in a single cell, whereas a single somatic mutation can undergo clonal expansion due to the replication of mtDNA being uncoupled from the cell cycle.

There are a few theories to explain clonal expansion of mtDNA mutations. Initially, the “survival of the smallest” model was proposed, where the deleted mtDNA genomes by being the smallest had a replicative advantage and would accumulate faster over time (Wallace, 1992). However, this theory only applies to mtDNA deletions but does not take into account mtDNA point mutations, which do not affect the size of the genome and still clonally expand during ageing (Greaves *et al.*, 2014).

Another theory, the “survival of the slowest” suggested that mitochondria with mutant mtDNA live longer because the respiratory chain is impaired and there is less ROS so less oxidative damage (de Grey, 1997). Such a model assumes the clonal expansion of mtDNA mutations has reached a threshold high enough to produce a defect in the respiratory chain. Over time these theories have been somewhat discarded.

The most recent and sustained theory is simply that ‘random intracellular genetic drift’ of mutated and wild-type mtDNA species get randomly amplified via relaxed replication, without any specific selective advantage or pressure needed (Elson *et al.*, 2001). Modelling studies suggest that relaxed replication may be sufficient to lead to clonal expansion in post-mitotic cells (Gross *et al.*, 1969; Chinnery and Samuels, 1999; Elson *et al.*, 2001).

1.5.6 Mitochondrial DNA mutations and disease

The mutational rate of mtDNA is several times higher than that of the nuclear DNA (Brown *et al.*, 1979; Linnane *et al.*, 1989) partly because mtDNA is localized physically close to the respiratory chain and hence more susceptible to receive oxidative damage, also because of the scarce mtDNA repair mechanisms and lack of protective histones. These factors together with a low fidelity polymerase γ (Kunkel and Loeb, 1981) and the constant turnover of the mtDNA make the mitochondrial genome more prone to mutations than its nuclear counterpart. Moreover, since the mtDNA is highly compact any mutations are likely to occur in protein-coding or tRNA regions and therefore have a downstream effect. A mutation can happen due to errors during mtDNA replication or repair (Schon *et al.*, 1989; Krishnan *et al.*, 2008).

Broadly, there are two main types of mtDNA mutations: point mutations and large-scale deletion.

Single mtDNA point mutations occur when a single base is substituted for another. Point mutations can be maternally inherited or somatic. More than half of the pathogenic mtDNA point mutations are located in mitochondrial tRNA genes, hence potentially producing a functional defect (Schaefer *et al.*, 2008). The most common and studied point mutations are the mt.3243A>G and mt.8344A>G, involved in mitochondrial myopathy, encephalopathy, lactic acidosis, and stroke-like episodes (MELAS) and myoclonic epilepsy with ragged red fibres (MERRF), respectively.

Large-scale mtDNA deletions remove or rearrange a big part of the mitochondrial genome that includes genes coding for proteins or tRNAs. The most well-known somatic deletion is the 4977 bp ‘common deletion’ flanked by two 13bp homologous repeat sequences at positions 8470-8482 and 13447-13459 (inclusive) (Schon *et al.*, 1989; Shoffner *et al.*, 1989). In some cases, one of these repeats is deleted. Further studies have shown the importance of these direct repeats in the formation of large-scale mtDNA deletions (Samuels, 2004; Samuels *et al.*, 2004; Guo *et al.*, 2010). The 4977 bp mtDNA common deletion (CD) is known to cause several diseases including Pearson’s syndrome, chronic progressive external ophthalmoplegia (CPEO) and Kearns-Sayre syndrome (KSS) (Holt *et al.*, 1988; Zeviani *et al.*, 1988; Moraes *et al.*, 1989). The mtDNA CD is also well-known to accumulate with age (Corral-Debrinski *et al.*, 1992; Lee *et al.*, 1994; Tengan *et al.*, 1997; Bua *et al.*, 2006; Gendron *et al.*, 2012); and it could even be implicated in cancer (Chen *et al.*, 2011).

Currently, it is not known exactly how the mtDNA CD can cause different disease phenotypes but some hypotheses argue that the nuclear genome could compensate for this defect, thereby allowing transition of mitochondrial phenotypes (Katada *et al.*, 2013); indicating that mtDNA deletions pose a potential for a phenotype that won't always occur. Besides, mtDNA CD could simply reveal a phenotype when heteroplasmy is present above a critical threshold. Conversely to point mutations, large-scale deletions are rarely inherited. They mainly localise in the major arc of the mitochondrial genome, between the two origins of replication, O_H and O_L. The mechanisms implicated in deletion formation are not fully elucidated, but very recent single-molecule analysis of the mtDNA CD revealed a replication impairment combined with abnormal break repair as the cause (Phillips *et al.*, 2017).

Phenotypic expression varies between different tissues, for instance high energy demanding post-mitotic tissues such as muscle and brain are thought to be more vulnerable to the effects of mtDNA mutations. This tissue specificity, seen in mitochondrial diseases, is likely to dictate to some extent the expression of a clinical phenotype.

Mitochondrial diseases are complex heterogeneous multi-systemic disorders typically affecting several high energy demanding organs such as skeletal muscle and nervous systems. Since a large proportion of OXPHOS genes are encoded by the nuclear genome, mitochondrial disease can either come from defects in the mtDNA or in the nDNA. Mitochondrial disease prevalence is difficult to estimate, but a recent study in the North East of England found the prevalence to be less rare than previously thought, affecting up to ~1 in 4,300 adults in the UK (Gorman *et al.*, 2015).

The first mtDNA point mutation linked to disease was mt.11778G>A in ND4 gene of complex I which would present as homoplasmic and be one of the pathogenic mutations of Leber's hereditary optic neuropathy (LHON) (Figure 1.4) (Wallace *et al.*, 1988).

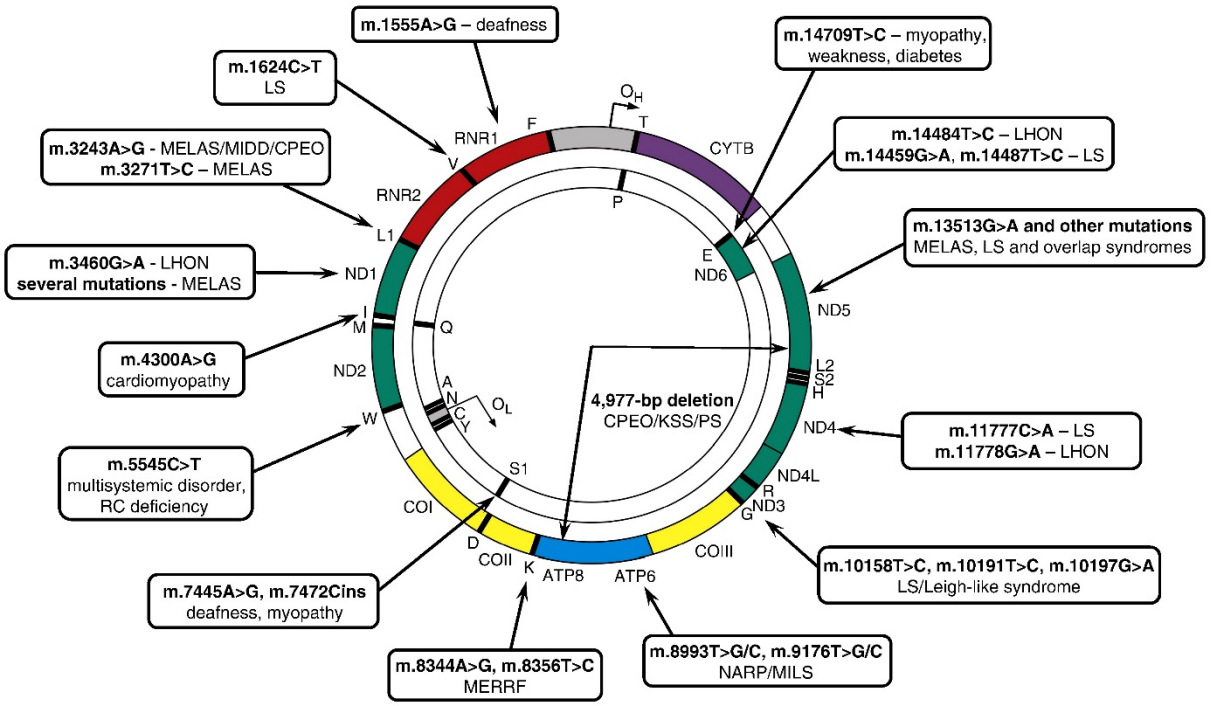

Figure 1.4. Genotype-phenotype correlations in human mitochondrial disease. MtDNA mutations are depicted with the associated clinical presentations. CPEO, chronic progressive external ophthalmoplegia; LHON, Leber hereditary optic neuropathy; LS, Leigh syndrome; MELAS, mitochondrial myopathy, encephalopathy, lactic acidosis, and stroke-like episodes; MERRF, myoclonic epilepsy and ragged red fibres; MILS, maternally inherited Leigh syndrome; NARP, neurogenic weakness, ataxia, and retinitis pigmentosa; PS, Pearson syndrome. Image taken from (Tuppen et al., 2010).

1.5.7 Mitochondrial DNA inheritance and the genetic bottleneck

Mitochondrial genetics differs from nuclear genetics in many aspects but mainly because the mitochondrial genome is inherited and transmitted through the maternal line, as opposed to the nuclear genome being inherited in a biparental diploidy Mendelian manner. Despite the predominance of this theory (Pyle *et al.*, 2015b), paternal inheritance of mtDNA has been observed in humans on a handful of cases (Schwartz and Vissing, 2002; Luo *et al.*, 2018) and some paternal mtDNA leakage has been reported in the animal kingdom (Gyllensten *et al.*, 1991; Kondo *et al.*, 1992; Zhao *et al.*, 2004; Sherengul *et al.*, 2006; Nunes *et al.*, 2013; Dokianakis and Ladoukakis, 2014) and remains a contentious area of debate.

Through a mammalian mtDNA genetic bottleneck, a mother can pass on different levels of heteroplasmic mutations to their offspring, thus either constraining or quickly segregating mtDNA mutant species.

In terms of female germ line, a germline bottleneck is thought to reduce the number of mtDNA molecules per cell during embryonic development. Indeed, a reduction of mtDNA in the germline of mice in some studies showed for the first time the existence of a genetic bottleneck (Cao *et al.*, 2007; Cree *et al.*, 2008; Wai *et al.*, 2008).

The constriction-expansion balance of mtDNA heteroplasmic subpopulations in the maternal germline is important in maintaining a purifying selection against deleterious mutations (Fan *et al.*, 2008; Stewart *et al.*, 2008).

1.5.8 Mitochondrial haplogroups

The evolution and geographic radiation of subgroups within the human population with mtDNA sequence variants led to the formation of mitochondrial haplogroups. These variants are homoplasmic and were fixed in the mitochondrial phylogenetic tree through radiation of maternal lineages many thousands of years ago. The origin of the mitochondrial eve is set in Africa, where it gave rise to macrohaplogroup L. MtDNAs radiated and from L others emerged, macrohaplogroups M and N, which left Africa and started a founder effect in the other continents (Wallace, 2015).

1.6 Mitochondrial DNA and Ageing

During the natural course of human ageing, somatic (acquired) mutations accumulate in the mitochondrial genome but it is still unclear how active the role of these mutations is and whether they cause the ageing observed or they are a consequence.

Although mtDNA mutations originating throughout life are assumed to be age-related, it is unknown whether they occur early or late in life. Some of these mutations could actually be passed down the maternal line but not detected with the technologies available. Recent work has pointed to the direction of inheritance of low-level heteroplasmic variants from the maternal line (Li *et al.*, 2010; Payne *et al.*, 2012; Guo *et al.*, 2013). This heteroplasmic variant level can vary markedly among different tissues of the same individual (He *et al.*, 2010).

One of the prevailing theories of ageing was initially proposed by Harman in the 1950s, the ‘free radical theory’ which postulates that ageing is due to the deleterious effect of endogenous reactive oxygen species (ROS), a by-product generated during normal activity of the OXPHOS system, inflicting progressive cumulative cellular dysfunction and thus tissue damage (Harman, 1956). Some years after, Harman’s original theory was renamed to ‘mitochondrial theory of ageing’ because mitochondria, namely the electron transport chain, are an important source of intracellular ROS production (Harman, 1972).

Since then, it has been commonly thought that mtDNA mutations in ageing are driven principally by a ‘vicious cycle’ of mitochondrial ROS leading to oxidative damage to mtDNA, causing respiratory chain dysfunction and further ROS production.

According to this theory, mtDNA mutations would be enhanced and propagated in an exponential manner, which is however, not the case. Many studies have failed to prove an increase in age-related oxidative damage (Tengan *et al.*, 1997; Mott *et al.*, 2001; Kennedy *et al.*, 2013; Itsara *et al.*, 2014). This lack of consistent evidence makes this theory inconclusive and arguable.

At the moment the theory of clonal expansion of pre-existing mutated mtDNA molecules seems to be more plausible than a continuous ROS vicious cycle, as

reviewed by *Pinto and Moraes*, who propose that ROS plays a simple stress-mediating role in the context of molecular damage (Pinto and Moraes, 2015).

Trifunovic and colleagues challenge the original oxidative damage theory since they found no increased ROS production in their study with mice with an error-prone polymerase, suggesting that respiratory dysfunction itself could be enough to trigger ageing and therefore no vicious cycle may be involved (Trifunovic *et al.*, 2005).

1.6.1 PolgA 'mutator' mouse model of mitochondrial ageing

A few years ago, two groups independently provided the first descriptions of a mouse model with a defective mtDNA polymerase (Trifunovic *et al.*, 2004; Kujoth *et al.*, 2005). These knock-in mice have a proofreading-deficient version of the mitochondrial DNA polymerase γ by a point mutation (D257A) in the catalytic *PolgA* subunit, which leads to accelerated accumulation of mtDNA mutations and a prematurely aged phenotype, i.e., hair loss, weight loss, greying, kyphosis, frailty, reduced subcutaneous fat, osteoporosis, thymic involution, loss of bone and muscle mass (Trifunovic *et al.*, 2004; Kujoth *et al.*, 2005).

'Mutator' mice homozygous for this allele (*PolG*$^{mut/mut}$) show a severe progeroid phenotype, whereas heterozygous mice (*PolG*$^{wt/mut}$) do not, and rather show a normal phenotype (Trifunovic *et al.*, 2004; Kujoth *et al.*, 2005).

It was reported by the Loeb group that mtDNA deletions were more abundant in *PolG*$^{mut/mut}$ mice in comparison to the *PolG*$^{wt/mut}$ ones, suggesting that deletions may be responsible for the reduced lifetime of homozygous mice (Vermulst *et al.*, 2008). However such finding has subsequently been refuted as the deletions seen were not true canonical deletions, i.e., smaller circular mtDNA species with part of the genome deleted, but rather were linear mtDNA species that were probably 'replication dead-ends' from the faulty pol γ (Williams *et al.*, 2010).

The previous papers focused on somatic mutations but in a recent paper by *Ross, Stewart and colleagues*, it was shown that mtDNA mutations could also be transmitted down the maternal germline and drive an ageing phenotype. In their study, mice which inherited low levels of germline mtDNA mutations had a shorter lifespan and a more severe aged phenotype compared to the ones that did not (Ross *et al.*, 2013).

Although the *PolgA* mouse has proved very useful for studies of mitochondrial deficiency and ageing, it does have some limitations in modelling the situation in humans. For example, it has continuous production of very high levels of somatic mtDNA mutations, whereas humans have low levels (possibly germline transmitted) with gradual clonal expansion; the ageing phenotype may well be driven more by mitochondrial dysfunction in stem cells (starting during embryogenesis), rather than in post-mitotic tissues in adult life. In this thesis, I did not use the standard *PolgA*

mouse model to study clonal expansion but I created a new mouse model as there are currently no good models of clonal expansion.

The mouse mitochondrial genome was completely sequenced in early 1980s showing mouse mtDNA overall sequence and organisation is very homologous to human mtDNA (Bibb *et al.*, 1981). Sequence homology is higher in mouse mitochondrial tRNA genes to their human analogues compared to rRNA genes and protein-coding genes. The overall locations of mouse mtDNA genes are in almost identical positions to human mtDNA, but the mouse mtDNA is shorter (16,299 bp) than the human because the D-loop region is shorter. The mtDNA common deletion spanning 4977 bp in humans is in fact shorter in mice, 3867 bp, but still involves the major mitochondrial arc (Figure 1.5) (Tanhauser and Laipis, 1995; Zhang *et al.*, 2013).

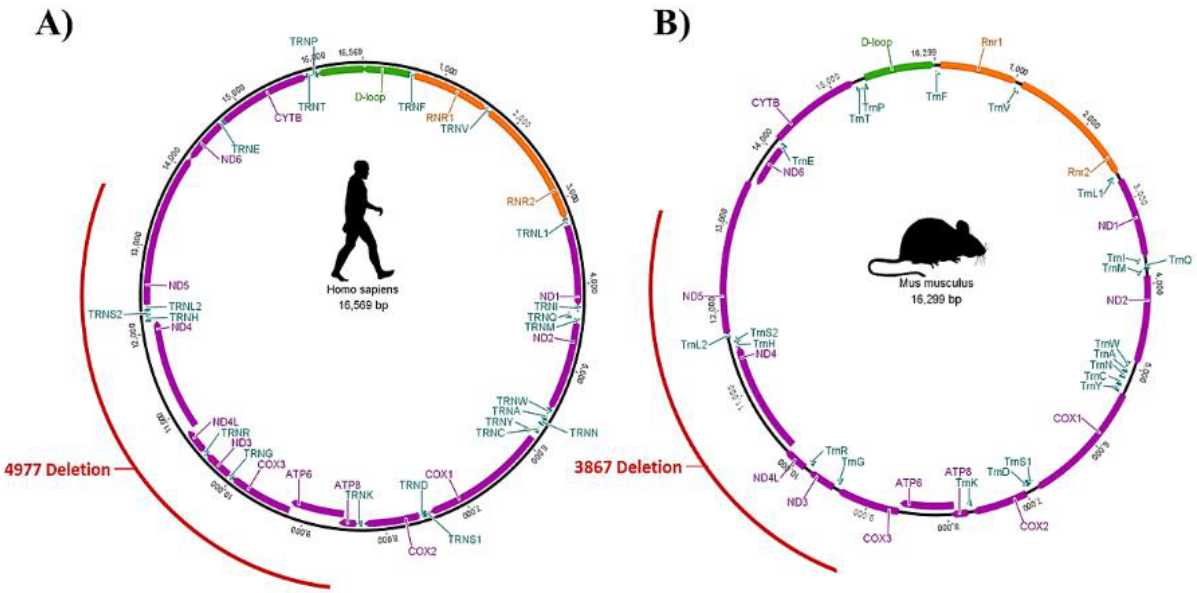

*Figure 1.5. Mitochondrial genome maps. Schematic representation of the mtDNA molecule and common deletion in humans (**A**) and mice (**B**). Image taken from (Kazachkova et al., 2013).*

1.7 Human Immunodeficiency Virus

The human immunodeficiency virus 1 (HIV-1) is the most prevalent and first discovered subtype of the HIV virus. HIV-1 is hereafter referred to as HIV in this thesis. HIV is an enveloped retrovirus that infects the host immune system cells and results in declining $CD4^+$ lymphocyte counts, leading to acquired immune deficiency syndrome (AIDS).

According to the World Health Organization, nearly 38 million people around the world were living with HIV in 2018.

The envelope of the virus, derived from the host cell membrane, is composed of surface glycoprotein 120 (gp120) and transmembrane glycoprotein gp41. The core of the virus is composed of capsid protein p24 and the p17 matrix core protein, which helps maintain viral structure. In the core, there are also two identical copies of single-stranded RNA (ssRNA) and three essential enzymes; reverse transcriptase (RT), protease and integrase.

After infection, the virus particle using its gp120 attaches to the receptor CD4 on the cell surface with the help of a co-receptor. The major co-receptors are CXCR4 and CCR5, primarily expressed in T-cells and macrophages, respectively but they can also express both. Binding of gp120 to CD4 receptor aided by the co-receptor results in a conformational change in gp120, allowing gp41 to unfold and insert its hydrophobic terminus into the host cell membrane. Gp41 draws the virus towards the host cell. After attachment, viral and host cell membranes fuse resulting in the viral RNA genome entering the cytoplasm of the cell where it is reverse-transcribed from ssRNA into proviral DNA using the HIV-1 reverse transcriptase (HIV-RT). This linear viral cDNA is integrated into the host cell nuclear DNA with the help of the viral integrase. Using the host cell machinery, it initiates transcription of viral mRNA species which are transported to the cytoplasm and translated into proteins being later cleaved by the protease, creating more virus particles and causing infection of nearby cells (Figure 1.6).

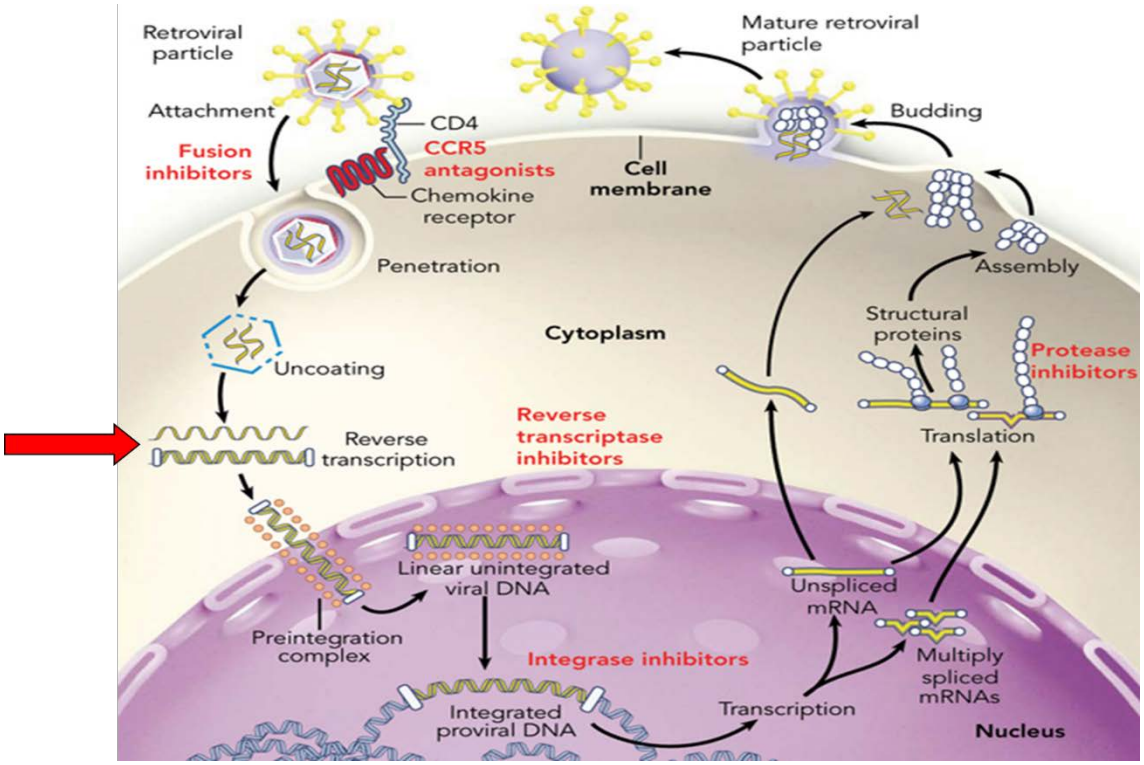

Figure 1.6. Replicative life cycle of HIV-1 and stages for the intervention of antiretroviral drugs (in red). Red arrow indicates the reverse transcription step, which is blocked by NRTIs and NNRTIs. Adapted from (Furtado et al., 1999).

1.7.1 Markers of HIV disease progression

CD4 T-cell count is commonly used to monitor the progress of HIV infection. However, decline in CD4 cell count can take several years to reach low levels. HIV-infected individuals with controlled viraemia have between 500-1500 cells/mm^3, which is considered a normal CD4 count. When CD4 count declines to less than 200 cells/mm^3, posing a risk of acquiring opportunistic infections and cancers, this is used to diagnose AIDS. The most common opportunistic infections in HIV are *Pneumocystis* pneumonia, Kaposi's sarcoma, cytomegalovirus, tuberculosis and candidiasis. Other AIDS-related infections include other bacterial, viral, fungal and protozoal infections. Recent results from the START study showed that initiation of antiretroviral therapy in HIV patients with a CD4 count of more than 500 cells/mm^3 was more beneficial than starting therapy after CD4 count had declined to 350 cells/mm^3 (Group *et al.*, 2015).

1.8 HIV treatment

1.8.1 Antiretroviral therapy (ART)

A variety of antiretroviral drugs can now target different stages of the HIV replication cycle. Entry into the host cell can be blocked by fusion inhibitors or chemokine receptor (CCR) antagonists. Antiretroviral regimens like nucleoside reverse transcriptase inhibitors (NRTIs) or nonnucleoside reverse transcriptase inhibitors (NNRTIs) lead to inhibition of reverse transcription. The action of viral integrase can be blocked by integrase inhibitors (INIs). Protease inhibitors (PIs) stop the viral protease.

Therefore the main classes are: NRTIs, NNRTIs, PIs, INIs, fusion inhibitors and CCR5 antagonists. Almost all patients are on highly active antiretroviral therapy (HAART) which is a combination of two NRTIs with a third class of drug, usually a PI, NNRTI or INI (Dieterich, 2006).

NRTIs are the longest established class and still the key mainstay of therapy. NRTIs inhibit transcription of viral RNA into proviral DNA. Zidovudine (also known as azidothymidine or AZT) was the first NRTI drug approved by the U.S. Food and Drug Administration in 1987 for the treatment of HIV infection. It was very widely used for many years, initially alone and later as part of HAART. Currently the most commonly used NRTIs include abacavir (ABC), lamivudine (3TC) and emtricitabine (FTC). Also very commonly used is tenofovir, as TDF (tenofovir disoproxil fumarate) or TAF (tenofovir alafenamide), which is an NtRTI (nucleo*tide* RTI). AZT, didanosine (ddI), zalcitabine (ddC) and stavudine (d4T) are also NRTIs but are no longer used in developed countries due to toxicity. AZT and d4T have however been widely used until recently in low income countries such as in sub-Saharan Africa.

1.8.2 NRTI antiretroviral drugs and mtDNA replication

In the case of thymidine analogues, they are incorporated into the mitochondria in a phosphorylated or unphosphorylated form. AZT undergoes a series of phosphorylations, until it reaches its active triphosphate form.

The first phosphorylation is done either by the thymidine kinase 1, if AZT is found in the cytoplasm, or by thymidine kinase 2, if it is found in the mitochondria (Arner and Eriksson, 1995). Both isoforms perform the same activity but in different cell compartments. Thymidylate kinase carries out the second phosphorylation, from AZT-monophosphate to AZT-diphosphate. Finally, nucleoside diphosphate kinase phosphorylates AZT into its triphosphate form, yielding the pharmacologically active AZT, which will then inhibit HIV reverse transcription (Lewis and Dalakas, 1995).

A membrane protein, named mitochondrial deoxynucleotide carrier, transports phosphorylated NRTIs and nucleosides into the mitochondria (Dolce *et al.*, 2001). However, this mechanism of NRTI entry into the mitochondria still needs further understanding.

AZT has a chemical structure very similar to the nucleotide thymidine, one of the DNA constituents (Figure 1.7). During the developing DNA chain, the phosphate group of thymidine binds with the 3' –OH functional group of the preceding nucleotide, and so forth. However, AZT does not have the 3' –OH group, instead it has an azido group (-N3) which cannot form a bond with the phosphate group from the following nucleotide (Lewis and Dalakas, 1995). Therefore, AZT incorporation by HIV reverse transcriptase into the viral elongating DNA chain will abruptly halt reverse transcription.

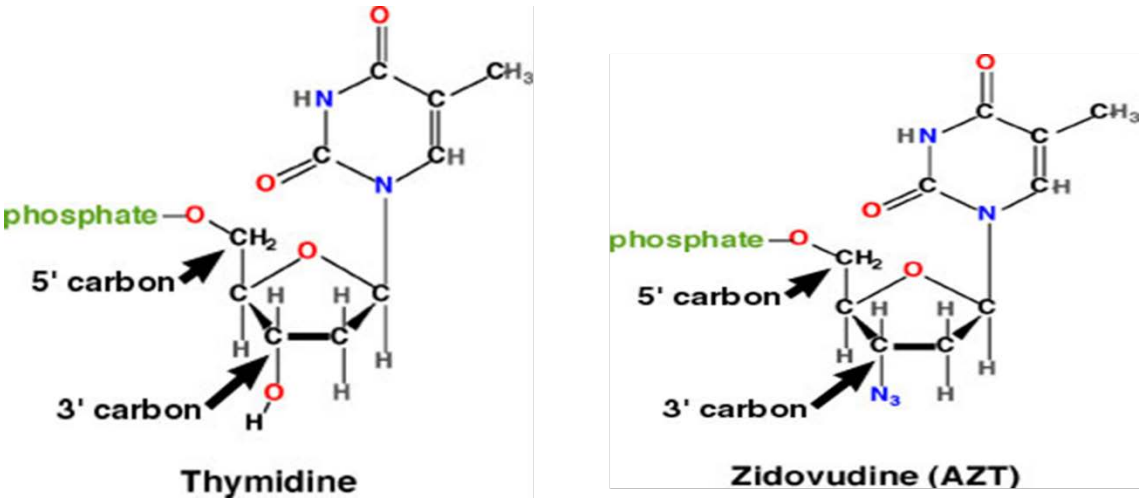

Figure 1.7. Diagram of the chemical structure from thymidine and zidovudine (AZT), an anti-HIV drug from the NRTI class. Adapted from Casiday and Frey (1998). Retrieved from http://www.chemistry.wustl.edu/~edudev/LabTutorials/HIV/DrugStrategies.html.

This process not only occurs during HIV reverse transcription but also during normal mtDNA replication by polymerase γ. The mitochondrial polymerase γ is not able to differentiate between thymidine and AZT given their analogy. As mentioned earlier, after their activation, NRTIs inhibit HIV reverse transcription and also polymerase γ, although the affinity of NRTIs for pol γ is estimated to be some orders of magnitude lower than that for HIV-RT. NRTIs' inhibition of mtDNA polymerase γ causes mtDNA depletion (content reduction) and leads to mitochondrial dysfunction, a process known as the polymerase γ hypothesis (Lewis and Dalakas, 1995).

Additionally, *Lim and Copeland* suggested that NRTIs not only inhibit the replication activity of the polymerase γ but also its inherent 3'-5' exonuclease activity (Lim and Copeland, 2001).

Some studies showed that antiretroviral switch from a highly toxic to a nontoxic NRTI allows the recovery of mtDNA content (McComsey *et al.*, 2005b), however more studies are needed to better understand this.

1.9 Pathogenesis of NRTI-induced mitochondrial toxicity

The hallmark toxicity of NRTIs is mitochondrial toxicity which clinically manifests as myopathy, neuropathy, lactic acidosis, lipodystrophy and very occasionally, hepatic failure. When NRTI-treated HIV positive patients first displayed these symptoms, they were recognised as being typical of hereditary mitochondrial diseases. Zidovudine-associated myopathy was first seen in several studies of treated patients (Helbert *et al.*, 1988; Dalakas *et al.*, 1990; Arnaudo *et al.*, 1991; Peters *et al.*, 1993). However, the molecular mechanism linking AZT-induced toxicity and muscle disease was not elucidated until some years later, when the polymerase γ hypothesis was proposed.

In studies of NRTI toxicity, mitochondrial damage can be biochemically measured in various ways such as looking at electron transport chain function, hydrogen peroxide production, mtDNA point mutations and deletions and mtDNA copy number (Koczor *et al.*, 2010).

The effects of anti-HIV therapy on mtDNA mutations have been studied using blood tissue (Bartley *et al.*, 2001; Martin *et al.*, 2003; McComsey *et al.*, 2005a; Ortiz *et al.*, 2011; Jitratkosol *et al.*, 2012; Liu *et al.*, 2013; Li *et al.*, 2017). However, blood is a mitotic tissue that replicates at a high rate, which might cause the loss of mtDNA mutations. Therefore, post-mitotic tissues such as brain and muscle tissues could be a better choice for looking at mtDNA mutations. The effect of anti-HIV therapy was studied using rodent cardiac muscle tissues, but comparable studies have not yet been performed on human cardiac muscle and brain tissues (Walker *et al.*, 2004a; Chan *et al.*, 2007; Balcarek *et al.*, 2010).

1.10 HIV and Ageing

The era of HAART has meant that HIV infection evolved from being a fatal infection to a now manageable chronic disease for most patients. Although antiretroviral therapy allowed for a higher life expectancy, it does not fully restore immune health in most infected individuals. Furthermore, several non-AIDS comorbidities are associated with long-term ART-treated HIV. But in general, it is not clear to what extent comorbidities are driven by residual effects of the virus or by the ART, likely both have a role.

Nowadays, antiretroviral treated HIV-infected persons achieve good immune reconstitution and an increased life expectancy, but nevertheless their average lifespan remains shorter compared to uninfected individuals, and they experience an increase in many of the common diseases and physiological changes of older age (Currier *et al.*, 2003; Valcour *et al.*, 2004; Brown and Qaqish, 2006; Desquilbet *et al.*, 2007; Erlandson *et al.*, 2013).

As mentioned before, given the known links between mitochondria and ageing (Taylor et al., 2003; Kujoth et al., 2005; Short et al., 2005; Bender et al., 2006; Bua et al., 2006; Vermulst et al., 2008), and mitochondria and HIV infection (Arnaudo et al., 1991; Shikuma et al., 2001; Cote et al., 2002; Miura et al., 2003), it is plausible that increased mitochondrial damage may be a biological mediator of ageing in HIV.

Previous work by *B. Payne and colleagues* has demonstrated that antiretroviral treated persons have an excess of cells containing mtDNA mutations, but the mechanism remains to be fully determined (Payne *et al.*, 2011). *In silico* modelling suggests that the increase may be consistent with an acceleration of clonal expansion of mtDNA mutations within cells, particularly in the setting of exposure to certain NRTI antiretroviral drugs. Conversely, other authors suggested that HIV infection or therapy may be mutagenic for mtDNA (Martin *et al.*, 2003; Walker *et al.*, 2004a; Jitratkosol *et al.*, 2012). Which model is correct will dictate the natural history of the mitochondrial defect in later life.

It is well established that certain NRTI antiretroviral drugs cause inhibition of the mtDNA polymerase γ leading to mtDNA depletion. It is therefore plausible that NRTI treatment also leads to increased mtDNA mutations, and that this may play a role in driving ageing phenotypes in HIV.

DdI is a strong inhibitor of pol γ and as such is expected to most likely affect clonal expansion (Lim and Copeland, 2001; Payne *et al.*, 2011). AZT is a weak inhibitor but potentially causes mutagenesis (Balcarek *et al.*, 2010; Cooper and Lovett, 2011). TDF and ABC do not inhibit pol γ and thus do not produce mtDNA depletion (Birkus *et al.*, 2002).

1.11 HIV, immune activation and chronic inflammation

HIV causes a massive decline in the T cell population, in particular CD4. However, in HIV infection, only 5-10% of immune cells that undergo apoptosis are actually HIV infected. CD4 T-cells that are not lost through the direct effects of HIV infection may instead be lost due to the host's immune response to the infection. This progressive CD4 lymphocyte loss is a hallmark of AIDS.

Infected T-cells are eliminated using some of the host's innate immune pathways.

Host cell interferon-γ-inducible protein 16 (IFI16) detects a build-up of viral transcripts inside the abortively infected cell, activating an inflammatory cascade within the cell (inducing interferon-β) which goes on to activate pyroptosis - the host cell self-destructs because of an inflammatory environment (Monroe *et al.*, 2014).

IFI16 activates caspase-1, which stimulates production of interleukin-1β. Inside the cell, IL-1β creates an inflammatory environment, which triggers pyroptosis (Man *et al.*, 2017). Pyroptosis is caspase-1 dependent (Doitsh *et al.*, 2014). IL-1β gets exposed to other neighbouring CD4 cells, undergoing pyroptosis as well and creating a chain reaction of CD4 cell loss. All of this propels a vicious cycle of chronic inflammation because of the proinflammatory signals that are being released which keep activating the host immune cells, leading to more cell death.

CD4 lymphocyte death following HIV infection can also be mediated through a different pathway. When integrase tries to integrate the viral cDNA into the host cell nuclear genome it creates DNA nicks to help with insertion. Host cell DNA-PK senses DNA breaks, triggering apoptosis (Cooper *et al.*, 2013). Apoptosis is very similar to pyroptosis, but pyroptosis is triggered by inflammation whereas apoptosis is triggered by damage signalling. If integrase succeeds and the cell produces virions, when HIV protease cleaves the viral precursors it can also cleave and activate other proteins

called caspase-3 and caspase-8, which will again trigger apoptosis. CD8 T-cells detect infected CD4 cells because these show viral surface proteins, they destroy them.

However, the majority of CD4 T-cell death is of uninfected ‘bystander’ cells, which leads to immune system failure (Holm and Gabuzda, 2005; Garg *et al.*, 2012; Garg and Joshi, 2017). When T-cells become exposed to HIV, even if they do not become infected by it, they display antigens in their surface, which are detected by dendritic cells transporting them to the lymph nodes. So uninfected T-cells that have ‘seen’ HIV will gather in lymph nodes. Within lymph tissues, pyroptosis will occur again, driven by endogenous inflammation.

This ‘bystander’ CD4 cell death was seen to be prevented by entry inhibitors, fusion inhibitors and NNRTIs, but not by the NRTI AZT (Doitsh and Greene, 2016); suggesting that elongation during reverse transcription is needed for the cell death events. Despite these recent findings, they do not fully explain why some HIV patients in ART still display persistent chronic inflammation. Additional important factors driving chronic inflammation in treated HIV include the presence of co-infections such as CMV (cytomegalovirus), as well as lifestyle factors.

Chronic immune activation and inflammation, leading to immune senescence is likely to be a major contributor to the age-related diseases that have been observed in HIV patients (Deeks, 2011; Nissen *et al.*, 2014).

1.12 HIV and neurocognitive disorders

Neurocognitive impairment (NCI) associated with HIV continues to be present in the HIV-infected population despite the widespread use of HAART. This excess of NCI is seen even when controlled for other comorbidities. A severe form of HIV-associated neurocognitive disorders (HAND), known as HIV-associated dementia (HAD), is less prevalent now owing to HAART, however mild and heterogeneous impairment, which include subclinical neuropsychological impairment (ANI) and mild cognitive motor disorder (MCI), are still persistent in up to one-half of people living with HIV (PLWH) in the US population, according to the CHARTER study (Heaton et al., 2010; Heaton et al., 2015). Recent European data, e.g. from the COBRA study, suggested lower rates than reported in the US data (Cole *et al.*, 2018; De Francesco *et al.*, 2018). The pattern of neurocognitive impairments in PLWH now more closely resembles that seen in other common neurodegenerative disorders, rather than that seen in HAD. The exact mechanisms whereby HIV causes NCI are not fully understood but are likely to be multifactorial, slowly changing and may plausibly include a strong 'legacy' effect of neuronal damage prior to initiation of HAART. The main current hypothesis is that persistent low-grade inflammation from monocytes and macrophages, vascular disease and microglial activation play a key role in causing HAND, even within the setting of successful HAART. Recently, it has become increasingly evident that impaired CNS function is linked to monocytic infection with HIV (Burdo *et al.*, 2013; McGuire *et al.*, 2015).

HIV infects and depletes CD4+ T lymphocytes, along with macrophages and dendritic cells. Many studies have reported the role of tissue macrophages acting as reservoir for HIV virus (Igarashi *et al.*, 2001; Groot *et al.*, 2008; Coleman and Wu, 2009; Koppensteiner *et al.*, 2012; Malim and Bieniasz, 2012; Abbas *et al.*, 2015). Similarly, microglial cells, a type of macrophage resident in the brain, express receptors linked to HIV tropism including CD4, CCR5, CXCR4 and CCR3 (Ghorpade *et al.*, 1998; Albright *et al.*, 1999). Microglia are therefore susceptible to HIV infection and spread (Cenker *et al.*, 2017), and are believed to be infected at a very early stage of the disease (An *et al.*, 1999). Microglia are long-lived cells which, due to the continuous cell division they are subject to, may provide an archive of HIV virus and therefore a persistent reservoir in the brain. Thus, viral reservoirs of latent and active infections present a challenge to antiretroviral therapy (Schnell *et al.*, 2011; Joseph *et al.*, 2015). Moreover, there is wide variability of ART penetrance across the blood-

brain barrier into the CNS. This effect has been quantified using the CNS penetration-effectiveness rank (CPE) (Letendre *et al.*, 2008). However such model has not proven consistent yet in improving treatment in HAND (Baker *et al.*, 2015).

Brains of HAND patients have displayed neuronal mitochondria with aberrant morphology compared to HIV-infected but not cognitively impaired peers (Avdoshina *et al.*, 2016; Fields *et al.*, 2016). Neurons are high energy demanding cells, containing large quantities of mitochondria per cell. Mitochondria in neurons provide ATP to axonal and dendritic terminals for healthy synapses and maintenance of energy homeostasis. Thus, neuronal dysfunction and neuronal loss are often associated with changes in mtDNA. In keeping with this hypothesis, *in vitro* studies have shown that HIV proteins may exhibit direct neurotoxicity associated with mitochondrial dysfunction. In particular, the viral envelope protein gp120 triggers neurotoxic pathways that lead to altered neuronal mitochondrial dynamics and function (Avdoshina *et al.*, 2016). HIV gp120 and HIV trans-activator of transcription (tat) are known to induce HIV-related neurotoxicity, and mitochondrial dysfunction by impairing neuronal mitophagy in human primary neurons (Teodorof-Diedrich and Spector, 2018). Tat has also been reported to increase mitochondrial fission in neurons (Rozzi *et al.*, 2018). These alterations are believed to elicit HIV-mediated neurodegeneration. Neurons are likely to be exposed to such viral proteins owing to the productive infection of adjacent glial cells. HIV does not infect primary neurons but does infect glial cells (also called neuroglia) including astrocytes. However, viral proteins like gp120 and tat do penetrate neurons *in vitro* and could therefore trigger molecular events to potentially cause neurocognitive impairment. HIV gp120 has also been found to induce apoptosis in *in vitro* human primary neurons and has been linked to HAD pathogenesis (Jana and Pahan, 2004). Gp120 not only has been observed to cause cell death in some types of neurons *in vitro* (Dawson *et al.*, 1993), but also *in vivo* in brains from rodents (Bansal *et al.*, 2000). Altogether these inflammatory factors have been proposed to contribute in the environment causing neuronal injury in HAND (Figure 1.8).

The possible role of ART in causing neurotoxicity, including by a mitochondrial mechanism was reported in some studies. Particularly, NRTI-associated peripheral neuropathy in HIV patients has been associated with mitochondrial toxicity (Moyle and Sadler, 1998; Dalakas, 2001; Dalakas *et al.*, 2001; Kallianpur and Hulgan, 2009; Lehmann *et al.*, 2011).

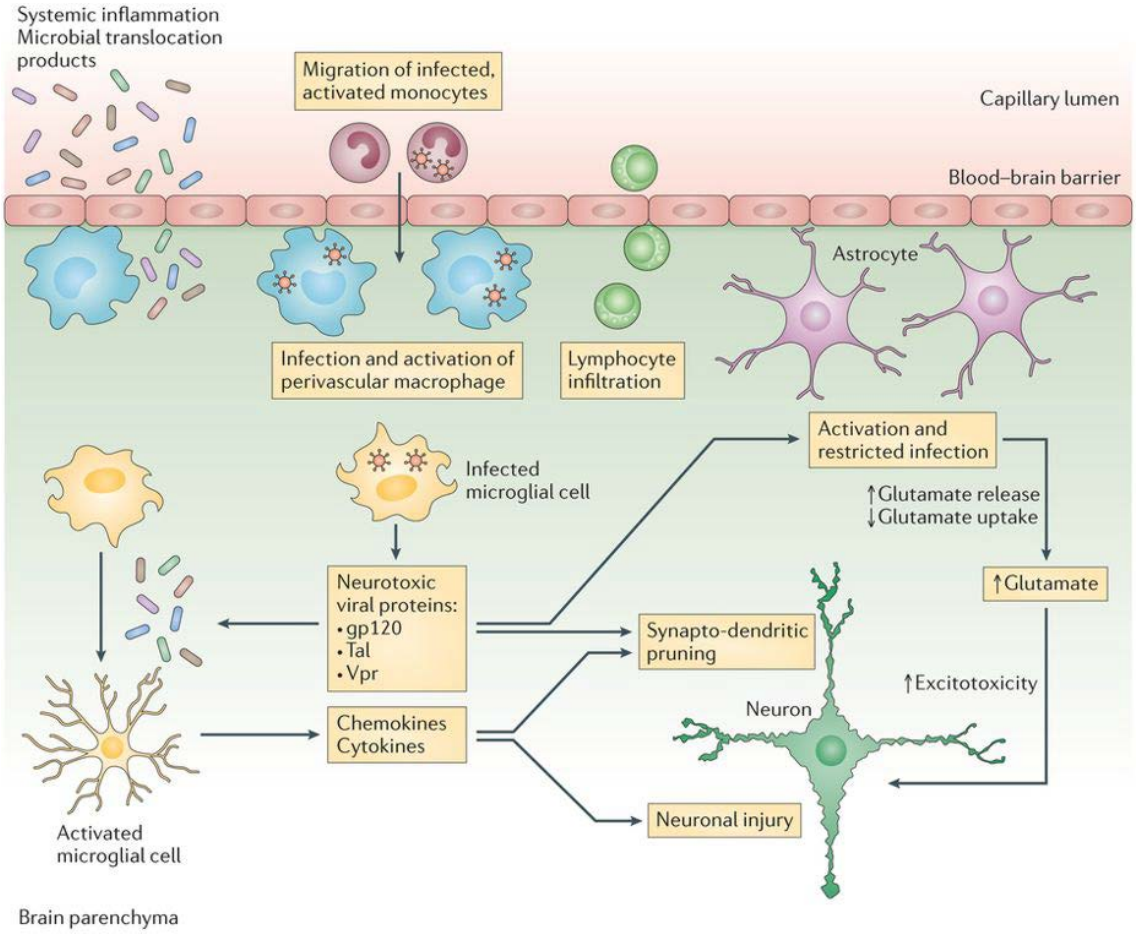

Figure 1.8. Neuropathogenic factors contributing to HIV-associated neurocognitive disorders. Infected macrophages and microglial cells release neurotoxic viral proteins that contribute to the activation of astrocytes and subsequent inflammation of the environment leading to neuronal injury. Image taken from (Saylor et al., 2016).

Optimal markers for HAND remain poorly defined, but have been recently reviewed elsewhere (Clifford and Ances, 2013; Clifford, 2017). Given the fact that thanks to ART HIV-infected individuals now live longer and have an increased burden of comorbidities, it is therefore more difficult to diagnose NCI that is truly HIV-related and not from age-associated neurocognitive disorders in this population. Current evaluation and management guidelines used in HAND patients show convergence in that NCI assessment should be performed only in symptomatic cases (Underwood and Winston, 2016).

1.13 Research Aims

The hypothesis was that mtDNA mutations are a mediator of ageing in HIV, by clonal expansion of mtDNA mutations leading to accelerated physiological decline.

The aims of the project were:

1) To develop a model of clonal expansion of mtDNA mutations in ageing.

2) To determine whether NRTI therapy accelerates clonal expansion.

3) To determine whether mtDNA damage contributes to the pathogenesis of HAND.

Chapter 2. Methods

2.1 Ethical guidelines

The human study was approved by the 'Newcastle and North Tyneside 2 Research Ethics Committee' (reference 17/NE/0015).

The mouse study was carried out under the Project Licence Number 70/8623. My personal licence (PIL) number was I7CC5B565.

2.2 *PolgA* mouse model

2.2.1 Breeding and husbandry

PolgA$^{wt/mut}$ mice were originally provided as a kind gift from Dr Michael Keogh (Newcastle University) and bred back to a C57BL/6J (B6, Charles River Laboratories) nuclear background as further explained in Chapter 4. C57BL/6J mice are the most widely used inbred strain, with minimal genetic drift, most well characterised and the first one to be sequenced. C57BL/6J, also known as black 6 mice, were used as a background strain for the generation of the *PolgA* WtN+ mouse model. The WtN+ derivative of the *PolgA* mutator mouse contained a germline mtDNA mutational burst on a wild-type inbred nuclear background; this clonal expansion mouse model was named 'WtN+' and is hereafter referred to as such in this thesis.

Mice were maintained on 12-hour light/dark cycles with *ad libitum* access to filtered water and normal mouse pellet diet. Mice were allocated into two study plans according to Home Office regulations, the methods described in this thesis were performed according to the relevant guidelines provided by the Project Licence regulations (see Appendix 10.3 for study plan details and Appendix 10.4 for the protocol for genetically altered animals).

2.2.2 Genotyping

Genotyping was carried out at weaning time, at 4 weeks old. Mice were genotyped as follows. QIAamp DNA Mini Kit (Qiagen) was used to extract total DNA from clipped ear tissue, as per manufacturer's guidelines. For the final elution stage, 200 µl Buffer AE were added to the centre of the membrane and allowed to incubate at room temperature for five minutes before centrifugation at full speed for one minute. DNA samples were stored in the -20°C freezer and used in subsequent analysis described in this thesis. The primer sequences used to genotype the mice are, CTTCGGAAGAGCAGTCGGGTG for the forward primer and GGGCTGCAAAGACTCCGAAGG for the reverse. Primers for genotyping annealed to the *PolgA* gene in chromosome 7. PCR reactions were performed in a 19 µl master mix containing nuclease-free H_2O, 1X Green GoTaq Reaction Buffer (Promega), 0.2 mM dNTP Mixture, forward and reverse primers (0.4 µM each), 0.25 U GoTaq DNA Polymerase to which was added 1 µl of DNA sample. Reactions were run on an Applied Biosystems® Veriti® 96 well thermal cycler (Thermo Fisher Scientific). PCR conditions consisted of one cycle at 94°C for 60 seconds; then 30 cycles of 94°C for 30 seconds, 60°C for 30 seconds, 72°C for 60 seconds; ending with 72°C for 3 minutes. Products were analysed on 1% agarose gel at 75V for 30 minutes. *PolgA*$^{wt/wt}$ is identified by a single 520 bp band while *PolgA*$^{mut/mut}$ is identified by a single 720 bp band size. For heterozygous *PolgA*$^{wt/mut}$ mice two bands at 520 bp and 720 bp were expected to be present as they have two alleles (Figure 2.1).

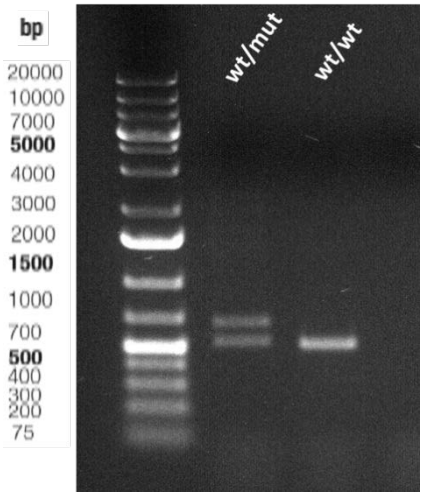

Figure 2.1. Agarose gel analysis of genotyping products of two mice brothers. Two bands (520 bp and 720 bp) are present for the first sample, heterozygous. One band (520 bp) is present for the second sample, wild-type. GeneRuler 1 kb Plus DNA Ladder SM1333 (Thermo Fisher Scientific) was loaded in the first lane.

2.2.3 Phenotypic testing

Mice were observed and clinically scored, blind to genotype and treatment, on a weekly basis. Phenotyping was carried out at 35 and 47 weeks of age (and 18 weeks for the clinical score values). Frequencies of interim measurements were subjected to change if weekly observation of mice suggested any problems. All phenotyping was done by a single female observer to minimise the effects of animal stress on the measurements.

2.2.4 Clinical scoring

Clinical scores were collected and registered for the defined criteria in the printed sheets in Appendix 10.1. A clinical score sheet was available to guide the scoring of the animals (Appendix 10.2). Scores included weight, appearance of the coat, skin tone, behaviour, posture and mobility, abdominal distension, foot colour and faeces. The animal had to be culled if: it had three separate scores of 2; it had a single score of 3; there was over 20% weight loss; there was persistent temperature below 33°C (if the temperature was low, animal was monitored a few times at 5 minute intervals to see if it recovered. Normally the scores are well correlated with the temperature. Low temperatures are only a concern if they are scoring considerably high as well).

Following our study plan guidelines, due to their genotype WtN+ animals had to be clinically scored once a week whereas wild-type animals were allowed to be scored at the established weeks (18, 35 and 47).

2.2.5 Open field tests

Mice in their home cages were first allowed 10 minutes to acclimatise to the room. Open field tests were carried out using a computer application called MouseTrapp (Neurolytical) (Mabrouk *et al.*, 2014) on a touch-screen tablet inside a white acrylic box with a specially cut slot for the tablet to slide into the bottom. Tablet was placed in the slot at the bottom of the opaque-walled test chamber, ensuring that the down arrow on the bottom left hand side was still exposed as this was used to stop recording the data at the end of the test. The mouse was gently placed in the centre of the 13.5 x 22 cm tablet surface and timed for 6 minutes after MouseTrapp was started. A clear plastic lid was used to cover the chamber. The observer stepped away from the cage to avoid looking inside and distracting the animal, which was allowed to ambulate freely. The open field test generated general locomotor activity data. For each session, a spreadsheet was automatically generated containing the number of steps the animal made, number of rears, distance travelled, length and velocity of each step. These features were important for assessing both the quality and quantity of animal movement and can be useful in studying animal motor function. The tablet and box were both cleaned with a 70% ethanol solution between tests in order to hide animal clues.

2.2.6 Metabolic treadmill tests

A metabolic treadmill test was carried out using the Metabolic Modular Treadmill (Columbus Instruments), to determine the consumption and production rates of oxygen and carbon dioxide. Only a selected group of representative females were chosen for this test (n=5 WtN+ and n=5 wild-type). The metabolic system, Oxymax, measured the concentration of these gases by comparing the amount being supplied into the treadmill chamber to that of gases leaving the chamber where the animal was placed. O_2 and CO_2 gas sensors were calibrated before the experiment began. O_2 and CO_2 values were adjusted and kept within range throughout the tests. Mice

were acclimatised for 15 minutes per day for 4 days prior to this test by being placed inside the enclosed motionless treadmill chamber.

For the experimental observations, mice were placed on the running lane inside the sealed chamber making sure they were settled before the experiment began. First, mice were rested for 15 minutes before running for 20 minutes at 12 m/min speed on the transparent treadmill as shown in Table 2.1. Oxymax software recorded gas exchange measures every 30 seconds. Chamber rear bumpers were occasionally used to gently push the mice on their hindquarters in case they slid back. The animals remained visible and it was ensured they were safe at all times. Each mouse performed the test once at each time point.

Step	Speed (m/min)	Ramp (s)	Hold (s)
1	0	0	900 (15 mins)
2	12	10	1200 (20 mins)

Table 2.1. Running protocol for the Metabolic Modular Treadmill. Total of 35 minutes, 5 minutes were allowed for system warm up. Data was collected every 30 seconds, as animals rested for the first 15 minutes and then they were ran for 20 minutes.

Once the exercise was over, the treadmill lane was cleaned and brushed with disinfectant spray first and then 70% ethanol solution.

2.2.7 Grip strength testing

Instrument was assembled prior to the performance of the front limbs grip test. Animals were held by the first proximal part of the tail and gently placed above the grid. The mouse was moved down until its front legs grabbed the grid approximately in the middle. While the mouse was grasping, its position was lowered to a horizontal position. The animal was pulled following the axis of the sensor until the grasp was released. The grip test measurement took 3 seconds from the first grasp to the release and the pulling movement was slow but regular. All these steps above were performed smoothly without abrupt movement. A constant velocity movement is the insurance of repeatable tests. The maximum force developed by the mouse was

displayed on the screen. Three repeats were performed per each mouse and values were recorded in grams.

2.2.8 Videos

The selected mice were videoed for 3 minutes after being placed on top of an upturned weighing box in a defined square area. Additionally, a brief video was also taken of the abdomen to look for abdominal distention, foot colour and detect faeces build up. These videos were performed to provide additional validation of the health scoring. Due to its format, videos are not included in this thesis but are available upon request.

2.2.9 Dissections

Mice were culled at three time points, 18, 36 and 48 weeks old. A longer time point of 76 weeks was also taken for a group of WtN+ females. All organs were harvested and weights were recorded (Appendix 10.5). Organs were snap-frozen as quickly as practicable, certainly within minutes following harvest. This is because basic mitochondrial histochemistry requires intact respiratory chain enzyme activities. Specimens were used in the following ways: mounted for cryosectioning, formalin fixed-paraffin-embedded (FFPE) tissue and stored for nucleic acid extraction. Any associated fat from the tissues was dissected out.

Specimens were mounted for cryosectioning using a sterile dissection kit, aimed to dissect two neat cubes of muscle tissue with well-preserved orientation from the centre of the specimen, each of 5-10 mm in each dimension. Skeletal muscle from mouse quadriceps was transversely oriented and mounted onto a strip of filter paper (Whatman) using a thin layer of OCT cryo-embedding matrix. Samples were snap-frozen by brief immersion in liquid-phase isopentane, cooled in liquid nitrogen (-160°C) and then transferred the mounted specimen into a specimen bag (pre-cooled in liquid nitrogen), sealed and placed in liquid nitrogen pending transfer to -80°C freezer for storage. Other tissues were snap-frozen in liquid nitrogen, then stored at -80°C.

FFPE tissue blocks were fixed in formalin for 24 hours and then the solution was changed to freshly made 70% ethanol, before being sent to the biobank for embedding of the FFPE tissue blocks.

2.3 DNA extraction from human tissues

2.3.1 Homogenisation and DNA purification from frozen human brain tissue

DNA from frozen human frontal cortex (grey matter) was either supplied as DNA extract by the biobanks, or extracted locally using commercial kits according to standard manufacturer's methods. Brain tissue from HIV positive subjects was processed in the Containment Level 3 laboratory.

The biobanks included TNRC (Texas Repository for AIDS Neuropathogenesis Research), CNTN (California NeuroAIDS Tissue Network), UCLA (National Neurological AIDS Bank, NNAB), Manhattan HIV Brain Bank (MHBB) and Edinburgh biobank.

DNA concentration was quantified using the Nanodrop ND-1000 Spectrophotometer (Labtech International).

2.4 DNA extraction from mouse tissues

2.4.1 Homogenisation of frozen mouse skeletal muscle and mouse colon

A maximum of 25 mg of frozen tissue was used for each sample. Skeletal muscle was placed in a porcelain mortar, chilled with liquid nitrogen and manually ground with a porcelain pestle until powdered. Liquid nitrogen was used to keep the samples and instruments cool at all times. Powdered tissue was carefully transferred into a 1.5 ml microcentrifuge tube. In between stages of this process, skeletal muscle tissue samples were kept in liquid nitrogen.

2.4.2 Homogenisation of frozen mouse brain

Frozen mouse brain was placed in a petri dish kept on dry ice in order to keep the sample frozen. Tissue from the frontal pole area was shaved using a sterile chilled scalpel and carefully transferred into a 1.5 ml microcentrifuge tube.

2.4.3 DNA purification from frozen mouse skeletal muscle, brain and colon

DNA isolation from homogenised skeletal muscle, colon and brain samples was performed using a QIAamp DNA Mini Kit (Qiagen) according to the manufacturer's guidelines as outlined in the 'DNA Purification from Tissues' protocol in the QIAamp DNA Mini and Blood Mini Handbook (05/2016). For the final elution stage, 200 µl Buffer AE were added to the centre of the membrane and allowed to incubate at room temperature for five minutes before centrifugation at full speed for one minute. DNA concentration was quantified using the Nanodrop ND-1000 Spectrophotometer.

2.5 Quantitative PCR to Measure Mitochondrial DNA Copy Number and Common Deletion Levels in Human Tissue

In order to measure mitochondrial DNA copy number (CN) in human homogenate tissue, a quantitative real-time PCR (qPCR) assay was used. The nuclear-encoded housekeeping gene Beta-2-microglobulin (*B2M*, Genbank accession ID: NM_004048, NG_012920.2 Chromosome 15) and the mitochondrially encoded NADH-ubiquinone oxidoreductase core subunit 1 gene (*MT-ND1*, Genbank accession ID: NC_012920.1) were used respectively as nDNA and mtDNA targets.

2.5.1 Mitochondrial DNA m.δ4977 bp common deletion level assay

The mitochondrial gene *MT-ND4* is usually lost during large-scale deletions, which involve the major arc of the mitochondrial genome, whilst *MT-ND1* remains undeleted in the molecule. A triplex *MT-ND1/MT-ND4/B2M* qPCR assay is used frequently to detect deletions (Pyle *et al.*, 2010; Pyle *et al.*, 2015a; Pyle *et al.*, 2016), but it will only detect relatively high deletion heteroplasmy levels (≥25%). The m.δ4977 bp mitochondrial 'common deletion' (CD), flanked by two 13 bp homologous repeat

sequences at positions m.8470-8482 and m.13447-13459 (inclusive), removes various genes including *MT-ND4* as depicted in Figure 2.2. A triplex qPCR assay with *CD/MT-ND1/B2M* amplicons was designed to allow low-level deletion detection (down to ~10^{-4}) and is a much more sensitive assay for deletions than the *MT-ND1/MT-ND4/B2M* assay. This assay is however specific to the CD, rather than detecting all major deletions.

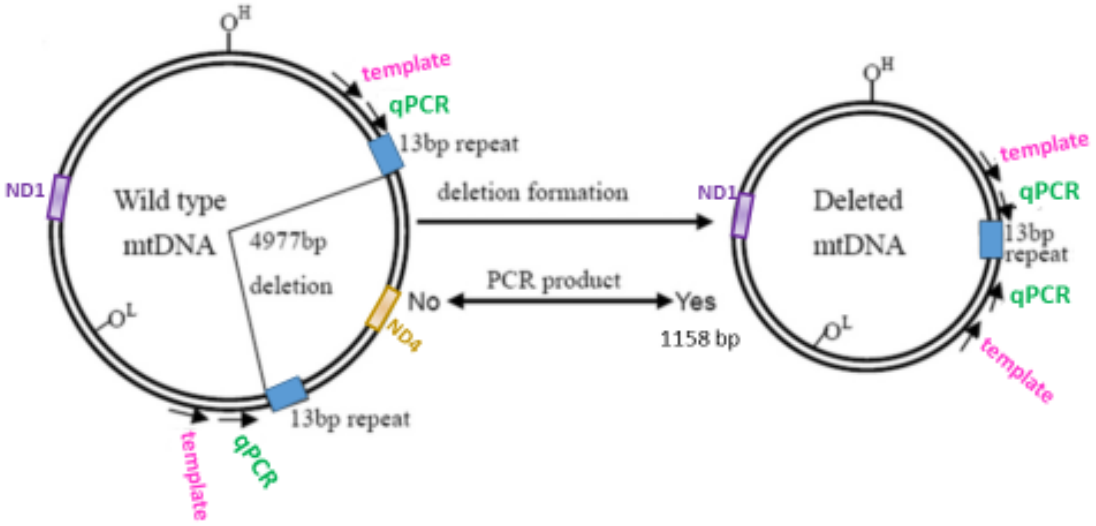

Figure 2.2. Schematic representation of the triplex qPCR assay used to detect the mtDNA 4977 bp common deletion. Depicted are the distribution of 13 bp homologous repeats for the common deletion (blue), MT-ND1 and MT-ND4 genes (purple and yellow respectively), the primers for template amplification (pink) and the primers for qPCR amplification (green). Image adapted from (Chen et al., 2011).

The proportional level of mitochondrial DNA molecules containing the m.δ4977 bp common deletion was quantified as previously done in our group (Samuels *et al.*, 2017) but the nuclear gene *B2M* was added to create a triplex real-time qPCR assay (*CD/MT-ND1/B2M* genes) so that mtDNA CN and CD levels could be calculated at the same time. The level of CD per mtDNA copy per cell was determined by comparison with the copy number of the *MT-ND1* gene (further explained in Section 2.5.7). The results were expressed on a logarithmic scale in line with the observed distribution of CD levels.

2.5.2 Preparation of reagents

All stock primers and probes (IDT) used in real time qPCRs were resuspended using Ambion® nuclease-free water (ThermoFisher Scientific) under the UV sterilizing PCR cabinet (UVP) to obtain working concentrations of 10 µM and stored at -20°C. All PCR reactions were set up on ice.

2.5.3 Generation of qPCR standard templates

Quantitative standards for the triplex *CD/MT-ND1/B2M* qPCR assay were prepared by PCR generated templates.

The *MT-ND1* and *B2M* standards were generated using a control DNA sample. The qPCR CD standard was generated using a DNA sample from a patient with progressive external ophthalmoplegia (PEO), kindly provided by Professor Rob Taylor (Newcastle University), with a known level of the δ4977 mtDNA common deletion. Primer sequences for the generation of the *ND1*, *B2M* and CD template are in Table 2.2.

Gene	Amplicon size (bp)	Forward Primer Sequence (5'-3')	Reverse Primer Sequence (5'-3')
B2M	1092	CGCAATCTCCAGTGACAGAA	GCAGAATAGGCTGCTGTTCC
MT-ND1	1040	CAGCCGCTATTAAAGGTTCG	AGAGTGCGTCATAGTTGTTC
CD	1158	TCCTAACACTCACAACAAAAC	GTTAGGTAGTTGAGGTCTAGG

Table 2.2. Primers used to generate standard templates using PCR for the human triplex qPCR assay.

PCR reactions were performed in a 24 µl PCR master mix containing: 1X MyTaq™ Reaction Buffer (includes dNTPs, $MgCl_2$ stabilizers and enhancers), one unit of MyTaq™ HS DNA Polymerase (Bioline), 400 nM of each forward and reverse primers and dH_2O. Approximately 30 ng of DNA was loaded into each reaction well of 0.2 ml 8-Strip PCR tubes (StarLab) and run on an Applied Biosystems® Veriti® 96 well thermal cycler (ThermoFisher Scientific). PCR conditions consisted of an initial denaturation at 95°C for one minute, followed by 30 cycles of denaturation at 95°C

for 15 seconds, annealing at 61°C (for *MT-ND1* and *B2M* genes) or 58°C (for CD template) for 15 seconds, extension at 72°C for 10 seconds.

2.5.4 Agarose gel electrophoresis

Amplified template PCR products (n=12) were pooled and mixed with Orange G loading buffer (50% glycerol, Orange G powder (Sigma Aldrich Company Ltd) and 50% water) and loaded into a single large well on a 1% agarose gel (1 g agarose (Bioline) in 100 ml 1X TAE buffer, and 0.4 mg/µl UltraPure™ ethidium bromide (Invitrogen)). GeneRuler 1 kb Plus DNA Ladder (ThermoFisher Scientific) and a negative PCR product used as a negative control were also mixed with Orange G dye and loaded into single separate wells. Agarose gels were electrophoresed at 75 V for one hour in 1X TAE buffer.

2.5.5 Purification and quantification of standard templates

Agarose gels were imaged using the UVP GelDoc-It™ imaging system (UVP). The gel-extracted fragment was extracted using the QIAquick gel extraction kit (Qiagen), as per manufacturer guidelines. Template concentrations were measured using the Nanodrop ND-1000 Spectrophotometer. Template DNA copy number concentrations were calculated using Equation 2.1. All template DNA was multiplexed together to obtain a starting copy number each of a 10^{10} ng/µl, which was then diluted 1:10 to obtain a 10^{9} ng/µl stock to be stored at -20°C until required.

$$Copy\ Number = [C \div (L\ x\ 2\ x\ 330)]\ x\ A$$

Equation 2.1. Formula used to calculate starting mitochondrial DNA copy number (copies/µl). C is DNA concentration in nanolitres (10^{-9}), L is amplicon length in base pairs and A is Avogadro's constant (6.023 x 10^{23}).

2.5.6 Quantitative PCR for mtDNA copy number quantification

All qPCR reaction plates were set up in a UV hood to minimise DNA contamination. The multiplexed 10^9 ng/µl DNA standards were diluted in a tenfold serial dilution of $1x10^8$ to $1x10^2$ ng/µl. The triplex qPCR mastermix was prepared in an 18 µl reaction volume containing 1X iTaq™ Universal Probes Supermix (Bio-Rad), 300 nM of each forward and reverse *B2M* and CD primers, 75 nM of each forward and reverse *MT-ND1* primers, 200 nM of each TaqMan™ probe and dH2O; with 2 µl of standard or DNA sample, loaded into a Hard-Shell 96-well PCR plate (Bio-Rad) covered with a Microseal® 'B' adhesive sealing film (Bio-Rad) to seal the plate. The qPCR amplification primers and Taqman™ probe sequences are found in Table 2.3 and Table 2.4, respectively.

Gene	Amplicon size (bp)	Forward Primer Sequence (5'-3')	Reverse Primer Sequence (5'-3')
B2M	231	CACTGAAAAAGATGAGTATGCC	AACATTCCCTGACAATCCC
MT-ND1	111	ACGCCATAAAACTCTTCACCAAAG	GGGTTCATAGTAGAAGAGCGATGG
CD	115	CCCACCATAATTACCCCCATAC	GGAGTAGAAACCTGTGAGGAAAGG

Table 2.3. Primers for the qPCR amplification of mitochondrial and nuclear genes used in the δ4977 mtDNA common deletion quantification and copy number assay. Primers from Integrated DNA Technologies.

All DNA standards were measured in duplicate and controls and DNA samples in triplicate on a CFX96 Touch™ Real-Time PCR detection system (Bio-Rad). The qPCR conditions were: initial denaturation at 95°C for three minutes; followed by 40 cycles of: denaturation at 95°C for 10 seconds, followed by annealing and extension at 62°C for one minute.

Gene	Fluorophore	Quencher	Probe Sequence (5'-3')
MT-ND1	HEX	BHQ_1	ACCCGCCACATCTACCATCACCCTC
B2M	FAM	BHQ_1	CCGTGTGAACCATGTGACTTTGTC
CD	Cy5	BHQ_2	CCTACCTCCCTCACCATTGG

Table 2.4. Taqman™ probes for the triplex qPCR assay. MT-ND1 gene was labelled with fluorescent HEX dye. Common deletion was labelled with fluorescent Cy5 dye. B2M was labelled with fluorescent FAM dye. Probes synthesised by Integrated DNA Technologies.

The CD probe was designed using Primer3 software online and it sits on the repeat region of the common deletion. All primers were screened using Primer-BLAST to confirm no nuclear gene homology (Ye *et al.*, 2012).

2.5.7 Determining mtDNA copy number and common deletion level in homogenate tissue

Analysis of the qPCR data was performed using Bio-Rad CFX manager 3.1 software. For each fluorophore, sample replicates with greater than 0.5 Ct standard deviation were removed from analysis and repeated in the following plate run. Control DNA samples were used in every plate to assess their Ct values were consistent throughout the consecutive plate runs. Intercept and slope values were averaged for every fluorophore (HEX, FAM and Cy5) across all qPCR plates in order to correct the starting quantity (SQ) data generated from the standard curve analysis. Standard curves were only acceptable when negative control contamination was above 35 Ct values and when efficiencies were greater than 85%. Raw data was exported into Microsoft Excel. MtDNA copy number was calculated as an average of each individual sample replicate Ct value, using Equation 2.2, and is reported in this thesis as copies per cell (copies/cell).

$$\text{mtDNA CN} = (\text{ND1 SQ mean}) \div (\text{B2M SQ mean} \div 2)$$

Equation 2.2. Calculation for mtDNA copy number using SQ mean values generated from Ct data using standard curves.

Common deletion level was calculated using Equation 2.3 and is reported in this thesis as common deletion per copy of mtDNA genome (CD/mtDNA genome copy).

$$\text{CD/mtDNA genome copy} = (\text{CD SQ mean}) \div (\text{ND1 SQ mean})$$

Equation 2.3. Calculation of common deletion level using SQ mean values generated from Ct data using standard curves.

2.6 Quantitative PCR to Measure Mitochondrial DNA Copy Number in Mouse Tissues

In order to measure mitochondrial DNA copy number in mouse homogenate tissue, a quantitative PCR assay was used. The nuclear-encoded housekeeping gene Beta-Actin (*β-Actin*) was used as the nuclear reference gene (Genbank accession ID: NC_000071.6, Chromosome 5) and the mitochondrially encoded NADH-ubiquinone oxidoreductase core subunit 5 gene (*MT-ND5*) (Genbank accession ID: NC_005089.1) was used as the mtDNA molecule reference. Reagents were prepared as described in Section 2.5.2.

2.6.1 Generation of qPCR standard templates

Quantitative standards for the duplex *MT-ND5/β-Actin* qPCR assay were prepared by PCR generated templates. The following steps for this protocol were carried out in a UV hood to minimise DNA contamination. Primer sequences for the generation of qPCR templates can be found in Table 2.5.

Gene	Amplicon size (bp)	Forward Primer 5'-3'	Reverse Primer 5'-3'
MT-ND5	1110	GCCCTTCACATAATTCCACTT	GGCTCCGAGGCAAAGTATAG
β-actin	1157	GATCGATGCCGGTGCTAAGA	GGAAAAGAGCCTCAGGGCAT

Table 2.5. Primers used to generate standard templates using PCR for the mouse duplex qPCR assay. Primers from IDT.

All PCR reactions were set up on ice. PCR reactions were performed in a 24 µl PCR master mix containing: 1X ImmoBuffer (Bioline), one unit of Immolase DNA Polymerase (Bioline), 4 mM $MgCl_2$, 0.2 mM of dNTPs, 0.3 µM of each forward and reverse primers and dH_2O. Approximately 20 ng of DNA was loaded into each reaction well of 0.2 ml 8-Strip PCR tubes (StarLab) and run on an Applied Biosystems® Veriti® 96 well thermal cycler (ThermoFisher Scientific). PCR conditions consisted of an initial Hot Start denaturation at 95°C for seven minutes, followed by 39 cycles of denaturation at 95°C for one minute, annealing at 55°C (for *MT-ND5*) or 63°C (for *β-Actin*) for one minute, extension at 72°C for two minutes, followed by a final extension step at 72°C for 10 minutes.

Agarose gels along with purification and quantification of standard templates were performed the same way as described in Sections 2.5.4 and 2.5.5.

2.6.2 Quantitative PCR for mtDNA copy number quantification

The multiplexed 10^9 ng/µl DNA standards were diluted in a tenfold serial dilution of $1x10^8$ to $1x10^2$ ng/µl. The duplex qPCR mastermix was prepared in a 18 µl reaction volume containing 1X iTaq™ Universal Probes Supermix (Bio-Rad), 300 nM of each forward and reverse *MT-ND5* and *β-Actin* primers, 200 nM of each TaqMan™ probe and Ambion® nuclease-free water (ThermoFisher Scientic); with 2 µl of standard or DNA sample, loaded into a Hard-Shell 96-well PCR plate (Bio-Rad) covered with a Microseal® 'B' adhesive sealing film (Bio-Rad) to seal the plate. The qPCR amplification primers and Taqman™ probe sequences are found in Table 2.6 and Table 2.7, respectively.

Gene	Amplicon size (bp)	Forward Primer 5'-3'	Reverse Primer 5'-3'
MT-ND5	134	ACCTAATTAAACACATCAACTTCCC	GACTCAGTGCCAGGTTGTAA
β-actin	137	CTGCTCTTTCCCAGACGAGG	AAGGCCACTTATCACCAGCC

Table 2.6. Primers for the qPCR amplification of mitochondrial MT-ND5 and nuclear β-Actin genes used for the determination of mtDNA copy number in mouse tissues. Primers from IDT.

All DNA standards were measured in duplicate and controls and DNA samples in triplicate on a CFX96 Touch™ Real-Time PCR detection system (Bio-Rad). The qPCR conditions consisted of an initial denaturation at 95°C for three minutes; followed by 39 cycles of: denaturation at 95°C for 10 seconds, followed by annealing and extension at 58°C for one minute.

Gene	Fluorophore	Quencher	Probe Sequence (5'-3')
MT-ND5	HEX	BHQ_1	ACACCACCACATCAATCAAATTCTCCTTCA
β-actin	FAM	BHQ_1	ATTGCCTTTCTGACTAGGTG

Table 2.7. Taqman™ probes for the duplex qPCR assay. MT-ND5 gene was labelled with fluorescent HEX dye. β-Actin was labelled with fluorescent FAM dye. Probes synthesised by Integrated DNA Technologies.

Mitochondrial DNA copy number was determined as described in Section 2.5.7, in this case for mouse *ND5* and *β-actin* were used instead of *ND1* and *B2M* in Equation 2.2.

2.7 Immunofluorescence

2.7.1 Cryosectioning and microtome sectioning

Skeletal muscle sections of 10 µm thickness were cut onto glass slides using the Cryo-star HM 560M cryostat which was maintained at -20°C. Skeletal muscle sections were left to air dry at room temperature for one hour before storing at -80°C until required for further use. After immunofluorescence staining, skeletal muscle sections were stored at -20°C.

Formalin-fixed paraffin-embedded (FFPE) colon blocks were sectioned at 4 µm onto glass slides using a microtome. FFPE colon slides were stored in the fridge at 4°C. After dewaxing and immunofluorescence staining, FFPE colon slides were kept at -20°C.

A 5X TBST solution was freshly prepared on the same day before the immunofluorescence protocols began, composed of 2 L of dH_2O, 121 g of Trizma® base (Sigma-Aldrich), 90 g NaCl (Sigma-Aldrich), 5 ml of Tween20 (Sigma-Aldrich) and pH adjusted to 7.6. A 1:5 dilution was performed to obtain 1X TBST working buffer.

2.7.2 Quadruple immunofluorescence for mouse skeletal muscle

Sections cut 10 µm thick were removed from the -80°C freezer and allowed to air dry for one hour before encircling each section using a hydrophobic pen. Sections were fixed in 10% formalin for ten minutes at room temperature in the fume hood followed by three five minute washes with 1X TBST. Sections were permeabilized in a gradient of freshly made methanol; 70% for ten minutes, 95% for ten minutes, 100% for twenty minutes, 95% for ten minutes and 70% for ten minutes before another three five minute washes with 1X TBST. Sections were protein blocked for one hour at room temperature with 10% normal goat serum (diluted in 1X TBST). Slides were

washed in 1X TBST for five minutes while M.O.M™ (mouse on mouse) working solutions were prepared. The M.O.M™ (Vector® Laboratories) Immunodetection kit was used to localize mouse primary antibodies on mouse tissues and reduce background staining caused by the presence of endogenous mouse IgG in the tissue section. The M.O.M™ Mouse IgG Blocking Reagent was prepared by adding two drops of stock solution to every 2.5 ml of 1X TBST. The M.O.M™ diluent was prepared by adding 600 µl of M.O.M™ Protein Concentrate stock solution to every 7.5 ml of 1X TBST. Sections were incubated for one hour at room temperature in 100 µl of the working solution of M.O.M™ Mouse IgG Blocking Reagent prepared as described. After that, a five minute wash with 1X TBST was performed before incubating the slides for five minutes at room temperature in 100 µl of the working solution of M.O.M™ diluent prepared as described. Slides were then washed for five minutes with 1X TBST. Approximately 100 µl of primary antibody cocktail diluted in M.O.M™ diluent was then applied to the OXPHOS sections from each sample and a no primary control (NPC) cocktail consisting of only laminin (muscle fibre boundary marker) antibody with M.O.M™ diluent was applied to the corresponding NPC sections. Primary antibody concentrations can be found at Table 2.8. Covered sections were incubated in a humidified chamber at 4°C overnight. The following day, slides were washed for two ten minute washes in 1X TBST on a shaking platform at 70 rpm. Approximately 100 µl of the secondary antibody cocktail was applied to all the sections, NPC and OXPHOS, and incubated in a humidified and dark chamber at 4°C for two hours. Secondary antibody concentrations can be found at Table 2.8. Sections were washed for two ten minute washes in 1X TBST on a shaking platform at 70 rpm. Sections were covered with approximately 100 µl of streptavidin conjugated secondary antibody (Alexa647) and incubated in a humidified and dark chamber for two hours at 4°C. Sections were washed for two ten minute washes in 1X TBST on a shaking platform at 70 rpm. Sections were then mounted in ProLong® Gold Antifade Mountant (ThermoFisher), left to air dry overnight and stored in the -20°C freezer.

Antibody	Company (Product number)	Dilution
Primary antibodies		
Rabbit anti-Laminin (polyclonal) (IgG)	Abcam (ab11575)	1:50
Mouse anti-MTCO1 (IgG2a)	Abcam (ab14705)	1:100
Mouse anti-NDUFB8 (IgG1)	Abcam (ab110242)	1:100
Mouse anti-VDAC1 (IgG2b)	Abcam (ab14734)	1:100
Secondary antibodies		
Anti-Rabbit Alexa Fluor 405	ThermoFisher Scientific (A-31556)	1:100
Anti-Mouse IgG2a Alexa Fluor 488	ThermoFisher Scientific (A-21131)	1:200
Anti-Mouse IgG2b Alexa Fluor 546	ThermoFisher Scientific (A-21143)	1:200
Anti-Mouse IgG1 biotin-XX	ThermoFisher Scientific (A10519)	1:200
Streptavidin Alexa Fluor 647	ThermoFisher Scientific (S32357)	1:100

Table 2.8. Primary and secondary antibodies used for quadruple immunofluorescence in mouse skeletal muscle sections. Information regarding dilution factor and manufacturer details are included.

2.7.3 Fluorescence microscopy for mouse skeletal muscle

Fluorescent images were captured at 20x magnification using the Celldiscoverer 7 widefield fluorescence microscope (ZEISS) containing filter cubes for the following wavelengths: 405, 488, 546 and 647nm. ZEN blue software was used to capture images. Exposure times were set for each channel to reduce background fluorescence and avoid over exposure before starting the image acquisition. Full skeletal muscle OXPHOS and NPC sections were scanned and tiled using the channel 405, laminin, as a reference. Tiled images were stitched and saved as a .czi file for image analysis. Snaps at 20x magnification were also taken for illustrative examples for publication.

Mean fluorescent intensities were quantified for each channel using an in-house analysis software coded for by MatLab 2015a for skeletal muscle fibres. Membrane marker laminin (405nm channel) was used to isolate individual fibres automatically. Any unwanted areas including folded tissue, fibres containing freezing artifacts or those over background were removed manually. The mean optical density (OD) for the 488, 546 and 649 channels was automatically measured in each individual fibre.

2.7.4 Quadruple immunofluorescence for mouse colon

FFPE sections cut 4 µM thick were incubated in a 37°C oven for five days. Slides were labelled accordingly and incubated in a 60°C oven for 45 minutes. Antigen retrieval buffer was prepared (EDTA pH 8.0, 0.416g per 500 ml dH_2O). Slides were deparaffinised and rehydrated through an alcohol series; 100% EtOH 1 (5 minutes), 100% EtOH 2 (5 minutes), 95% EtOH (5 minutes), 70% EtOH (5 minutes) and placed in dH_2O for 5 minutes. Antigen retrieval was carried out using a pressure cooker for 40 minutes. Sections were transferred to dH_2O quickly to prevent the sections from drying before three five minute washes in 1X TBST. Each section was encircled using a hydrophobic pen. Sections were blocked with 10% NGS in 1X TBST for one hour at room temperature. About 100 µl of primary antibody cocktail was then applied to the OXPHOS sections from each sample and 10% NGS was applied to the corresponding NPC sections. Primary antibody concentrations can be found at Table 2.9. Covered sections were incubated in a humidified chamber at 4°C overnight.

Antibody	Company (Product number)	Dilution
Primary antibodies		
Rabbit anti-TOMM20 (IgG)	Abcam (ab186734)	1:100
Mouse anti-ATPB (IgG1)	Abcam (ab14730)	1:100
Mouse anti-MTCO1 (IgG2a)	Abcam (ab14705)	1:50
Mouse anti-UQCRFS1 (IgG2b)	Abcam (ab14746)	1:100
Mouse anti-NDUFB8 (IgG1)	Abcam (ab110242)	1:50
Secondary antibodies		
Anti-Rabbit IgG Alexa Fluor 488	ThermoFisher Scientific (A-11008)	1:200
Anti-Mouse IgG1 Alexa Fluor 647	ThermoFisher Scientific (A-21240)	1:200
Anti-Mouse IgG2a Alexa Fluor 546	ThermoFisher Scientific (A-21133)	1:200
Anti-Mouse IgG1 biotin-XX	ThermoFisher Scientific (A10519)	1:200
Streptavidin Alexa Fluor 647	ThermoFisher Scientific (S32357)	1:200
Anti-Mouse IgG2b Alexa Fluor 546	ThermoFisher Scientific (A-21143)	1:200
Hoechst 33342	ThermoFisher Scientific (H3570)	1:1000

Table 2.9. Primary and secondary antibodies used for quadruple immunofluorescence in mouse colon sections. Information regarding dilution factor and manufacturer details are included.

The following day, sections were washed for two ten minute washes in 1X TBST on a shaking platform at 70 rpm. If slides were stained for complex I and III then a biotin labelled secondary antibody diluted in 10% NGS was applied and sections incubated for two hours at room temperature. Sections were washed for two ten minute washes in 1X TBST. About 100 µl of the secondary antibody cocktail was applied to all the sections, NPC and OXPHOS, and incubated at 4°C for two hours. Secondary antibody concentrations can be found at Table 2.9. Sections were washed for two ten minute washes in 1X TBST. Hoechst was added to all the sections as a nuclear counterstain and incubated in the dark at room temperature for 15 minutes. Sections were washed for two ten minute washes in 1X TBST. Sections were then mounted in ProLong® Gold Antifade Mountant (ThermoFisher), left to air dry overnight and stored in the -20°C freezer.

2.7.5 Confocal microscopy for mouse colon

Images were captured using the Nikon A1 upright confocal microscope containing filters for the following wavelengths: 405, 488, 546 and 647nm. Nikon NIS-Elements software was used to capture images. For the NPC sections, one image was captured using the 20x objective and for the OXPHOS sections, five representative images across the whole section were captured using the 20x objective.

Fluorescence in the 405nm channel was used to define the nuclear boundary of the colonic crypts and thus to identify them during analysis. ImageJ Fiji software (Schindelin *et al.*, 2012) was used to manually circle individual colonic crypts and determine the mean fluorescence intensity of each channel within a 20x image.

2.7.6 Quantitative immunofluorescence

Quadruple immunofluorescence data generated from skeletal muscle fibres and colonic crypts was analysed using an R script written by Dr John Grady (Newcastle University). Values for each channel were corrected for non-specific background by subtracting the OD in the NPC from those generated from the OXPHOS labelled section. Values obtained were log transformed. Z-scores were generated for each channel, using the mitochondrial mass marker levels of VDAC (for fibres) or TOMM20 (for colonic crypts) to normalise the values.

Fibres and colonic crypts were classified as normal (z>-3), intermediate positive (z from -3 to -4.5), intermediate negative (z from -4.5 to -6) or negative/deficient (z<-6) for each protein i.e., complex I, III, IV and V for colonic crypts, and complex I and IV for fibres. Fibres (VDAC) and colonic crypts (TOMM20) were also classified by levels of mitochondrial mass markers as very low, low, normal, high or very high. Z-plots were then produced. This protocol has been validated for skeletal muscle by members of our lab (Rocha *et al.*, 2015).

2.8 Laser microdissection of single cells

Individual cells were captured by laser microdissection using a Zeiss Laser Capture Microdissection microscope with Palm Robo v4.6 using the Closecut + AutoLPC function for glass slides. Cut settings were as follows: energy = 46 and focus = 74 and the LPC settings were: energy = 15 and delta = 5. Two 0.2 ml eppendorfs were inserted in the TubeCollector and 15 µl of lysis buffer was added to each cap. Eppendorfs were kept on ice, prior to being quickly centrifuged to bring the tube contents to the bottom before incubating.

2.8.1 Single cell lysis buffer

Lysis buffer was made up of 0.5 M Tris-Hcl, 0.5% Tween 20 and 1% Proteinase K immediately before the laser microdissection experiment and kept on ice. Captured cells in 15 µl of lysis buffer were quickly centrifuged and incubated at 55°C for 16 hours (Liu, 2010), followed by 10 minutes at 95°C. Lysates were stored at -20°C.

2.9 Mitochondrial DNA enrichment for Next Generation Sequencing

The entire mitochondrial genome was enriched before being deep-sequenced using Illumina MiSeq. Two overlapping primer sets were used to amplify the mtDNA by long-range PCR, in both human and mouse mtDNA.

2.9.1 Long-Range PCR and agarose gel electrophoresis

Human mitochondrial DNA was enriched using long-range PCR (LR-PCR). Two overlapping amplicons covering the entire human mtDNA were amplified using two primer sets as previously described by members of our lab (Coxhead *et al.*, 2016). Long-range PCR reactions were performed in a 24 µl master mix containing nuclease-free H_2O, 1X Takara PrimeSTAR GXL Buffer (Mg^{2+} plus), 0.2 mM dNTP Mixture, forward and reverse primers (0.2 µM each), 0.625 U Takara PrimeSTAR GXL DNA Polymerase (Takara Bio Company) and 1 µl of DNA sample. Reactions were run on an Applied Biosystems® Veriti® 96 well thermal cycler (Thermo Fisher Scientific).

PCR conditions consisted of an initial denaturation at 94°C for one minute, followed by 35 cycles of denaturation at 98°C for 10 seconds, annealing at 60°C for 15 seconds and extension at 68°C for 10 minutes, and one with a final extension step at 72°C for 10 minutes. LR-PCR primer sequences can be found in Table 2.10.

Fragment	Amplicon size (bp)	Forward Primer Sequence (5'-3')	Reverse Primer Sequence (5'-3')
1	9932	CCCTCTCTCCTACTCCTG	CAGGTGGTCAAGTATTTATGG
2	9066	CATCTTGCCCTTCATTATTGC	GGCAGGATAGTTCAGACG

Table 2.10. Forward and reverse primer sequences and product sizes covering the entire human mitochondrial genome for enrichment prior to next generation sequencing. Primers from IDT.

Fragment 1 spanned from position m.6222 to m.16133 and fragment 2 from m.15295 and m.7773, mapped in Figure 2.3.

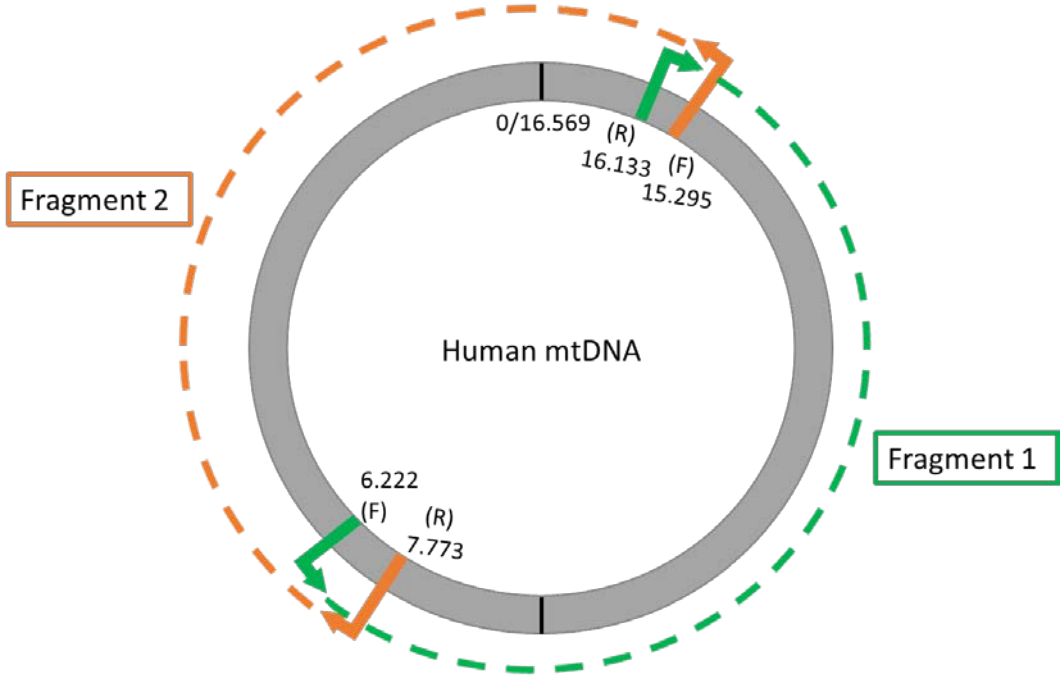

Figure 2.3. Schematic of the human mitochondrial genome, mapped with the two overlapping fragments used for amplification. Numbers indicate the primer base pair positions. (F) indicates binding position for the forward primer and (R) for reverse.

Long-range PCR reactions for mouse mtDNA amplicons were performed as described above for human. For mouse mtDNA, PCR conditions consisted of an initial denaturation at 98°C for 30 seconds, followed by 35 cycles of denaturation at 98°C for 30 seconds, annealing at 54°C (fragment 1) or 50°C (fragment 2) for 30 seconds and extension at 68°C for 12 minutes, and one with a final extension step at 72°C for 10 minutes.

Two sets of overlapping primers were used to cover the entire mouse mitochondrial genome using LR-PCR. Mouse LR-PCR primer sequences can be found in Table 2.11.

Fragment	Amplicon size (bp)	Forward Primer Sequence (5'-3')	Reverse Primer Sequence (5'-3')
1	9109	GAAAGCGTTCAAGCTCAAC	CATGAAGCGTCTAAGGTGTG
2	8825	CCATCTTAGTTTTCGCAGC	ACTTTGACTTGTAAGTCTAGG

Table 2.11. Primer sequences and product sizes for the LR-PCR amplification of mouse mitochondrial genome used for next generation sequencing. Primers from IDT.

Fragment 1 spanned from position m.1628 to m.10737 and fragment 2 from m.10059-m.2315, mapped in Figure 2.4.

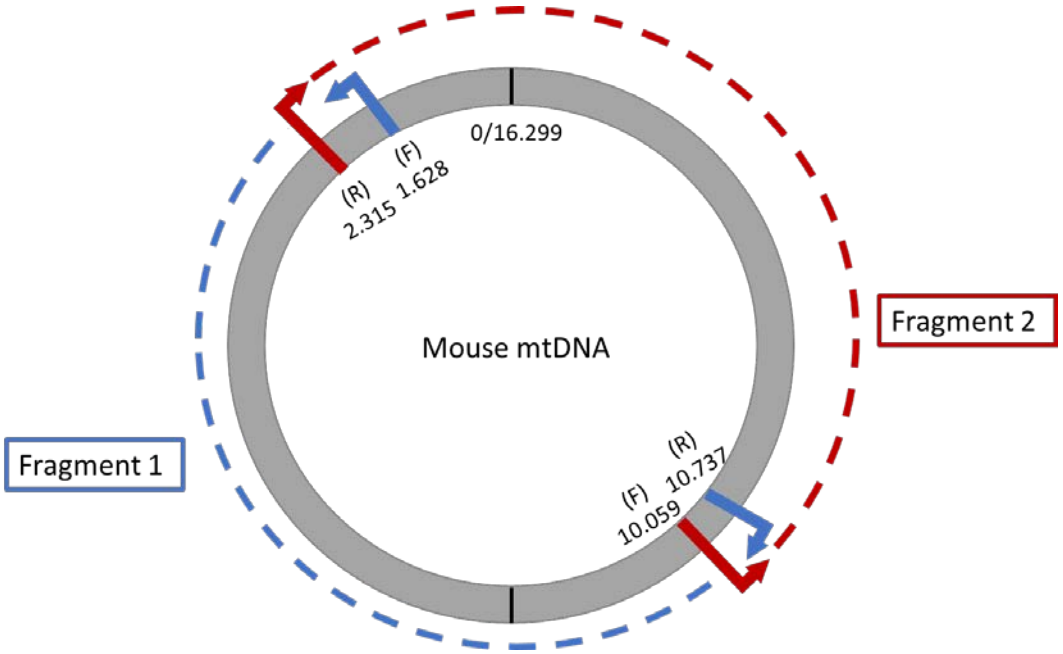

Figure 2.4. Schematic of the mouse mitochondrial genome, mapped with the two overlapping fragments used for amplification. Numbers indicate the primer base pair positions. (F) indicates binding position for the forward primer and (R) for the reverse primer.

Products were analysed on a 0.8% agarose gel containing SYBR Safe DNA Gel Stain (Thermo Fisher Scientific) at 55V for 1h in 1X TAE buffer. 5 µl of Orange G loading buffer (50% glycerol, Orange G powder (Sigma Aldrich Company Ltd) and

50% water) was mixed with 5 µl of PCR product. GeneRuler 1kb Plus DNA ladder SM1333 (Thermo Fisher Scientific) was loaded in the first lane.

2.10 Next Generation Sequencing (NGS) using Illumina MiSeq platform

2.10.1 Rationale for choosing NGS for mitochondrial DNA

NGS, or massively parallel sequencing, has become a potent and prevailing tool in research with a great potential for the study of mtDNA mutations. MtDNA mutations present at a low heteroplasmy level (<~20%) cannot be detected by conventional sequencing technologies such as Sanger Sequencing. More powerful instruments are necessary for the study of low-level mtDNA heteroplasmy. Technologies with high depth and breadth of coverage enable the investigation of very low-level variants (down to 2% heteroplasmy level or lower), whilst providing coverage of the entire mtDNA genome.

Illumina GA/MiSeq platform is a high throughput sequencing technology, and has proved cost-efficient for sequencing large numbers of small genomes such as mtDNA. The Illumina platforms have sequencing error rates that compare favourably with most other platforms.

2.10.2 Product purification and pooling

After enrichment of mtDNA, the LR-PCR products were purified using the AgenCourt AMPure XP bead technology (Beckman Coulter). This system utilizes paramagnetic bead technology for high-throughput purification of PCR amplicons by binding 100 bp and larger amplicons to the beads. Using a washing procedure, excess reaction components and contaminants can be removed. AMPure XP beads were added to the samples in a ratio of 1.8 µl bead:1 µl PCR product, pipette mixed thoroughly and incubated for five minutes to allow PCR products to bind to the magnetic beads. The PCR plate was then placed onto the Magnet Plate (96S Super Magnet Plate, ALPAQUA) for two minutes to separate beads from the solution. The cleared solution was aspirated from the plate without disturbing the brown bead ring, which was then washed twice with freshly made 70% ethanol. The bead ring was left to air dry a few minutes to ensure all traces of ethanol were removed. After removal from the magnet

plate, beads were eluted into 30 µl of nuclease-free H_2O, pipette mixed thoroughly and incubated at room temperature for one minute. The PCR plate was then placed back onto the Magnet Plate for one minute to separate beads from the solution and the eluate was transferred to a new PCR plate. The concentration of the samples was measured using the Qubit™ dsDNA Broad Range Assay kit (ThermoFisher Scientific) on the Qubit 3.0 Fluorometer as per manufacturer's guidelines.

MtDNA fragments originating from the same individual sample were then pooled together to a concentration of 10 ng/µl per sample. Two subsequent dilutions were performed on the same day as the library preparation began, to get to a final concentration of 0.2 ng/µl per sample.

2.10.3 Library preparation

The library preparation was performed using the Nextera XT DNA Library Preparation Kit (Illumina Inc., CA, USA) in order to "tagment", amplify, normalise and pool the samples. Multiplexed pools were sequenced using Illumina MiSeq v3.0 sequencing platform in 250 bp paired-end reads. To avoid run-specific amplification variation, wild-type and WtN+ mouse samples were randomly mixed in every sequencing run.

2.11 Bioinformatics analysis pipeline

Paired-end fastq files were obtained from the MiSeq platform. Bioinformatic sequence analysis and variant calling is described as follows. All bioinformatics steps were performed as part of an in-house custom pipeline scripted by Fiona Robertson. The post-run fastq files of each sample were first assessed for quality via FASTQC v. 0.11.5 (Andrews, 2010), before all duplicate reads were removed by Fastuniq v. 1.1 (Xu *et al.*, 2012). Thereupon, de-duplicated read sets were aligned to the selected genome using BWA, v. 0.7.15, invoking the mem module (Li and Durbin, 2009), against genome versions GRCh37 (GCA_000001405.1, human), or mm10 (GCA_000001635.2, mouse). Sorting and indexing of alignments was performed using Samtools v.1.3.1 (Li *et al.*, 2009). Variant calling was preformed using VarScan v.2.3.7 (Koboldt *et al.*, 2012) and then annotated via the ENSEMBL VEP tool. v90 (Zerbino *et al.*, 2018), with merged cache files:

homo_sapiens_merged_vep_90_GRCh37 and mus_musculus_merged_vep_90_GRCm38, with inclusion of the respective dbSNP databases - sourced: NCBI (Sherry *et al.*, 2001). Python scripts were used to extract coverage data. Further custom scripts are available (upon request) for downstream filtering of variant annotation data to ease further analysis and visualisation.

2.12 Post-bioinformatic quality control

Post-bioinformatic quality control was performed in order to ensure high-quality comparisons. Samples were removed if coverage was <99% at a minimal depth of 1000x (further explained for each results Chapter). Heteroplasmic variants were defined as >2% but <98%. Homoplasmic variants were defined as >98%.

2.13 Statistical Analyses

Graphs were produced in Prism v5.04 and all statistical analysis were performed in IBM SPSS Statistics v23. Specific tests used are described in the methods and results chapters. *P*-values <0.05 were considered significant.

Chapter 3. Investigating the relationship between mitochondrial DNA damage in human brain and HIV infection

3.1 Introduction

Patients with long-term treated HIV exhibit features of premature and accelerated biological ageing. Mitochondrial dysfunction and mtDNA damage are also well-recognised in people living with HIV (PLWH). Largely these phenomena are considered to be complications of antiretroviral therapy (ART), especially with certain drugs of the nucleoside analogue reverse transcriptase inhibitor (NRTI) class. Whilst NRTIs principally inhibit HIV reverse transcriptase, they may also inhibit the mtDNA polymerase, pol γ, leading to mtDNA depletion (Arnaudo *et al.*, 1991; Casademont *et al.*, 1996; Dalakas *et al.*, 2001; Lim and Copeland, 2001; Cote *et al.*, 2002; Walker *et al.*, 2004b; Buffet *et al.*, 2005; Haugaard *et al.*, 2005; Cherry *et al.*, 2006). More recently, it has been demonstrated, by our group and others, that NRTI therapy may also result in an increase in somatic mtDNA mutations in several tissues including skeletal muscle, blood, and the renal tract (Martin *et al.*, 2003; Lehmann *et al.*, 2011; Payne *et al.*, 2011; Jitratkosol *et al.*, 2012; Samuels *et al.*, 2017). In addition, there is some limited evidence that HIV per se may also reduce mtDNA content, at least in lymphocytes (Miura *et al.*, 2003).

Neurocognitive impairment remains prevalent in PLWH in the mild forms of HIV-associated neurocognitive disorder (HAND). NRTI-induced neurotoxicity in the brain was reported in a few studies in mice (Zhang *et al.*, 2014; Zhang *et al.*, 2015). However to this date, only a single study has looked at mtDNA in human brain in HIV infection but within the context of methamphetamine use, showing association between mitochondrial injury, HIV DNA levels and neurocognitive function (Var *et al.*, 2016).

It is therefore plausible that HIV infection and/or ART is associated with an excess of mtDNA damage in the brain and therefore with HAND.

3.2 Experimental Aims

This study aimed to determine whether antiretroviral treated HIV-infected persons have evidence of mtDNA damage in the brain, and whether this potentially contributes to neurocognitive impairment.

3.3 Methodology

3.3.1 Cohort of brain samples

Snap-frozen post-mortem frontal grey matter samples were obtained from the National NeuroAIDS Tissue Consortium (NNTC) (https://nntc.org/), the Edinburgh Brain and Tissue Bank (www.ed.ac.uk/clinical-brain-sciences/research/edinburgh-brain-and-tissue-bank), and the Newcastle Brain Tissue Resource (NBTR) (https://nbtr.ncl.ac.uk/). Frontal cortex brain tissue was processed as previously described in Section 2.3. Both HIV positive cases and HIV negative controls were studied. In light of the known associations between mtDNA changes and age, controls of comparable age range were specifically included to the cases, but also older controls to determine whether the effects of HIV/ART on brain mtDNA mirrored those seen in normal ageing. Donors with other (non-HIV associated) brain pathology and with opportunistic infections of the brain were excluded. Maximum time to autopsy was 24h. Clinical and neurocognitive testing data were taken from the last antemortem study visit (maximum 6 months antemortem). Brain bank donors had given informed consent for retention of their tissue for research purposes, and the present study was approved by local research ethics committee (ref. 17/NE/0015).

3.3.2 Real-time PCR for mtDNA copy number and common deletion assay

MtDNA content was expressed relative to cell content and was measured in triplicate by multiplex real-time qPCR amplification of mitochondrial gene *MT-ND1* and the nuclear-encoded housekeeping gene *B2M*. In addition to mtDNA quantification, proportional levels of the 4977 bp mtDNA ‘common deletion’ (CD) were expressed relative to mtDNA content, and measured by allele-specific qPCR as detailed in Section 2.5, where primers and probe sequences for this assay are also found.

Data for mtDNA copy number (CN) and CD levels were age-normalised by correcting for the regression coefficient for age in the HIV negative control group.

3.3.3 Next generation sequencing of human mitochondrial DNA

Whole human mtDNA was enriched using long-range PCR. Primer sequences and LR-PCR details found in Section 2.9.1.

MtDNA point variants were measured on an Illumina MiSeq platform as described in Section 2.10. Paired-end fastq files were obtained from the MiSeq platform. Bioinformatic sequence analysis and variant calling is described in Section 2.11. MtDNA point variants present at 2% to 98% heteroplasmy were reported.

3.3.4 Large-scale mtDNA deletions

Screening for large-scale mtDNA deletions was performed by LR-PCR in fragment 1 amplicon of the human mtDNA used for sequencing in Section 2.9.1.

3.3.5 Neurocognitive testing

Neurocognitive testing data used in the present study included the following parameters and were provided by Dr David Moore (HIV Neurobehavioral Research Program, University of California). Primary neurocognitive diagnosis ranged in four categories: neurocognitively normal, subclinical neuropsychological impairment (ANI), mild cognitive motor disorder (MCI) and HAD; in accordance to the “Frascati Criteria” classification (Antinori *et al.*, 2007). These HAND sub-classifications were extensively reviewed elsewhere (Table 3.1) (Clifford and Ances, 2013). Frascati criteria classifies HAND based on poor neurocognitive function in at least two cognitive domains and the degree of impairment of daily activities.

	Neurocognitive status	Functional Status
Asymptomatic Neurocognitive Impairment (ANI)	1 SD below mean, 2 cognitive domains	No Impairment in activities of daily living
Mild Neurocognitive Disorder (MND)	1 SD below mean, 2 cognitive domains	Impairment in activities of daily living
HIV Associated Dementia (HAD)	2 SD below mean, 2 cognitive domains	Marked impairment in activities of daily living

Table 3.1. Categories of HIV-associated neurocognitive disorder (HAND), Frascati criteria. Of note, for HAND diagnosis other etiology of dementia must be ruled out and confounding effect of substance use or psychiatric illness must be considered. Neurocognitive testing should include evaluating at least five domains including attention-information processing, language, abstraction-executive, complex perceptual motor skills, memory (including learning and recall) simple motor skills or sensory perceptual skills. Appropriate norms must be available to determine the number of domains in which performance is below 1 standard deviation (SD). Functional status is typically evaluated by self report but may be corroborated by a collateral source. No agreed upon measures exist for HAND criteria. Table and information taken from (Clifford and Ances, 2013).

Other neurocognitive outcome data were composite scores including Global T-Score, Global Deficit Score (GDS) and Abstraction Executive Domain Deficit Score. Global T-Score and Global Deficit Score were obtained from the same tests however the former showing normalised test scores and the latter categorised into deficit scores. The component tests of the cognitive batteries used are detailed in Appendix 10.6.

Abstraction executive functioning domain was specifically studied as this may best capture frontal lobe function and therefore maps to the anatomical location of the study samples.

The GDS approach is used to detect and classify HIV-associated neurocognitive disorders (Blackstone *et al.*, 2012). GDS is a continuous measure that takes into account the deficits across the neuropsychological tests by converting T-scores into deficit scores from 0 (no impairment) to 5 (severe impairment) and then averages them into a global deficit score (Table 3.2).

Descriptor	T scores	Deficit Score
Normal	≥ 40	0
Mild	39-35	1
Mild-to-Moderate	34-30	2
Moderate	29-25	3
Moderate-to-Severe	24-20	4
Severe	≤ 19	5

Table 3.2. Scores and descriptors for the global deficit score. A cut-off score of ≥ 0.5 is used to determine impairment on the GDS (Blackstone et al., 2012).

3.3.6 Statistical analysis

Statistical testing was performed using SPSS 24 (IBM). Log_{10} transformation of CD values were used to approximate a normal distribution and allow for parametric testing. Non-parametric testing (Spearman correlation) was used for analyses of mtDNA point variants.

3.4 Results

The study included a total of 90 donors (50 HIV positive, 40 HIV negative). Donor demographic and clinical characteristics are detailed in Table 3.3.

Variable	**HIV- controls**	**HIV+ cases**
Number of samples	N=40	N=50
Age at death, years (range)	66.1±18.3 (29-91)	49.2±9.6 (32-70)[a]
Gender (M/F)	28/12	40/7[a]
CD4 cell count, cells/µl (range)	-	143±193 (2-1043)
Log_{10} HIV RNA plasma viral load (range)	-	3.9±1.6 (1.6-6)
Number of patients on any ART at last assessment (yes/no)	-	(31/11)[b]
Number of patients ever on ART during disease duration (yes/no)	-	(39/3)[b]
Nadir CD4 cell count (range)	-	62±67 (0-257)
CD4/CD8 cell count (range)	-	0.25±0.4 (0.01-1.82)

Table 3.3. Demographic characteristics of HIV-uninfected controls and HIV+ cases used for the analysis. N is number. ART is antiretroviral therapy. Gender is displayed as the number of males/females. All other values are displayed as mean ± standard deviation. Range are (minimum – maximum) values. [a]Age at death and gender information only available for n=47 HIV+ cases. [b]ART information only available for n=42 HIV+ patients.

Detailed list of antiretroviral drug regimens for HIV patients, at time of death (considered time of last assessment) and for previous exposure, can be found in Appendix 10.7, together with a list of drug abbreviations.

3.4.1 Cellular mitochondrial DNA content

There was a borderline significant inverse correlation between mtDNA content and age at death in the combined group of cases and controls (r=-0.2, n=90, p=0.05). This association was however highly significant within the HIV-negative controls (r=-0.5, n=40, p=0.001), but not in HIV+ cases (r=-0.1, n=50, p=0.4) (Figure 3.1).

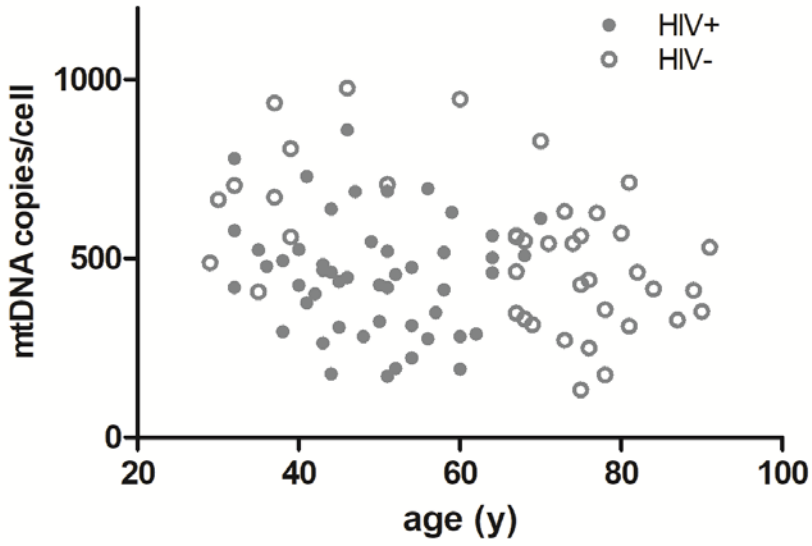

Figure 3.1. Mitochondrial DNA copy number levels against age at death for HIV positive cases and HIV negative controls. MtDNA content correlated significantly with age at death in controls but not in HIV+ cases. Every dot represents a sample. Y is for years.

Given the large literature linking changes in mtDNA with age, along with the strong effect observed here in our HIV- controls, all subsequent analyses of mtDNA content were corrected for age at death based on the data for HIV negative control subjects as described previously (regression coefficient, -5.512 mtDNA copies per year).

It was then determined whether HIV status independently affected mtDNA content. Decreased mtDNA content (age-corrected mtDNA genome copies per cell) was associated with positive HIV status (mean (SE); HIV+, 726 (24), n=47; HIV-, 887 (28), n=40; unpaired t-test, p<0.001; Figure 3.2).

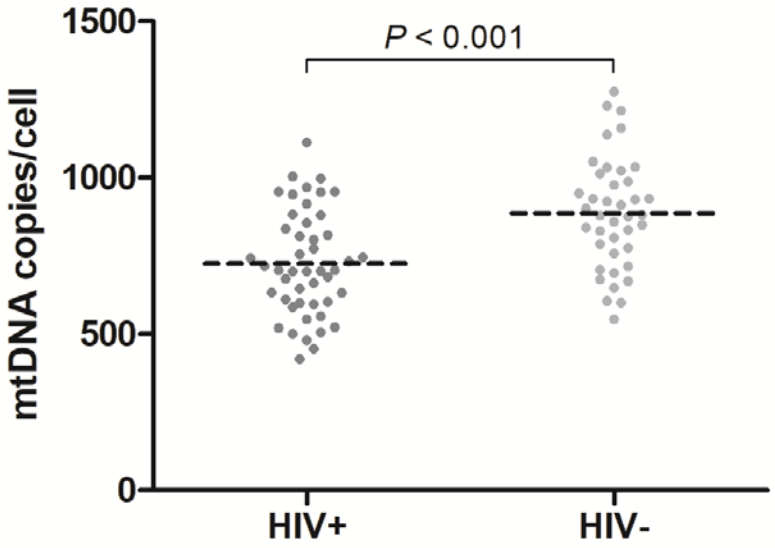

Figure 3.2. Mitochondrial DNA copy number levels (age-corrected) for HIV positive cases and HIV negative controls. HIV positive status was associated with lower mtDNA content. Every dot represents a sample. P is p-value. Dotted line at mean.

The effect of HIV clinical and treatment factors on mtDNA content amongst HIV positive cases was then investigated. There were no significant correlations between mtDNA content and immunological parameters or HIV viral load: current CD4 lymphocyte count (r=0.14, n=44, p=0.4; Figure 3.3A); current CD8 lymphocyte count (r=0.05, n=24, p=0.8; Figure 3.3B); $\log_{10}$ HIV-1 RNA plasma viral load (r=-0.22, n=44, p=0.14; Figure 3.3C); nadir CD4 lymphocyte count (r=0.16, n=24, p=0.5; Figure 3.3D); current CD4/CD8 ratio (r=-0.11, n=23, p=0.6; Figure 3.3E).

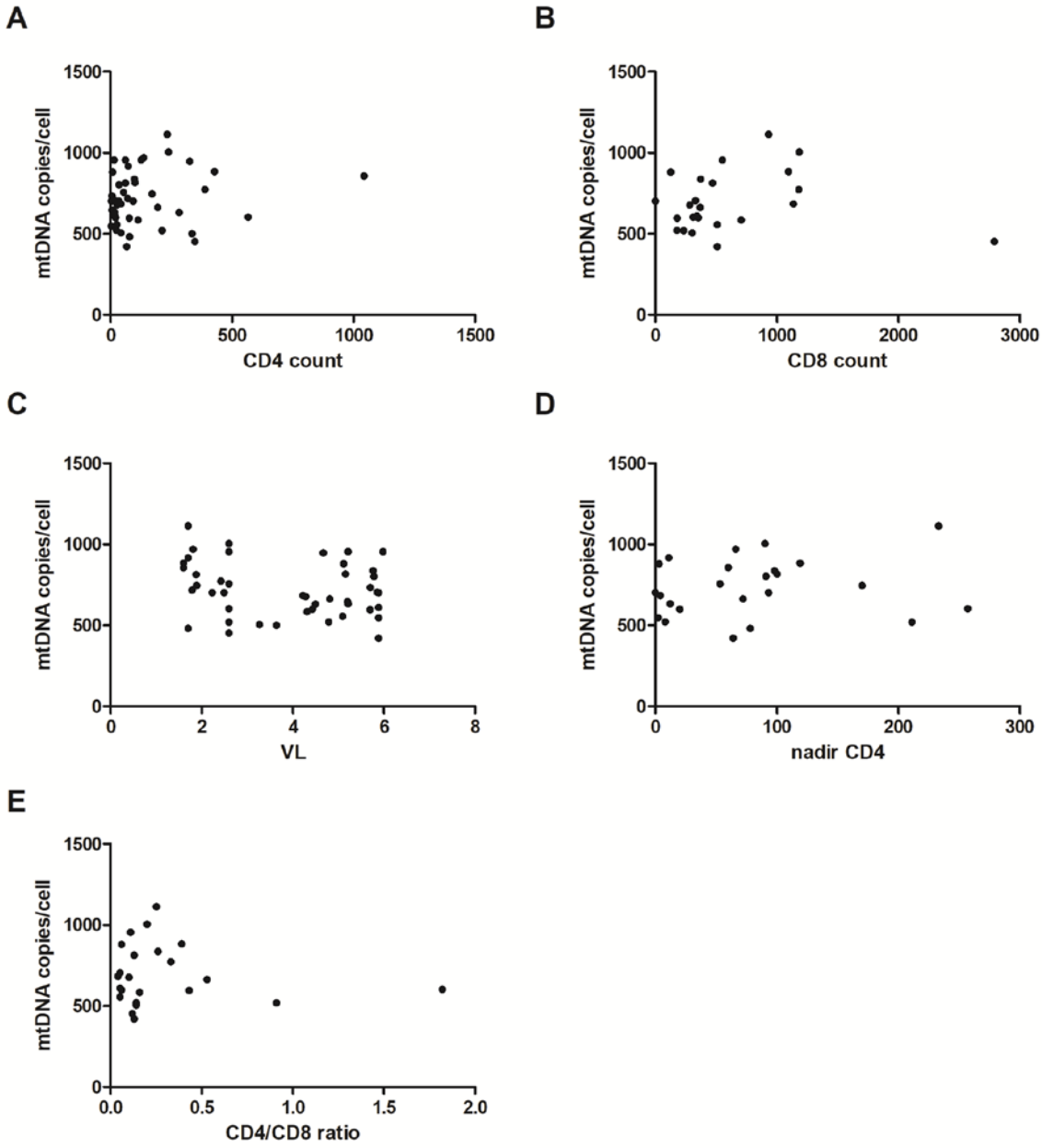

*Figure 3.3. Mitochondrial DNA copy number levels (age-corrected) against HIV immunological parameters for HIV positive cases. MtDNA content showed no significant correlation with CD4 cell count (**A**), CD8 cell count (**B**), log_{10} HIV-1 RNA plasma viral load (VL) (**C**), nadir CD4 (**D**) or CD4/CD8 cell ratio (**E**). Every dot represents a sample.*

Furthermore, there was no association between ART and mtDNA content, based either on current exposure to any ART at the time of last assessment (on ART, 722 (30), n=31; not on ART, 717 (52), n=11; p=0.9, Figure 3.4), or history of exposure to one or more of those NRTIs which most strongly inhibit the mitochondrial pol γ *in vitro*, that is, the di-deoxy-nucleoside analogues [d-drugs]: didanosine (ddI), zalcitabine (ddC), stavudine (d4T) (d-drug, 692 (35), n=23; no d-drug, 752 (40), n=17; p=0.27, Figure 3.5).

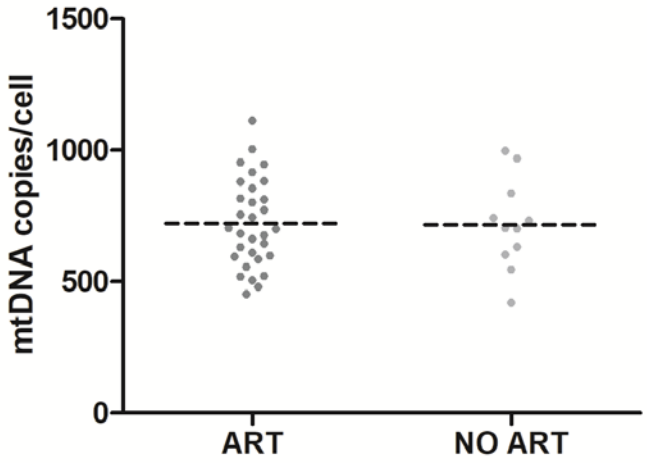

Figure 3.4. Mitochondrial DNA copy number levels (age-corrected) for HIV positive cases who were taking (ART) or not (NO ART) any antiretroviral medication at the time of their last assessment. MtDNA content levels were not significantly different regarding exposure to any ART or not. Every dot represents a sample. Dotted line at mean.

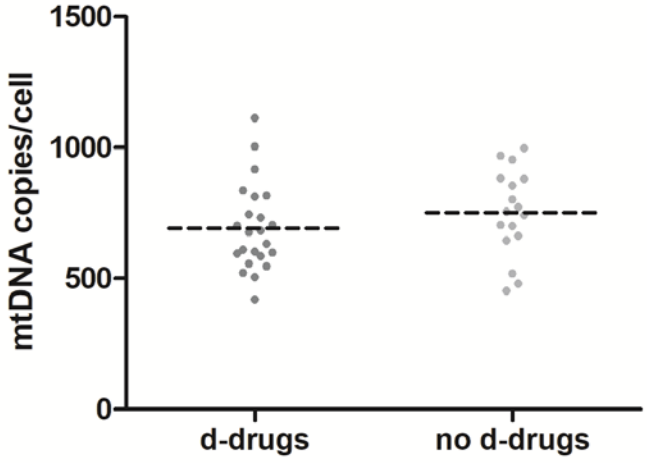

Figure 3.5. Mitochondrial DNA copy number levels (age-corrected) for HIV positive cases who took d-drugs or not (no d-drugs) at any point throughout their course of treatment. MtDNA content levels were not associated with exposure to d-drugs. D-drugs: ddI, ddC and d4T. Every dot represents a sample. Dotted line at mean.

Specific analysis of the individual d-drugs showed no significant association between mtDNA copy number and the d-drug exposure (ever exposed compared with never exposed) for ddI (ddI 694 (42), n=18; no ddI, 737 (33), n=22; p=0.4; Figure 3.6A), ddC use (ddC 774 (59), n=10; no ddC, 699 (29), n=30; p=0.2; Figure 3.6B) or d4T use (d4T 671 (35), n=21; no d4T, 769 (37), n=19; p=0.06; Figure 3.6C). Although it has relatively low potential of pol γ inhibition, zidovudine (AZT) is also considered to be mitochondrially toxic. AZT did not show a significant association between its use and mtDNA copy number (AZT, 743 (36), n=23; no AZT, 683 (38), n=17; p=0.3; Figure 3.6D).

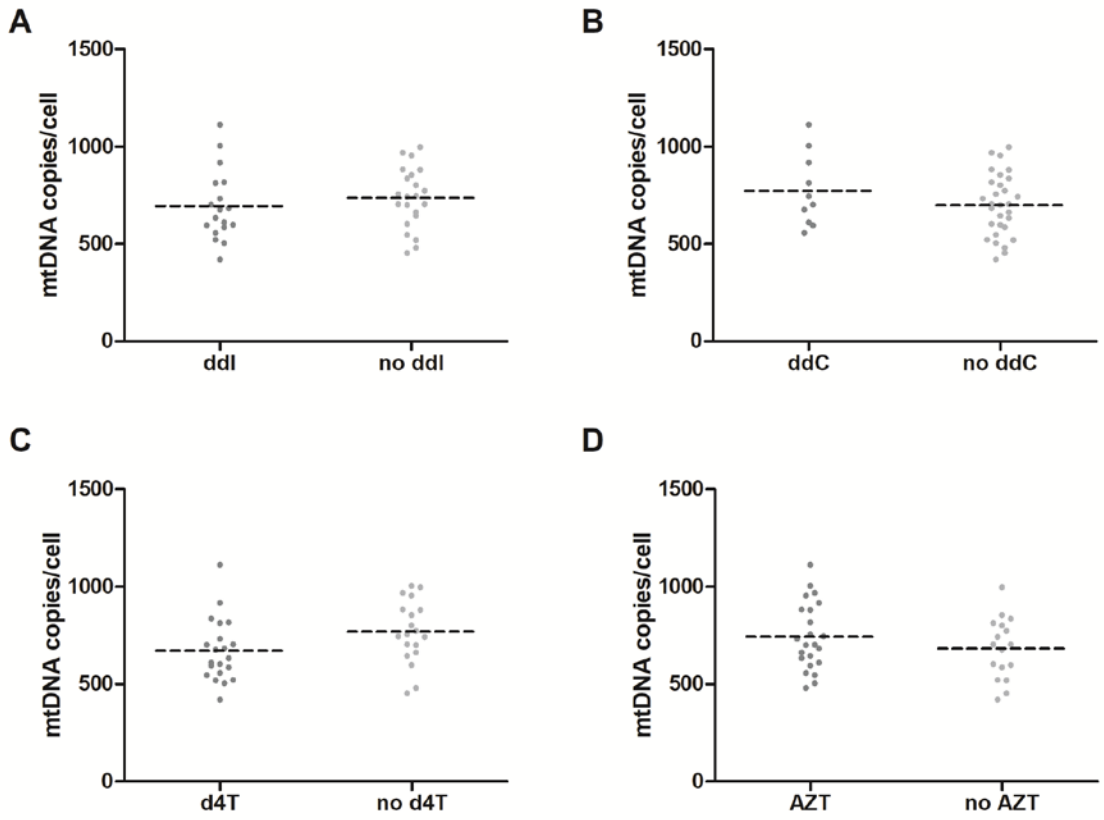

*Figure 3.6. Mitochondrial DNA copy number levels (age-corrected) for HIV positive cases who took specific antiretroviral drugs or not at any point throughout their course of treatment. MtDNA content levels were not associated with exposure to ddI (**A**), ddC (**B**), d4T (**C**) and AZT (**D**). Every dot represents a sample. Dotted line at mean.*

3.4.2 MtDNA large scale deletions and δ4977 common deletion levels

No large-scale mtDNA rearrangements were detectable by LR-PCR. Using the sensitive CD-specific qPCR assay, the total burden of mt.δ4977 deletion mutation was estimated at the whole-tissue level. MtDNA common deletion levels were significantly correlated with age at death in both HIV+ patients (r=0.3, n=50, p=0.04) and more strongly in uninfected controls (r=0.5, n=40, p=0.0005) (Figure 3.7).

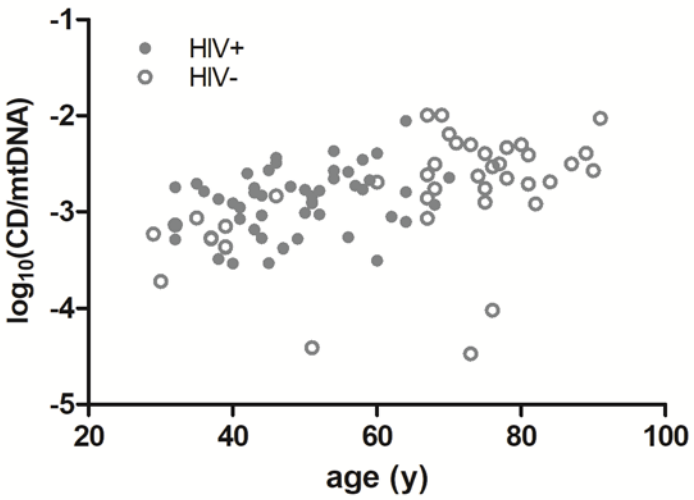

Figure 3.7. Mitochondrial DNA common deletion levels against age at death for HIV positive cases and HIV negative controls. Common deletion content showed a significant correlation with age at death in both HIV+ cases and controls. Every dot represents a sample. Log_{10} is a logarithmic scale for CD relative to mtDNA. Y is for years.

Again correcting for age at death based on data from HIV negative controls (regression coefficient, 0.0158 log_{10}CD/mtDNA per year), positive HIV status was independently associated with higher proportional levels of the CD (log_{10}CD, mean (SE); HIV+, -3.67 (0.05), n=47; HIV-, -3.86 (0.08), n=40; p=0.046; Figure 3.8).

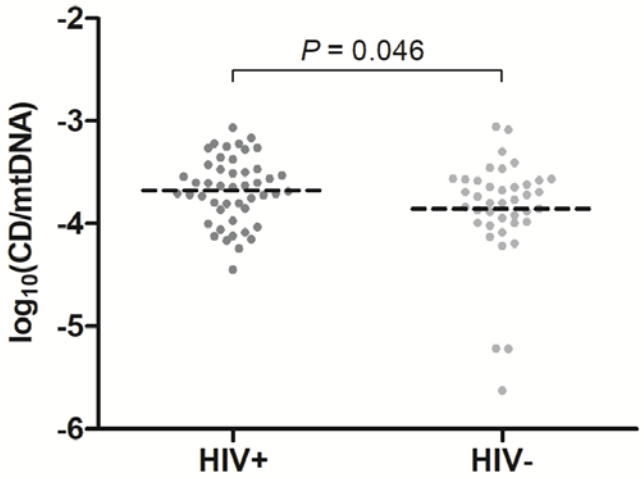

Figure 3.8. Mitochondrial DNA common deletion levels (age-corrected) for HIV positive cases and HIV negative controls. MtDNA CD levels were higher in HIV positive cases compared to HIV negative controls. Log_{10} is a logarithmic scale of 10. Every dot represents a sample. P is p-value. Dotted line at mean.

Amongst HIV positive cases, there were no significant correlations between mtDNA CD levels and immunological parameters or HIV viral load: current CD4 lymphocyte count (r=-0.13, n=44, p=0.4; Figure 3.9A); current CD8 lymphocyte count (r=0.13, n=24, p=0.6; Figure 3.9B); log_{10} HIV-1 RNA plasma viral load (r=-0.06, n=44, p=0.7; Figure 3.9C); nadir CD4 lymphocyte count (r=-0.05, n=24, p=0.8; Figure 3.9D); current CD4/CD8 ratio (r=0.05, n=23, p=0.8; Figure 3.9E).

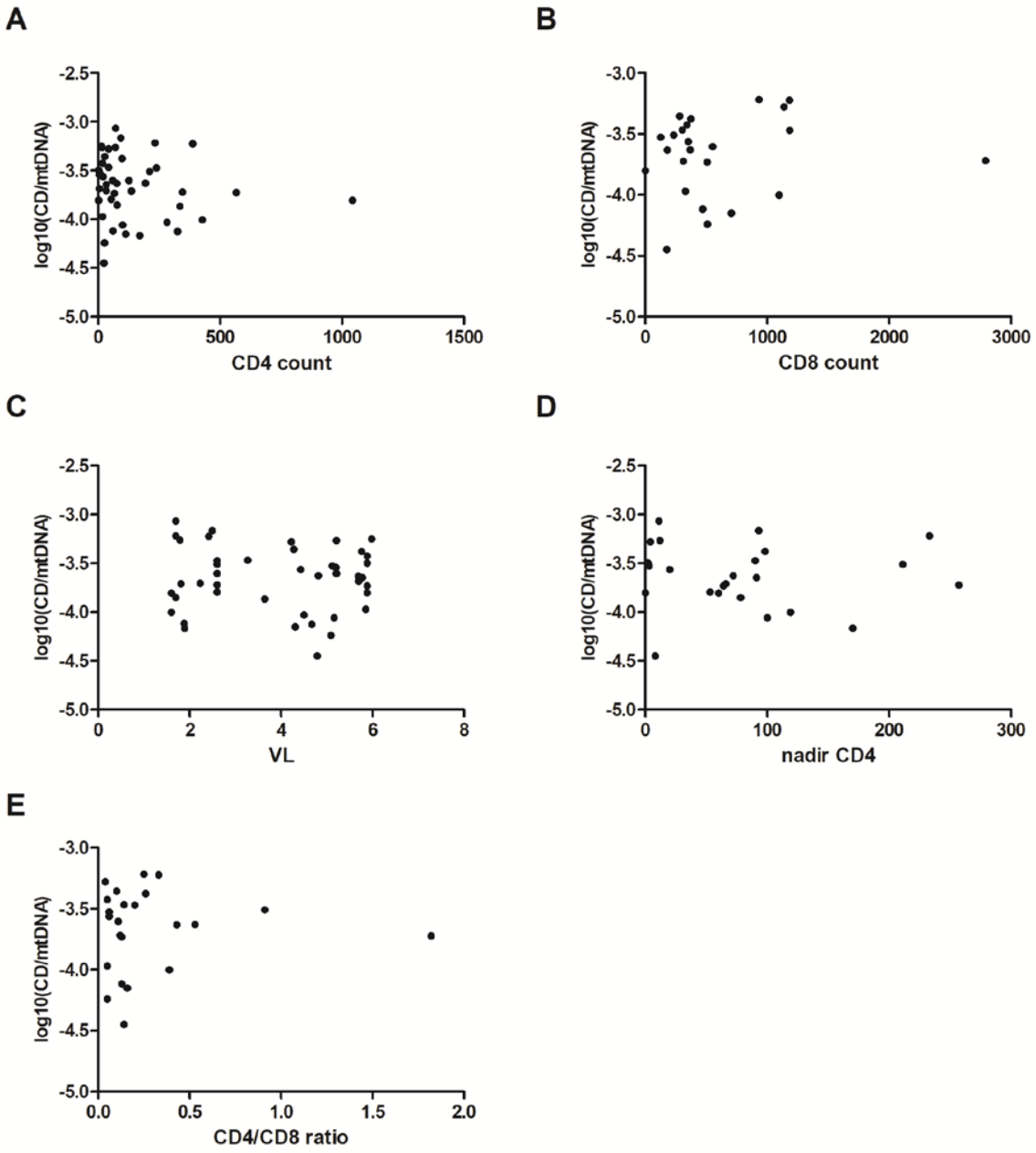

*Figure 3.9. Mitochondrial DNA common deletion levels (age-corrected) against HIV immunological parameters for HIV positive cases. Common deletion content showed no significant correlation with CD4 cell count (**A**), CD8 cell count (**B**), log_{10} HIV-1 RNA plasma viral load (VL) (**C**), nadir CD4 (**D**) or CD4/CD8 cell ratio (**E**). Every dot represents a sample.*

Furthermore, there was no association between ART and mtDNA CD levels, based either on current exposure to any ART (on ART, -3.70 (0.06), n=31; not on ART, -3.66 (0.07), n=11; p=0.7; Figure 3.10), or specific history of d-drug exposure as defined before (d-drugs, -3.68 (0.08), n=23; no d-drugs, -3.66 (0.06), n=17; p=0.8; Figure 3.11).

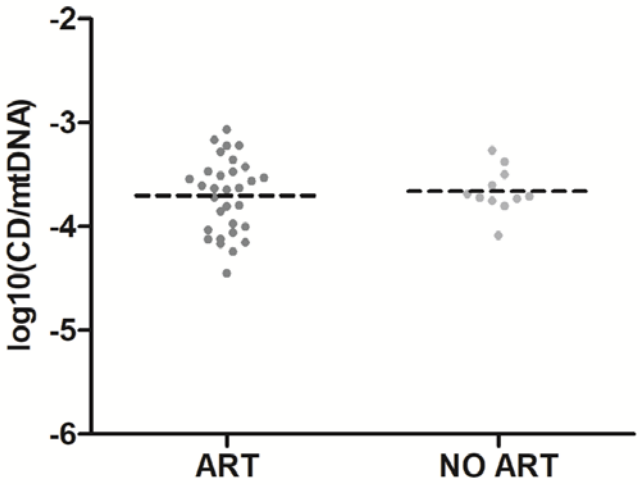

Figure 3.10. Mitochondrial DNA common deletion levels (age-corrected) for HIV positive cases who were taking (ART) or not (NO ART) any antiretroviral medication at the time of their last assessment. MtDNA CD levels were not significantly different regarding exposure to any ART or not. Every dot represents a sample. Dotted line at mean.

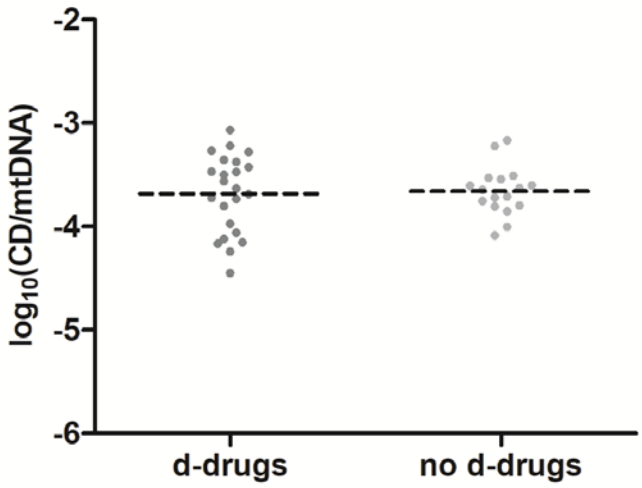

Figure 3.11. Mitochondrial DNA common deletion levels (age-corrected) for HIV positive cases who took d-drugs or not (no d-drugs) at any point throughout their course of treatment. MtDNA CD did not vary with d-drug exposure. Dotted line at mean.

Specific analysis of the individual d-drugs showed no significant association between mtDNA CD and the d-drug exposure (ever exposed compared with never exposed) for ddI (ddI -3.67 (0.09), n=18; no ddI, -3.68 (0.05), n=22; p=0.9; Figure 3.12A), ddC (ddC -3.65 (0.1), n=10; no ddC, -3.68 (0.05), n=30; p=0.8; Figure 3.12B) or d4T use (d4T -3.67 (0.08), n=21; no d4T, -3.68 (0.06), n=19; p=0.9; Figure 3.12C). AZT did not show a significant association between its use and mtDNA CD (AZT, -3.6 (0.07), n=23; no AZT, -3.75 (0.08), n=17; p=0.18) (Figure 3.12D).

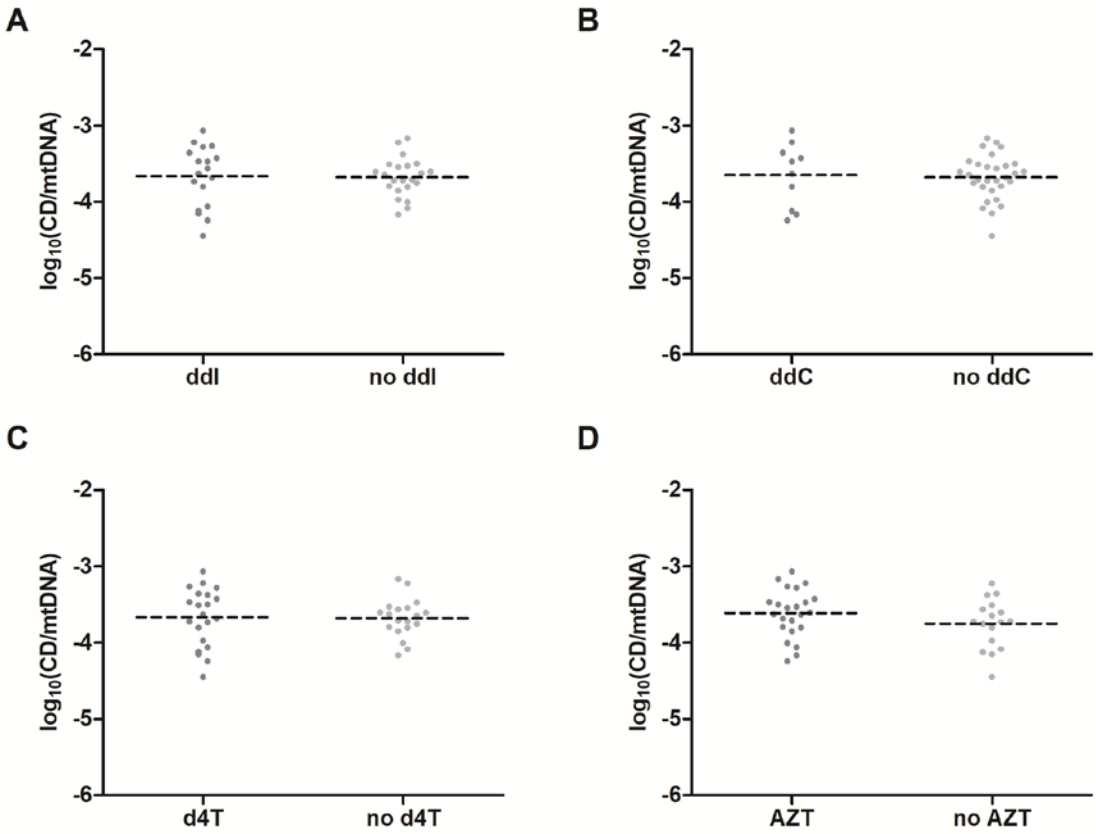

*Figure 3.12. Mitochondrial DNA common deletion levels (age-corrected) for HIV positive cases who took specific antiretroviral drugs or not at any point throughout their course of treatment. MtDNA CD levels were not associated with exposure to ddI (**A**), ddC (**B**), d4T (**C**) and AZT (**D**). Every dot represents a sample. Dotted line at mean.*

3.4.3 Neurocognitive impairment and mtDNA

The association between mtDNA content and neurocognitive impairment was investigated. Based on the categorical classification of NCI (normal, ANI, MCI, HAD) no association was seen (one-way ANOVA, p=0.33; Figure 3.13).

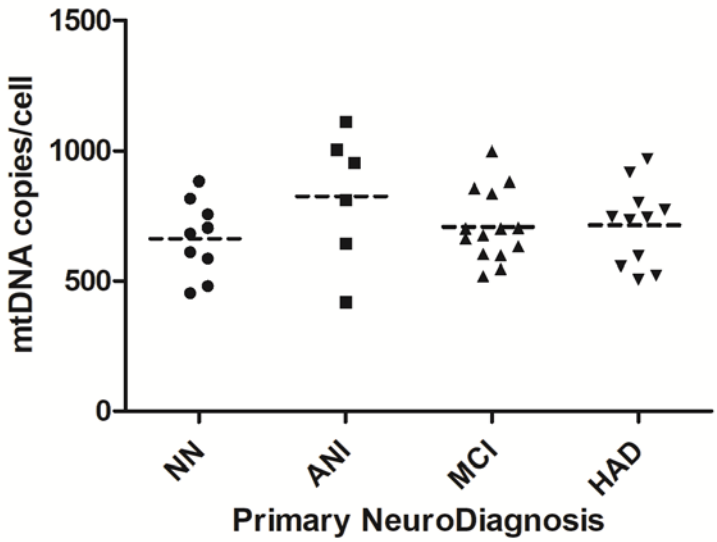

Figure 3.13. Mitochondrial DNA copy number levels (age-corrected) for HIV+ patients clustered in groups regarding their neurocognitive diagnosis (NN: neurocognitively normal; ANI: subclinical neuropsychological impairment; MCI: mild cognitive motor disorder; HAD: HIV-associated dementia). There was no difference between the groups in their mtDNA content.

This lack of association was also true of global T-score (r=-0.20, n=30, p=0.28; Figure 3.14A), and global deficit score (GDS; r=0.15, n=30, p=0.4; Figure 3.14B). In view of the anatomical site of tissue studied, the frontal cortex, executive function was also assessed. Here there was a trend towards association between deficit score for this cognitive domain and mtDNA content albeit not reaching statistical significance (r=0.31, n=33, p=0.077; Figure 3.14C).

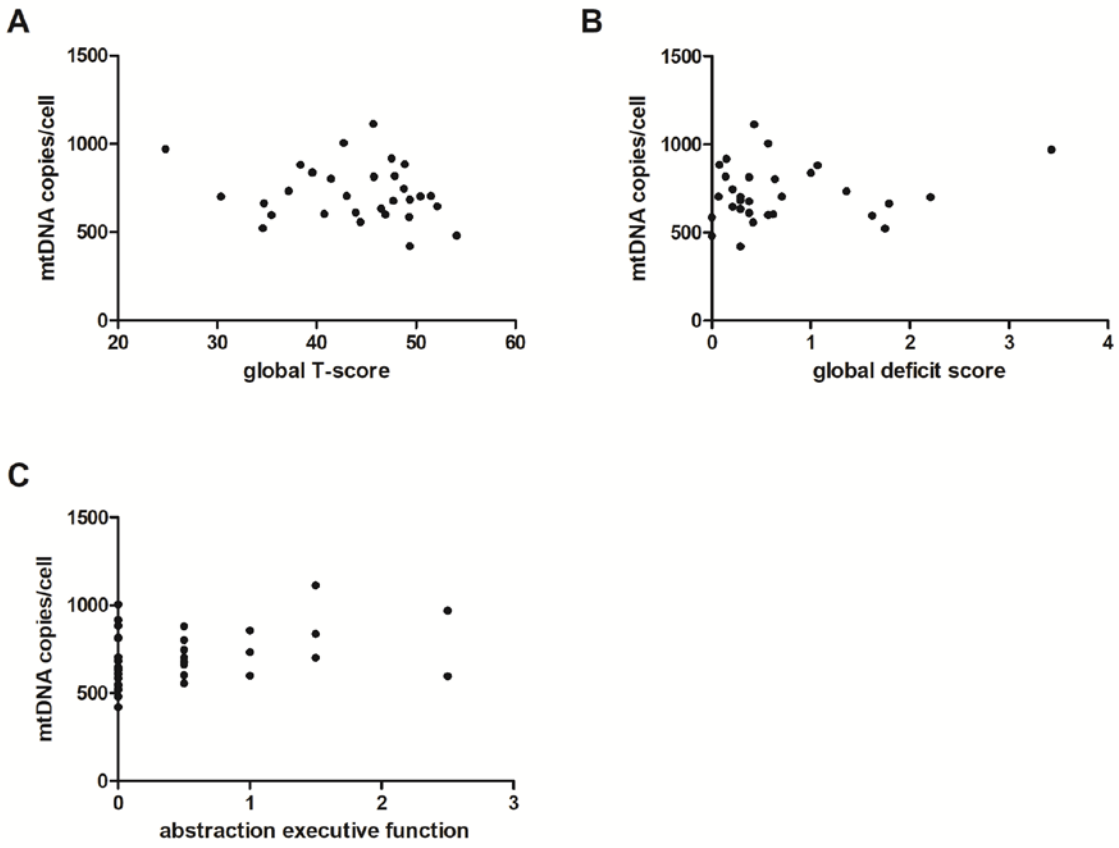

*Figure 3.14. Mitochondrial DNA copy number levels (age-corrected) against HIV neurocognitive testing parameters for HIV positive cases. MtDNA content showed no significant correlation with neurocognitive function assessments including global T-score (**A**), global deficit score (**B**) and abstraction executive domain deficit score (**C**). Every dot represents a sample.*

Regarding mtDNA CD, based on the categorical classification of NCI (one-way ANOVA p=0.37; Figure 3.15), global T-score (r=-0.10, n=30, p=0.6; Figure 3.16A), GDS (r=0.09, n=30, p=0.6; Figure 3.16B), or executive function (r=0.23, n=33, p=0.20; Figure 3.16C), no associations were seen between neurocognitive function and mtDNA CD levels.

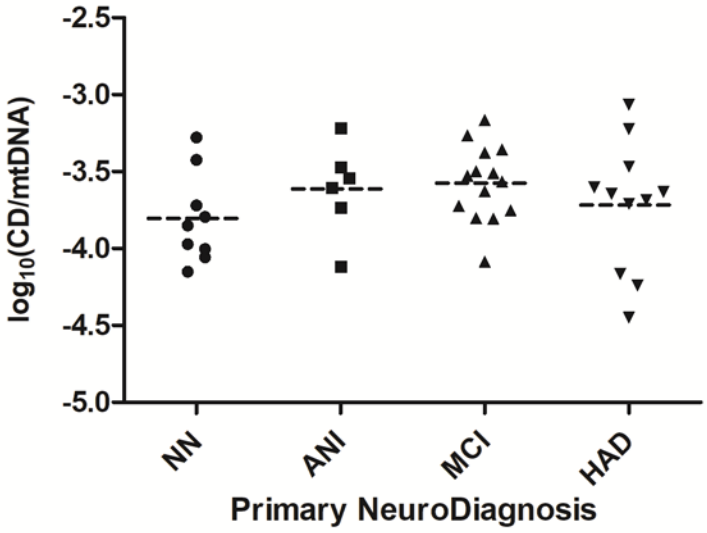

Figure 3.15. Mitochondrial DNA common deletion levels (age-corrected) for HIV+ patients clustered in groups regarding their neurocognitive diagnosis. There was no difference between the groups regarding mtDNA CD burden.

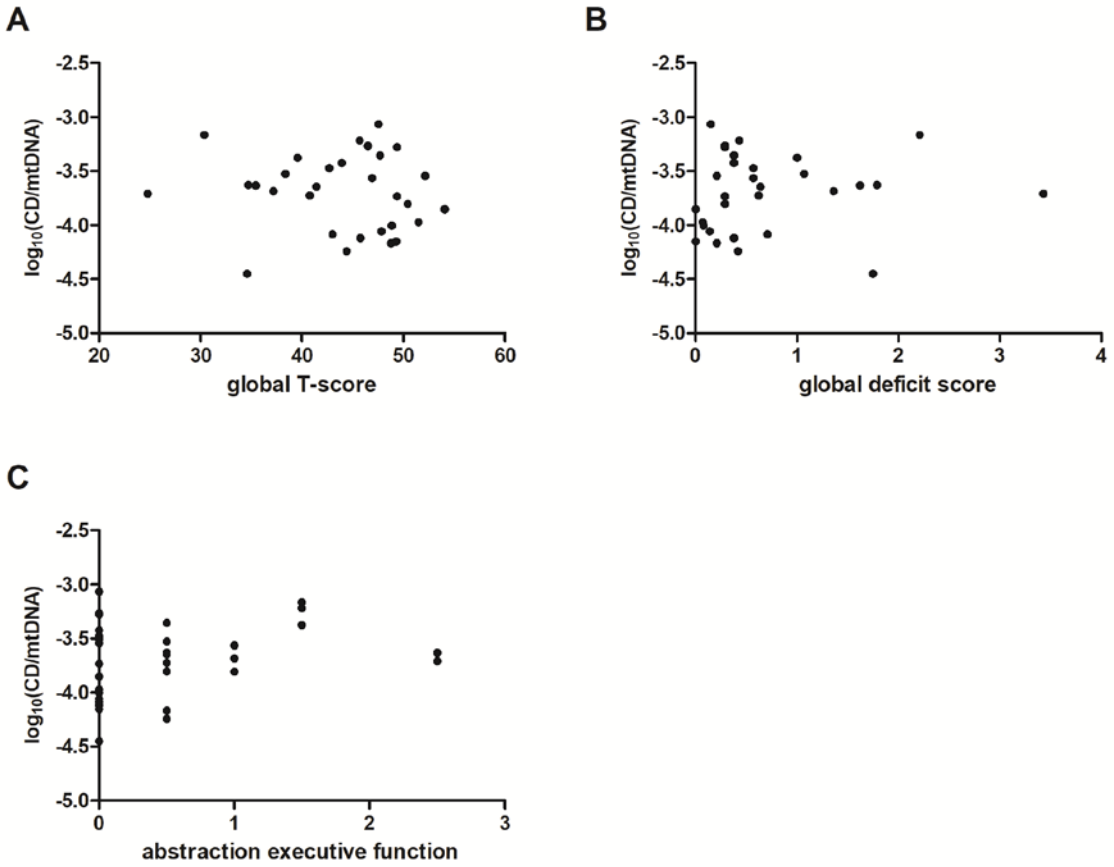

*Figure 3.16. Mitochondrial DNA common deletion levels (age-corrected) against HIV neurocognitive testing parameters for HIV positive cases. MtDNA CD showed no significant correlation with neurocognitive function assessments including global T-score (**A**), global deficit score (**B**) and abstraction executive domain deficit score (**C**). Every dot represents a sample.*

There was no association between mtDNA content and CD levels in HIV+ cases, in uninfected controls and in both groups pooled (r=0.10, p=0.4, n=87; Figure 3.17).

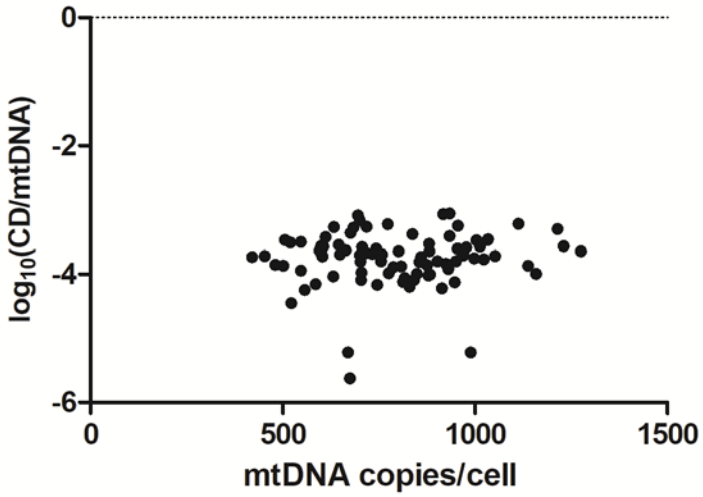

Figure 3.17. Mitochondrial DNA copy number levels (age-corrected) against mitochondrial DNA common deletion levels (age-corrected) for both HIV positive cases and HIV negative controls. No correlation was found between mtDNA content and CD in the HIV+ and HIV- cohort.

CD4 T-cell levels were analysed for HIV+ cases regarding the neurological subcategories and there were no significant differences (mean (SE); NN, 171 (41), n=19; ANI, 152 (58), n=13; MCI, 123 (49), n=23; HAD, 151 (38), n=27; Kruskal-Wallis test, p=0.3; Figure 3.18).

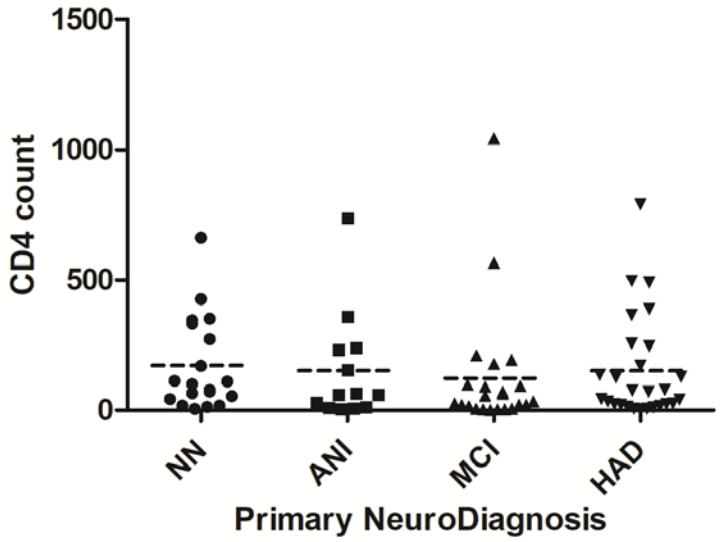

Figure 3.18. CD4 T-cell count values for HIV+ patients clustered in groups regarding their neurocognitive diagnosis. There was no difference between the groups in terms of CD4 T-cell levels.

HIV patient RNA plasma viral load values (log_{10} transformed, viral log) showed no differences between the neuro subcategories (NN, 3.6 (0.4), n=19; ANI, 3.6 (0.5), n=12; MCI, 4.3 (0.3), n=22; HAD, 4 (0.3), n=27; Kruskal-Wallis test, p=0.6; Figure 3.19).

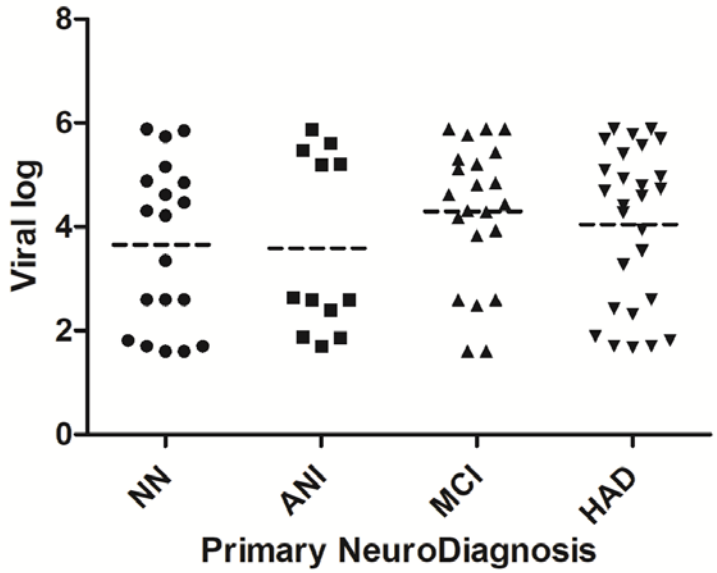

Figure 3.19. Plasma viral values for HIV+ patients clustered in groups regarding their neurocognitive diagnosis. There was no difference between the groups in terms of HIV RNA plasma viral load values (viral log). Viral log is log_{10} of viral load (in viral copies/mL). Dotted line at mean.

3.4.4 Deep resequencing of human mtDNA point variants

Bioinformatic analysis was performed as described in Section 2.11. Samples were removed if coverage was <99% at a minimal depth of 1000x (see coverage graph in Appendix 10.8). 86 samples (48 cases, 38 controls) achieved adequate sequence coverage and quality for analysis. Homoplasmic mtDNA variants (defined here as base positions with a variant present at ≥ 98% frequency) were examined in order to establish that background mtDNA sequence context was not a confounder of the analyses of heteroplasmic mtDNA point variants. A median of 30 (IQR, 12.75-34) homoplasmic variants per sample in HIV positive cases was observed, which did not differ significantly from HIV negative controls (median 23.5, IQR 11.75-33, Mann Whitney p=0.3). Furthermore, the number of homoplasmic variants per sample showed no correlation with age at death (Spearman; HIV+, r=0.07, p=0.6; HIV-, r=-0.05, p=0.8), or with number of heteroplasmic variants per sample (HIV+, r=-0.16, p=0.3; HIV-, r=0.22, p=0.19).

Heteroplasmic mtDNA point variants were therefore next analysed. Protein coding and D-loop variants were the most abundant in both HIV+ and HIV- subjects (Figure 3.20).

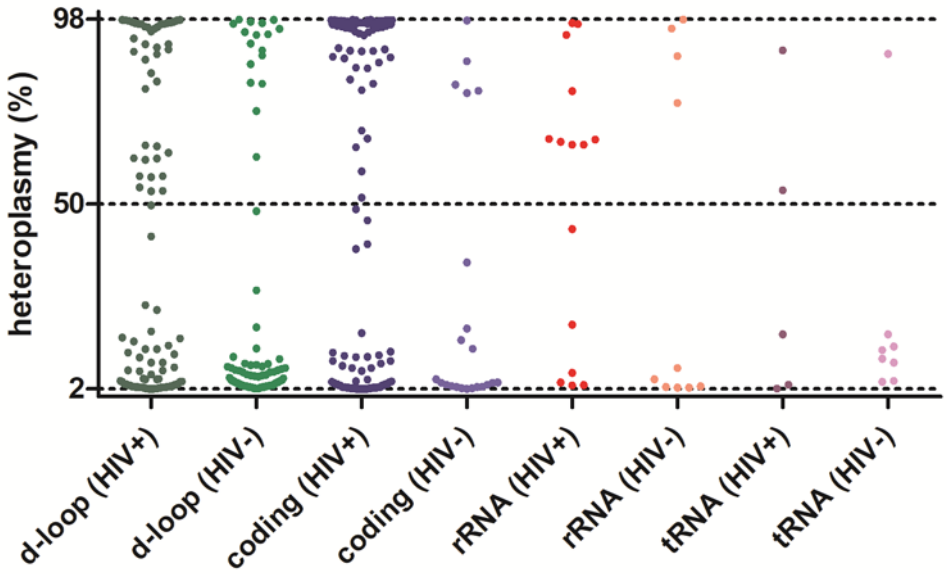

Figure 3.20. Heteroplasmic mtDNA point variants detected by deep resequencing (Illumina MiSeq). Every dot is an mtDNA variant. Y axis is heteroplasmy frequency. D-loop are variants found in the mtDNA displacement loop. Coding are variants in the protein-coding regions. rRNA is ribosomal RNA. tRNA is transfer RNA.

Total variant load, expressed here as the number of base positions showing heteroplasmic mtDNA variants, was a median of 2 per sample (IQR 1-4) in both HIV positive cases and HIV negative controls. For both groups, variants were most commonly seen in the mtDNA non-coding D-loop (mean of 2.6 variants per sample, -2.64 $\log_{10}$ per base position), followed by protein-coding genes (1.6 variants per sample, -3.85 $\log_{10}$ /bp). rRNA variants (0.3 per sample, -3.92 $\log_{10}$ /bp) and tRNA variants (0.1 per sample, -4.16 $\log_{10}$ /bp) were comparatively rare (Figure 3.21). Within protein-coding regions, mtDNA variants were classed as synonymous substitutions, where amino acid sequence is not modified, and non-synonymous substitutions, altering the amino acid sequence of the protein. Synonymous variants were not significantly different between HIV+ and HIV- samples (p=0.6) (Figure 3.21). There was a handful of HIV+ samples that appeared to have an excess of non-synonymous variants compared to the HIV- group but statistically this did not reach significance (p=0.1) (Figure 3.21).

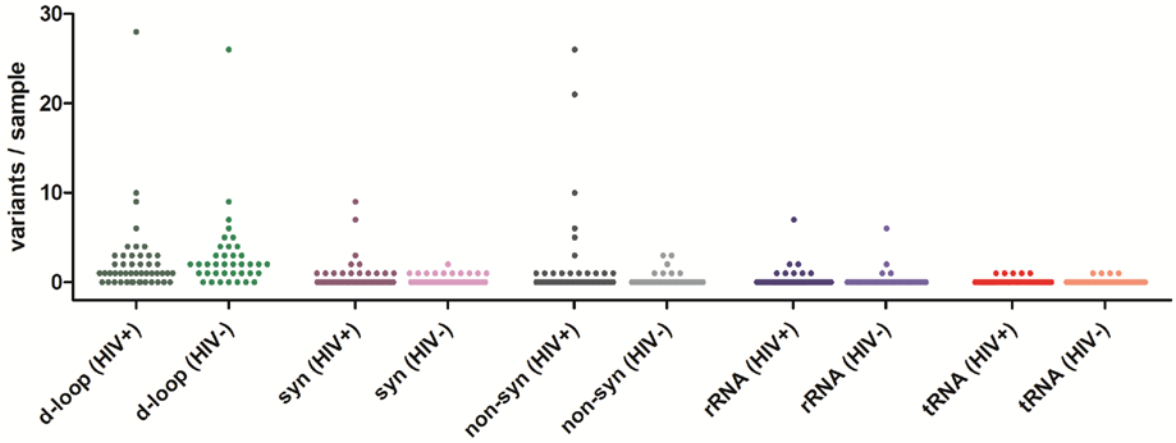

Figure 3.21. Heteroplasmic mtDNA point variants per sample. Number of base positions showing variants per case, according to HIV status and variant type. Every dot represents a sample. D-loop are variants found in the mtDNA displacement loop. Syn is for synonymous variants. Non-syn is for non-synonymous variants. rRNA is ribosomal RNA. tRNA is transfer RNA.

Similar to the findings for mtDNA content and mtDNA deletions, there was a significant effect of age on the number of heteroplasmic mtDNA point variants in HIV negative controls (r=0.43, p=0.007, Figure 3.22). However, after correction of variant load per case for this age effect, there remained no significant difference between HIV positive cases and HIV negative controls (p=0.19).

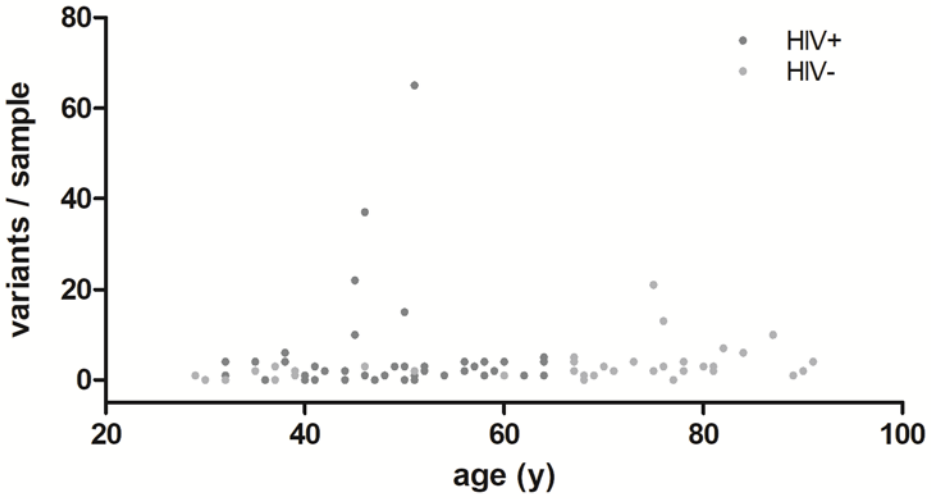

Figure 3.22. Number of base positions showing variants per case, according to age and HIV status. Y is for years.

Finally, as mtDNA point variants present at high heteroplasmy levels are likely to have greater functional effects than those at low levels, a variant burden per sample was weighed for variant heteroplasmy levels (expressed here as variants per bp per 10^6 mtDNA genome copies). Again there was a significant association of variant burden with age in HIV negative controls (r=0.34, p=0.038, Figure 3.23), but no effect in HIV positive (r=0.17, p=0.2).

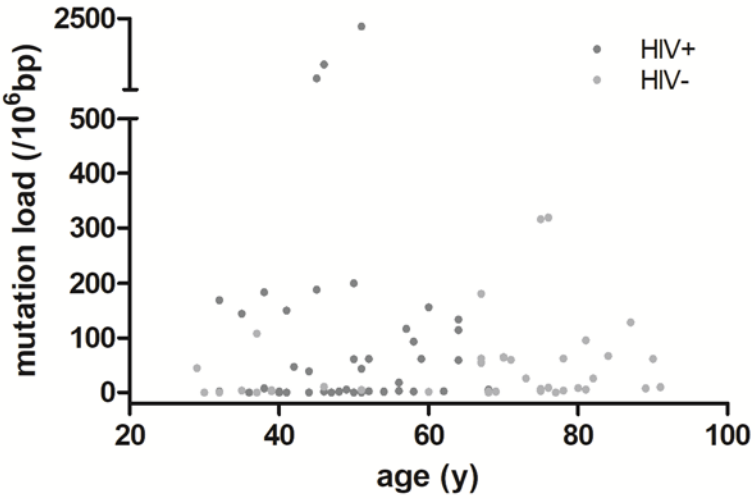

Figure 3.23. MtDNA variants per case, weighted for variant heteroplasmy. Bp is base pairs. Y is for years.

3.5 Discussion

This study aimed to understand mtDNA damage in the human brain at the whole-tissue level in the setting of HIV infection, antiretroviral treatment and ageing. On all measures studied, the expected changes with age were observed: decreased mtDNA copy number, increased deletions, and increased point mutations.

Although increased mtDNA point mutations with age are expected, to this author's knowledge, this is the first study to report mutations using an NGS approach which captures the whole mtDNA genome in this setting.

The multiplex qPCR was used to determine mtDNA copy number and prevalence of the age-associated mt.δ4977 common deletion in frontal cortex tissue of HIV positive cases and age-adjusted HIV-uninfected controls. Regarding cellular mtDNA content, mitochondrial DNA copy number was significantly lower in HIV-positive cases compared to HIV-uninfected controls. Within the HIV+ cohort, mtDNA CN was not associated with any of the established HIV disease progression biomarkers, CD4 T-cell count and HIV RNA viral load. Other disease-monitoring markers: CD4/CD8 ratio, nadir CD4 count and CD8 lymphocyte count were also not associated with mtDNA content. Similarly, no significant association was found between mtDNA content and ART at the time of last assessment, whether that be ART in general, any polymerase-γ inhibiting ART, or specific mitochondrially toxic medications. Regarding 4977 bp common deletion levels, mtDNA age-associated CD was significantly higher in HIV-positive cases compared to HIV-uninfected controls. Within the HIV+ cohort, mtDNA CD was not associated with any of the established HIV disease progression biomarkers and other T cell count markers. As observed for mtDNA content, there was no association found between mtDNA CD and any of the ART parameters. Furthermore, there was no effect of mtDNA parameters, mtDNA CN and age-associated common deletion, on neurocognitive impairment measurements.

Taken together, these data showed for the first time that mtDNA quantity and quality decrease in the frontal cortex of the brain of PLWH. Increasing age was associated with an increase in mtDNA mutation load (both mtDNA point variants and deletions), and a decrease in cellular mtDNA content. These findings are in keeping with the published literature on mtDNA changes in the ageing human brain. In the case of both mtDNA content and mtDNA deletions, HIV infection appeared to augment these age-associated changes. By a simple analogy, the observed effects of HIV were

equivalent to ~32 year (for mtDNA content) and ~12 year (for mtDNA deletions) age advancement. Interestingly the data (Figure 3.22 and 3.23) also seemed to show a trend towards the same phenomenon for mtDNA point variants, but this did not reach statistical significance.

Most prior data on mtDNA changes in PLWH have suggested that the predominant driver of mtDNA depletion and mutation is ART, and especially the historical NRTIs which inhibit pol γ. In contrast, these results show strong effects of HIV infection per se, but not of ART or of specific NRTIs. One of the explanations could be because the penetration of ART into the CNS is variable, but drug levels are always significantly lower than those seen in plasma. As NRTI-induced mitochondrial toxicity is dose-dependent, it is plausible that drug levels achieved in the CNS are below a threshold at which significant mtDNA damage will occur. Another possibility, not mutually exclusive, is that the cells of the CNS are more sensitive to the effects of HIV itself on mtDNA compared with many other tissues. Thus when observing changes in mtDNA, the HIV effect is dominant over any ART effect.

A plausible hypothesis to argue why HIV infection itself resulted in the reduction in mtDNA quantity and quality in the brain of HIV+ individuals compared to HIV-uninfected controls could be explained by a HIV-mediated neurotoxicity associated with mitochondrial dysfunction. As previously described in the literature, a number of HIV viral proteins have been shown to be released *in vitro* from HIV-infected cells, including lymphoid, monocytic and glial cells, during viral replication and to infect these cells in the central and peripheral nervous system, where they also act as viral reservoirs, posing a challenge for ART (Furtado *et al.*, 1999; Coleman and Wu, 2009; Castellano *et al.*, 2017; Castellano *et al.*, 2019).

The nature of post-mortem brain tissue samples used in this study inevitably places some limits on the generalisability of these findings to healthy PLWH. Whilst cases with other CNS pathology or opportunistic infections were excluded, the HIV cohort as a whole shows advanced HIV (mean CD4 cell count 143 cells/µL). In a larger and more homogenous set of cases, it would be important to establish whether consistent viral suppression and immune reconstitution is associated with attenuation of the observed changes in mtDNA.

3.6 Conclusion

In conclusion, PLWH with predominantly advanced disease, have abnormalities of mitochondrial DNA quality and quantity in the brain. These changes appear to augment those seen due to the normal ageing process, giving weight to the hypothesis that HIV infection may adversely affect biological pathways of ageing including the maintenance of mitochondrial function.

Chapter 4. Generation of the *PolgA* 'WtN+' mouse model of clonal expansion of mitochondrial DNA mutations in ageing

4.1 Introduction

MtDNA mutations reach high levels within individual cells by a process known as clonal expansion. Recent data suggest that the accumulation of mtDNA mutations within tissues with ageing is likely to be predominantly due to the clonal expansion of existing mutations within cells, rather than high levels of mutagenesis (Greaves *et al.*, 2014). It is not currently known however whether clonal expansion is a modifiable process which can affect the rate of physiological ageing.

The *PolgA* 'mutator' mouse contains an error-prone mtDNA polymerase γ. The homozygous mouse produces very high levels of mtDNA mutations, and has a premature ageing phenotype with early death (Trifunovic *et al.*, 2004; Kujoth *et al.*, 2005). More recently, it has been appreciated that female heterozygous *PolgA* mice produce offspring with germline mtDNA mutations. These germline mutations enhance the phenotype and indeed can lead to a mildly accelerated ageing phenotype even when bred back to a wild-type nuclear background (Ross *et al.*, 2013). Trapping germline heteroplasmic mtDNA mutations on a wild-type nuclear background therefore potentially provides a model with which to study clonal expansion.

4.2 Aims of this investigation

To develop and characterise a mouse model with which to define the natural history of clonal expansion of mtDNA mutations and their effect on physiological ageing.

4.3 Methodology

4.3.1 PolgA 'WtN+' mouse model generation

The 'WtN' derivative of the *PolgA* 'mutator' mouse, as described by Ross and colleagues (Ross *et al.*, 2013), contains 'trapped' germline mtDNA mutations, bred back to a wild-type inbred nuclear background (C57BL/6J). This method was adapted by breeding once through a homozygous *PolgA* female in order to produce offspring with a larger 'burst' of germline mtDNA mutations. These were then 'trapped' by breeding back to the wild-type nuclear background. I termed this derivative 'WtN+' to denote the greater expected number of germline mtDNA mutations. Maternal generations of WtN+ mice were produced as follows. *PolgA*$^{wt/mut}$ females (n=5) in G0 (generated from a homozygous mother) produced *PolgA*$^{wt/wt}$ female offspring (G1) which were used to produce *PolgA*$^{wt/wt}$ female offspring (n=5) in G2 and in turn to produce the experimental animals (G3) (Figure 4.1). Since mtDNA is exclusively maternally transmitted, germline mtDNA mutations were passed down the maternal line. It was anticipated that this breeding strategy would lead to a high degree of similarity in germline mtDNA mutations between experimental animals of the G3 generation, thus facilitating easier comparison of clonal expansion of these specific mutations within different groups.

As a control group, mice without germline mtDNA mutations were generated by crossing C57BL/6J females with male littermates of the breeding WtN+ females.

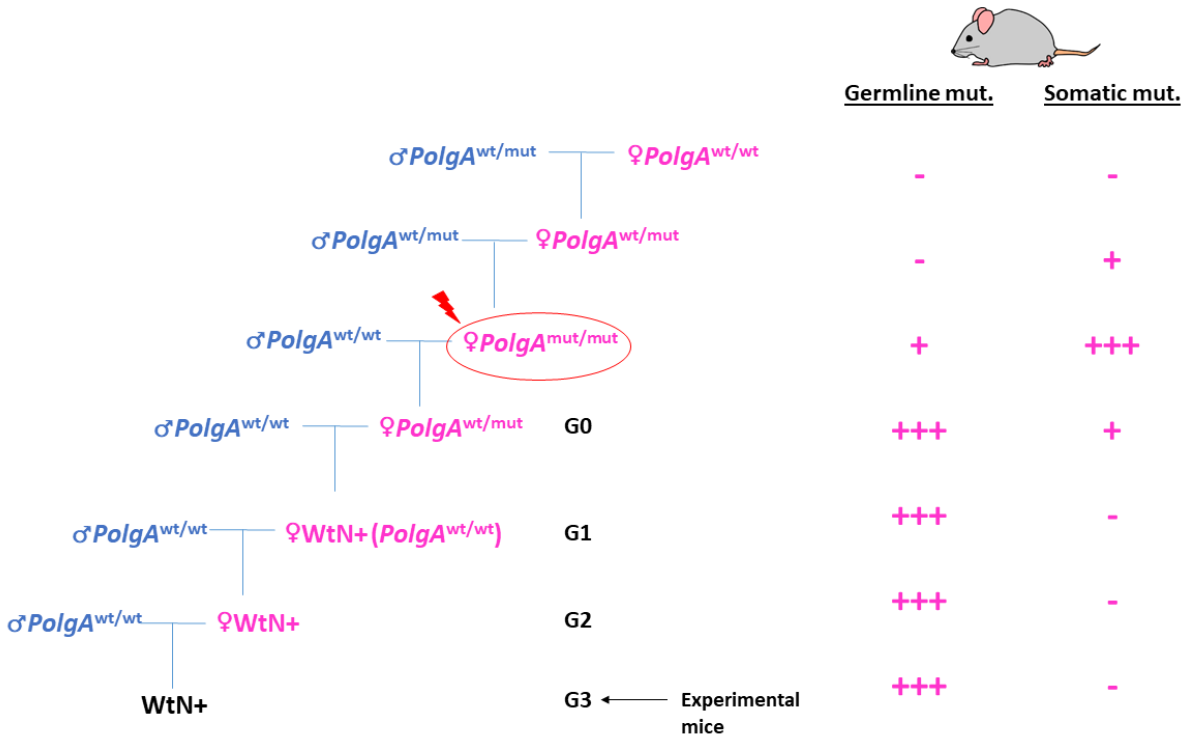

Figure 4.1. Generation of WtN+ mice. Two intercrosses were needed to generate one female PolgA$^{mut/mut}$*. Homozygous* PolgA$^{mut/mut}$ *females were initially generated to create a large germline mtDNA mutational 'burst'.* PolgA$^{mut/mut}$ *mothers produced offspring with multiple germline heteroplasmic mtDNA mutations. Backcrossing to wild-type male mice restored wild-type polymerase function, but retained germline mtDNA mutations. G2 females were used to generate the experimental mice (G3). Thus, all experimental mice would start with the same pool of germline mutations.*

This breeding programme encountered fertility issues, which improved with successive generations. Average litter size (abortions and early neonatal deaths of pups were not counted) for G0 mothers was 2.5, for G1 was 6.5 and for G2 was 6.4. The proportion of successful crosses, i.e., the ones that resulted in a litter of at least one live pup, was 40% for G0 mothers, 67% for G1 and 83% for G2. When breeding wild-type animals, the average litter size was 7 and the successful crosses were at 90%.

Detailed mitochondrial cellular and molecular analyses in the experimental mice, G3, by age and genotype are presented in Chapter 6. Further phenotypic data are presented in Chapter 5.

4.3.2 Tissue processing

Clipped ear tissue was taken at weaning (age ~4 weeks) and was used for genotyping (described in Section 2.2.2), qPCR for mtDNA content, and next generation sequencing to define the pool of transmitted germline mtDNA mutations. All other tissues were dissected during organ harvesting. Dissecting of mouse tissues was previously explained in Section 2.2.9. DNA used for qPCR and NGS was extracted from tissue homogenates as described in Section 2.4.

4.3.3 Real-time PCR for mtDNA copy number

MtDNA content was expressed relative to cell content and was measured in triplicate by multiplex real-time qPCR amplification of mitochondrial gene *MT-ND5* and the nuclear-encoded housekeeping gene *β-Actin*. Primers and probe sequences for this assay are found in Section 2.6.

4.3.4 Next generation sequencing of mouse mitochondrial DNA

Whole mouse mtDNA was enriched using long-range PCR. Primer sequences and LR-PCR details found in Section 2.9.1.

MtDNA point variants were measured on an Illumina MiSeq platform as described in Section 2.10. Paired-end fastq files were obtained from the MiSeq platform. Bioinformatic sequence analysis and variant calling is described in Section 2.11. Ensembl sequence reference used was mm10 (NC_005089.1). MtDNA point variants present at 2% to 98% heteroplasmy were reported.

4.3.5 Quadruple immunofluorescence for mouse tissues

Quadruple immunofluorescence staining and quantification for mouse colon and skeletal muscle was performed as detailed in Section 2.7.

4.3.6 Statistical analysis

Statistical testing was performed using SPSS 24 (IBM). Non-parametric testing (Spearman correlation and Kruskal-Wallis tests) was used for analyses of mtDNA point variants.

4.4 Results

All experimental animals were generated from the same *PolgA*$^{mut/mut}$ grandmother. In this Chapter, a comparison of mitochondrial parameters in the female mice of each generation is reported. For the comparisons presented here, mice in each generation (G0-G3) were culled at a very similar time point, ~70 weeks [±5w] of age. Deep sequencing results were all obtained from ear tissue at 4 weeks old.

4.4.1 Cellular mitochondrial DNA content in mouse tissue homogenates

MtDNA content (mtDNA genome copies per cell) did not vary significantly in ear snip tissue between the four female mice generations used for breeding of the experimental colony (mean (SE) mtDNA copies/cell; G0, 72 (4), n=5; G1, 81 (8), n=5; G2, 86 (9), n=5; G3, 73 (4), n=38; one-way ANOVA, p=0.55; Figure 4.2).

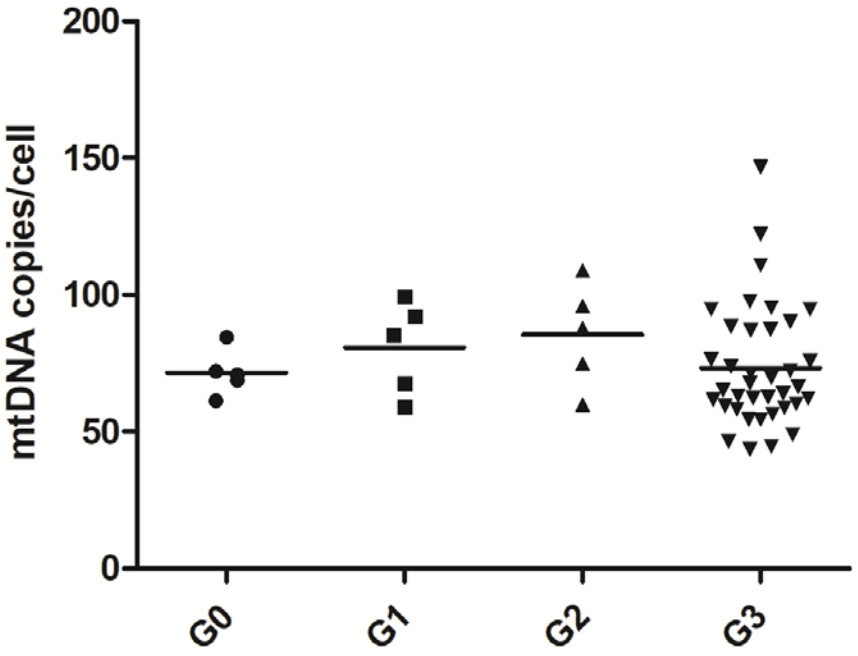

Figure 4.2. Mitochondrial DNA copy number levels in ear tissue for the four mouse generations used for breeding of the experimental colony. Ear snipped tissue was taken during mice weaning. MtDNA CN in ear was not significantly different between generations at 4 weeks old. G stands for generation. Every dot represents a mouse. Line at mean.

MtDNA copy number in homogenised colon was significantly higher in G0 compared with female WtN+ mice of generations G2 and G3 (G0, 329 (16), n=3; G2, 154 (9), n=5; G3, 195 (5), n=6; one-way ANOVA, p<0.0001; Figure 4.3). G1 was not included in the statistical analysis owing to a single data point, but appears comparable to G2/G3. Tukey's multiple comparison test also showed a significant increase in mtDNA content from G2 to G3 (p<0.05).

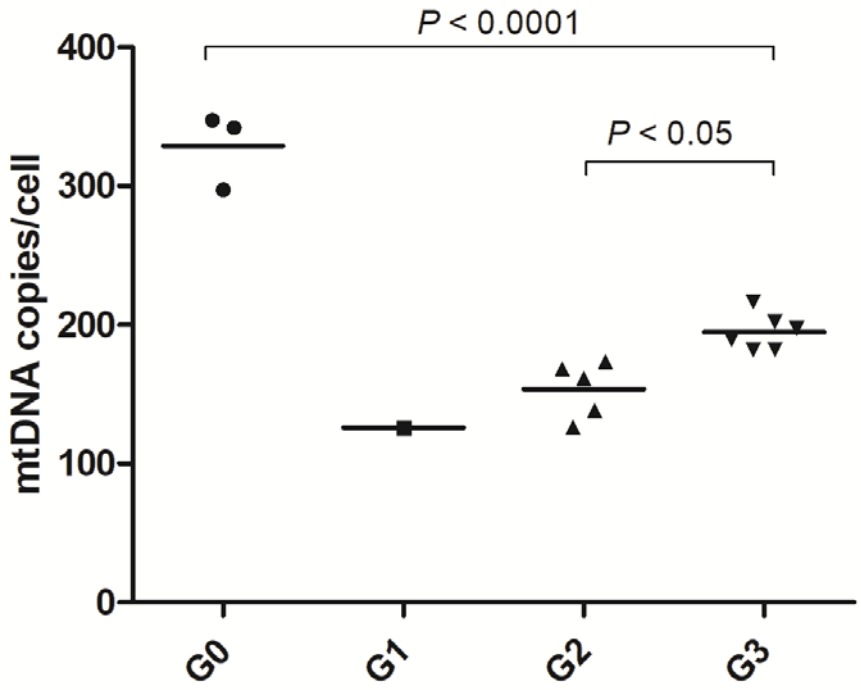

Figure 4.3. Mitochondrial DNA copy number levels in homogenised colon for the four mouse generations used for breeding of the experimental colony. MtDNA CN in colon was significantly different between generations 0, 2 and 3. G stands for generation. Every dot represents a mouse. Top p-value is for one-way ANOVA between G0, G2 and G3. P-value between G2 and G3 is for Tukey's multiple comparison test. Line at mean. All mice were culled at ~70 weeks [±5w] of age.

MtDNA copy number in homogenised skeletal muscle did not differ significantly between female mice generations (G0, 2315 (232), n=3; G2, 2426 (440), n=5; G3, 1573 (204), n=6; one-way ANOVA, p=0.15; Figure 4.4). G1 was not included in statistical analysis as single data point only.

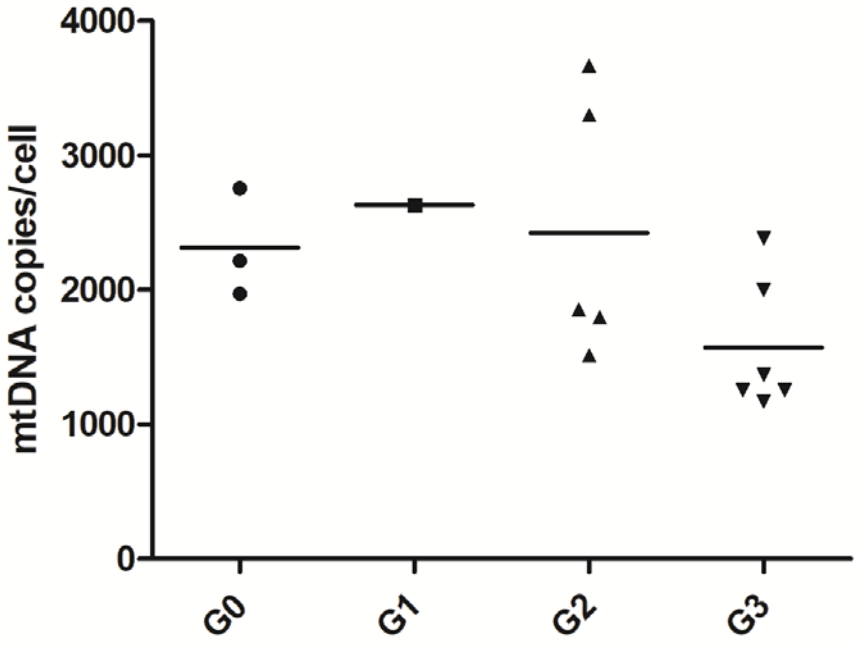

Figure 4.4. Mitochondrial DNA copy number levels in homogenised skeletal muscle for the four mouse generations used for breeding of the experimental colony. MtDNA CN in skeletal muscle was not significantly different between generations 0, 2 and 3. G stands for generation. Every dot represents a mouse. Line at mean. All mice were culled at ~70 weeks [±5w] of age.

MtDNA content in homogenised frontal cortex was significantly high in G0 compared with the other female mice generations, G2 and G3 (G0, 1862 (87), n=2; G2, 826 (106), n=5; G3, 618 (118), n=6; one-way ANOVA, p=0.0005; Figure 4.5). G1 was not included in statistical analysis as single data point only. Tukey's multiple comparison test showed no difference in mtDNA content from G2 to G3.

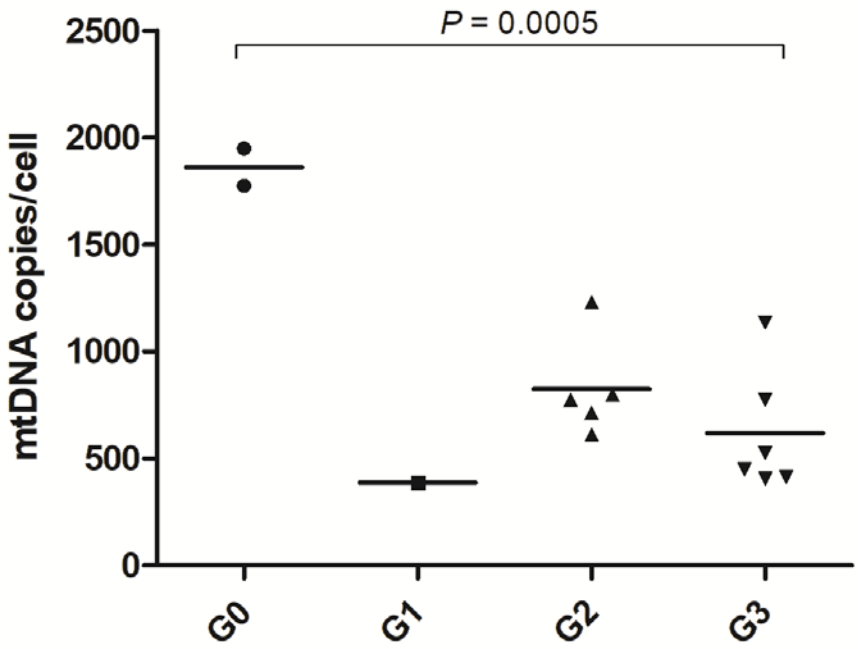

Figure 4.5. Mitochondrial DNA copy number levels in homogenised frontal cortex for the four mouse generations used for breeding of the experimental colony. MtDNA CN in brain was significantly different between generations 0, 2 and 3. G stands for generation. Every dot represents a mouse. P is p-value for one-way ANOVA between G0, G2 and G3. Line at mean. All mice were culled at ~70 weeks [±5w] of age.

4.4.2 Deep resequencing of mouse mtDNA point variants

Next generation sequencing of the mitochondrial genome using Illumina MiSeq, of ear snip samples from the mice pedigree was performed. Generations of WtN+ mice sequenced were as follows: G0 (n=5, *PolgA*$^{wt/mut}$), G1 (n=1, *PolgA*$^{wt/wt}$), G2 (n=5, *PolgA*$^{wt/wt}$) and G3 (n=27, i.e., a subset, *PolgA*$^{wt/wt}$).

Additionally, ear snip mtDNA of founder heterozygous *PolgA* mice (F0 hets, n=4) was sequenced in order to descriptively compare purely somatic mtDNA variants, expected on the F0 hets, to purely germline mtDNA variants, expected in the WtN+ cohort.

G0 mice (as they were heterozygous for the *PolgA* genotype) should contain a small number of somatic mtDNA variants in addition to germline variants. G1-G3 should contain almost entirely germline variants, as there were almost no somatic mtDNA variants expected in wild-type C57BL/6J mice.

MtDNA variants were only reported if they had greater than 2% heteroplasmy based on the observation that variants at >1% heteroplasmy are almost never seen in wild-type C57BL/6J mice. In fact, wild-type C57BL/6J mice sequencing results showed no mtDNA variants (data not plotted).

The distribution of variants across the mouse mitochondrial genome was plotted along with their heteroplasmy levels (Figure 4.6). Variants in the G0 mice appeared relatively evenly distributed across the mtDNA genome. Variants in the WtN+ mice of generations G1 to G3 were clearly clustered at specific base positions, reflecting the transmission only of a subset of initial variants. Variants in the F0 heterozygous mice were very minimal. Transmission of specific variants is analysed further below.

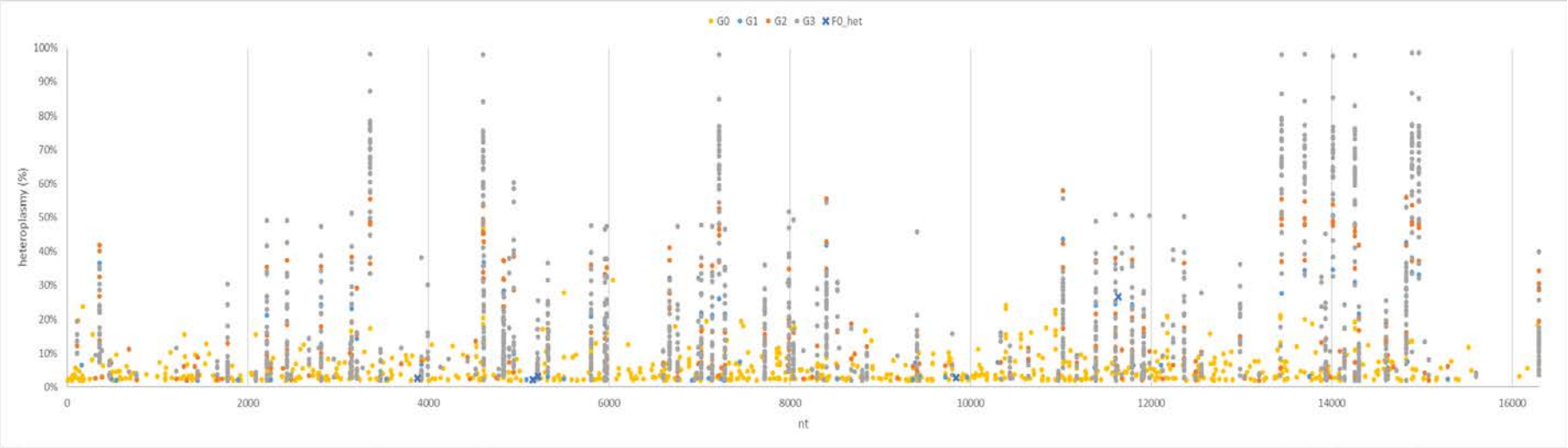

Figure 4.6. Distribution of variants across the mouse mitochondrial genome. Each dot represents an individual variant detected in an individual animal in ear snip mtDNA at 4 weeks of age. Y axis is the variant heteroplasmy. G stands for generation. F0 het are founder heterozygous.

The heteroplasmy levels of variants of each type were analysed in each generation of mice. MtDNA point variants were filtered and categorised according to whether they were non-coding variants (NC, principally in the D-loop); protein-coding variants, which were further sorted into non-synonymous substitutions, altering the amino acid sequence of the protein, and synonymous if the amino acid sequences were not modified; rRNA and tRNA variants. Median and maximum heteroplasmy levels increased significantly in all mtDNA variant types across successive generations. Coding gene variants, both synonymous ($p<0.0001$) and non-synonymous ($p<0.0001$), increased significantly in heteroplasmy more rapidly than other variant types (Figure 4.7). Non-coding ($p=0.038$), rRNA ($p<0.0001$) and tRNA ($p<0.0001$) variants also increased significantly in heteroplasmy throughout generations G0-G3. Heteroplasmy levels in F0 heterozygous mice were low for all variant types.

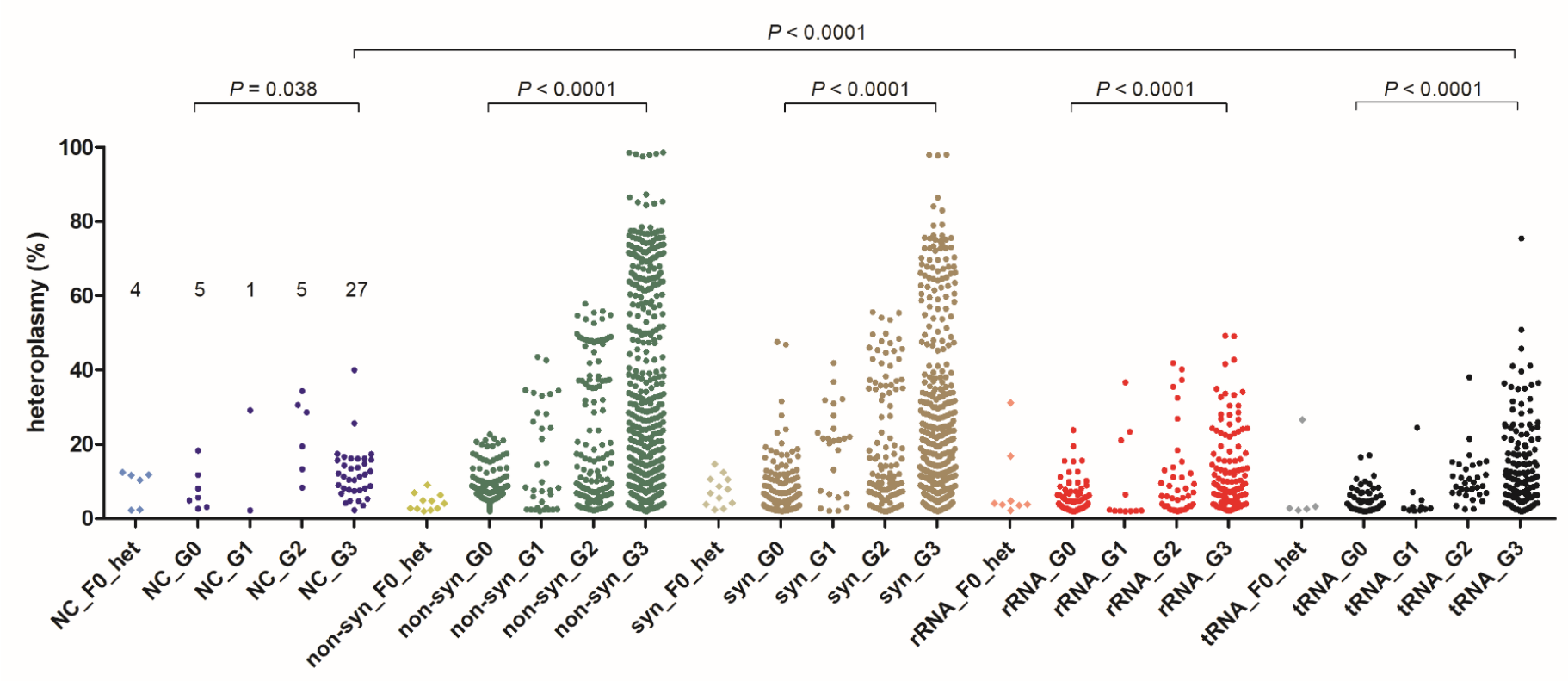

Figure 4.7. Effect of variant type on tolerated heteroplasmy level by generation. Each dot is an individual variant in an individual mouse. Y axis is heteroplasmy frequency. G stands for generation. Values on the first group (4, 5, 1, 5, 27) are the number of mice per generation. P is p-value. Top p-value is for comparison of all variant types in G3. NC is non-coding; non-syn is non-synonymous; syn is synonymous; rRNA is ribosomal RNA; tRNA is transfer RNA. F0 het are founder heterozygous.

The same data were expressed in terms of number of variants observed at any heteroplasmy level by variant type in each generation of mice, normalised to the number of nucleotide ‘at risk’, i.e., nucleotide positions of that type. It was shown that for each variant type, the variant frequency of coding ($p<0.0001$), rRNA ($p<0.0001$) and tRNA ($p=0.011$) variants significantly decreased with successive generations which did not reach statistical significance for non-coding variants, but the number of observations were small (Figure 4.8). Again, variant frequency in F0 heterozygous mice was low for all variant types.

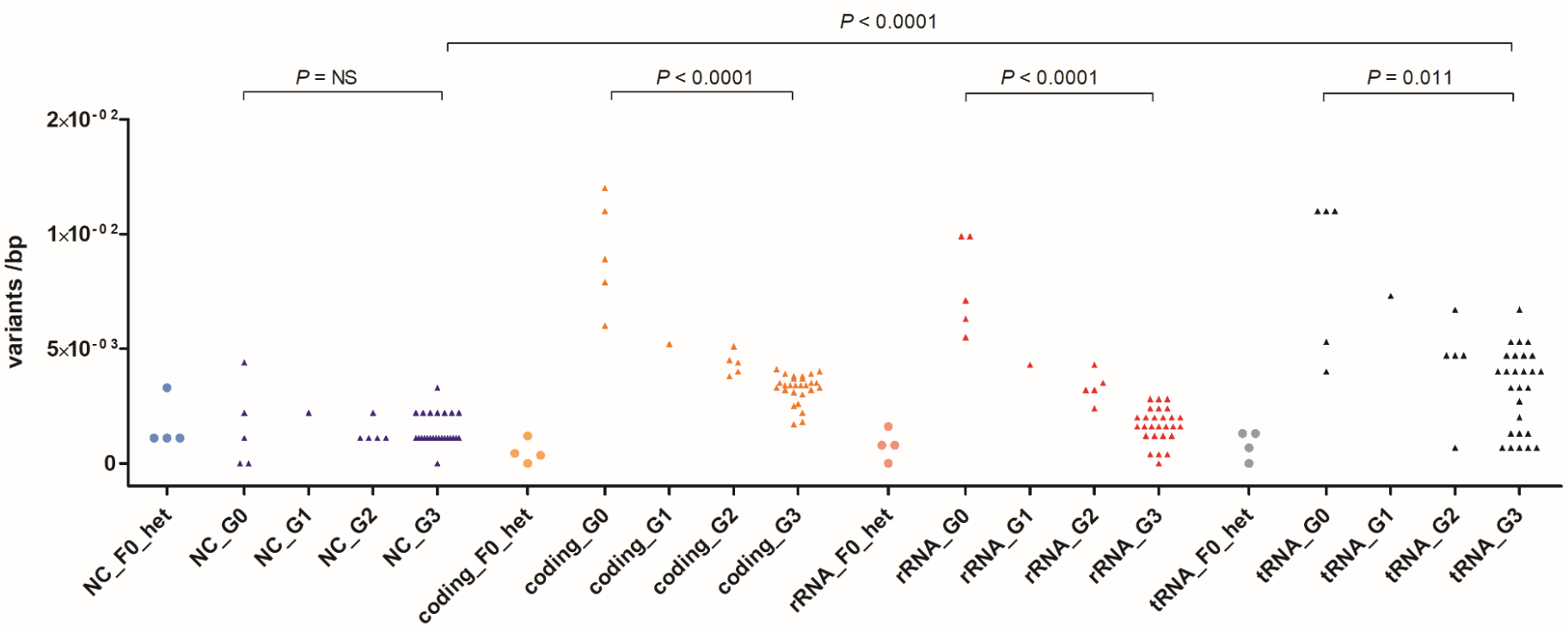

Figure 4.8. Effect of variant type on variant frequency by generation. Each dot is an individual mouse. Y axis is mtDNA variants per base pair. G stands for generation. P is p-value for nonparametric one-way ANOVA between G0, G2 and G3. Top p-value is for comparison of all variant types in G3. NC is non-coding; coding is protein-coding variants; rRNA is ribosomal RNA; tRNA is transfer RNA. NS is non-significant. F0 het are founder heterozygous.

From the same dataset again, each variant seen was weighted by its heteroplasmy level. This metric therefore combined variant count and heteroplasmy data and is considered as a measure of overall ‘mutational burden’. These data suggested that coding gene variants were better tolerated than other variant types across generations as they reached higher mutational burdens ($p=0.002$; Figure 4.9). As per previous analysis, F0 heterozygous mice had very minimal mutational burden in comparison to the WtN+ mice of interest.

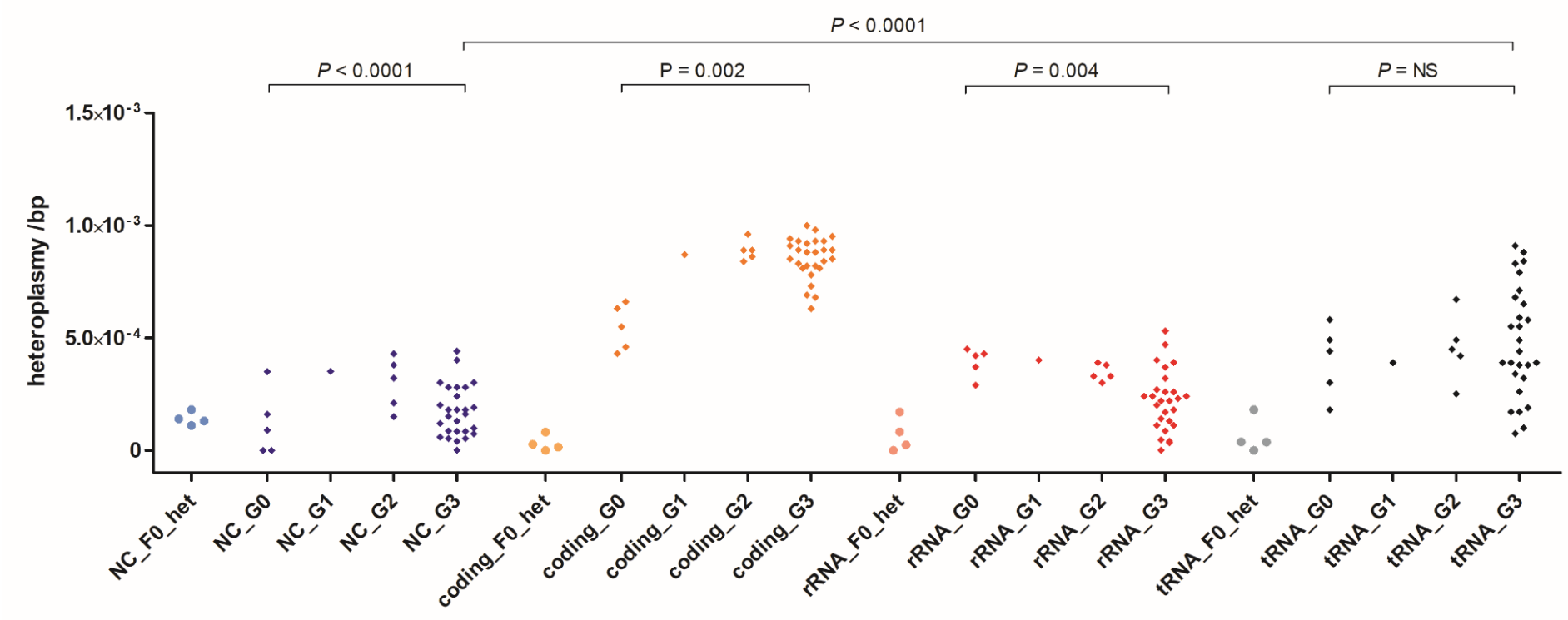

Figure 4.9. Effect of variant type of variant load by generation. Y axis is heteroplasmy per base pair. G stands for generation. P is p-value for nonparametric one-way ANOVA between G0, G2 and G3. Top p-value is for comparison of all variant types in G3. NC is non-coding; coding is protein-coding variants; rRNA is ribosomal RNA; tRNA is transfer RNA. NS is non-significant. F0 het are founder heterozygous.

The transmission of individual mtDNA variants within mother/offspring pairs was examined and categorised according to mtDNA variant type. First, the heteroplasmy level shifts between mother and offspring were plotted, as mean shift and SEM for each variant transmission observed (as each mother produced multiple offspring with differing variant heteroplasmy levels). This analysis showed that there was a clear relationship between maternal and offspring variant heteroplasmy levels, but there were clear shifts away from the expected line. There was also a spread of heteroplasmy levels for each individual variant within multiple offspring of the same mother (Figure 4.10). In order to determine whether there was systematic selection against certain variant types, the slopes of the regression lines were then compared for each variant type (Figure 4.11).

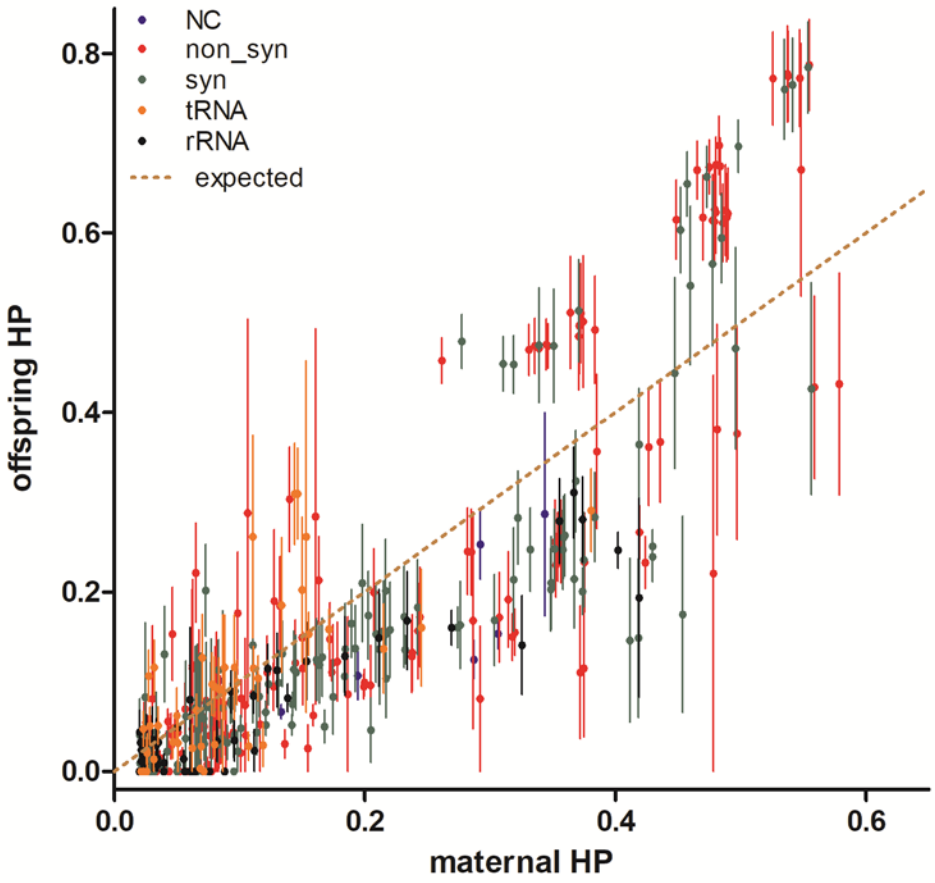

Figure 4.10. Shift in heteroplasmy level of mtDNA variant type between WtN+ mother and offspring. X axis is maternal heteroplasmy and Y axis is offspring heteroplasmy. Dots are mean and vertical lines are SEM for each variant observed. NC is non-coding; non-syn is non-synonymous; syn is synonymous; rRNA is ribosomal RNA; tRNA is transfer RNA. Expected is a positive linear correlation line of r=1 and slope=1.

All slopes produced from linear regression for non-coding, non-synonymous, synonymous, rRNA and tRNA variant shifts between mother and offspring were different from the expected slope=1. Slopes suggested selection against non-coding (slope 0.6, 95% CI [0.4, 0.8]), rRNA (slope 0.7, 95% CI [0.64, 0.79]) and tRNA (slope 0.76, 95% CI [0.61, 0.91]) variant shifts. There was also a selection for protein-coding non-synonymous (slope 1.2, 95% CI [1.17, 1.27]) and synonymous (slope 1.08, 95% CI [1.02, 1.14]) variant shifts. Slopes also differed significantly between each other ($p<0.0001$; Figure 4.11). This fitted with the above data suggesting that coding gene variants were subject to less negative selection than other variants. The explanation for the 'positive selection' of synonymous/non-synonymous variants could be that the genetic bottleneck allowed random drift (including drift to higher heteroplasmy levels),

especially of those variants that were already at quite high heteroplasmy levels. So it was those variants that drifted upwards that were more likely to get passed on.

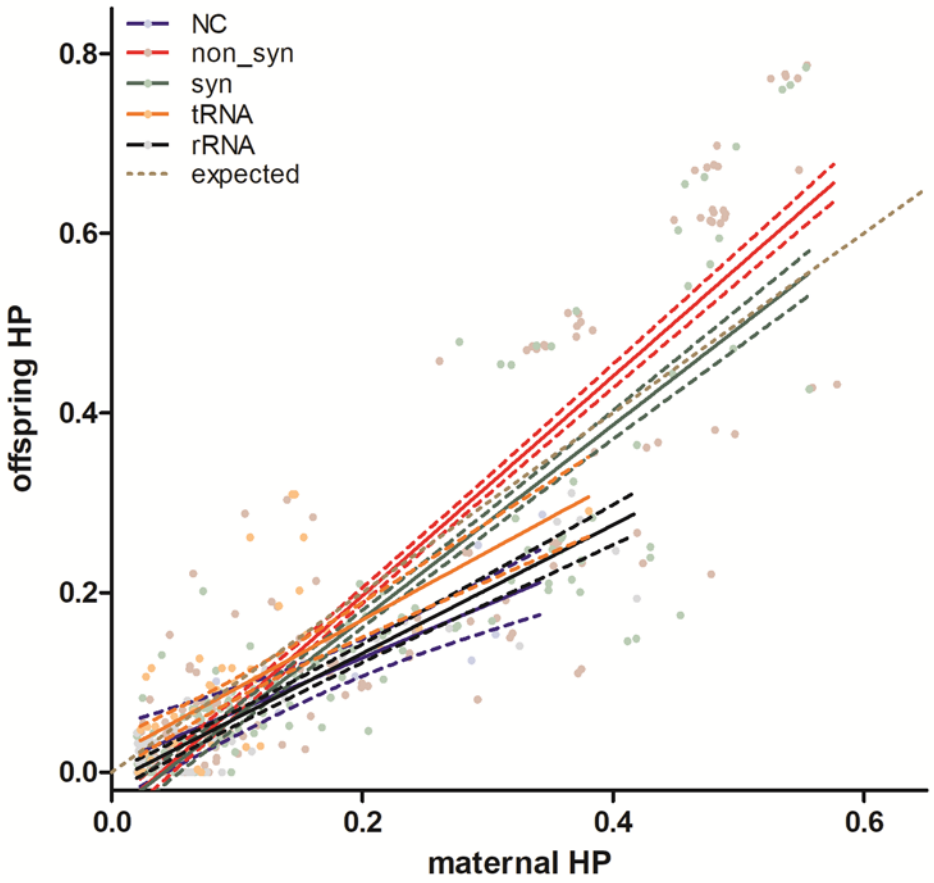

Figure 4.11. Shift in heteroplasmy level according to mtDNA variant type between WtN+ mother and offspring. X axis is maternal heteroplasmy and Y axis is change in variant heteroplasmy between mother and offspring. Dots are samples. Solid lines are regression lines plotted for each variant type and dotted lines are 95% confidence interval for each line. NC is non-coding; non-syn is non-synonymous; syn is synonymous; rRNA is ribosomal RNA; tRNA is transfer RNA. Expected is a positive linear correlation line of r=1 and slope=1.

Since complex I (CI) defects are the most frequently encountered type of OXPHOS dysfunction, specific complex I non-synonymous mtDNA variants between generations G0-G3 were analysed. Complex I mtDNA variant counts (Figure 4.12A) and variant frequency per bp (Figure 4.12B) significantly decreased by generation, as observed in the protein-coding mtDNA variants in previous analyses shown above Figure 4.8. In the same way as described for coding variants, CI non-synonymous variants significantly reached higher mutational burdens (Figure 4.12C).

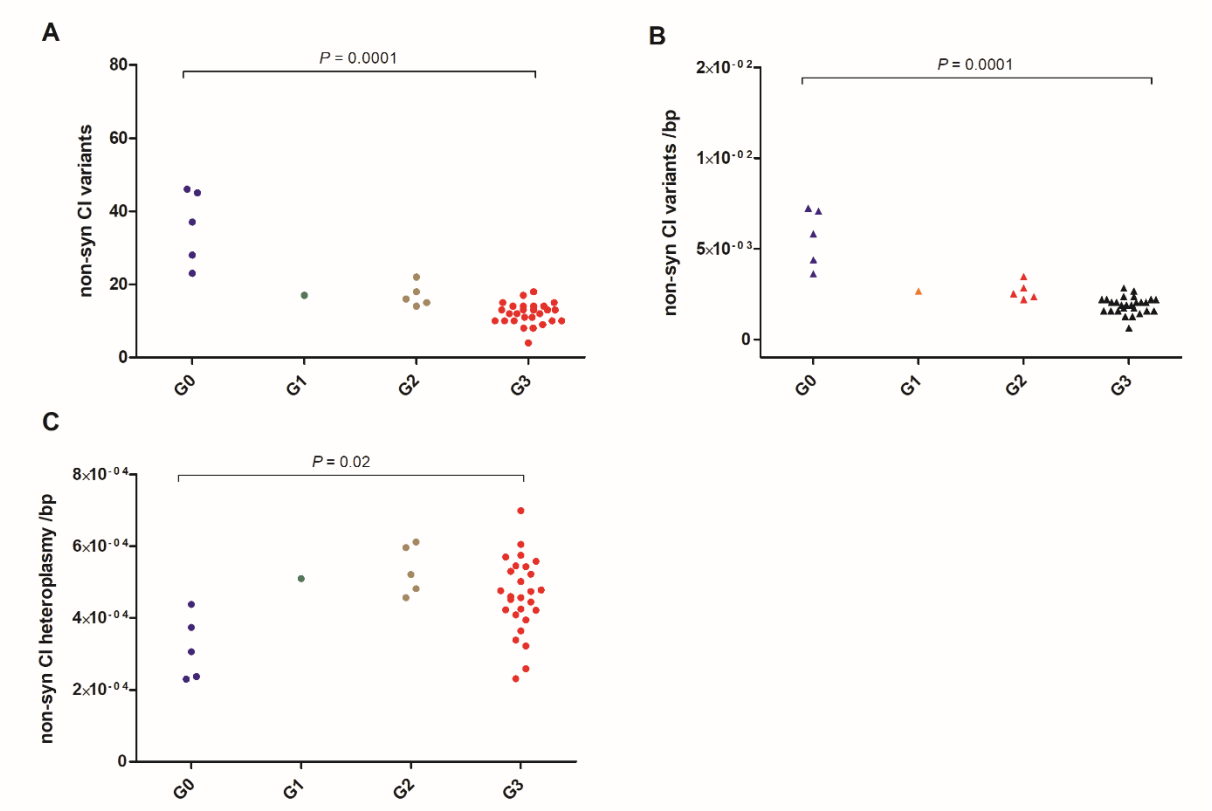

*Figure 4.12. Complex I non-synonymous mtDNA variants by generation. (**A**) Number of complex I non-synonymous mtDNA variants by generation. (**B**) Variant frequency by generation. Y axis is variants per base pair. (**C**) Variant load by generation. Y axis is heteroplasmy per base pair. Each dot is an individual mouse. P is p-value for nonparametric one-way ANOVA between G0, G2 and G3. G stands for generation.*

4.4.3 Immunofluorescence for mitochondrial respiratory complexes activity

Quadruple immunofluorescence was used to detect OXPHOS activity in mitochondrial respiratory chain complexes I, III, IV and V, in individual colonic crypts. Complex deficiency was expressed as a z-score, relative to young healthy control (C57BL/6J) mice. Z-scores above -3 were considered normal, below -6 were deficient. For each complex, colonic crypts classified as z<-3 included those below the normal threshold; z<-4.5 included intermediate and deficient; and z<-6 only included fully deficient crypts. Log_{10}-transformed values of complex deficiency were used.

In successive generations of WtN+ female mice, there was a decrease in the proportion of complex I deficient crypts (z<-3), which was significant between G2 and G3 (p=0.03; Figure 4.13A). This is in keeping with the decrease in number of mtDNA mutations seen in successive generations. Data in G3 are shown for the late time point (~70w [±5w]).

Complex III deficient colonic crypts (z<-3) significantly decreased between G2 and G3 of WtN+ female mice (Figure 4.13B). Complex IV and complex V were not significantly affected throughout any of the generations G1-G3, but deficiency of these complexes was very rare (Figure 4.13C/D).

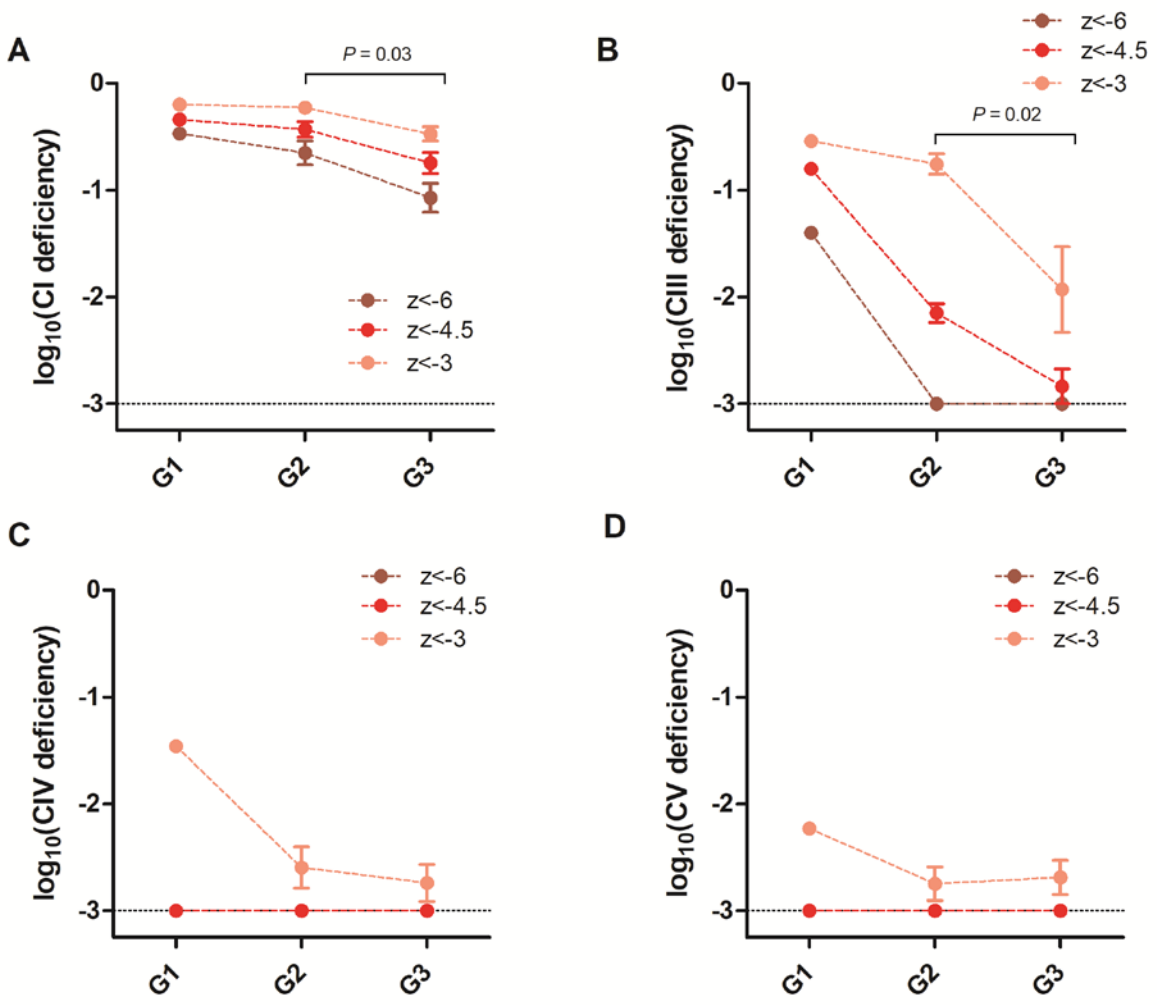

*Figure 4.13. OXPHOS complexes deficiency in colonic crypts of female WtN+ mice throughout generations 1, 2 and 3. Levels of complex I (**A**), complex III (**B**), complex IV (**C**) and complex V (**D**) deficiency were plotted. Severe overall deficiency was only seen in complex I. G stands for generation. Z is z-score. CI is complex I. CIII is complex III. CIV is complex IV. CV is complex V. Dots are mean ± SEM for each generation and deficiency z-score. Shading represents different cut-offs for classing crypts as deficient (z-scores of <-6 / <-4.5 / <-3). P is p-value for unpaired t-test of z<-3 between G2 and G3.*

Quadruple immunofluorescence was used to detect OXPHOS activity in complexes I and IV in individual skeletal muscle fibres. For each complex, individual fibres were classified into groups as per colonic crypts. For complex I, there was a trend of decreasing proportions of deficient fibres across generations G0 to G1, becoming near absent in G2/G3, although this did not reach statistical significance (Figure 4.14A). Defects were minimal in all generations for complex IV (Figure 4.14B).

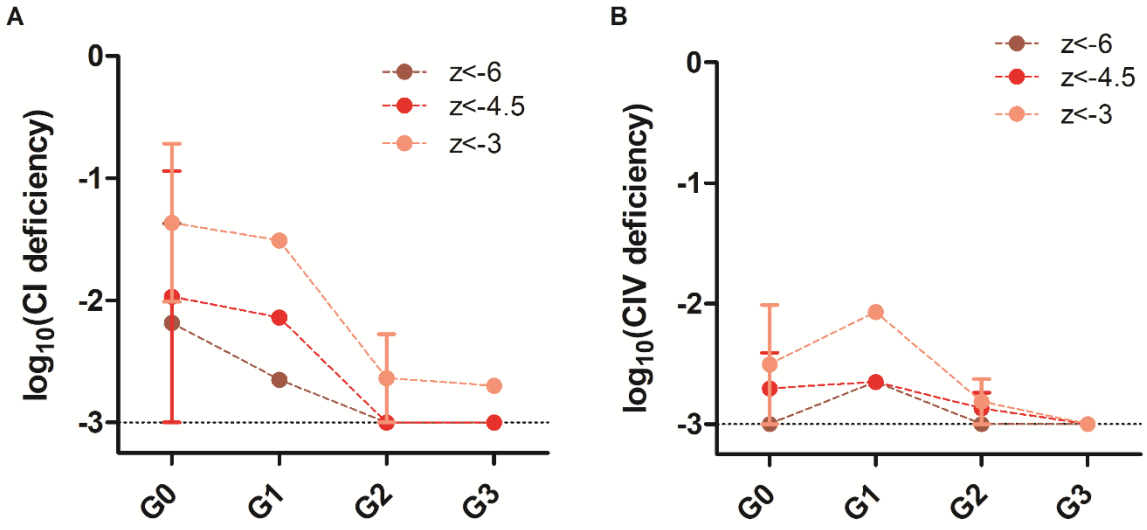

*Figure 4.14. OXPHOS complexes deficiency in skeletal muscle fibres of female WtN+ mice throughout generations 0, 1, 2 and 3. Levels of complex I (**A**) and complex IV (**B**) deficiency were plotted. G stands for generation. Z is z-score. CI is complex I. CIV is complex IV. Dots are mean ± SEM for each generation and deficiency z-score. Shading represents different cut-offs for classing crypts as deficient (z-scores of <-6 / <-4.5 / <-3).*

4.5 Discussion

The WtN+ derivative of the *PolgA* mutator mouse contained a germline mtDNA mutational burst on a wild-type inbred nuclear background (C57BL/6J). There were some challenges in breeding the mice. Initial intercrosses to produce a homozygous mutant female were successful as was generation of heterozygous female offspring from this female, which were expected to contain high levels of germline mtDNA mutations (G0). Low fecundity was however encountered at the stage of breeding from the G0 female mice by back-crossing them with wild-type male mice to restore polymerase γ function in the offspring. As founder heterozygous *PolgA* mice, i.e., those without germline mtDNA mutations, usually breed well, it is assumed that the high numbers of germline mutations introduced may have been responsible for the low fertility, small litter sizes and miscarriages that were observed. *Ross, Stewart and colleagues* found that the germline-transmitted mtDNA mutations that they introduced into heterozygous mice (*PolgA*$^{wt/mut}$) led to reduced fertility, together with other health impairments. These mice produced low litter sizes when intercrossed with male heterozygous 'mutator' mice to generate homozygous (*PolgA*$^{mut/mut}$) mice. However, backcrossing with wild-type mtDNA improved litter sizes (Ross *et al.*, 2013). These findings by the Larsson group somewhat contradicted the observations in this study, as I observed reduced fertility also when backcrossing to wild-type. However, as our G0 heterozygous animals were the offspring of a homozygous *PolgA*$^{mut/mut}$ mother, rather than a heterozygous mother as used in the original Ross paper, the greater burden of germline mtDNA mutations that I generated is likely to have further exacerbated low fecundity. Once the G1 generation of WtN+ mice was established, breeding was then normal or near normal.

To further investigate fecundity in this mouse model, future work could examine oocytes and embryos from these mice to determine whether I am seeing embryonic lethality or adult infertility.

Cellular mtDNA content in mouse tissue homogenates from the offspring of the homozygous *PolgA*$^{mut/mut}$ mother showed no significant difference in ear tissue taken at early life stage, 4 weeks old, between G0-G3 female generations. Such lack of difference indicates that successive generations of these female mice produced from the mutator mouse were born with a very similar amount of mtDNA content and that the germline mtDNA mutations introduced did not have an effect on mtDNA copy

number in early life. Similarly, no differences in mtDNA CN were observed in skeletal muscle at 70 weeks of age, which correlates with the findings obtained in quadruple immunofluorescence for complex I and complex IV, showing minimal defects. In contrast, mtDNA CN in colon at 70 weeks of age was significantly elevated in G0 when compared to the following generations. The regulation of colon mtDNA CN in successive generations G1-G3 may indicate a compensatory response, as G1-G3 showed a decrease in respiratory chain complex I deficiency. At the age of 70 weeks, mtDNA CN levels in frontal cortex were also significantly higher in G0, and decreased in successive generations G1, G2 and G3, again suggesting a possible compensatory regulation of mtDNA levels in response to the germline mtDNA mutational burst. Unfortunately, no immunofluorescence or sequencing was performed in these brain samples, as the main focus of this investigation were colon and skeletal muscle.

The results for the ear clipped tissue (age ~4 weeks) cannot be compared in the same manner as the other tissues, because colon, skeletal muscle and brain were taken at the point of euthanasia (age ~70 weeks). MtDNA content in ear tissue accounted for purely mtDNA germline transmission whereas colon, skeletal muscle and brain results were likely to be subjected to clonal expansion of germline mtDNA mutations (and in the case of G0 only, also of somatic mtDNA mutations).

Deep sequencing of the mitochondrial genome in ear clipped specimens obtained at weaning showed that, although the increase in heteroplasmic variants across generations was significant for all types, high levels of heteroplasmy were achieved mostly in protein-coding gene variants (synonymous and non-synonymous) in generation 3 as opposed to rRNA and tRNA variants. Protein-coding region mtDNA variants were tolerated to reach higher levels. In contrast, rRNA and tRNA variants did not reach high heteroplasmy levels in the last generation, indicating a plausible mechanism for selection against these mutations during germline transmission (results from Figure 4.7). These findings disagree with those from *Stewart and colleagues'* where they saw a strong purifying selection against non-synonymous variants but less intense in rRNA or tRNA variants in mtDNA mutator mice (Stewart *et al.*, 2008), whereas here protein-coding variants seemed to be less selected against compared to tRNA mutations. Moreover, *Stewart et al* did not look at all the mtDNA variant types and track each variant's heteroplasmy in the way presented in this investigation, making our data more reliable.

In terms of overall variant frequency, mtDNA sequencing indicated a strong selection against mutations in protein-coding genes, rRNA and tRNA genes, as showed in previous Figure 4.8. Such purifying pattern of mtDNA variants per bp is consistent with the known maternal germline purifying selection (Stewart *et al.*, 2008; Stewart and Larsson, 2014).

Founder heterozygous *PolgA* mice were sequenced in order to compare their mtDNA variant load to that of the WtN+ mice. Basically, newly formed somatic mtDNA mutations (which should be all that F0 heterozygous contain) did not reach very high heteroplasmy levels compared with the variants seen in the WtN+ animals. This probably suggests that the series of embryonic bottlenecks that the mtDNA variants pass through once ‘trapped’ in the germline of WtN+ mice allows them to progressively ‘ratchet up’, hence the increases in heteroplasmy seen with each generation, from the initial low heteroplasmy levels seen for somatic mtDNA variants.

Number of mtDNA variants per base pair are also lower in the F0 heterozygous than any of the WtN+ mice (Figure 4.8), but this is likely because the WtN+ mice were generated through a homozygous mutator mother, which will create a lot more new variants than a heterozygous mother.

Quadruple immunofluorescence in colon showed complex I deficiency decreased within generations G1-G3 in WtN+ female mice. The same significantly decreasing trend of deficiency was observed for complex III between G1-G3, however complex IV and V were not affected. Comparison of these changes to those seen for the mtDNA mutations on deep sequencing, showed that the earlier generations (which had the highest levels of respiratory chain deficiency) were those with the highest numbers of mutations at baseline, rather than those with the highest baseline heteroplasmy levels.

Skeletal muscle showed no significant complex I and complex IV defect levels across generations, presumably because mtDNA point mutations generally need to achieve extremely high heteroplasmy levels to cause OXPHOS defects in skeletal muscle, as opposed to mtDNA deletions.

Overall, the level of all respiratory complexes deficiency decreased along generations.

Z-scores of -3 to -4.5, which have been termed as ‘intermediate positive’ for studies of human skeletal muscle, should be interpreted with caution in the present study because no previous studies have validated criteria for respiratory chain intermediate crypts in mice. However, in order to make analysis more practical, z-scores of -3 were used as a cut-off above which values were considered normal and below abnormal.

4.6 Conclusion

This breeding strategy successfully produced a new derivative of the *PolgA* mouse ‘WtN+’ which transmitted multiple mtDNA point mutations down the maternal line. These mutations showed a full range of heteroplasmy levels, and showed expected features of drift of mutation levels within mother/offspring pairs, and selection against certain mutation types.

Breeding through a homozygous *PolgA* mother led to an increase in germline mtDNA mutations, but at the expense of reduced fertility in its offspring.

Point mutations were well conserved through successive generations of WtN+ mice, suggesting that this model can be taken forward as a tool in which to track the clonal expansion of these mutations over time.

Chapter 5. Phenotypic characterization of the *PolgA* 'WtN+' mouse

5.1 Introduction

Phenotyping scoring systems are an important tool for evaluating mouse models of various diseases. The mtDNA 'mutator' mouse contains a deficient proofreading pol γ, which accumulates high levels of somatic mtDNA mutations during its life and a premature progeroid phenotype including hair loss, weight loss, shortened lifespan, reduced subcutaneous fat, greying, sarcopenia, kyphosis, anaemia and cardiac hypertrophy (Trifunovic *et al.*, 2004; Kujoth *et al.*, 2005; Trifunovic *et al.*, 2005). These features of accelerated ageing in homozygous mutator mice were not detected in heterozygous mice, even though they showed higher mtDNA mutations compared to wild-type mice (Trifunovic *et al.*, 2004; Vermulst *et al.*, 2007). However, it was later reported that despite the motor function in heterozygous mice not being affected, significant metabolic defects were reported showing that both homozygous and heterozygous *PolgA* mice exhibit mitochondrial dysfunction (Dai *et al.*, 2013), although possibly reached at a different threshold in each genotype.

In the present study, a series of non-invasive methods were used to phenotype the WtN+ mice, our derivative of the *PolgA* mtDNA 'mutator' mouse, and compared with wild-type control mice (wt). The use of standardised phenotypic tests has become common practice when developing mouse models in order to characterise particular genotypes and link them to behavioural phenotypes.

Open field activity tests are a popular assessment tool used to investigate animal ambulatory behaviour and locomotor function, although the animal's intrinsic response to stimuli and exploration is not fully understood. Metabolic treadmill tests are widely used as a way to characterise the cardiovascular fitness of mice (Petrosino *et al.*, 2016), of importance because age-related cardiomyopathy has previously been reported in mutator mice (Zhang *et al.*, 2003; Dai *et al.*, 2010). Moreover, exercise has been proven to alleviate the muscle ageing phenotype in the mutator mice (Safdar *et al.*, 2011; Safdar *et al.*, 2016) not by reducing the mtDNA mutational load but by decreasing the non-mutational oxidative DNA damage. Forelimb grip strength tests have been used for many years to detect skeletal muscle dysfunction in mice, particularly in rodent models of neuromuscular disorders (Takeshita *et al.*, 2017). The International Mouse Phenotyping Consortium (IMPC)

created a phenotyping pipeline called IMPReSS which is seen as the gold-standard for mouse phenotyping methodology; in which open field and grip strength tests are considered mandatory tests and calorimetry (metabolic treadmill) as non-mandatory (Dickinson *et al.*, 2016).

Modelling the age-related changes across the lifespan of mice aims to make a correlation to those observed in humans. Studies comparing life phases in C57BL/6J mice and humans showed that although they both have different maturational rates, i.e. rates in mice are faster than humans; there are some life phase equivalents between them (Figure 5.1). Adult mice from 12-24 weeks (3-6 months) would be equivalent to humans ranging from 20-30 years old. Mice from 40-56 weeks (10-14 months) would correlate to 38-47 years in humans; and finally an old stage of 72-96 weeks in mice would correlate to 56-69 years old in humans (data from The Jackson Laboratory website).

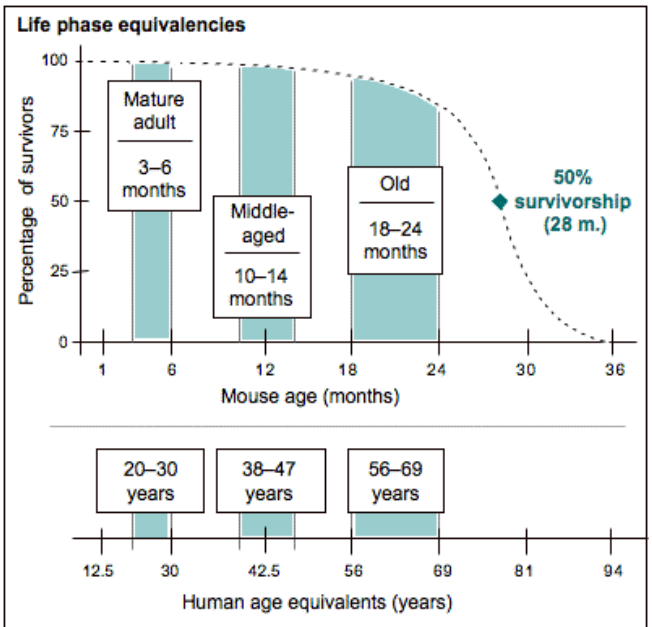

Maturational rate comparisons

Ages	Mouse vs. human
Birth–1 month	150 times faster
1–6 months	45 times faster
6+ months	25 times faster

Figure 5.1. Life history stages in C57BL/6J mice in comparison to human beings. Data adapted from Flurkey, Currer, and Harrison, 2007. "The mouse in biomedical research" in James G. Fox (ed.), American College of Laboratory Animal Medicine series (Elsevier). Figure taken from the JAX® website.

5.2 Aims of this investigation

The goal was to use functional assessments to determine the phenotype of the animals in the study, *PolgA* WtN+ mice, in three representative lifespan time points; 18, 35 and 47 weeks old, representing young, early middle-aged and late middle-aged mice.

5.3 Methodology

5.3.1 Mouse cohort

Mice were sexed during genotyping. Genotyping was carried out at 4 weeks old, which was the weaning time, and littermates were separated in different cages according to genotype and sex. Further genotyping details were detailed in Section 2.2.2.

5.3.2 Phenotypic testing

Phenotypic tests included clinical scoring, open field tests, metabolic treadmill and grip strength tests as described in Section 2.2.

5.3.3 Statistical analysis

Differences between mice groups were carried out using two-way ANOVA, or two-tailed unpaired t-test as appropriate. When one-way ANOVA was significant, a post test for multiple comparisons between means was performed if relevant. $P<0.05$ was used to define statistical significance.

5.4 Results

5.4.1 Body weight

Weight measurements were recorded during clinical scoring as detailed in Section 2.2.4. Mice were weighed at a similar time of day to avoid circadian fluctuations. Whilst regular weights were performed for monitoring animal welfare, the three key phenotyping time points (18, 35, 47 weeks) are presented here as outcome data (Figure 5.2). Data were analysed for both sexes and genotypes: WtN+ females, WtN+ males, wild-type females and wild-type males.

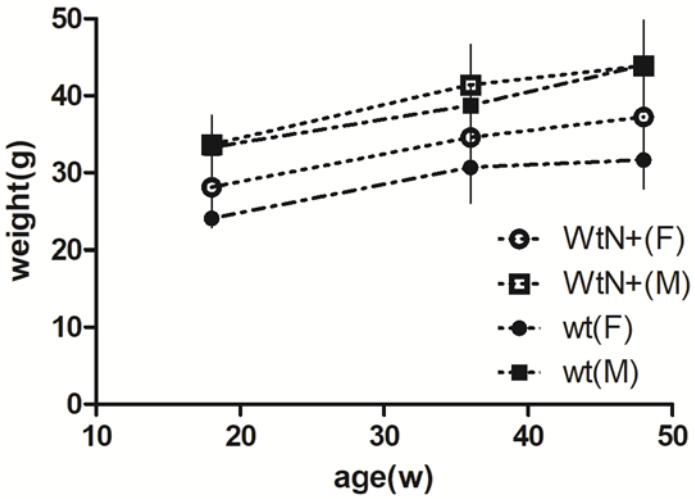

Figure 5.2. Growth curves of WtN+ and wt mice. This plot shows the mice body weight at the three key time points (18, 35, 47w; the dot is mean and error bars are SEM; weights from ±1w). (F) is female and (M) is male. (g) is grams and (w) is weeks.

A two-way ANOVA was performed for each sex, to assess whether there was an interaction between age and genotype on weight. For females, both age ($p<0.0001$) and genotype ($p=0.0004$) are significantly associated with weight. For males, only age is associated ($p<0.0001$) with weight. In both sexes, there was no interaction between age and genotype on weight.

Upon tissue dissections, all organs were weighed and there were no consistent effects of WtN+ genotype observed.

5.4.2 Open field tests

Data were retrieved from the tablet tracking software following open field testing. Measurements were used from the first 300 seconds (5 minutes) of the test where the mouse was allowed to freely explore the open field. Locomotor activity collected by the MouseTrapp (Neurolytical) software included: number of touches (n), number of rears (n) (number of times the mouse stood on its hind paws), total distance moved (cm), average velocity (cm/millisecond) and average step length (total number of touches divided by total distance travelled, in cm).

On one-way ANOVA there was no significant difference between any of the groups at 35 and 47 weeks old in any of the measures; the number of touches or steps (Figure 5.3A), the rearing events (Figure 5.3B), the distance explored (Figure 5.3C), the velocity of the mice (Figure 5.3D) and step length throughout the duration of the test (Figure 5.3E).

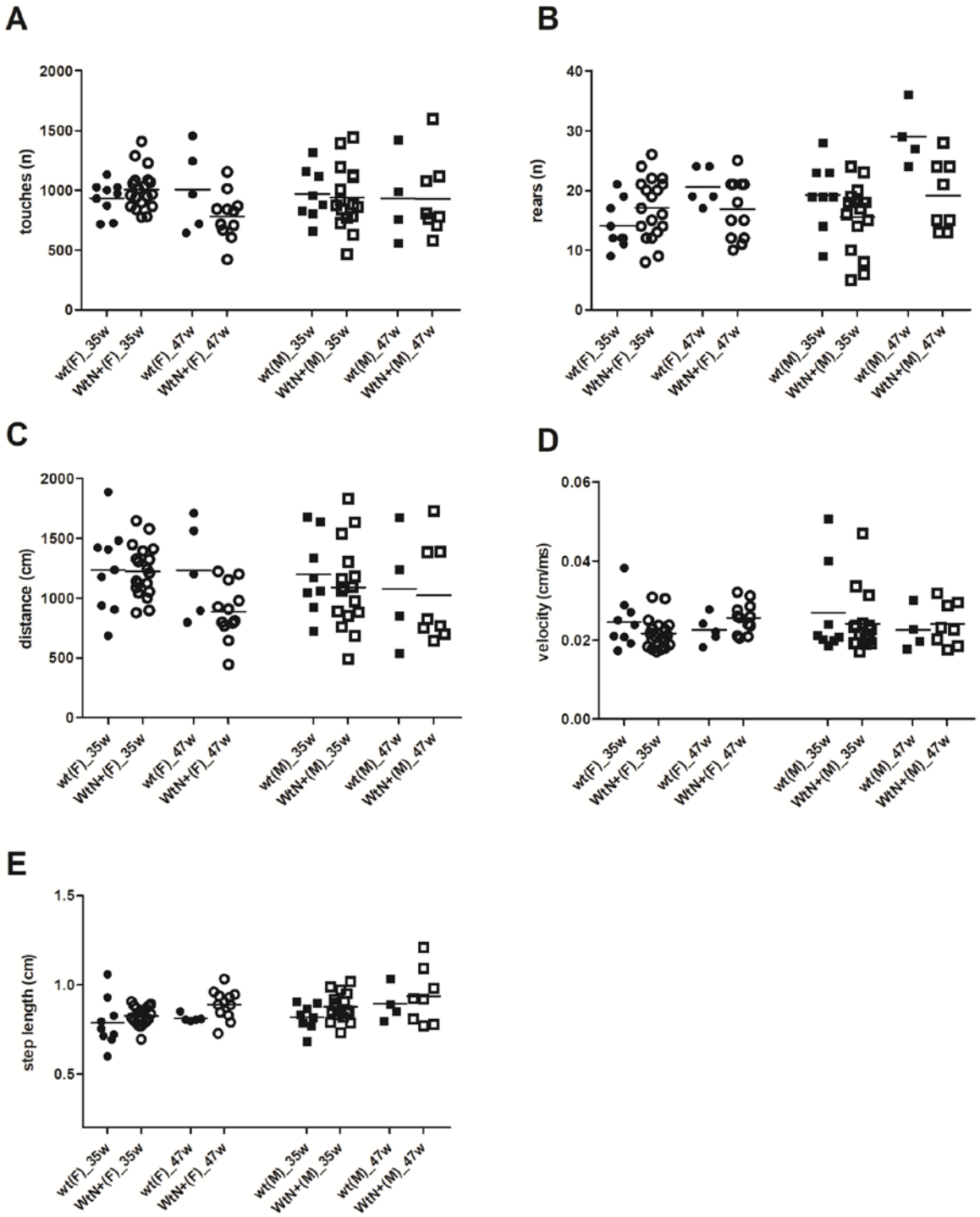

*Figure 5.3. Dot plot figures showing the open field test values for both sexes, genotypes and age. Open field values measured were number of touches (**A**), number of rears (**B**), distance explored by the mice (**C**), the velocity they kept (**D**) and the step length (**E**). Each dot represents an individual animal. Line at mean. (n) is number. (cm) is centimetre. (cm/ms) is centimetre per millisecond. (F) is female and (M) is male. W is weeks.*

For open field activity tests, a longer time point of 75 weeks was also taken for a subset of WtN+ females (n=5) along with the time points of 35 and 47 weeks. This 75-week female time point was then compared to the previous time points in WtN+ female mice only. One-way ANOVA showed significant differences between the WtN+ females at the three time points (35, 47 and 75 weeks) in number of touches ($p=0.0006$; Figure 5.4A), distance moved ($p<0.0001$; Figure 5.4C), velocity ($p=0.002$; Figure 5.4D) and step length ($p=0.02$; Figure 5.4E) but not in rearing behaviour (Figure 5.4B). Despite these statistically significant differences, none of the parameters appeared to show a progressive change with ageing.

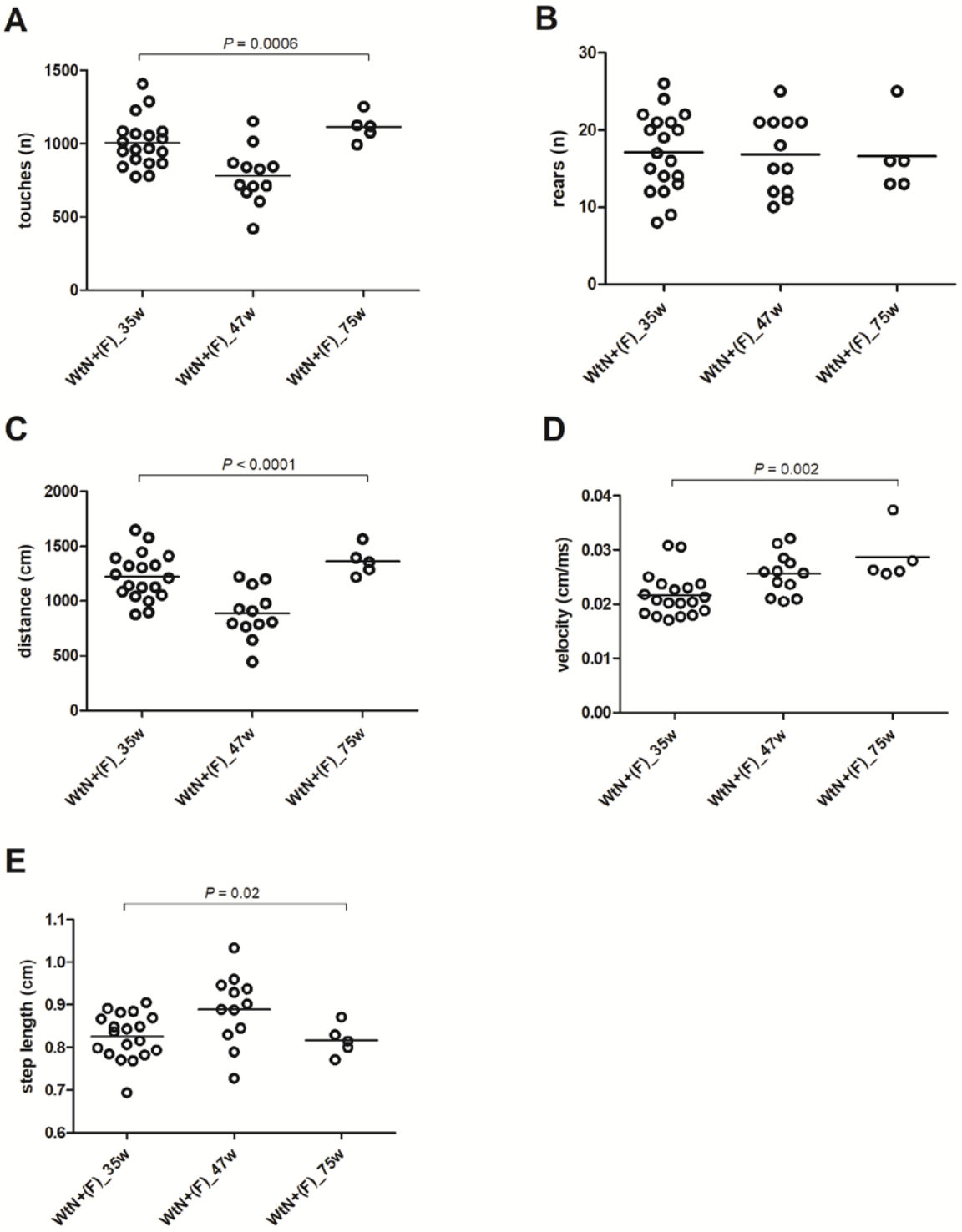

*Figure 5.4. Dot plot figures showing the open field test values for WtN+ females across the three time points (35, 47 and 75 weeks old). Open field values measured were number of touches (**A**), number of rears (**B**), distance explored by the mice (**C**), the velocity they kept (**D**) and the step length (**E**). Dots represent individual mice. Line at mean. (n) is number. (cm) is centimetre. (cm/ms) is centimetre per millisecond. (F) is female. W is weeks. P-values are one-way ANOVA.*

5.4.3 Metabolic treadmill tests

Metabolic parameters were measured while the mice were at rest during the first 15 minutes and for the following 20 minutes during exercise. Owing to the complexity of the protocol, metabolic treadmill was performed on a subset of representative females (n=5 WtN+ and n=5 wild-type). The metabolic treadmill provided cardio-metabolic parameters including volume of oxygen consumption (VO_2), volume of carbon dioxide produced (VCO_2), and respiratory exchange ratio (RER) through indirect calorimetry and heat production. The gas measurements for oxygen and carbon dioxide were normalized to animal body weight and expressed in ml/kg per hour. RER is the unit-less ratio of the rate of carbon dioxide production to the rate of oxygen consumption (VCO_2/VO_2). When the animal is metabolizing pure fat for energy, its RER is close to 0.70, whereas if it is using pure carbohydrates, RER is close to 1.0 (Issekutz *et al.*, 1962). Accordingly, an indication of maximal exertion is achieved when RER is ≥ 1.0 but none of the mice were exerted to this level since it was not the objective of this study.

Generally, resting parameters were all lower at 47 weeks than 35 weeks, suggesting that mice became less active at rest as they aged (Figure 5.5A-D).

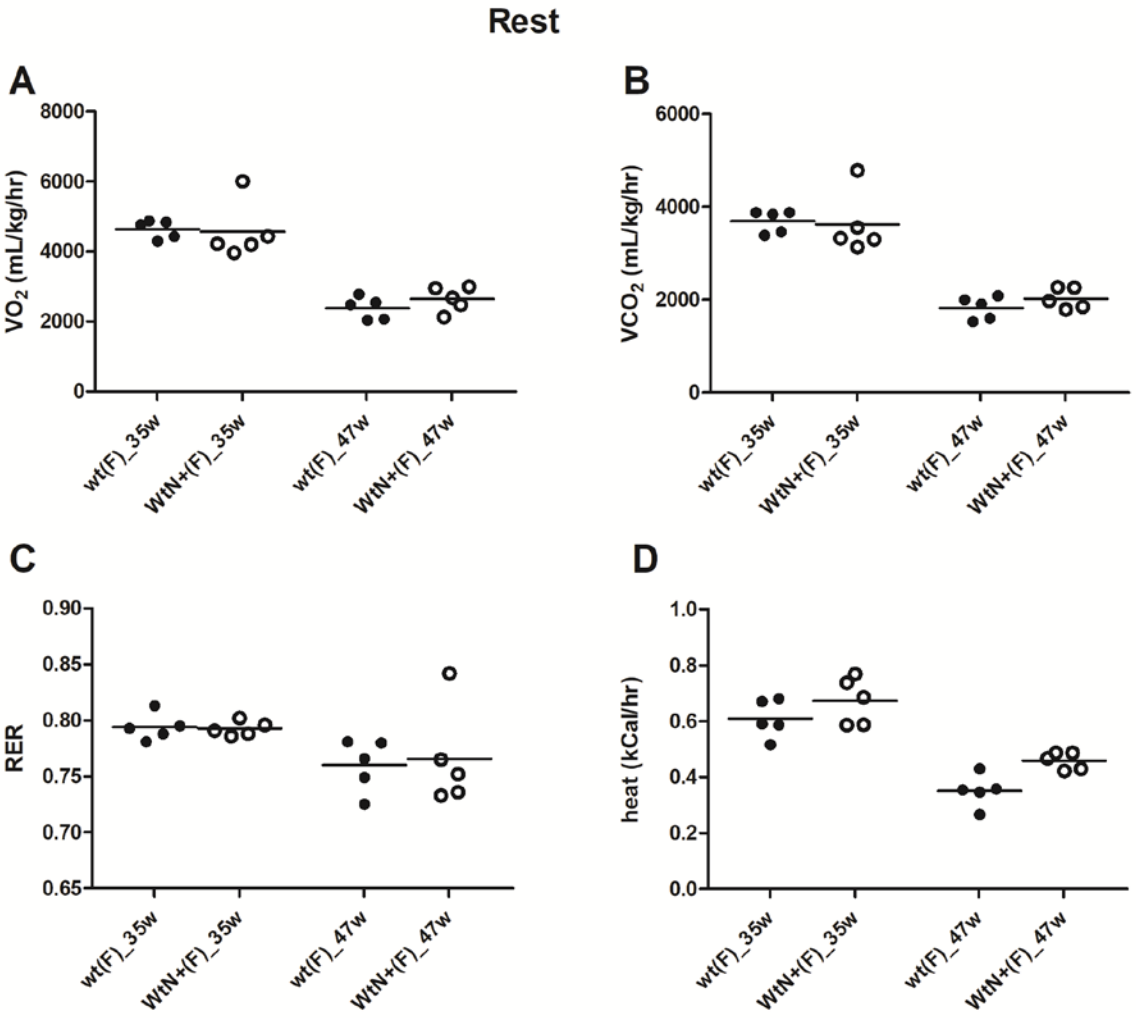

*Figure 5.5. Dot plots showing the metabolic treadmill values at rest for both genotypes and age. Values were oxygen consumption (**A**), CO_2 produced (**B**), respiratory exchange ratio (RER, **C**) and heat produced (**D**). Each dot is the measurement of a single mouse. Line at mean. (F) is female. W is weeks.*

A two-way ANOVA for genotype and age was performed to assess the effect of these factors on metabolic values. Age was found to be significantly associated with all the cardio-metabolic measures at rest, VO_2 ($p<0.0001$), VCO_2 ($p<0.0001$), RER ($p=0.02$) and heat ($p<0.0001$). Genotype was only significantly associated with heat production ($p=0.02$) but not with the rest of the parameters. No significant interactions between age and genotype were detected on any of the metabolic treadmill parameters (Table 5.1).

	Age	genotype
VO_2	$p<0.0001$	NS
VCO_2	$p<0.0001$	NS
RER	$p=0.02$	NS
Heat	$p<0.0001$	$p=0.02$

Table 5.1. Tabular results of two-way ANOVA by age and genotype of the metabolic treadmill values (VO_2, VCO_2, RER and heat). NS is non-significant. P is p-value.

During exercise, no significant differences by age or genotype (or interaction of age and genotype) was found in any of the parameters (Figure 5.6A-D).

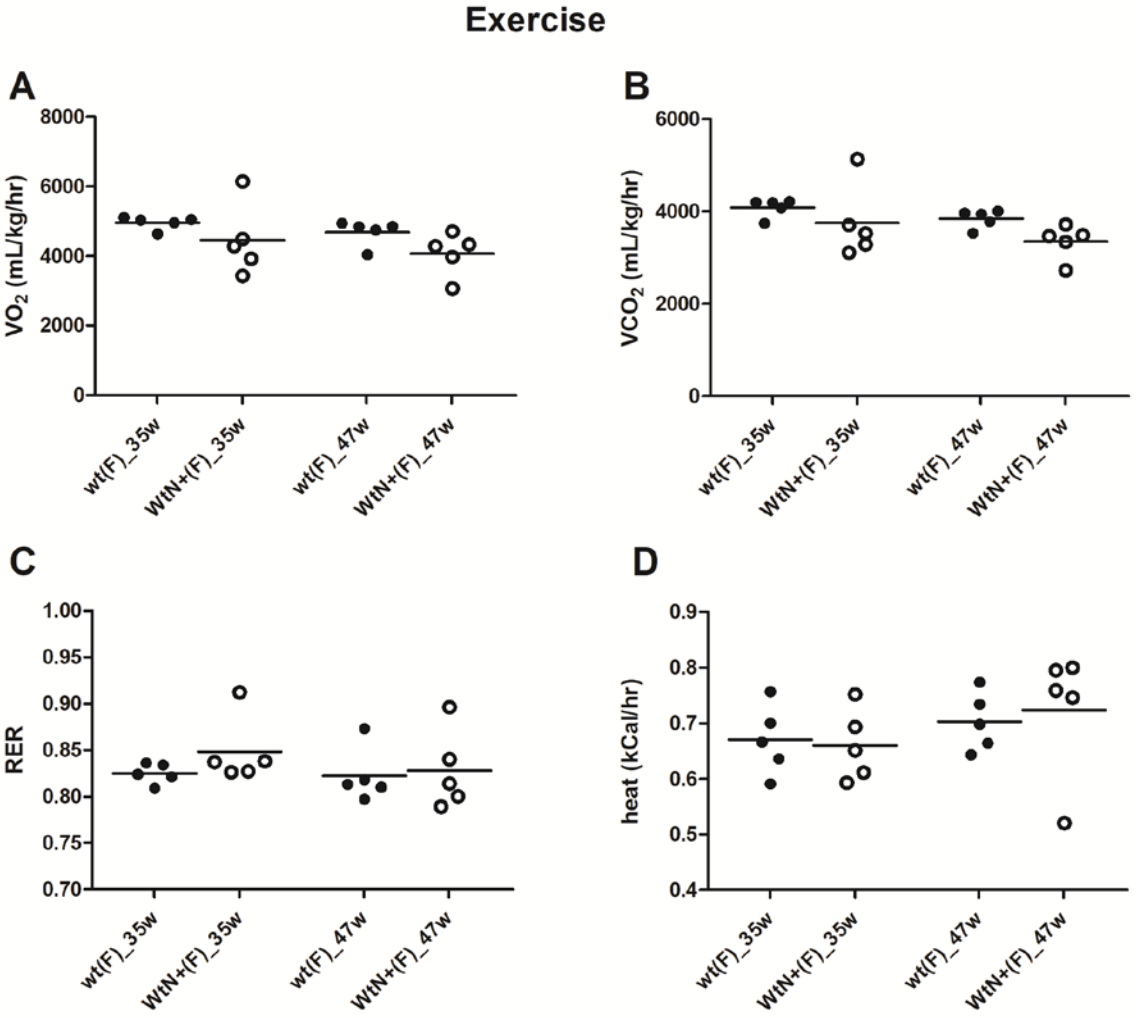

*Figure 5.6. Dot plots showing the metabolic treadmill values during exercise for both genotypes and age. Values were oxygen consumption (**A**), CO_2 produced (**B**), respiratory exchange ratio (RER, **C**) and heat produced (**D**). Each dot is the measurement of a single mouse. Line at mean. (F) is female. W is weeks.*

For metabolic treadmill, a longer time point of 75 weeks was also taken for a subset of WtN+ females (n=5) along with the primary outcome time points of 35 and 47 weeks. This 75-week time point was then compared to the previous time points in WtN+ female mice only. At rest, one-way ANOVA between the WtN+ females in the three established time points (35, 47 and 75 weeks) showed a significant decrease in volume of oxygen consumption ($p<0.0001$; Figure 5.7A), volume of carbon dioxide produced ($p<0.0001$; Figure 5.7B) and mouse heat production ($p<0.0001$; Figure 5.7D) but not in RER (Figure 5.7C) over the time studied. Moreover, post tests for trend analysis in VO_2 ($p<0.0001$), VCO_2 ($p<0.0001$) and heat ($p<0.0001$), showed a significant linear decreasing trend.

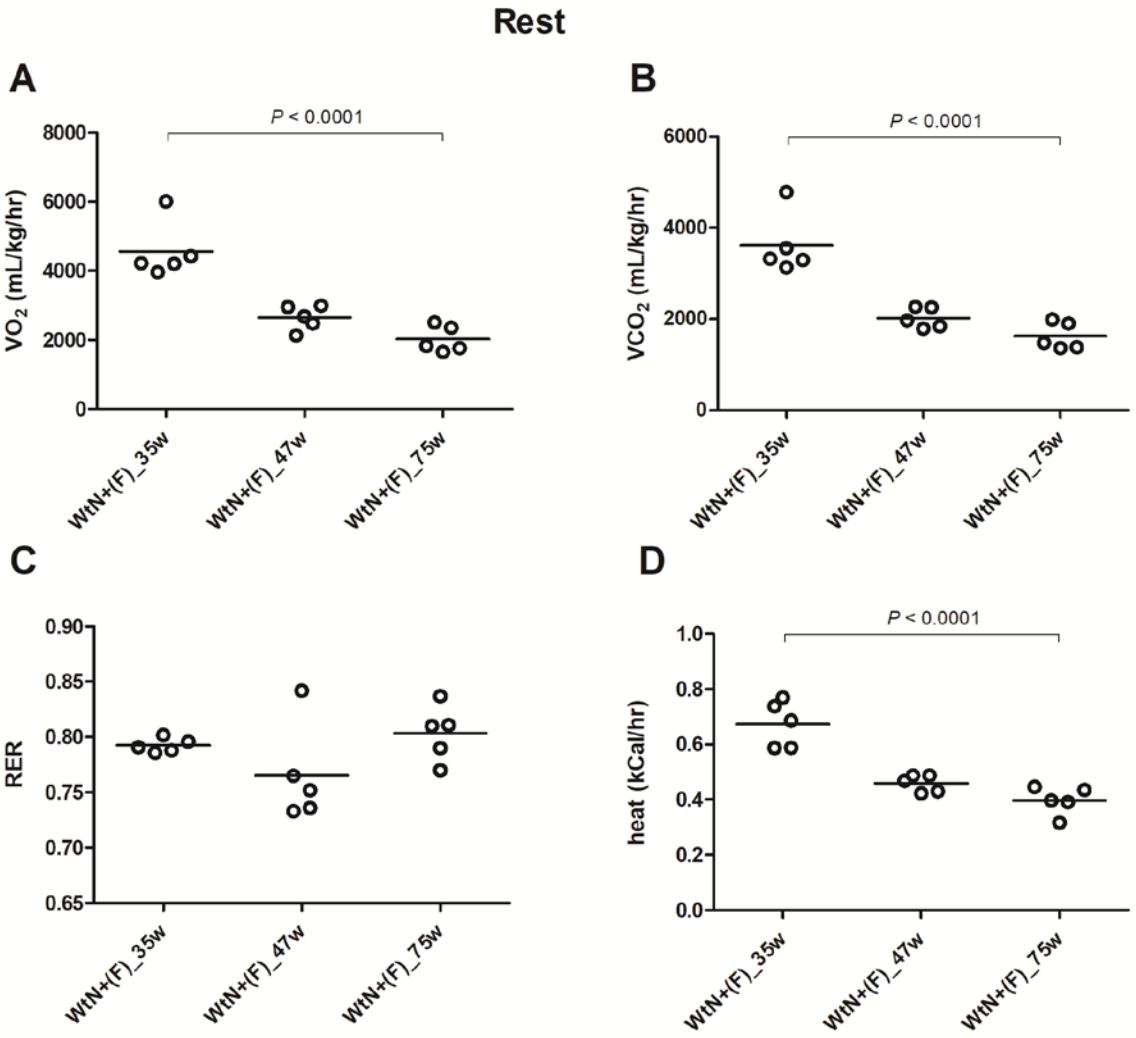

*Figure 5.7. Dot plots showing the metabolic treadmill values at rest for WtN+ females at the three time points (35, 47 and 75 weeks). Values were oxygen consumption (**A**), CO_2 produced (**B**), respiratory exchange ratio (RER, **C**) and heat produced (**D**). Each dot is the measurement of a single mouse. Line at mean. (F) is female. P-values are one-way ANOVA. W is weeks.*

During exercise, one-way ANOVA between the WtN+ females showed no significant changes in the metabolic treadmill values (Figure 5.8A,C,D) except for a significant decrease of CO_2 produced over time (p=0.04; Figure 5.8B). Post-test for linear trend in CO_2 also showed a significant linear trend (p=0.01).

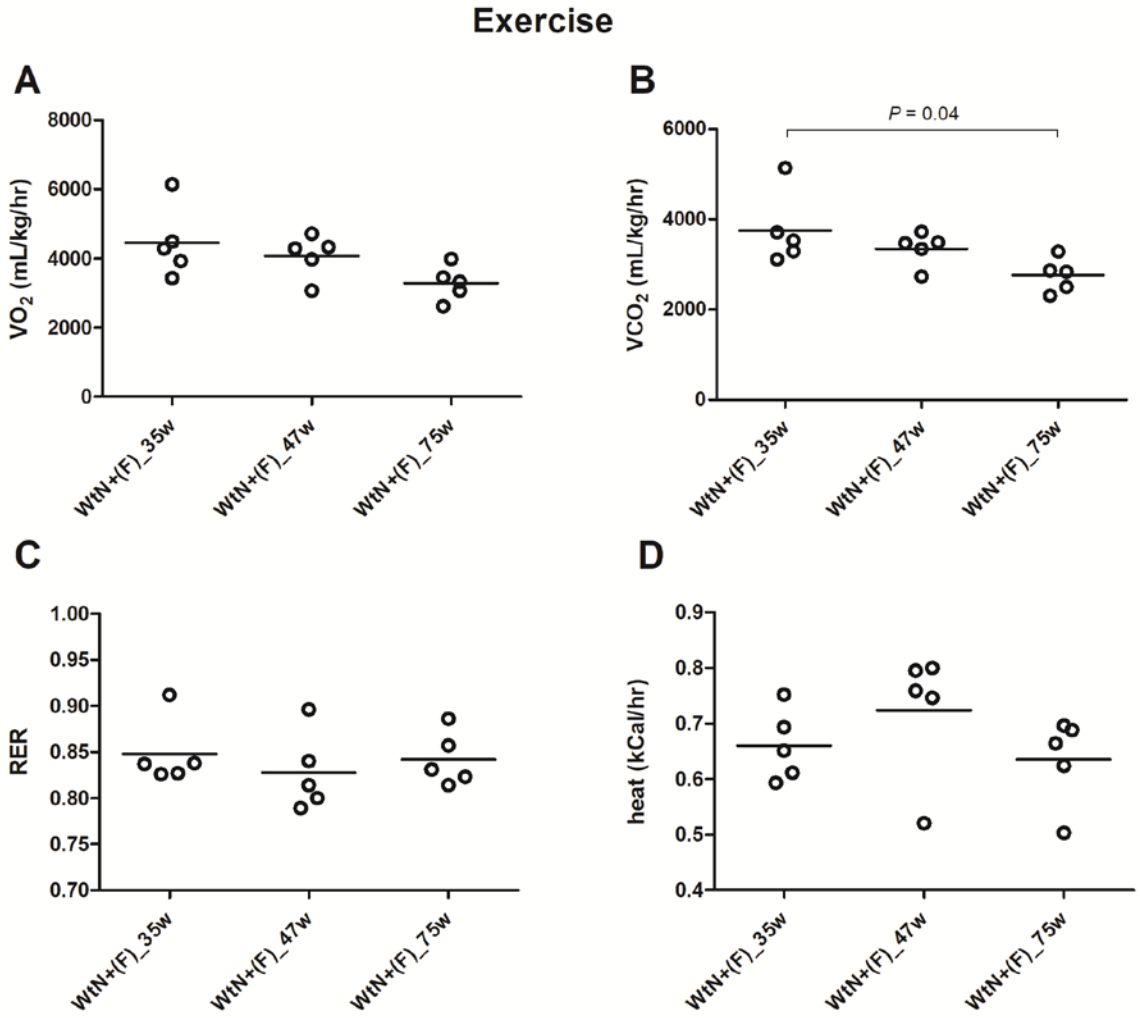

*Figure 5.8. Dot plots showing the metabolic treadmill values during exercise for WtN+ females at the three time points (35, 47 and 75 weeks). Values were oxygen consumption (**A**), CO_2 produced (**B**), respiratory exchange ratio (RER, **C**) and heat produced (**D**). Each dot is the measurement of a single mouse. Line at mean. P-values are one-way ANOVA. W is weeks.*

5.4.4 Forelimb grip strength

Grip strength measurements were recorded as described in Section 2.2.7. The three repeats measured were averaged and grip strength values were adjusted for the weight of each mouse, in order to control for the effects of growth and sex.

Data were analysed for both sexes and genotypes: WtN+ females and males, wild-type females and males (Figure 5.9).

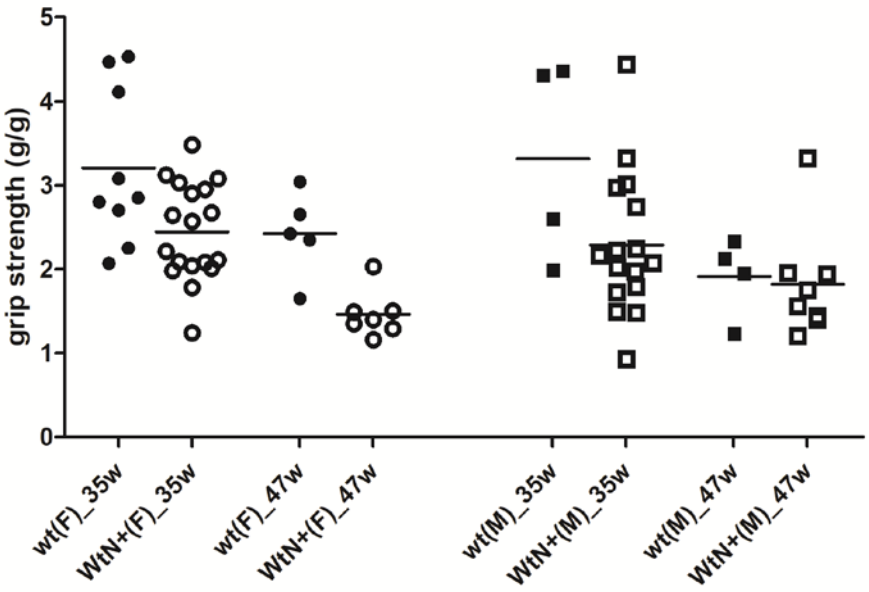

Figure 5.9. Dot plots showing the grip strength values for both sexes, genotypes and age. Each dot is the mean of three grip strength measurements from a single mouse. Line at mean. (F) is female and (M) is male. (g/g) is the grip strength in grams adjusted for the mouse body weight in grams. W is weeks.

Two-way ANOVA showed that both genotype ($p=0.0004$) and age ($p<0.0001$) were significantly associated with grip strength, but there was no interaction between genotype and age on grip strength.

5.5 Discussion

All the *in vivo* functional phenotypic tests aimed to complement each other. There was a significant direct impact of age on weight in both sexes, meaning the mice got heavier as they aged which is in keeping with what is already well-known for inbred male and female mice with a C57BL/6J nuclear background (Figure 5.10). Additionally, WtN+ animals were heavier than wt for females only. The relevance of this finding is not clear, and could be explained by a 'batch effect' as by necessity of the breeding scheme, WtN+ and wt animals were drawn from different litters.

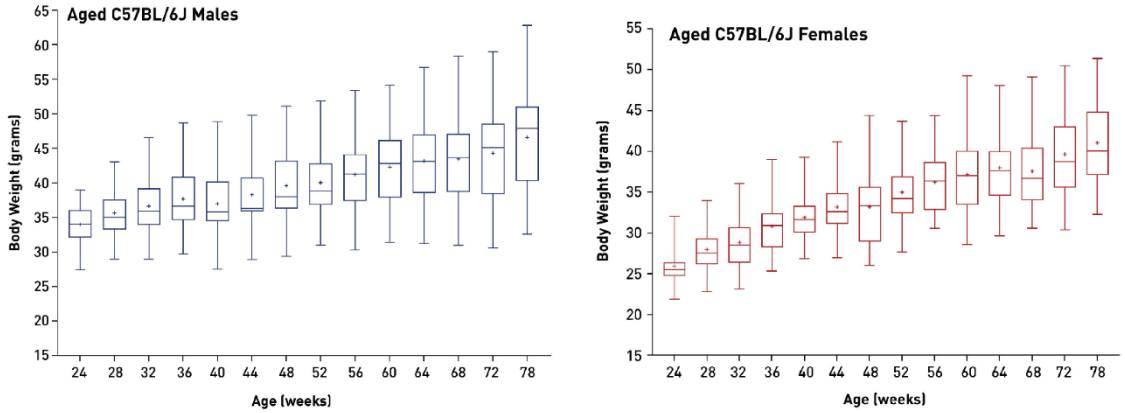

Figure 5.10. Body weight information for aged C57BL/6J (000664) mice from The Jackson Laboratory. Figures taken from the JAX® website. Boxes extend from the 25th to 75th percentile. Box line shows median weight and + shows mean weight. Whiskers for maximum and minimum weights.

The study of the exploratory behaviour in an open field was performed as a single test. Open field tests were first developed in the 1930s in order to assess explorative drive, locomotor activity, thigmotaxis behaviour and anxiety in rodents. As such, open field reflects a combination of physical and behavioural functions. The incorporation of a touch-screen tablet with a specific software tailored to mice allowed for testing of basic locomotor parameters of interest in this study. When looking at wild-type and WtN+ female and male mice in the two time points, 35 and 47 weeks old, there was no significant change in any of the parameters. When comparing the female WtN+ groups to the extended time point, 75 weeks old, there were some significant differences between the groups, however they were not consistent across the locomotor parameters and it was concluded that there was no progressive age-related deterioration in open field parameters in WtN+ mice.

To establish the cardio-metabolic phenotype of mice, the metabolic treadmill was used to functionally assess the metabolic rate. Oxygen consumption (VO_2) and expiration of CO_2 were the key outputs. Impaired levels of cardio-metabolic fitness could not be detected in WtN+ compared with wild-type animals. It could be argued that the metabolic variables reported in this animal assay might not be sufficiently sensitive to detect small impairments in cardiovascular fitness. For a more stringent and human-equivalent assessment, more variables could ideally have been investigated, such as lactate concentrations, the threshold at which aerobic metabolisms shifts to anaerobic metabolisms etc. However, these values are quite difficult to assess in mouse studies as the one presented here, and those tests that were performed here provide an adequate screen in keeping with recommended phenotyping protocols.

At rest, both wt and WtN+ mice became less metabolically active as they aged, however, during exercise none of the metabolic parameters measured showed any significant differences.

Forelimb grip strength measurements provided information regarding muscle strength. Grip strength (adjusted for body mass) decreased with age in both WtN+ and wt animals. In addition, grip strength was lower in WtN+ compared with wt animals, suggesting some impairment of skeletal muscle function resulting from WtN+ genotype.

5.6 Conclusion

Overall, these findings suggest that the mtDNA mutational burden bred into the WtN+ mice did not reach the threshold needed for a limiting or impaired locomotor and behavioural phenotype, but may cause some decrease in muscle strength.

Chapter 6. Mitochondrial, cellular and molecular analyses in the WtN+ mouse cohort

6.1 Introduction

The generation and the phenotyping of the WtN+ mouse have been discussed in Chapter 4 and Chapter 5, respectively, and this present Chapter describes its cellular and molecular analyses.

6.2 Experimental Aims

This work aimed to characterise at the cellular and molecular level the mitochondrial dysfunction resulting from mtDNA mutations in the *PolgA* WtN+ mouse cohort in comparison with wild-type (wt) controls.

6.3 Methodology

In total 95 animals were included in the experimental plan. In order to standardise as much as possible the germline mutations between animals, 62 WtN+ experimental animals were generated (G3 in the WtN+ breeding strategy, see Section 4.3.1), all originating from the same WtN+ grandmother. As a control group, 33 wild-type mice were generated by crossing wild-type black 6 (C57BL/6J) females with *PolgA*$^{wt/wt}$ (WtN+) males from the breeding colony.

6.3.1 Tissue processing

Clipped ear tissue was taken at weaning (age ~4 weeks) and was used for genotyping (described in Section 2.2.2), qPCR for mtDNA content, and next generation sequencing to investigate mtDNA mutations. All other tissues were dissected during organ harvesting. Dissecting of mouse tissues was previously explained in Section 2.2.9. DNA used for qPCR and NGS was extracted from tissue homogenates as described in Section 2.4.

6.3.2 Real-time PCR for mtDNA copy number

MtDNA content was expressed relative to cell content and was measured in triplicate by multiplex qPCR amplification of mitochondrial gene *MT-ND5* and the nuclear-encoded housekeeping gene *β-Actin*. Primers and probe sequences for this assay are found in Section 2.6.

6.3.3 Next generation sequencing of mouse mitochondrial DNA

Whole mtDNA genomes were enriched using long-range PCR. Primer sequences and LR-PCR details found in Section 2.9.1.

MtDNA point variants were measured on an Illumina MiSeq platform as described in Section 2.10. Paired-end fastq files were obtained from the MiSeq platform. Bioinformatic sequence analysis and variant calling is described in Section 2.11. Ensembl sequence reference used was mm10 (NC_005089.1). MtDNA point variants present at 2% to 98% heteroplasmy were reported. Coverage graph is found in Appendix 10.9.

6.3.4 Quadruple immunofluorescence for mouse tissues

Quadruple immunofluorescence staining and quantification for mouse colon and skeletal muscle was performed as detailed in Section 2.7. Microscope snaps of a colon (Figure 6.1A) and a skeletal muscle (Figure 6.1B) section are shown below as an example of a WtN+ 48-week mouse.

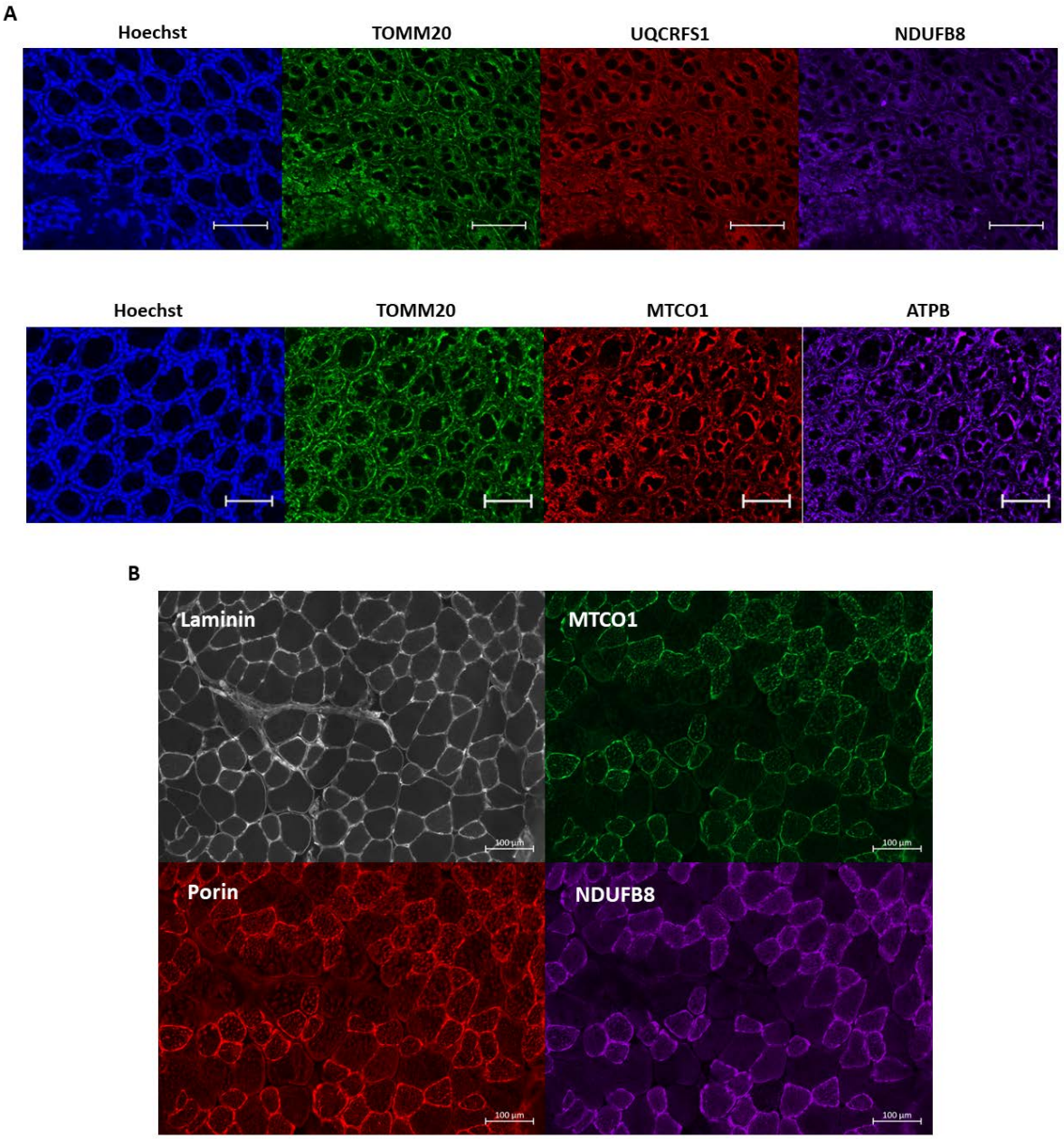

Figure 6.1. Representative immunofluorescence images of a colon and skeletal muscle section of a WtN+ female mouse at 48 weeks. (A) Example of representative immunofluorescence images for FFPE colon section of a WtN+ female mouse at 48 weeks. Hoechst was used as a nuclear counterstain as the colonic crypt boundary. TOMM20 is the mitochondrial mass marker. Staining was performed in serial sections for a NDUFB8 (complex I) and UQCRFS1 (complex III) batch, and a subsequent MTCO1 (complex IV) and ATPB (complex V) batch. (B) Example of representative immunofluorescence images for frozen skeletal muscle section of a WtN+ female mouse at 48 weeks. Laminin is a membrane marker used to define individual fibres. Porin is the mitochondrial mass marker. MTCO1 was used for complex IV and NDUFB8 for complex I. Scale bar is 100 µm.

Additionally, z-score plots were produced to visually give a representation of the level of deficiency for each complex. An example of a z-score plot is found below for complex I and III (Figure 6.2A) and complex IV and V (Figure 6.2B).

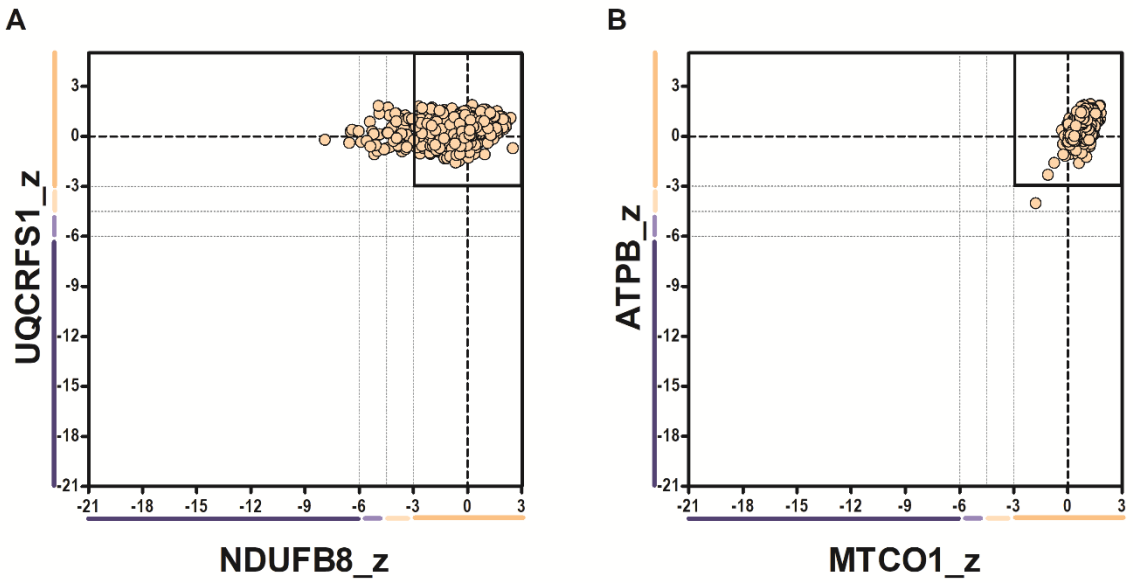

*Figure 6.2. Mitochondrial respiratory chain profiles from immunofluorescence results for FFPE colon of a WtN+ female mouse at 48 weeks. Graph (**A**) demonstrates z-scores distribution for complex I (NDUFB8) and complex III (UQCRFS1); and graph (**B**) for complex IV (MTCO1) and complex V (ATPB). Each point is the z-scores for (**A**) complex I and III or (**B**) complex IV and V for a single colonic crypt. Bars on the X and Y axis indicate category of z-scores: dark blue is negative, light blue is intermediate negative, light beige is intermediate positive and orange is normal. Dashed lines mark the boundaries of these categories.*

6.3.5 Statistical analysis

Statistical testing was performed using SPSS 24 and Prism V5. Non-parametric testing (Spearman correlation) was used for analyses of mtDNA point variants. When one-way ANOVA was significant, a post test for multiple comparisons between means was performed if relevant.

6.4 Results

6.4.1 Cellular mitochondrial DNA content in mouse tissue homogenates

MtDNA content (mtDNA genome copies per cell) did not vary significantly in ear snip tissue between experimental female and male wild-type and WtN+ mice at baseline 4 weeks old (wild-type F, 79 (6), n=16; WtN+ F, 73 (4), n=38; wild-type M, 66 (4), n=24; WtN+ M, 68 (3), n=26; one-way ANOVA, p=0.2; Figure 6.3).

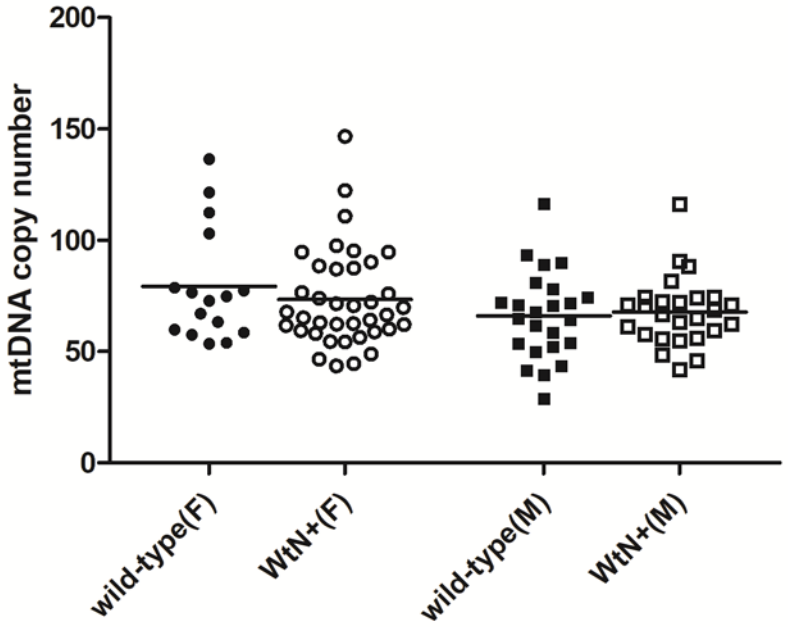

Figure 6.3. Mitochondrial DNA copy number levels in baseline ear tissue of wild-type and WtN+ mice. MtDNA CN in ear was not significantly different between female and male wild-type and WtN+ mice. Every dot represents an individual mouse. Line at mean. (F) is female and (M) is male.

Cellular mitochondrial DNA copy number in homogenised colon throughout the three key harvesting time points (18, 36 and 48 weeks) in wild-type and WtN+ females did not vary (wild-type 18w, 146 (8), n=6; WtN+ 18w, 158 (10), n=6; wild-type 36w, 128 (7), n=4; WtN+ 36w, 139 (7), n=6; wild-type 48w, 141 (9), n=5; WtN+ 48w, 140 (8); one-way ANOVA, p=0.3; Figure 6.4A).

A longer time point of 76 weeks was also taken for a subset of WtN+ females (n=6). This 76-week harvesting female time point was then compared to the previous time points in WtN+ female mice to assess for an age-related trend in mtDNA CN. This analysis showed a significant difference between time points 18, 36, 48 and 76 weeks (one-way ANOVA, $p<0.0001$; Figure 6.4B). Tukey's multiple comparison test showed that mtDNA CN in colon of WtN+ females at 76 weeks was significantly higher compared to all the previous harvesting time points (Figure 6.4B).

Colon mtDNA copy number throughout the three key time points (18, 36 and 48 weeks) did not vary in wild-type and WtN+ males (wild-type 18w, 144 (9), n=10; WtN+ 18w, 156 (8), n=7; wild-type 36w, 149 (11), n=4; WtN+ 36w, 157 (9), n=9; wild-type 48w, 136 (9), n=4; WtN+ 48w, 138 (9), n=8; one-way ANOVA, p=0.5; Figure 6.4C).

MtDNA copy number in colon was not significantly different between genotypes and sex regardless of age at death (wild-type F, 139 (5), n=15; WtN+ F, 158 (6), n=24; wild-type M, 143 (6), n=18; WtN+ M, 151 (5), n=24; one-way ANOVA, p=0.1; Figure 6.4D).

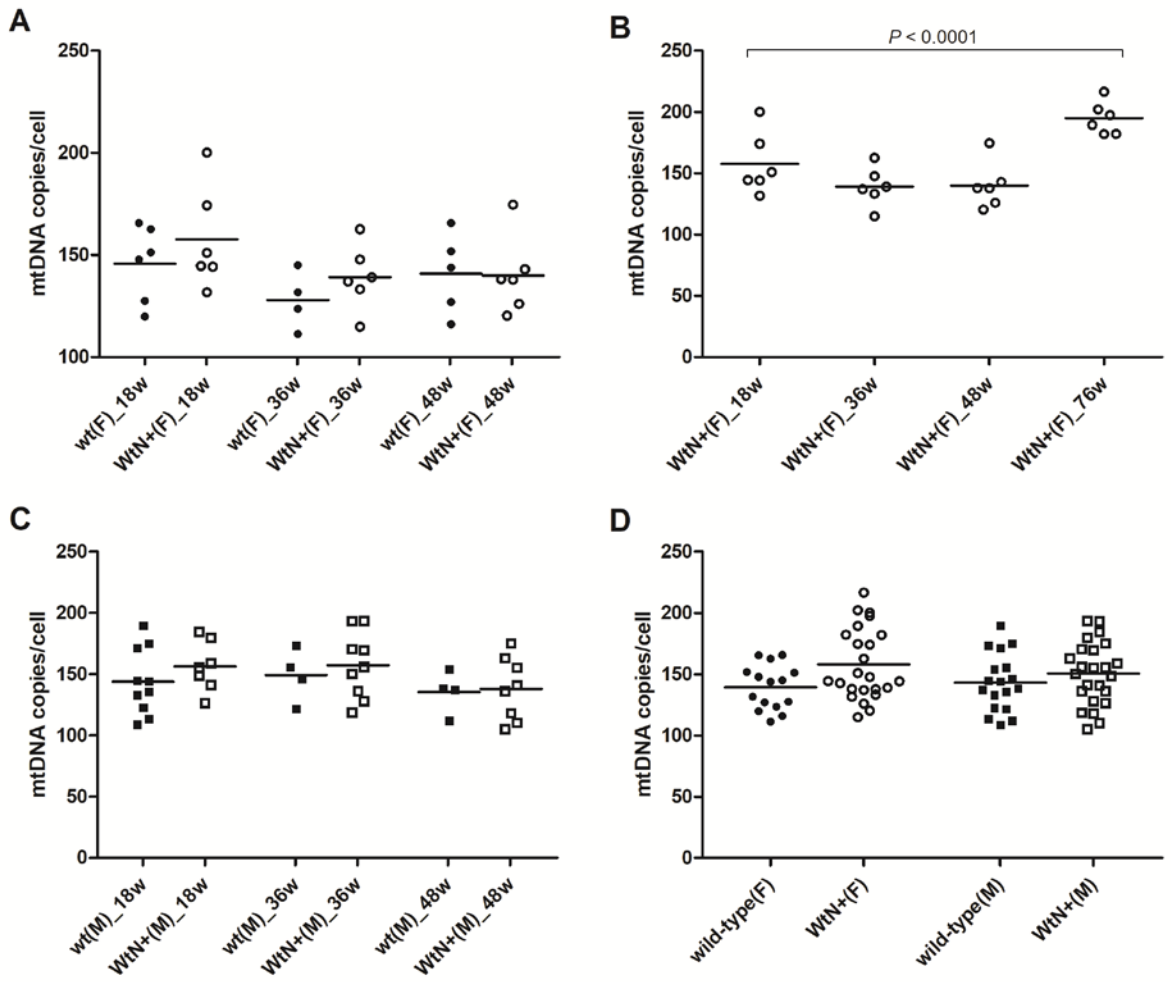

*Figure 6.4. Mitochondrial DNA copy number levels in homogenised colon. (**A**) MtDNA CN in colon of female wild-type and WtN+ mice at 18, 36 and 48 weeks old was not significantly different. (**B**) MtDNA CN levels in colon of female WtN+ mice at 18, 36, 48 and 76 weeks old. MtDNA CN in colon was significantly increased in WtN+ females at the 76-week harvesting time point. P is p-value for one-way ANOVA. (**C**) MtDNA CN levels in colon of male wild-type and WtN+ mice at 18, 36 and 48 weeks old was not significantly different. (**D**) MtDNA CN levels in colon of female and male wild-type and WtN+ mice was not significantly different. Every dot represents an individual mouse. Line at mean. (F) is female. (M) is male. W is weeks.*

Cellular mitochondrial DNA copy number in homogenised skeletal muscle throughout the three key harvesting time points (18, 36 and 48 weeks) in wild-type and WtN+ females did not vary (wild-type 18w, 1773 (359), n=6; WtN+ 18w, 1662 (128), n=6; wild-type 36w, 1500 (198), n=4; WtN+ 36w, 1402 (258), n=6; wild-type 48w, 1240 (244), n=5; WtN+ 48w, 1422 (201); one-way ANOVA, p=0.7; Figure 6.5A).

The longer 76-week time point taken for a subset of WtN+ females (n=6) was then compared to the previous time points in WtN+ female mice which showed no significant difference between time points 18, 36, 48 and 76 weeks (one-way ANOVA, p=0.8; Figure 6.5B).

MtDNA CN in homogenised skeletal muscle was significantly different throughout the three key harvesting time points (18, 36 and 48 weeks) in wild-type and WtN+ males (one-way ANOVA, p=0.0002; Figure 6.5C). When analysis stratified by genotype was performed, mtDNA copy number significantly decreased at the oldest time point in comparison with the younger time points in both wild-type (wt 18w, 1645 (125), n=10; wt 36w, 1386 (83), n=4; wt 48w, 862 (28), n=4; one-way ANOVA, p=0.003; Figure 6.5C) and WtN+ males (WtN+ 18w, 1207 (114), n=7; WtN+ 36w, 1551 (161), n=9; WtN+ 48w, 921 (48), n=8; one-way ANOVA, p=0.005; Figure 6.5C).

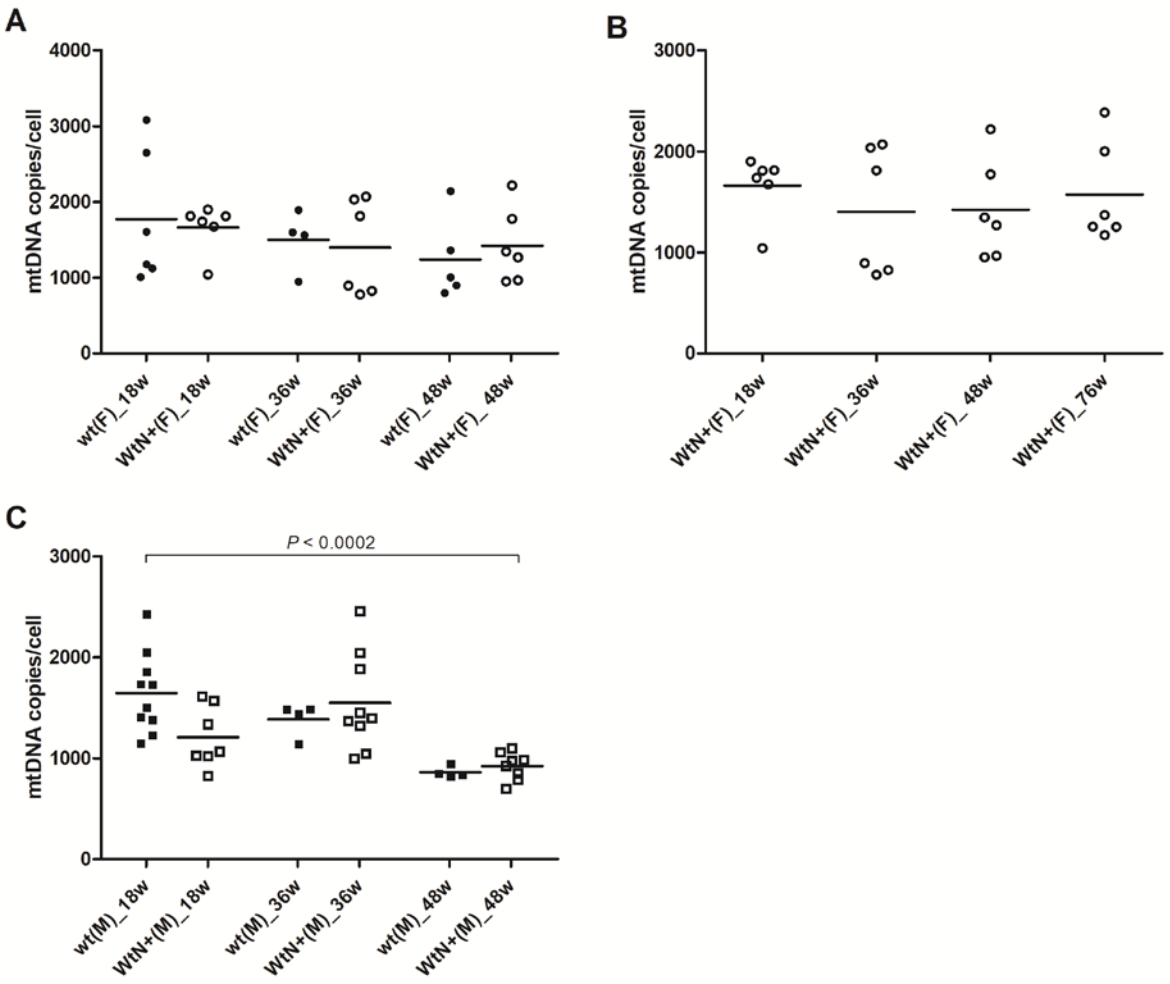

*Figure 6.5. Mitochondrial DNA copy number levels in homogenised skeletal muscle. (**A**) MtDNA CN in skeletal muscle of female wild-type and WtN+ mice at 18, 36 and 48 weeks old was not significantly different. (**B**) MtDNA CN levels in skeletal muscle of female WtN+ mice at 18, 36, 48 and 76 weeks old was not significantly different. (**C**) MtDNA CN levels in skeletal muscle of male wild-type and WtN+ mice at 18, 36 and 48 weeks old. MtDNA CN in skeletal muscle was significantly different between wt and WtN+ males between the harvesting time points. P is p-value for one-way ANOVA. Every dot represents an individual mouse. Line at mean. (F) is female. (M) is male. W is weeks.*

6.4.2 Deep resequencing of mouse mtDNA point variants

Next generation sequencing of samples from baseline ear snip, homogenised colon and skeletal muscle was performed for WtN+ and wild-type female mice. MtDNA variant counts (which included the number of non-coding, tRNA, rRNA and protein-coding variants) observed in ear snip were correlated to those in colon and skeletal muscle for the same mouse. Slopes of the regression lines were used to determine whether there was any evidence of systematic loss or gain of variants between baseline and the age of euthanasia. Slopes for colon and skeletal muscle did not differ significantly from the expected correlation line of slope=1, or from each other. There was therefore no evidence that mtDNA variants were systematically lost or gained in colon (regression line slope 0.99, 95% CI [0.95, 1.025]) or skeletal muscle (regression line slope 1.024, 95% CI [0.99, 1.062]) compared with baseline ear snip (Figure 6.6).

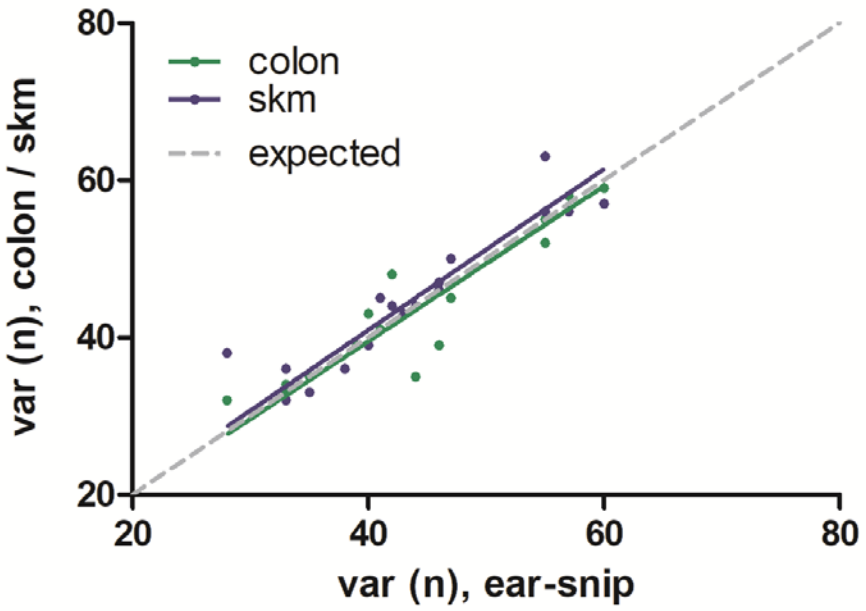

Figure 6.6. Correlation of number of mtDNA variants per ear snip vs colon and skeletal muscle for experimental WtN+ female mice. Var (n) is the count of the number of all mtDNA variants with heteroplasmy 2%-98%. MtDNA variants shown for all time points, 18, 36, 48 and 76 weeks. Every dot represents an individual mouse. Expected is a positive linear correlation line of slope=1.

I then considered the mtDNA 'mutation load' in each mouse by summing the variant heteroplasmy levels for each mtDNA variant type. This measure therefore encompasses both the number of variants and their heteroplasmy levels. Again the slope of the regression lines were examined to see if there was evidence of systematic gain or loss of mutation load between baseline (ear snip) and the age at euthanasia. On comparing colon with ear snip tissue, there was evidence of a slight but statistically significant selection against tRNA variants (regression line slope 0.8, 95% CI [0.61, 0.99]), but no selection was observed for non-synonymous complex I (regression line slope 1.0, 95% CI [0.95, 1.1]) or rRNA (regression line slope 0.95, 95% CI [0.88, 1.012]) variants (Figure 6.7).

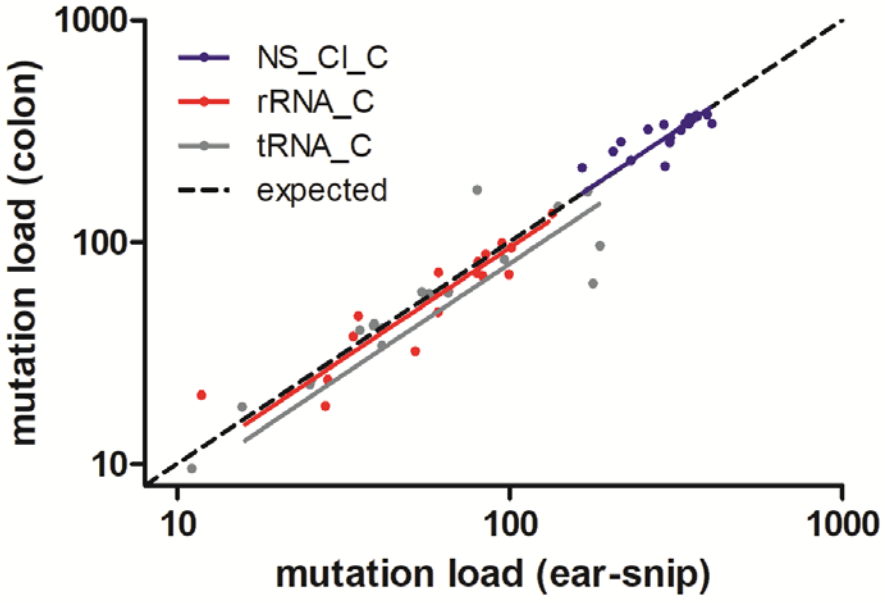

Figure 6.7. MtDNA mutation load for ear snip tissue in relation to homogenised colon in WtN+ mice. Load refers to total heteroplasmy load for each variant type. Every dot represents an individual mouse. NS_CI refers to the mtDNA non-synonymous complex I mutations. rRNA is the ribosomal RNA mtDNA variants. tRNA is the transfer RNA mtDNA variants. C is colon. X and Y axis are expressed as log_{10} values. Expected is a positive linear correlation line of slope=1.

As found for colon, the mutation load of skeletal muscle in relation to ear snip tissue for all three mtDNA variant types sat very close to the expected line. However, in skeletal muscle no variant type showed a significant difference from expected (Figure 6.8). No selection was observed against tRNA (regression line slope 1.08, 95% CI [0.97, 1.2]), non-synonymous complex I (regression line slope 0.99, 95% CI [0.91, 1.07]) or rRNA (regression line slope 1.0, 95% CI [0.95, 1.05]) variants.

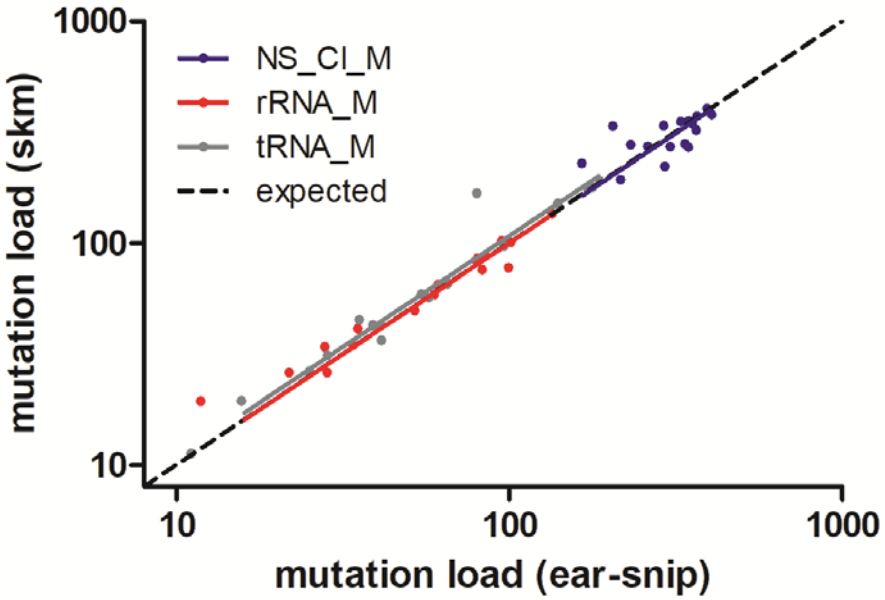

Figure 6.8. MtDNA mutation load for ear snip tissue in relation to homogenised skeletal muscle (skm) in WtN+ mice. Load refers to total heteroplasmy load for each variant type. Every dot represents an individual mouse. NS_CI refers to the mtDNA non-synonymous complex I mutations. rRNA is the ribosomal RNA mtDNA variants. tRNA is the transfer RNA mtDNA variants. M is skeletal muscle. X and Y axis are expressed as log_{10} values. Expected is a positive linear correlation line of r=1 and slope=1.

I next considered the heteroplasmy levels of individual mtDNA variants in paired ear snip and colon or skeletal muscle samples. Most mtDNA variants were seen at very similar heteroplasmy levels in colon compared with ear snip. There were a small number of mtDNA variants which were only detected in one or other of the tissues (i.e., lying on x or y axis). Distribution of the vast majority of variants sat very close to the expected line, suggesting very little selection.

As in the analyses described above for mutation count and mutation load, I again used the slope of the regression line to determine whether there was any systematic gain or loss of variant heteroplasmy between baseline and age of euthanasia. In this analysis, I saw a very slight, but statistically significant, overall decrease in variant heteroplasmy, including all mtDNA variant types for colon (slope 0.95, 95% CI [0.93, 0.97]) and skeletal muscle (slope 0.93, 95% CI [0.91, 0.95]) (Figure 6.9).

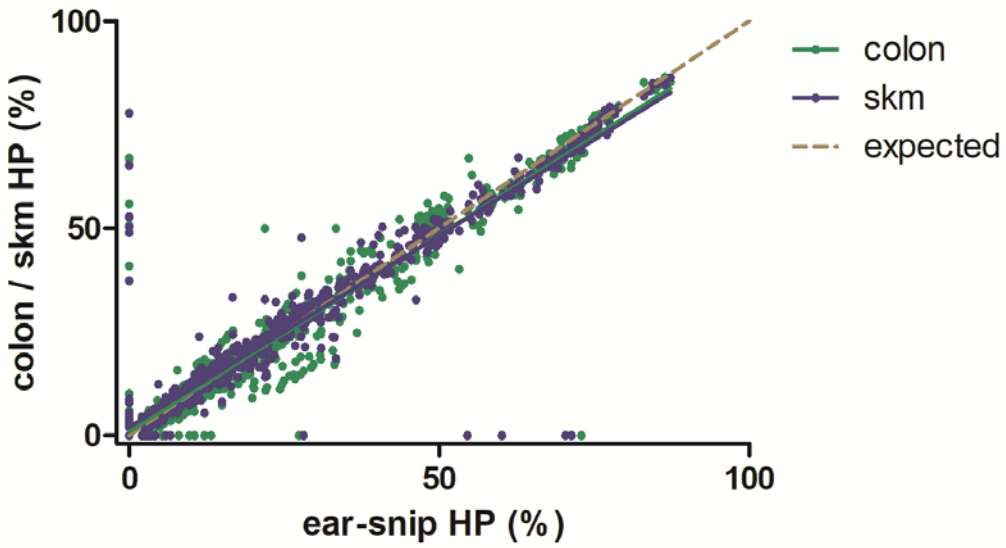

Figure 6.9. Correlation of number of mtDNA heteroplasmies per ear snip vs colon and skeletal muscle for experimental WtN+ mice. MtDNA variants shown for all variant types and all time points, 18, 36, 48 and 76 weeks. HP is heteroplasmy. Every dot represents a variant. Expected is a positive linear correlation line of slope=1.

When examining the effect of mtDNA variant type on the correlation of variant heteroplasmy levels in ear snip and colon, I observed that it was only the non-synonymous mtDNA variants that showed a small but significant selection against the expected (regression line slope 0.92, 95% CI [0.89, 0.96]) (Figure 6.10).

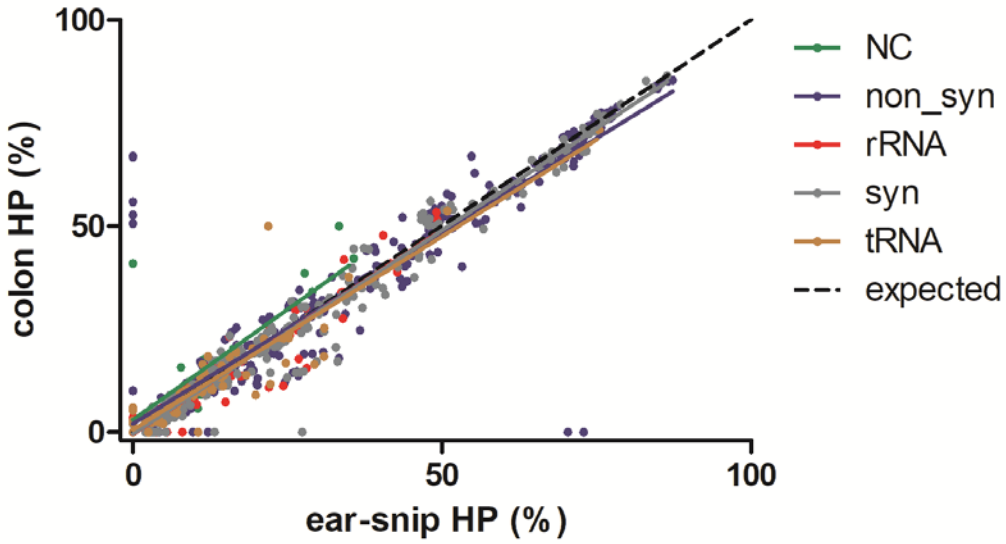

Figure 6.10. MtDNA heteroplasmy levels for ear snip variants in relation to colon in WtN+ mice per variant type. MtDNA heteroplasmy shown for specific variant types in all time points. Every dot represents a variant. HP is heteroplasmy. NC is non-coding. Non_syn is non-synonymous. Syn is synonymous. rRNA is ribosomal RNA. tRNA is transfer RNA. Expected is a positive linear correlation line of slope=1.

When examining the effect of mouse age on the correlation of variant heteroplasmy levels in ear snip and colon, I observed that mtDNA variants in colon of older mice appeared to show greater spread in distribution (i.e., to sit further from the expected line) (Figure 6.11). This observation is consistent with there being increased drift of variants from baseline with increasing age of the animal. This effect is analysed further below.

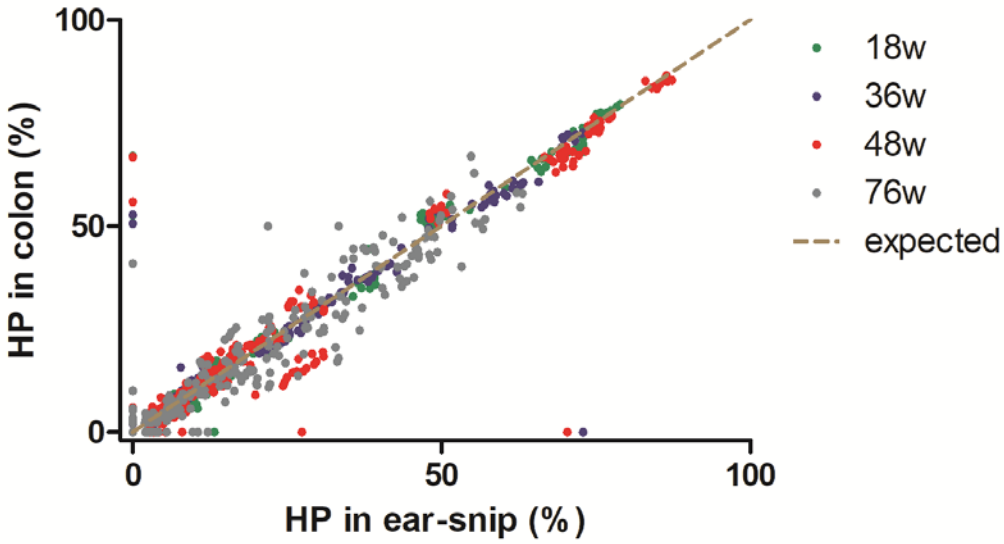

Figure 6.11. MtDNA heteroplasmy levels for ear snip variants in relation to colon in WtN+ mice at 18, 36, 48 and 76 weeks. MtDNA heteroplasmy shown for all variant types. Every dot represents a variant. HP is heteroplasmy. W is weeks. Expected is a positive linear correlation line of slope=1.

From the previous plot, there was a suggestion that the spread, i.e., degree of shift from baseline to colon, was wider at 48 and 76 weeks compared to the earlier time points. Therefore an analysis of the residuals (r^2) of the regression lines of best fit was performed. Higher residuals indicate greater differences between observed and predicted variant heteroplasmy levels. This would indicate greater dispersion of the variant heteroplasmy from baseline. One-way ANOVA of the residuals across all time points (18, 36, 48 and 76 weeks) was highly significant ($p<0.0001$) and showed a significant linear trend of increasing residuals with increasing mouse age ($p<0.0001$) (Figure 6.12). This suggests that drift of variant heteroplasmy levels from baseline does increase with age in mouse colon.

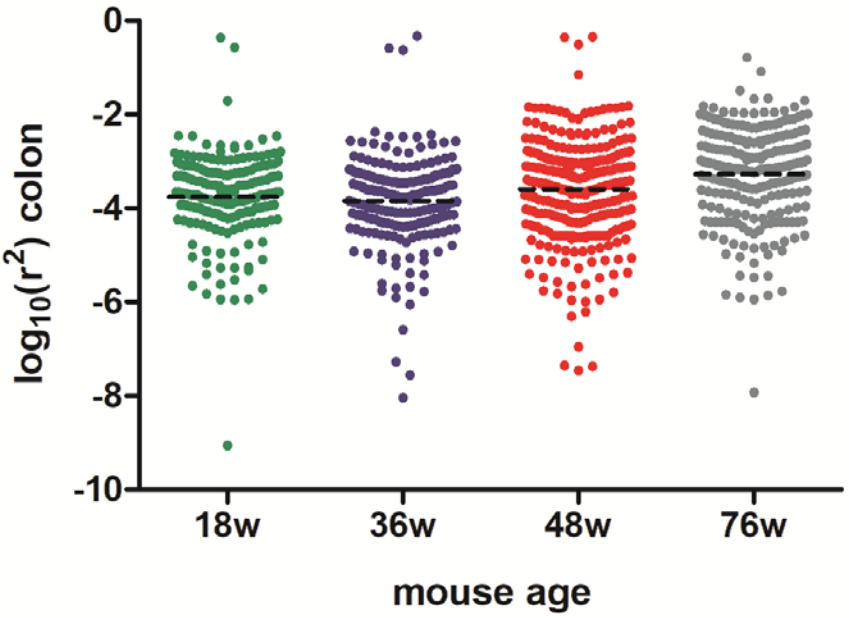

Figure 6.12. Distribution of residuals from baseline ear snip to colon in WtN+ mice at 18, 36, 48 and 76 weeks old. Residuals (r^2) were transformed into log_{10} values (Y axis).

Similarly to colon, when correlating the heteroplasmy levels of individual variants in ear snip and skeletal muscle, the distribution of mtDNA variants was very close to expected. In skeletal muscle there did not seem to be a change in variant distribution with mouse age (Figure 6.13).

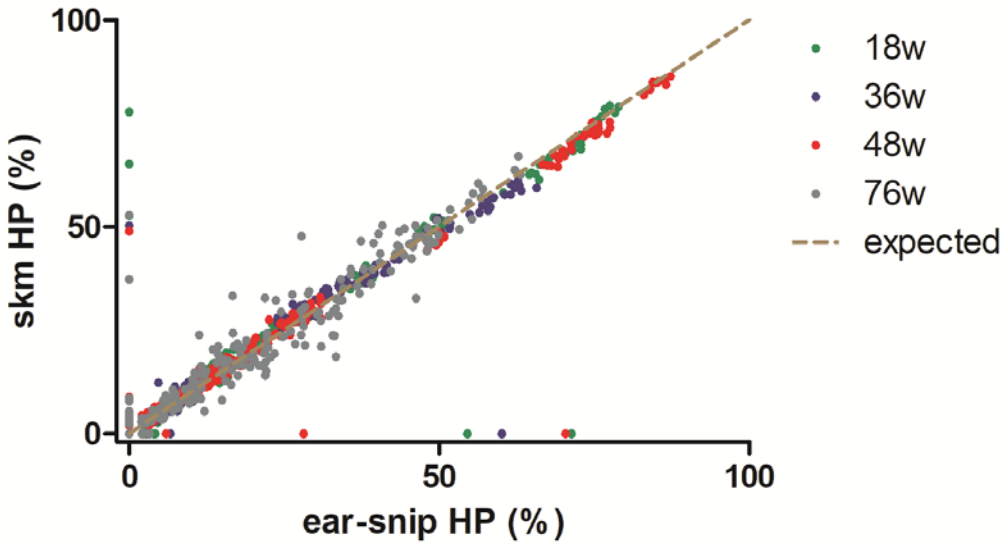

Figure 6.13. MtDNA heteroplasmy levels for ear snip variants in relation to skeletal muscle in WtN+ mice at 18, 36, 48 and 76 weeks. MtDNA heteroplasmy shown for all variant types. Every dot represents a variant. HP is heteroplasmy. W is weeks. Expected is a positive linear correlation line of slope=1.

When specific mtDNA variant types were analysed, non-synonymous mtDNA variants showed a small but significant selection against the expected (regression line slope 0.9, 95% CI [0.86, 0.94]) (Figure 6.14) as previously seen in colon.

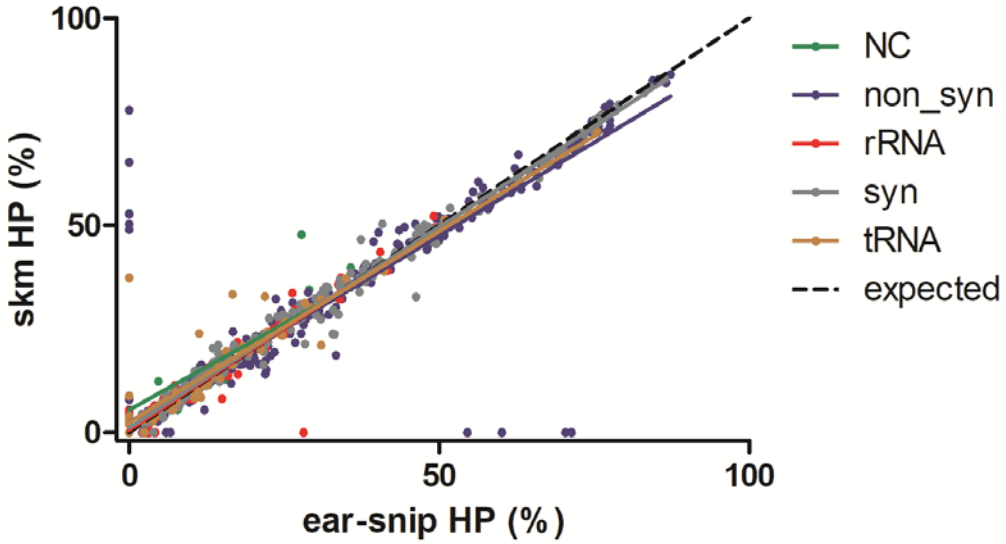

Figure 6.14. MtDNA heteroplasmy levels for ear snip variants in relation to skeletal muscle in WtN+ mice per variant type. MtDNA heteroplasmy shown for specific variant types in all time points. Every dot represents a variant. HP is heteroplasmy. NC is non-coding. Non_syn is non-synonymous. Syn is synonymous. rRNA is ribosomal RNA. tRNA is transfer RNA. Expected is a positive linear correlation line of slope=1.

Again, the residuals of the regression line of best fit were compared across the time points to determine if there was an increased drift of variant heteroplasmy from baseline with increasing mouse age in skeletal muscle. Although the residuals were significantly different between time points for skeletal muscle, this was driven by the residuals being lower at 48 weeks than the other time points and there was no significant trend with age as previously seen in the colon samples (Figure 6.15).

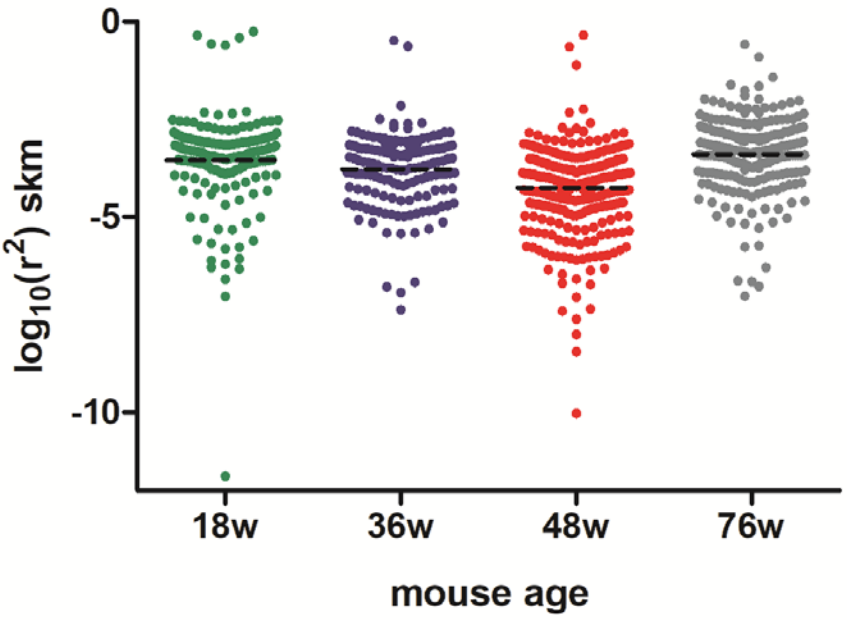

Figure 6.15. Distribution of residuals from baseline ear snip to skeletal muscle in WtN+ mice at 18, 36, 48 and 76 weeks old. Residuals (r^2) were transformed into log_{10} values (Y axis).

6.4.3 Immunofluorescence for mitochondrial respiratory complexes activity

The proportion of complex I-deficient colonic crypts increased over time in WtN+ mice (non-linear (quadratic) model fit, r=0.76, p<0.001; Figure 6.16).

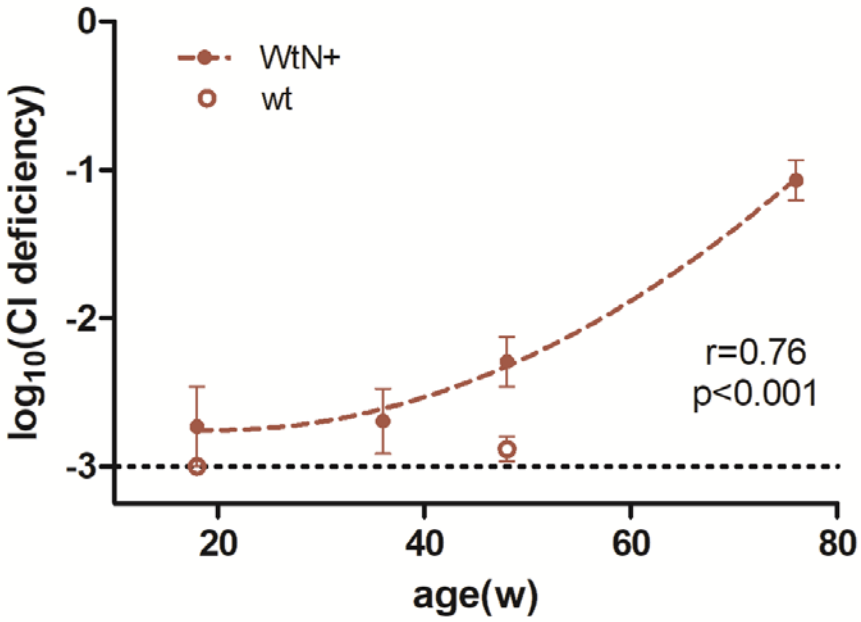

Figure 6.16. Levels of complex I deficiency in colonic crypts of WtN+ and wild-type mice over time. Time points used for WtN+ were 18, 36, 48 and 76 weeks. Wild-type values are shown for time points 18 and 48 weeks. Values plotted in the graph are deficiency z-scores of <-6. Y axis is log_{10}-transformed values of complex I deficiency. Dots are mean ± SEM for each time point. (w) is weeks.

The increase in proportion of CI-deficient colonic crypts in WtN+ mice was additionally analysed by different severity of CI-deficiency according to z-score cut-off (-6, -4.5, -3). All these classes of CI-deficient colonic crypts increased with time in WtN+ mice (Figure 6.17).

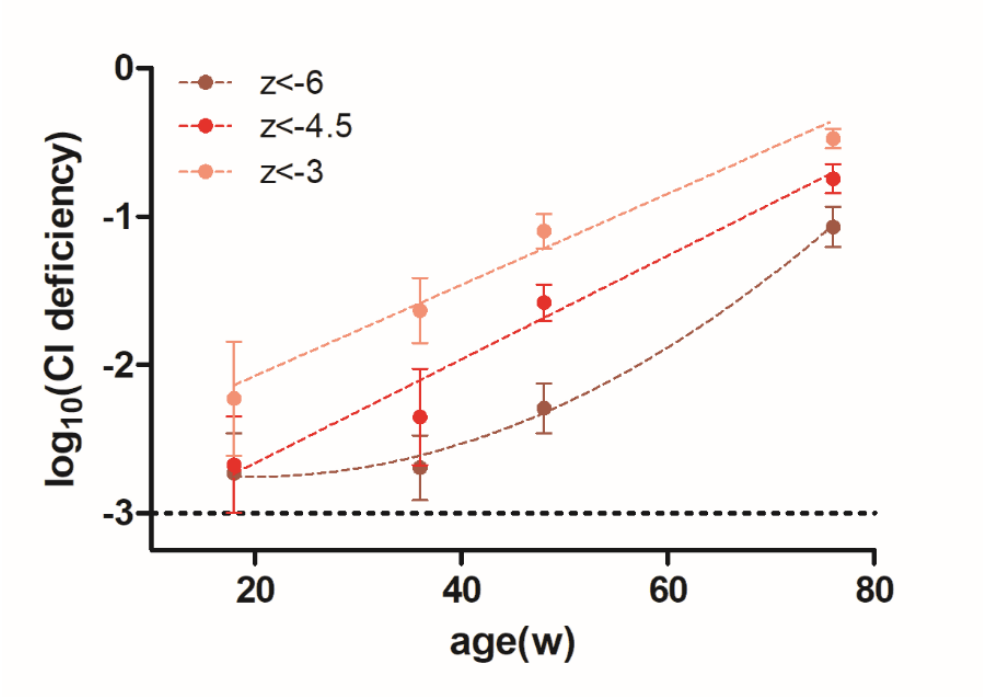

Figure 6.17. Complex I deficiency over time in colonic crypts of WtN+ mice. Different z-score cut-offs show the relative contribution of different degrees of complex I deficiency. Regression lines for z-score <-4.5 and <-3 cut-offs are linear whereas for <-6 it is quadratic. Shading represents different cut-offs for classing crypts as deficient (z-scores of <-6/<-4.5/<-3). Y axis is log_{10}-transformed values of complex I deficiency. Dots are mean ± SEM for each time point and deficiency z-score. (w) is weeks.

The proportions of complex I, III, IV and V deficient crypts at 48 weeks were analysed for WtN+ and wild-type mice. The two sexes were pooled for this analysis as there was no evidence of an effect of sex on the outcomes of interest. Complex I deficiency at the 48-week time point was significantly higher in WtN+ than in wild-type mice (z<-6 mean (SE), wt, -2.88 (0.08), n=9; WtN+, -2.29 (0.17), n=11; Welch's t-test, p=0.007; Figure 6.18A). Differences were not statistically significant for the other complexes III, IV and V (Figure 6.18B, C and D, respectively).

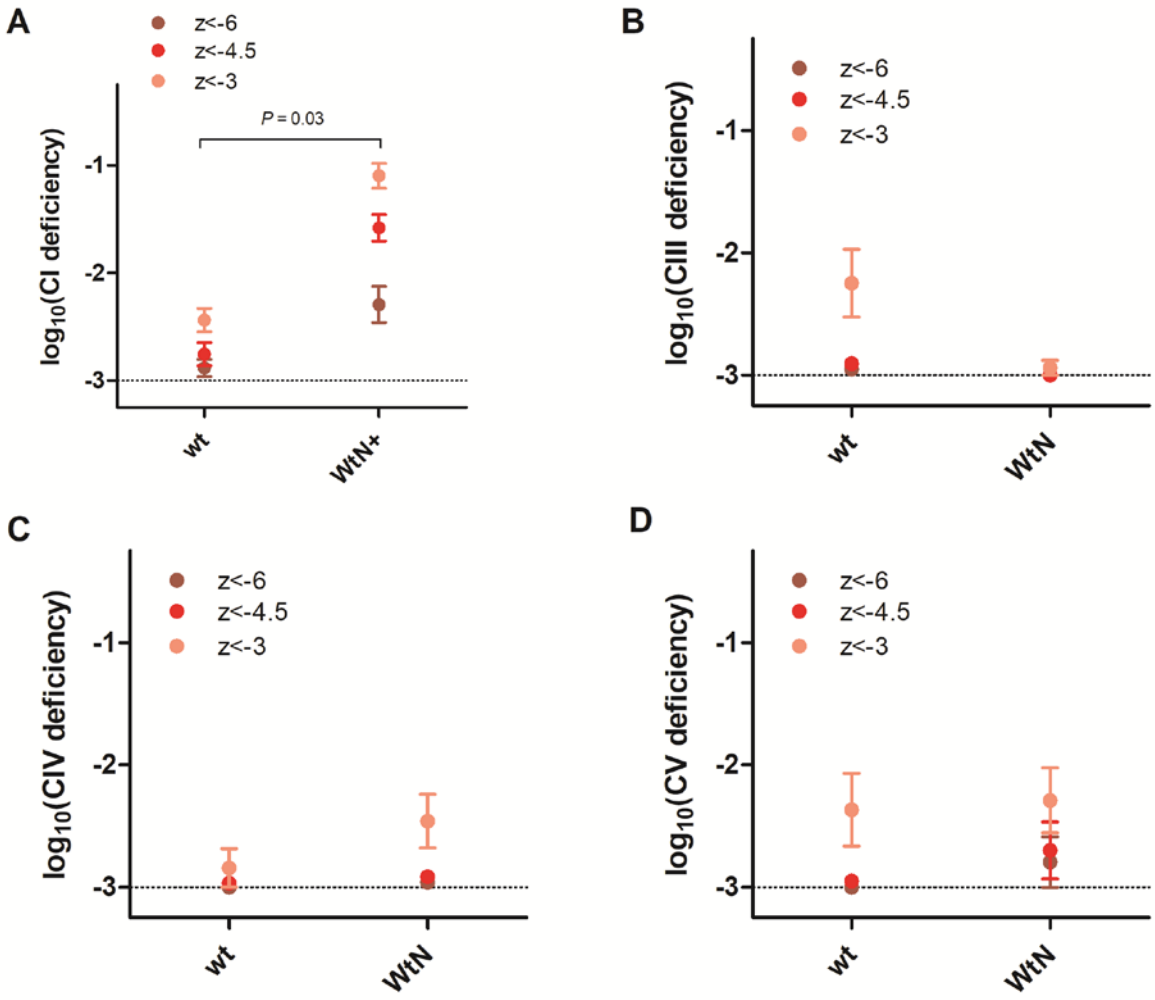

*Figure 6.18. OXPHOS complexes deficiency in colonic crypts of wild-type and WtN+ mice at 48 weeks. Levels of complex I (**A**), complex III (**B**), complex IV (**C**) and complex V (**D**) deficiency in wt and WtN+ mice colon were plotted. Z is z-score. CI is complex I. CIII is complex III. CIV is complex IV. CV is complex V. Dots are mean ± SEM for each genotype and deficiency z-score. Shading represents different cut-offs for classing crypts as deficient (z-scores of <-6 / <-4.5 / <-3). P is p-value for unpaired t-test with Welch's correction of z<-6 between wt and WtN+.*

The same immunofluorescence analyses were performed in skeletal muscle, but no significant complex I and IV defects were observed between the WtN+ and wild-type mice (data not plotted).

A linear regression model was then used to investigate the relationship between complex I deficiency in colon with age and mtDNA mutation types. In order to adjust for any differences in number and types of variants at baseline between groups of mice of different ages, this model contained age along with the variant type of interest. A specific linear regression analysis was performed for every mtDNA variant type and showed none of the mutation types, whether measured by total count or mutation load (summed heteroplasmy), correlated significantly with complex I defect after adjustment for the age of the mouse (Table 6.1).

Mutation type	**Regression coefficient (95% CI)**	**P-value**
Total HP (count)	0.01 (-0.03, 0.05)	0.6
Coding gene (count)	0.01 (-0.03, 0.05)	0.7
Non-syn coding gene (count)	0.00 (-0.08, 0.07)	0.9
Non-syn CI (count)	-0.03 (-0.12, 0.06)	0.5
rRNA (count)	-0.02 (-0.19, 0.16)	0.9
tRNA (count)	0.08 (-0.08, 0.23)	0.3
Non-syn CI (summed HP)	0.00 (0.00, 0.01)	0.6
rRNA (summed HP)	0.00 (-0.01, 0.01)	0.8
tRNA (summed HP)	0.00 (-0.01, 0.01)	1.0

Table 6.1. Correlations between complex I defects in colon, baseline mutation loads and age. Values shown for WtN+ mice cohort. Linear regression model used. Table is of regression coefficients (B, with 95% CI), and p-value. 95% CI overlapping 0, and p>0.05 indicate no significant effect of that factor (mutation load or count) on the outcome (complex I defect). Count is the number of mtDNA variants for that mutation type. HP is heteroplasmy. Summed HP refers to the total heteroplasmy load for each variant type.

6.5 Discussion

As expected, mtDNA CN at baseline in ear snip was not significantly different between the experimental WtN+ mice cohort and wild-type control mice. This is reassuring, as it suggests that mtDNA depletion is unlikely to be a confounding factor in our analyses of the effects of the mtDNA mutations present in the WtN+ genotype. MtDNA CN in colon was not different between wild-type and WtN+ mice at most time points. However, in mice aged to 76 weeks there was an increase in mtDNA CN compared to younger animals. This is likely to suggest a compensatory response to mitochondrial respiratory chain deficiency as this was the time point at which mice showed the highest levels of CI deficiency. In contrast to our findings in colon, mtDNA CN in skeletal muscle of the male groups decreased with age in both WtN+ and wild-type mice, perhaps in keeping with a decrease in activity levels with age.

Our comparisons of heteroplasmy levels of variants between baseline (ear snip) and colon or skeletal muscle samples allowed us to determine whether there was any systematic selection against certain variant types during the life of the animal. Any such effects were very small, however there was evidence of slight selection against tRNA and non-synonymous variants. These selection effects appeared to be much weaker than those observed in the germline (see Chapter 4), suggesting that once the heteroplasmic mtDNA variants are established in the germline they cannot be strongly selected against in tissues during the animal's lifespan. Future work could test this effect in a highly replicative tissue such as blood to see if there is more post-embryonic selection possible, as has been described for human mtDNA pathogenic mutations such as m.3243A>G.

The amount of drift of mtDNA variants in colon compared to baseline significantly increased with age (as determined by comparison of the regression residuals). This linear increase with age was not observed for skeletal muscle. The older WtN+ mice time point, 76 weeks, showed more spread away from the expected line than at earlier time points, suggesting that over the life of the mouse, the heteroplasmy levels of mutations in colon are able to progressively drift further away from baseline.

Overall, these sequencing findings indicate that mtDNA point mutations in the WtN+ mouse appear to be functionally important in colon but not in skeletal muscle. This is in keeping with expectations, as colonic crypts are a well-established model of the

clonal expansion of mtDNA point mutations with age, whereas it is mtDNA deletions that mainly affect skeletal muscle.

In a similar way, on immunofluorescence analyses of tissue sections, I observed mosaic CI deficiency in colonic crypts but not in skeletal muscle fibres. Again, this confirmed the pathogenic potential of mtDNA point mutations in ageing colon but not muscle. These respiratory chain defects in colon were almost exclusively of CI, with minimal defects of CIII, CIV and CV. This presumably reflects the fact that it is far more likely for mtDNA point mutations to affect CI genes as they comprise a much larger proportion of the mtDNA genome.

The CI defects in colon increased progressively with mouse age. Linear regression analyses confirmed that this effect was explained by the increasing age of the mice, and not by differences in baseline mutation levels (counts or loads). Any effect of the baseline mutation levels very largely disappeared once age was corrected for. Overall, this fits very well with a model of clonal expansion, as it suggests that age drives the complex I defect, largely regardless of the baseline mutation count. In other words, even quite high levels of mutations at baseline cannot lead to respiratory chain defects within individual colonic crypts until there has been sufficient time for clonal expansion to occur.

6.6 Conclusion

Overall, these experiments demonstrate that the WtN+ mouse model that I have developed appears to have several characteristics that make it a promising model for the age-associated clonal expansion of mtDNA point mutations:

1. A pool of mtDNA mutations present at baseline with a range of heteroplasmy levels;
2. Drift of the heteroplasmy levels of these mutations which increases over time in colon, in keeping with the turnover of mtDNA in colonic crypts;
3. A progressive increase in the proportion of CI deficient crypts with age, which is not mediated by a change in the overall number or heteroplasmy level of mutations in homogenised tissue.

These CI deficient crypts are assumed to represent the end-point of clonal expansion of mtDNA point mutations. This assumption will be empirically tested in Chapter 7.

Chapter 7. Clonal expansion of mtDNA mutations leading to complex I deficiency in single colonic crypts

7.1 Introduction

In the preceding chapters I have described the generation of a new derivative of the *PolgA* mouse, 'WtN+', which contains multiple heteroplasmic mtDNA point mutations, transmitted via the maternal germline, along with a wild-type nuclear background. As described in Chapter 6, this mouse appeared to have a number of characteristics that suggested it was a feasible model for studying the clonal expansion of mtDNA point mutations in ageing and disease, including antiretroviral treatment.

In order to confirm that the increases in the proportions of CI-deficient colonic crypts observed in the WtN+ mouse were due to the clonal expansion of mtDNA mutations within individual crypts it was necessary to perform molecular studies comparing CI-deficient and normal crypts to the homogenised colon.

A few studies report capturing of single colonic crypts in frozen tissue by laser microdissection (Taylor *et al.*, 2003; Greaves *et al.*, 2012; Baines *et al.*, 2014; Kauppila *et al.*, 2016), but to date no studies have reported mtDNA isolation in FFPE colon tissue due to the difficulty in successfully obtaining good DNA yield and quality. Given that the identification of CI-deficient crypts requires the use of immunohistochemistry on FFPE tissue (as opposed to histochemistry on unfixed frozen tissue), it is highly desirable to be able to study mtDNA in colonic crypts from FFPE tissue.

7.2 Experimental Aims

To confirm that the clonal expansion of mtDNA mutations has caused the observed complex I deficiency at a single crypt level.

7.3 Methodology

7.3.1 Laser microdissection of single colonic crypts

FFPE colon sections were cut on to uncharged and noncoated glass slides at 4 µm for laser microdissection and underwent immunofluorescence staining and microscopy imaging as described in Sections 2.7.4 and 2.7.5, respectively. Images of immunofluorescently labelled colon sections were used as a map to then manually find the complex I deficient crypts under brightfield illumination on the laser microdissection microscope. Single mouse colonic crypts were laser microdissected as described in Section 2.8 (Figure 7.1).

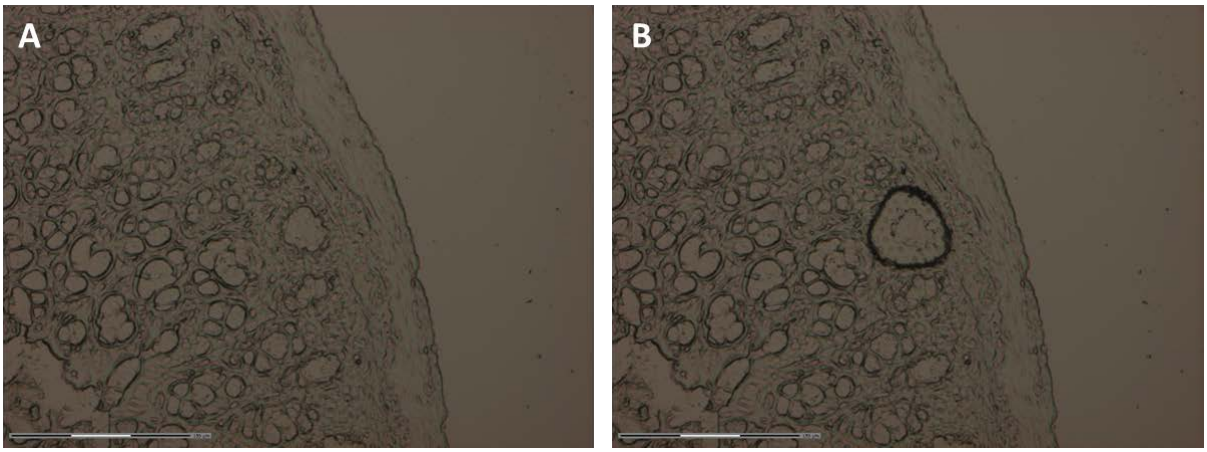

*Figure 7.1. Example of a laser microdissected colonic crypt from a WtN+ mouse used in this study. Images of the colon section taken before (**A**) and after (**B**) dissecting out of a single mouse colonic crypt. Scale bar is 150 µm.*

Laser microdissection of single colonic crypts and optimal amplification of DNA sequences for subsequent deep sequencing had to undergo several rounds of optimisation. Optimisation work included LR-PCR from single and pooled colonic crypts, which was not successful, testing of different number of crypts in a pool, qPCR on pools of single crypts and different sizes of PCR amplicons. Pools of colonic crypts were tested from two until 20, and DNA amplicons were obtained in pools of 15 colonic crypts. Real-time qPCR performed in some representative single colonic crypts gave Ct values of 33-40, which indicated very low amounts of mtDNA, in keeping with the failure of PCR amplification for sequencing from single colonic crypts. Different sizes of amplicons were also tested in primers amplifying interest areas of mtDNA complex I, and the best fragments to use were three ~600bp amplicons and three ~300bp amplicons.

For each sample, 15 single colonic crypts were cut and pooled. Every time single cell(s) or single colonic crypt(s) term is used in this Chapter, it will refer to a pool of 15 single colonic crypts.

As the respiratory chain defects I had observed on immunofluorescence staining were overwhelmingly affecting CI, I studied CI-deficient crypts and compared them with CI-normal crypts and with the homogenised colon from the same mouse.

7.3.2 Next generation sequencing of mouse mitochondrial DNA

Primers for the amplicons of the complex I region in the mitochondrial genome were designed to amplify areas with specific mtDNA variants previously seen at >10% heteroplasmy levels in homogenate colon tissue of WtN+ mice.

Mouse mtDNA was enriched using a PCR protocol consisting of the same reagents as were used for the LR-PCR protocol (Section 2.9.1). PCR conditions consisted of an initial denaturation at 95°C for three minutes, followed by 45 cycles of denaturation at 95°C for 30 seconds, annealing at 55°C for 30 seconds and extension at 68°C for 30 seconds, and one with a final extension step at 72°C for five minutes. Primer sequences for the six fragments amplified are found in Table 7.1.

Fragment	Amplicon size (bp)	Forward Primer Sequence (5'-3')	Reverse Primer Sequence (5'-3')
1	666	AGAGAAGGTTATTAGGGTGG	TTGTTTCTGCTAGGGTTGAG
2	710	TCACTATTCGGAGCTTTACG	GGATAAGGTGTTTAGGTAGC
3	310	ACTCGCCTAATTTATTCCACTTCAC	TCCTGCCAATCTAGTTGAGGTC
4	643	AATCGGTTCTATTCCACTGC	GCTAGATTAGCTAGACTTGC
5	322	ACTGCTAATTCATGCTTCCATGT	GTGACTCAGTGCCAGGTTGT
6	301	AGTTAGATCCCCAAGTCTCTGGA	TGATTTTTCATGTCATTGGTCGCA

Table 7.1. Primers for the amplification of mitochondrial genome fragments from complex I used for next generation sequencing of mouse single colonic crypts. Primers from IDT.

MtDNA point variants were measured on an Illumina MiSeq platform as described in Section 2.10. Paired-end fastq files were obtained from the MiSeq platform. Bioinformatic sequence analysis and variant calling is described in Section 2.11. Ensembl sequence reference used was mm10 (NC_005089.1). MtDNA point variants present at 2% to 98% heteroplasmy were reported. Coverage graph is found in Appendix 10.10.

Fragment 1 spanned from position m.2665 to m.3331; fragment 2 from m.3131-m.3841; fragment 3 from m.4793-m.5102; fragment 4 from m.10627-m.11270; fragment 5 from m.11629-m.11950; and fragment 6 from m.13815-m.14115. Fragments are mapped in Figure 7.2.

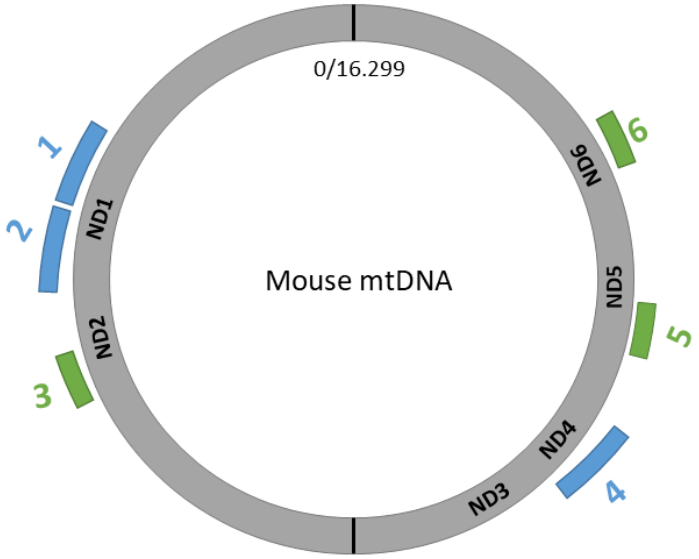

Figure 7.2. Schematic of the mouse mitochondrial genome, mapped with the amplified fragments from complex I used for next generation sequencing of mouse single colonic crypts. Fragments in blue (1, 2 and 4) are longer amplicons (~600bp). Fragments in green (3, 5 and 6) are shorter amplicons (~300bp).

7.4 Results

Complex I deficiency was established using immunofluorescence for complex I, using NDUFB8 subunit antibody. Single colonic crypts were categorised as normal if the fluorescence for NDUFB8 was in the normal range (z-score>-3), and deficient if NDUFB8 z-score values fell below -6, as described in Section 2.7.6.

For the study of single colonic crypts presented in this Chapter, only representative females from the 48-week time point were used; two wild-type: mouse 104 and mouse 111; and two WtN+: mouse 76 and mouse 77. For each WtN+ mouse, one normal complex I and two complex I deficient single colonic crypt pools were analysed.

Nine mtDNA mutations with varying levels of heteroplasmy found initially in the sequencing results of homogenised colon of representative mice, were used to design the NGS primers for the sequencing of the six fragments across complex I genes in single colonic crypts. The heteroplasmy levels of these pre-specified mutations were then analysed in the normal and CI-deficient single colonic crypts of the WtN+ mice (Table 7.2) and in the normal single crypts of the wild-type. These pre-specified mutations were all non-synonymous complex I mtDNA variants, and therefore expected to have a functional effect on CI within cells.

Position	WtN+ (76)			WtN+ (77)			
	Normal	Def	Def	Normal	Def	Def	Ref>Alt
mt.2812	9.69%	×	×	19.19%	×	×	C>T
mt.3205	×	18.58%	33.31%	×	10.76%	16.69%	C>T
mt.3352	89.86%	25.46%	20.74%	×	41.58%	67.92%	C>T
mt.4829	2.47%	35.12%	46.67%	5.84%	33.12%	24.56%	C>G
mt.4833	2.31%	34.93%	46.80%	×	33.05%	24.07%	C>T
mt.4944	30.47%	6.41%	2.33%	×	×	3.50%	T>C
mt.11025	10.93%	71.89%	80.22%	×	53.86%	53.50%	G>A
mt.11790	5.46%	×	3.47%	×	×	×	T>A
mt.14013	83.71%	41.03%	27.16%	80.42%	42.26%	55.85%	G>T

Table 7.2. MtDNA heteroplasmy levels for the non-synonymous complex I mutations chosen from homogenate colon and used to investigate clonal expansion in single colonic crypts. MtDNA heteroplasmy levels are shown for the two WtN+ mice studied (mouse 76 and 77), in complex I normal and deficient single colonic crypts; whereas these mutations were not found in the wild-type mice. × means variant not present. Ref is reference base, Alt is alternate base. Normal means non-deficient complex I. Def means complex I deficient.

Deep sequencing of homogenised colon was done for the whole mitochondrial genome (results for the mouse cohort were discussed in Chapter 6). Mutation load, the overall summed heteroplasmy of non-synonymous complex I variants, in WtN+ mice was higher in CI-deficient colonic crypts than in CI normal crypts or in homogenised colon (Figure 7.3). Note that in Figure 7.3 I am initially presenting the analysis of all non-synonymous CI mutations captured by the MiSeq assay, whether part of the pre-specified set of mutations or not. I later show this analysis restricted only to those pre-specified mutations (see below).

As expected, mutation loads in crypts from wild-type mice were very low, although were slightly higher than seen in colon homogenate (where no mutations were seen). This may reflect low levels of somatic mtDNA mutations in colon of these mice, or may reflect an increase in assay noise due to amplifying from very low starting quantities of mtDNA in single crypts.

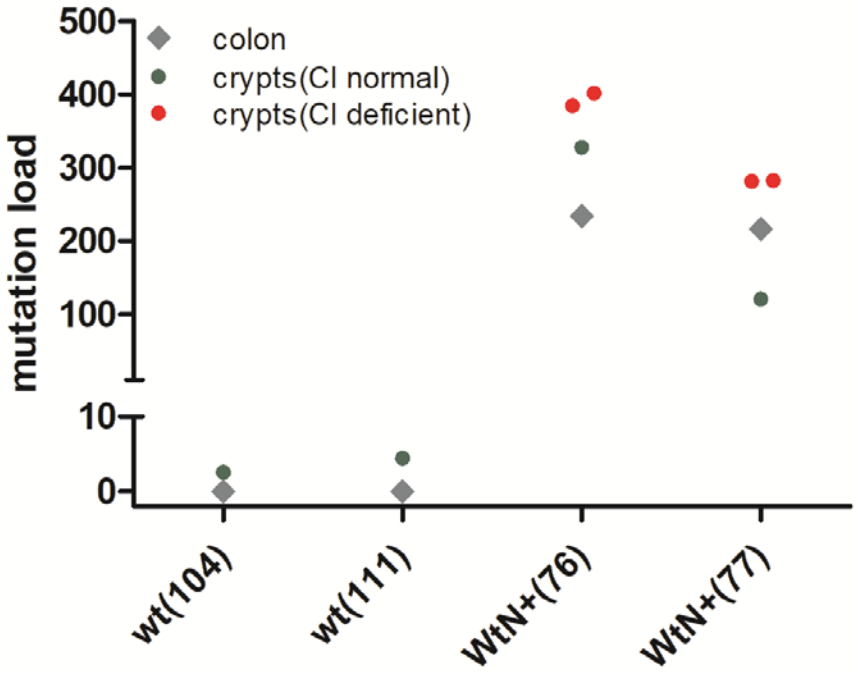

Figure 7.3. All mtDNA mutational load for non-synonymous complex I variants in wild-type and WtN+ mice. Grey box is mutation load for homogenate colon, which includes all mtDNA non-synonymous CI variants. Red dot is mutation load for complex I deficient crypts. Green dot is mutation load for complex I normal crypts. Red and green dots represent results for the non-synonymous CI variants present in the six fragments sequenced in single colonic crypts.

Although the amplicons were designed to detect specific non-synonymous CI mtDNA mutations, other CI variants and tRNA mutations were also captured. Unlike for CI mutations, tRNA mutation loads did not appear to segregate with CI-deficient crypts (Figure 7.4). This suggests that it is indeed non-synonymous CI mutations that are driving CI deficiency in single crypts, and not other mutation types.

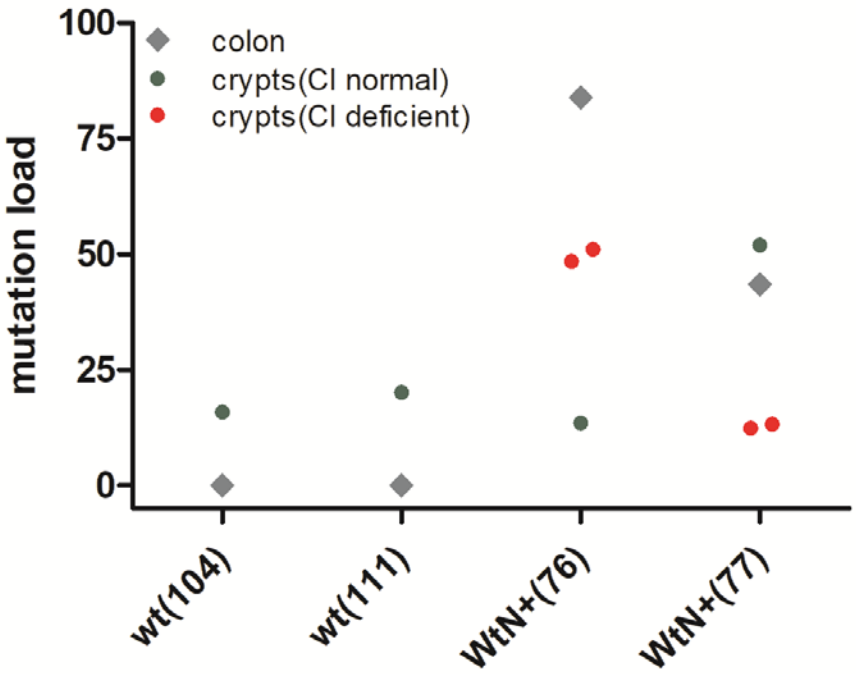

Figure 7.4. All mtDNA mutational load for tRNA variants in wild-type and WtN+ mice. Grey box is mutation load for homogenate colon. Red dot is mutation load for complex I deficient crypts. Green dot is mutation load for complex I normal crypts.

I then performed the same analysis of mutation load restricted only to the pre-specified mtDNA non-synonymous complex I mutations shown in Table 7.2. The distribution pattern was very similar to that found before for all non-synonymous CI mutations with higher mutation loads in CI-deficient single crypts of WtN+ mice compared with CI-normal crypts or colon homogenate (Figure 7.5). None of these mutations were seen in single crypts of wild-type mice.

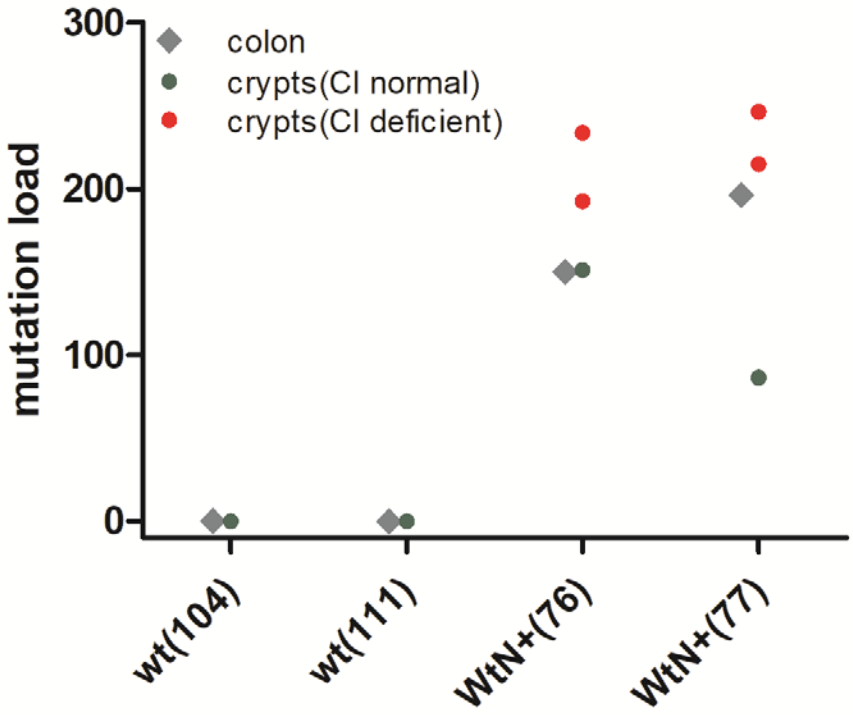

Figure 7.5. Pre-specified mtDNA non-synonymous complex I mutations in wild-type and WtN+ mice. These only include the pre-specified list of mutations from Table 7.2 seen in the homogenate colon for that mouse. Grey box is mutation load for homogenate colon. Red dot is mutation load for complex I deficient crypts. Green dot is mutation load for complex I normal crypts.

Next, analysis of the heteroplasmy levels of the specific mtDNA mutations between CI-deficient and normal crypts was performed, by comparing each to its heteroplasmy level in homogenised colon of the same mouse. The fold-change of heteroplasmy for every pre-specified mtDNA mutation between homogenised colon and single crypts was calculated by dividing the heteroplasmy of the mutation in the normal or CI-deficient colonic crypt by the heteroplasmy of the same mutation in the colon homogenate of the same WtN+ mouse. In the two WtN+ mice, there was a significant increase in heteroplasmy of mtDNA non-synonymous CI mutations in single colonic crypts compared to the respective colon homogenate (fold-change mean 2.6, 95% CI [1.2, 4]). In CI-normal single colonic crypts, mutation heteroplasmy levels were numerically lower than in colon homogenate although this did not quite reach statistical significance (fold-change mean 0.64, 95% CI [0.24, 1.05]) (Figure 7.6). Fold changes of heteroplasmy levels relative to colon homogenate in CI-deficient single crypts were significantly higher than for CI-normal crypts (p=0.021).

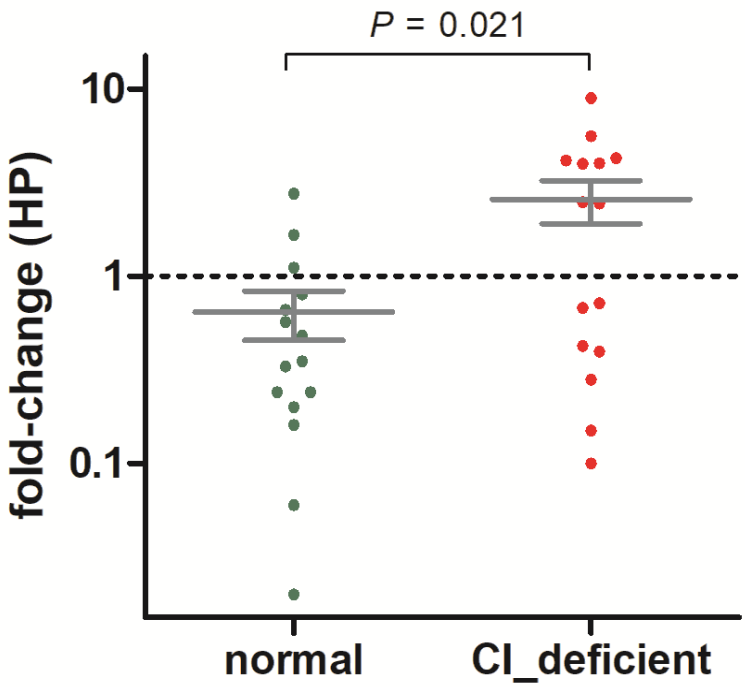

Figure 7.6. Fold-change of heteroplasmy levels for the pre-specified mtDNA non-synonymous complex I mutations in WtN+ mice. These only include the pre-specified list of mutations from Table 7.2 seen in the homogenate colon for that mouse. Data plotted for both WtN+ mice. Dotted line at 1 indicates homogenate colon heteroplasmy levels. Each dot is an individual pre-specified mtDNA point mutation. Red dot is mutation load for complex I deficient crypts. Green dot is mutation load for complex I normal crypts. P is p-value for t-test. HP is heteroplasmy. Lines at mean and error bars are SEM.

Finally, I investigated whether the CI-deficiency in individual crypts was driven by the clonal expansion of a specific mtDNA mutation. From the protein-coding, non-synonymous complex I variants included in this assay, four mtDNA variants were clearly identified which strongly segregated with complex I deficiency in colonic crypts: mt.3205C>T, found in *MT-ND1*, S(serine)/L(leucine); mt.4829C>G, found in *MT-ND2*, P(proline)/A(alanine); mt.4833C>T, found in *MT-ND2*, T(threonine)/I(isoleucine); and mt.11025G>A, found in *MT-ND4*, A(alanine)/T(threonine) (Figure 7.7). Of these, mt.11025G>A appeared likely to have the greatest effect as it reached the highest heteroplasmy levels in CI-deficient single crypts along with very low heteroplasmy levels in CI-normal crypts.

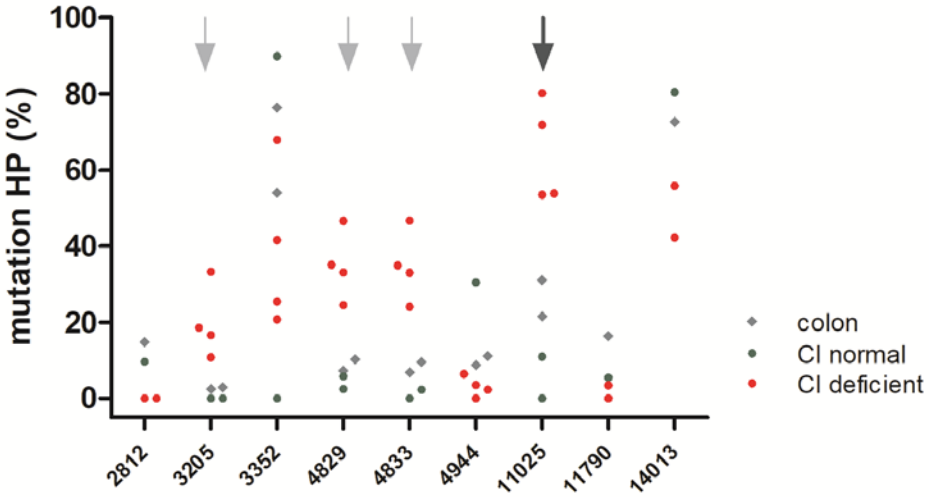

Figure 7.7. Heteroplasmy levels for the pre-specified individual mtDNA non-synonymous complex I mutations detected in WtN+ mice. These only include the pre-specified list of mutations from Table 7.2 seen in the homogenate colon for that mouse, represented on the X axis. Arrows indicate specific mtDNA mutations which segregate with complex I deficiency. Of these, mt.11025 (darker arrow) appears to be the most important. Grey box is mutation load for homogenate colon. Red dot is mutation load for complex I deficient crypts. Green dot is mutation load for complex I normal crypts. HP is heteroplasmy.

7.5 Discussion

In humans, a pathogenic homoplasmic mtDNA point mutation in the *MT-ND4* gene of complex I (mt.11778G>A) is associated with LHON. This mtDNA mutation and a few others in *MT-ND1*, *MT-ND4* and *MT-ND6* are the primary causative variants in the majority of LHON cases, which show a specific clinical phenotype affecting the optic nerve cells and presenting with visual loss (Yu-Wai-Man *et al.*, 2002; Carelli *et al.*, 2004).

The above example sets a precedent for how single mtDNA point variants in pathogenic locations of complex I genes can trigger mitochondrial dysfunction in specific organs. In the case presented in this Chapter, four mtDNA point mutations were identified as the main drivers of complex I deficiency in single colonic crypts of WtN+ mice.

When comparing these mtDNA point mutations driving complex I deficiency in single colonic crypts to their heteroplasmy levels in homogenised colon, a substantial shift was found in heteroplasmy, being higher in single crypts compared to colon homogenates. Such finding explains why although the total mutational load in colon homogenate is relatively low, within single colon cells the individual mtDNA point mutations can accumulate to high levels and therefore cause a biochemical defect, as observed in immunofluorescence for complex I.

Differences in heteroplasmy levels of non-synonymous complex I mutations were able to explain the mosaic pattern of complex I normal and deficient crypts. This effect of non-synonymous complex I variants was not apparent from looking at the sequencing data for the homogenates only. This parallels very well published observations in human colon in ageing, where there was no substantial increase in overall mutation burden with age, but the proportion of mitochondrially-deficient crypts increases with age due to clonal expansion (Baines *et al.*, 2014; Greaves *et al.*, 2014).

Seven subunits of complex I are encoded by the mitochondrial genome, *ND1-ND6* and *ND4L*, and are thought to be in charge of pumping protons; whereas the 38 remaining subunits making up complex I are nuclear encoded, and are thought to be responsible for oxidation of NADH and electron transfer (Janssen *et al.*, 2006).

In this study, the mtDNA mutation which showed the most dramatic segregation with CI deficiency in single crypts, mt.11025G>A, was found in the gene *ND4*. It could be argued that this non-synonymous substitution may affect the assembly of the whole of complex I as *ND4* is assembled at a late stage, together with *ND5*, in the hydrophobic membrane arm (Mathiesen and Hagerhall, 2002). *ND4* is therefore essential for the assembly of the membrane arm of complex I, which is the first complex responsible for proton translocation in the OXPHOS system (Figure 7.8).

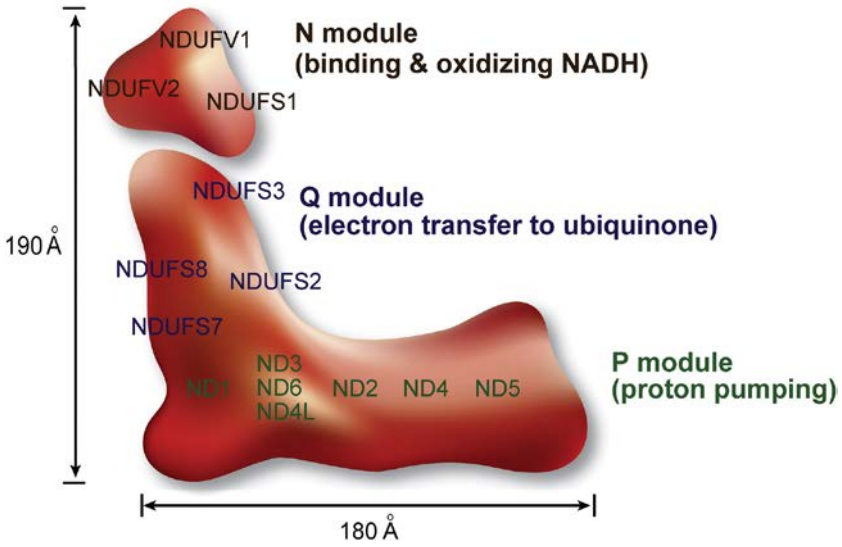

Figure 7.8. Schematic graph of mammalian mitochondrial complex I structure. The proton pumping module of complex I, located in the hydrophobic membrane arm, is composed of the seven subunits encoded by mtDNA, ND1-ND6 and ND4L. Image taken from (Mimaki et al., 2012).

Pathogenic mutations in mitochondrial *ND4* assembly causing defects or truncations in humans have not been reported in the literature, but they could be key for the proper anchorage of complex I to the mitochondrial inner membrane.

The other two mtDNA mutations likely to be driving CI-deficiency (mt.4829C>G and mt.4833C>T) were found in the *ND2* gene. *ND2* is also found in the membrane arm of complex I, according to the current model of complex I assembly (Figure 7.8), and is rarely affected by pathogenic mutations in humans. In a single case though, a mutation in *ND2* was found to be pathogenically associated with LHON (Brown *et al.*, 1992). In patient-derived cells containing a non-synonymous mutation in *ND2* (mt.4681) found at above 95% heteroplasmy, there was evidence of a complex I defect presenting with Leigh Syndrome (Ugalde *et al.*, 2007).

At this point, it is not clear to which extent these mutations disrupt the conformation of these subunits, but it is plausible that single deleterious mtDNA point mutations need to be present at high heteroplasmy levels in single cells in order to produce deficiency. It is also possible that the CI deficiency initially observed during immunofluorescence was driven by more than one mtDNA non-synonymous point mutation that have clonally expanded at the single crypt level.

A potential limitation of studying pooled crypts could be argued. By pooling crypts, I was more likely to see multiple high level heteroplasmies, whereas if a true single crypt were studied I may be more likely to observe a single high level clonally expanded mtDNA variant. Studying pooled crypts would therefore actually make it harder to detect clonal expansion of individual mutations, but I was nevertheless able to do this successfully (Figures 7.5/7.6). This approach has therefore proven successful in being able to demonstrate that this is a model of clonal expansion.

7.6 Conclusion

There were shifts in mtDNA mutation heteroplasmy levels in single colonic crypts compared with the homogenate tissue. This is strong direct evidence of clonal expansion of mtDNA point mutations leading to a mosaic pattern of CI deficiency. This confirms that the observations described in Chapter 6 are indeed the result of clonal expansion, and confirms that our WtN+ mouse model is a feasible model for studying clonal expansion *in vivo*.

Chapter 8. Investigating the effects of antiretroviral drug exposure on clonal expansion of mtDNA mutations in 'WtN+' mice

8.1 Introduction

The first FDA-approved antiretroviral drug, AZT, was reported to cause mitochondrial myopathy in HIV-treated patients (Helbert *et al.*, 1988; Dalakas *et al.*, 1990; Peters *et al.*, 1993). Some studies showed cessation of AZT therapy to stop or alleviate myopathy clinical symptoms (Helbert *et al.*, 1988; Masanes *et al.*, 1998).

The polymerase γ hypothesis stated that NRTIs cause mitochondrial toxicity by inhibiting pol γ during mtDNA replication (Lewis, 2003). Biochemical studies defined the affinity of NRTIs to be greater for the mitochondrial pol γ than for other nuclear DNA polymerases (Kakuda, 2000). A "hierarchy" of pol γ *in vitro* inhibition was then proposed for specific NRTIs: ddC>ddI>d4T>>3TC>TDF>AZT>ABC (Johnson *et al.*, 2001; Lim and Copeland, 2001; Lewis *et al.*, 2003).

AZT is a relatively weak polymerase γ inhibitor but has been hypothesised to also cause mtDNA mutagenesis (Balcarek *et al.*, 2010; Cooper and Lovett, 2011), likely by inhibiting mitochondrial thymidine kinase 2 (TK2) leading to imbalance of dNTP pools (Rylova *et al.*, 2005; Akman *et al.*, 2008). In addition, inhibition of pol γ by incorporation of AZT into the elongating mtDNA chain may make AZT less likely to be efficiently removed from the mtDNA by the pol γ (Lim and Copeland, 2001).

As reported in the literature, mouse models have been used to study effects of antiretroviral drugs, in particular NRTIs and protease inhibitors (Koczor *et al.*, 2010; Koneru *et al.*, 2014; Zhang *et al.*, 2014; Zhang *et al.*, 2015). Studies in mice showed that AZT exposure *in utero*, without HIV infection, led to cardiac dysfunction (Walker *et al.*, 2004a), and damaged cardiomyocytic mitochondria were observed in mice exposed to AZT/3TC *in utero* and postnatally (Bishop *et al.*, 2004). MtDNA damage in heart tissue of AZT-treated mice was found in a subsequent study (Chan *et al.*, 2007). These findings are relevant for human studies since AZT was frequently used, either alone or in combination, to treat HIV-infected pregnant women to prevent mother-to-child transmission of HIV, as well as their newborn infants. There was also some evidence reported linking AZT to mild cardiomyopathy in humans, but this has not been conclusively proven by subsequent studies (Herskowitz *et al.*, 1992). It was

also observed that the active form of AZT, AZT-triphosphate, altered mitochondrial dynamics in myoblast cultured cells (Nomura *et al.*, 2017). AZT-treated animals show abnormal mitochondrial morphology as well as reduced mtDNA content, mitochondrial RNA and polypeptide synthesis in skeletal muscle compared with untreated animals (Lewis *et al.*, 1992).

It has previously been demonstrated that NRTI exposure is associated with an excess of mtDNA mutations in HIV positive people. I have hypothesised that this increase in mtDNA mutations results in accelerated clonal expansion of pre-existing (age-associated) mtDNA mutations, rather than increased mutagenesis. This effect on mtDNA might plausibly drive phenotypic features of ageing in people living with HIV. To date, it has not been possible to test this hypothesis empirically as there has not been a good model in which to study the age-associated clonal expansion of mtDNA mutations within a feasible timescale.

The *PolgA* WtN+ mouse model that I have described in the preceding chapters is therefore a potential tool for assessing the causative effects of NRTIs on mtDNA mutations and the ageing phenotype. This rodent model was used which demonstrates physiological ageing within a feasible timescale in order to investigate clonal expansion.

8.2 Experimental Aims

To determine whether NRTI therapy modifies the rate of clonal expansion of mtDNA mutations and the ageing phenotype.

8.3 Methodology

The WtN+ mouse cohort was used for the following investigation. The generation, phenotyping and cellular and molecular analyses of the WtN+ mouse have been described in Chapters 4, 5 and 6, respectively.

8.3.1 Zidovudine dosage in WtN+ female mice

Retrovir (zidovudine, AZT) syrup 50 mg/5ml was acquired as a liquid formulation (ViiV Healthcare, GlaxoSmithKline). To achieve a human equivalent dose of 120 mg/kg/d, 24.7 mg AZT were added per 30 ml bottle of drinking water. Dosing per ml of drinking water was calculated based on anticipated daily volumes of water consumed per mouse. Prior to commencing the experiment, the palatability of Retrovir was tested on a separate pilot cage of mice to ensure it did not affect oral intake and adjustments were made to the drinking water if necessary. It was confirmed that the AZT did not affect oral water intake.

Weight loss and anaemia were recognised adverse effects of the genotype and/or NRTI treatment, with humane limits of >30% weight loss, and clinical score >moderate (10-14).

8.3.2 Tissue processing

Clipped ear tissue was taken at weaning (age ~4 weeks) and was used for qPCR for mtDNA content and next generation sequencing to investigate mtDNA mutations. All other tissues were dissected during organ harvesting. Dissecting of mouse tissues was previously explained in Section 2.2.9. DNA used for qPCR and NGS was extracted from tissue homogenates as described in Section 2.4.

8.3.3 Real-time PCR for mtDNA copy number

MtDNA content was expressed relative to cell content and was measured in triplicate by multiplex real-time qPCR amplification of mitochondrial gene *MT-ND5* and the

nuclear-encoded housekeeping gene *β-Actin*. Primers and probe sequences for this assay are found in Section 2.6.

8.3.4 Next generation sequencing of mouse mitochondrial DNA

Whole mtDNA genomes were enriched using long-range PCR. Primer sequences and LR-PCR details found in Section 2.9.1.

MtDNA point variants were measured on an Illumina MiSeq platform as described in Section 2.10. Paired-end fastq files were obtained from the MiSeq platform. Bioinformatic sequence analysis and variant calling is described in Section 2.11. Ensembl sequence reference used was mm10 (NC_005089.1). MtDNA point variants present at 2% to 98% heteroplasmy were reported.

8.3.5 Quadruple immunofluorescence for mouse tissues

Quadruple immunofluorescence staining and quantification for mitochondrial respiratory chain defects in mouse colon and skeletal muscle was performed as detailed in Section 2.7.

8.3.6 Phenotypic testing

Phenotypic tests included clinical scoring, open field tests, metabolic treadmill and grip strength tests as described in Section 2.2. Effects of AZT were analysed in the phenotypic tests performed.

8.3.7 Statistical analysis

Specific statistical analysis were carried out using correlation, linear regression, ANOVA, or two-tailed unpaired t-test as appropriate. When ANOVA was significant, a post test for multiple comparisons between means was performed if relevant.

8.4 Results

8.4.1 Zidovudine-induced toxicity

Three cages of WtN+ female mice (n=14 mice in total) were dosed via drinking water with AZT. They were 20 weeks of age at the start of treatment. This age was chosen to ensure that only adult mice were exposed to AZT, in order to model exposure to AZT in an HIV positive person for a finite period during adulthood. The treatment had been first checked for palatability without any problems.

After 7 weeks of AZT treatment, of an intended 12 weeks, a subset of mice (n=6) developed rapid onset of weight loss (ranging from 18-30%), anaemia, lethargy and dehydration (Figure 8.1). Due to toxicity, this subset of WtN+ female mice reached a pre-specified humane endpoint and were culled at 27 weeks, by schedule 1 method. This occurred after 7 weeks of exposure to AZT.

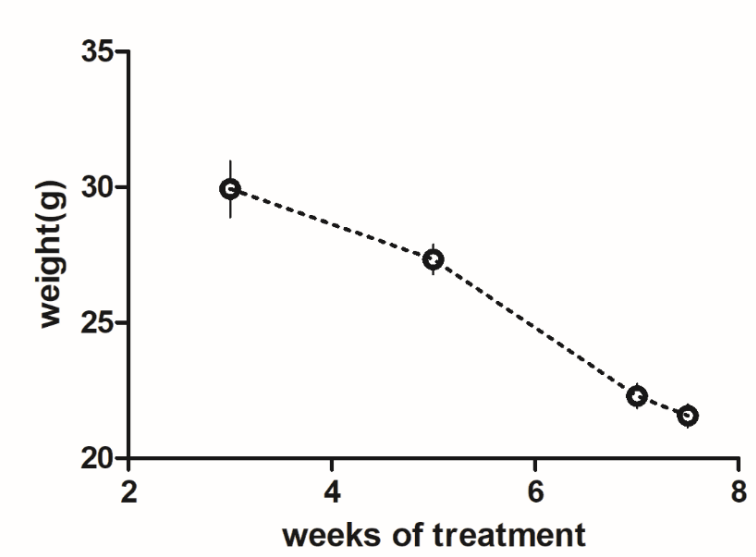

Figure 8.1. Body weights for WtN+ female mice on AZT treatment for 7 weeks during which they developed toxicity. This subset of mice (n=6) developed weight loss very quickly. The dot is mean and error bars are SEM. (g) is grams.

Other littermate mice (n=8) who had also had 7 weeks of AZT treatment however showed no weight loss, only mild anaemia, and no other adverse effects. These mice were monitored daily and soaked diet was given as a precaution, until weights were confirmed to have remained stable, and any mild anaemia had resolved. This group remained well and were able to complete the planned protocol of AZT treatment.

Those mice not experiencing toxicity were treated for 12 weeks. After stopping the drug dosing, a period of washout was allowed before harvesting of the animal. This washout period was designed to allow any inhibition of pol γ caused by AZT to resolve. Thus, when tissues were harvested, I should observe any effects of altered clonal expansion, but not the acute effects of current AZT treatment, such as mtDNA depletion.

From these eight AZT-treated WtN+ mice, four were culled at 36 weeks and four at 48 weeks. The WtN+ AZT mice harvested at 36 weeks therefore had AZT treatment for 12 weeks and then a washout period of 3 weeks before euthanasia. The WtN+ AZT harvested at 48 weeks, had AZT treatment for 12 weeks as well and then a longer washout period of 15 weeks before euthanasia (Figure 8.2).

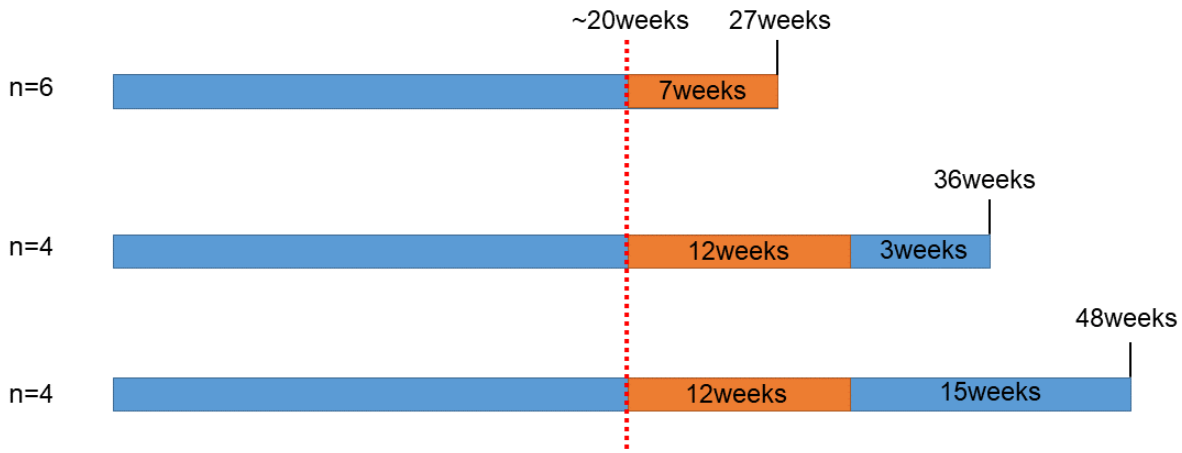

Figure 8.2. Timeline of AZT drug dosing and washout. Three groups of mice (n=14) were dosed with zidovudine liquid formulation diluted in drinking water. All WtN+ female mice started treatment at 20 weeks. The first cage (n=6) was dosed for 7 weeks before having to be euthanised due to toxicity at 27 weeks. The second cage (n=4) was dosed for 12 weeks and had a 3-week washout period without the drug before harvesting at 36 weeks. The third cage (n=4) was dosed for 12 weeks too and had a 15-week washout period before harvesting at 48 weeks. Orange is the duration of AZT treatment. N is number.

8.4.2 Cellular mitochondrial DNA content in mouse tissue homogenates

MtDNA content (mtDNA genome copies per cell) did not vary significantly in homogenised colon between female WtN+ AZT-treated and untreated mice at 36 weeks old (mean (SE) mtDNA copies/cell; WtN+ 36w AZT, 123 (10), n=4; WtN+ 36w, 139 (7), n=6; unpaired t-test, p=0.2; Figure 8.3A). At 48 weeks, mtDNA CN in colon was significantly lower in WtN+ AZT compared to untreated WtN+ mice (WtN+ 48w AZT, 114 (7), n=4; WtN+ 48w, 140 (8), n=6; unpaired t-test, p=0.048; Figure 8.3A).

Cellular mtDNA content was not significantly different in homogenised skeletal muscle between female WtN+ AZT and untreated mice at 36 (WtN+ 36w AZT, 1694 (70), n=4; WtN+ 36w, 1402 (258), n=6; unpaired t-test, p=0.4) and 48 weeks old (WtN+ 48w AZT, 1982 (196), n=4; WtN+ 48w, 1422 (201), n=6; unpaired t-test, p=0.09; Figure 8.3B).

MtDNA content in homogenised frontal cortex was not significantly different between WtN+ AZT and untreated mice at 48 weeks (WtN+ 48w AZT, 1020 (99), n=4; WtN+ 48w, 990 (134), n=6; unpaired t-test, p=0.9; Figure 8.3C).

MtDNA CN was not different in the tail of WtN+ AZT mice compared to the untreated WtN+ mice at 48 weeks (WtN+ 48w AZT, 142 (16), n=4; WtN+ 48w, 140 (8), n=6; unpaired t-test, p=0.9; Figure 8.3D).

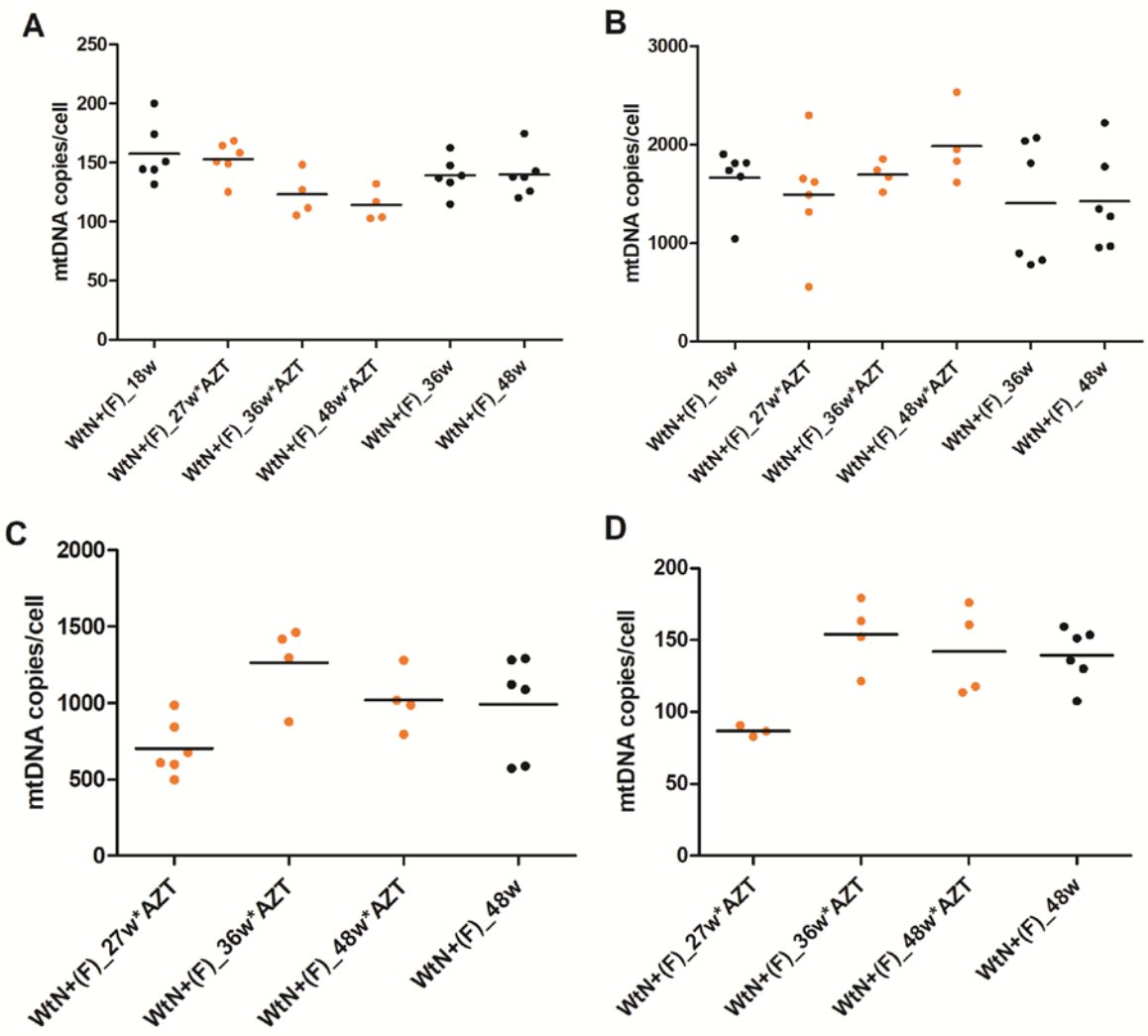

*Figure 8.3. Mitochondrial DNA copy number levels in homogenised tissues of female AZT-treated WtN+ and untreated WtN+ mice. (**A**) MtDNA CN in colon of WtN+ AZT at 27, 36 and 48 weeks, and WtN+ at 18, 36 and 48 weeks. MtDNA CN in colon was not significantly different in AZT-treated and untreated groups at 36 weeks but it was significantly lower in AZT-treated compared to untreated at 48 weeks. (**B**) MtDNA CN in skeletal muscle of the same groups was not significantly different between the 36 and 48-week groups. (**C**) MtDNA CN in frontal cortex for AZT groups and untreated 48-week WtN+ mice. MtDNA CN in brain was not significantly different between the 48-week groups. (**D**) MtDNA CN in tail of AZT groups and untreated 48-week WtN+ mice. MtDNA CN in tail was not significantly different between the 48-week groups. Every dot represents an individual mouse. Line at mean. (F) is female. W is weeks.*

Despite small differences in mtDNA at different time points and in different tissues, in general there was no consistent trend of mtDNA copy number levels across the tissues tested.

8.4.3 Deep resequencing of mouse mtDNA point variants

Next generation sequencing of samples from baseline ear snip, homogenised colon and skeletal muscle were analysed in order to make comparisons of AZT-treated to untreated WtN+ female mice. MtDNA variant counts (which included the number of non-coding, tRNA, rRNA and protein-coding variants) observed in ear snip were correlated to those in colon and skeletal muscle for the same mouse, in the AZT-treated and untreated WtN+ mouse groups. There was no effect of AZT on the correlation of variant numbers between baseline (ear snip) and colon or skeletal muscle (Figure 8.4). This suggests that AZT treatment was not associated with systematic loss or gain of variants.

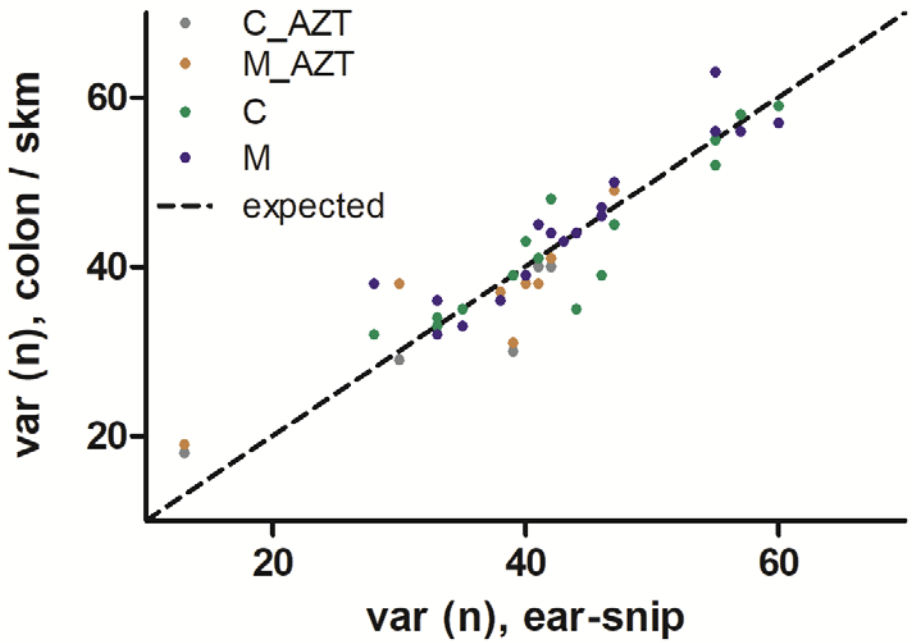

Figure 8.4. Correlation of number of mtDNA variants per ear snip vs colon and skeletal muscle for WtN+ AZT-treated and untreated mice. Var (n) is the count of the number of all mtDNA variants with heteroplasmy 2%-98%. MtDNA variants shown for 36-week and 48-week AZT time points, but excluded the 27-week toxicity time point. Every dot represents an individual mouse. C is colon. M is skeletal muscle. C_AZT is colon for AZT-treated. M_AZT is skeletal muscle for AZT-treated.

The mutation load, the overall summed heteroplasmy for each mtDNA variant type, of colon was also well correlated to that of the ear snip tissue. As observed for the untreated WtN+ mice, there was a very slight selection against tRNA variants in colon (regression line slope 0.87, 95% CI [0.78, 0.97]). No selection was observed for non-synonymous complex I (regression line slope 0.9, 95% CI [0.75, 1.05]) and rRNA (regression line slope 0.8, 95% CI [0.6, 1.002]) variants in colon of AZT-treated mice (Figure 8.5).

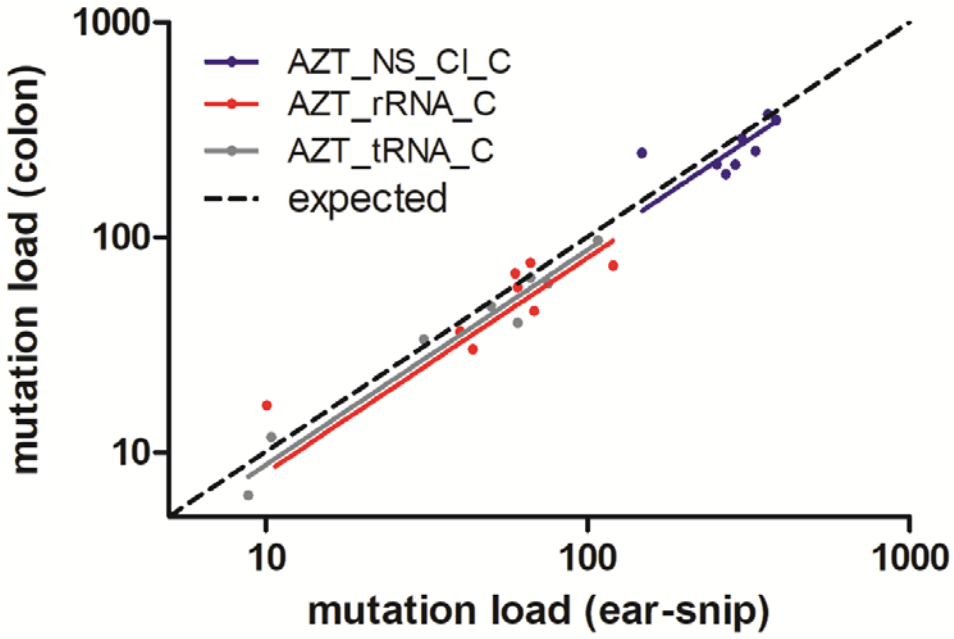

Figure 8.5. MtDNA mutation load for ear snip tissue in relation to homogenised colon in WtN+ AZT-treated mice. Load refers to total heteroplasmy load for each variant type. Every dot represents an individual mouse. NS_CI refers to the mtDNA non-synonymous complex I mutations. rRNA is the ribosomal RNA mtDNA variants. tRNA is the transfer RNA mtDNA variants. C is colon. X and Y axis are expressed as log_{10} values. Expected is a positive linear correlation line of slope=1.

I next examined the correlation between heteroplasmy levels of individual variants in ear snip and colon of AZT-treated mice. At both 48 weeks (regression line slope 0.84, 95% CI [0.76, 0.92]) and 36 weeks (slope 0.9, 95% CI [0.84, 0.96]) (Figure 8.6), there was evidence of slight selection against mtDNA variant heteroplasmy levels in colon.

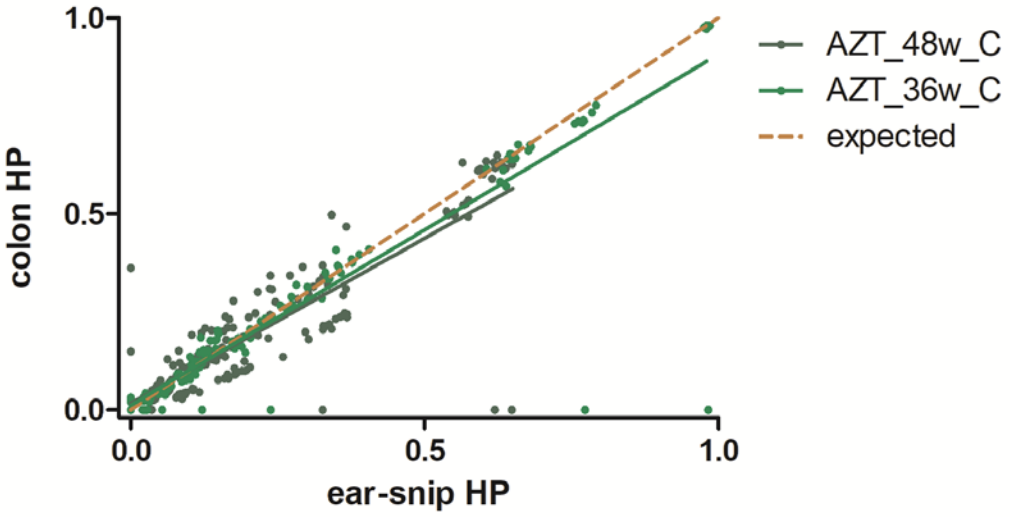

Figure 8.6. MtDNA heteroplasmy levels for ear snip variants in relation to colon in WtN+ AZT-treated mice. MtDNA heteroplasmy shown for all variant types at 36-week and 48-week AZT time points, but excluded the 27-week toxicity time point. Every dot represents a variant. C is colon. HP is heteroplasmy. Expected is a positive linear correlation line of slope=1.

Residuals (r^2) are the difference between observed and expected values on the regression line of best fit. Therefore, the distribution of variant heteroplasmy residuals is a measure of how much drift there is in heteroplasmy from baseline ear snip to colon. In the AZT-treated WtN+ mice, I observed that the drift of mtDNA mutations in colon increased. AZT treatment was associated with a significant increase in the dispersion of mtDNA mutation heteroplasmy in colon compared with baseline. This dispersion was greater at the 48-week compared with the 36-week time point. One-way ANOVA was significant ($p<0.0001$), and further post hoc test showed a significant difference between AZT-treated and untreated residuals in colon at 36 weeks ($p<0.0001$) and at 48 weeks ($p<0.0001$) (Figure 8.7A). Residuals in colon showed a significant progressive increase with age in AZT-treated mice (slope significantly non-zero, $p=0.006$) as opposed to no significant effect on treatment naïve mice (slope not different from zero, $p=0.6$) (Figure 8.7B).

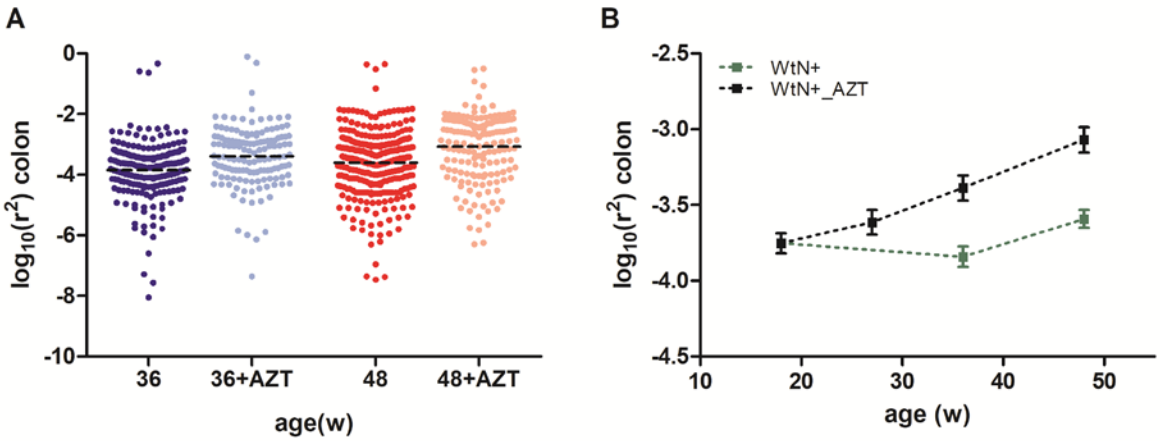

*Figure 8.7. Distribution of residuals in colon in AZT-treated and untreated WtN+ mice. (**A**) Dispersion of residuals from baseline ear snip to colon in both groups, 36 and 48 weeks old. (**B**) Increase of residuals in colon for all time points measured in AZT (black) and treatment naïve (green) mice. 27-week toxicity time point is included. Dots are mean ± SEM for each time point.*

The same analyses were then applied to skeletal muscle. No effect of AZT treatment was observed in the correlation of total mutation load (summed heteroplasmy) between baseline ear snip and skeletal muscle mtDNA variants in non-synonymous complex I, rRNA and tRNA positions (Figure 8.8).

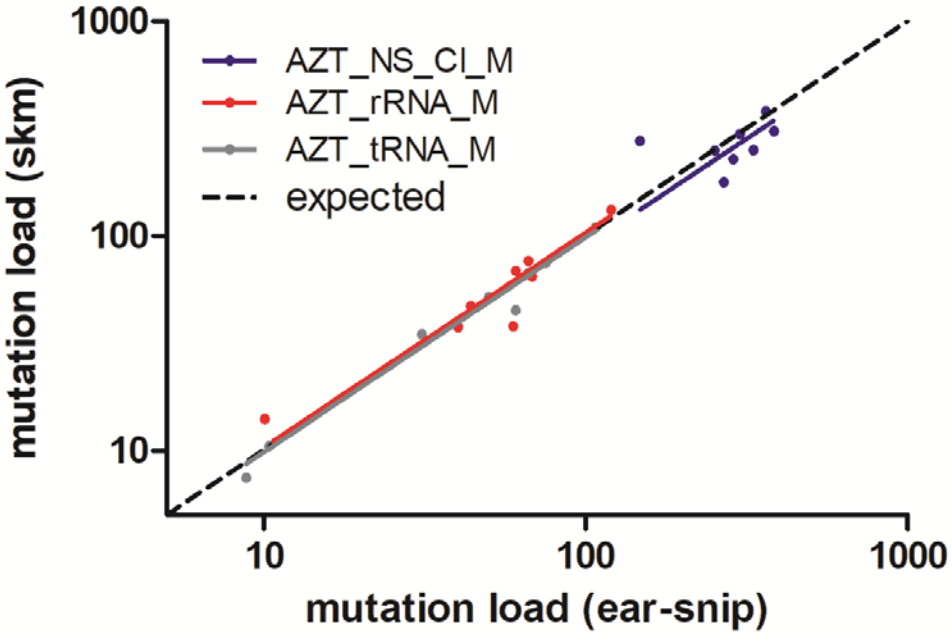

Figure 8.8. MtDNA mutation load for ear snip tissue in relation to homogenised skeletal muscle (skm) in WtN+ AZT-treated mice. Load refers to total heteroplasmy load for each variant type. Every dot represents an individual mouse. NS_CI refers to the mtDNA non-synonymous complex I mutations. rRNA is the ribosomal RNA mtDNA variants. tRNA is the transfer RNA mtDNA variants. M is skeletal muscle. X and Y axis are expressed as log_{10} values. Expected is a positive linear correlation line of slope=1.

Next, I examined the heteroplasmy levels of individual mtDNA variants in skeletal muscle compared with ear snip of AZT-treated WtN+ mice. In both the 48-week group (regression line slope 0.86, 95% CI [0.79, 0.92]) and the 36-week (slope 0.93, 95% CI [0.88, 0.98]) there was slight selection against variant heteroplasmy in skeletal muscle (Figure 8.9).

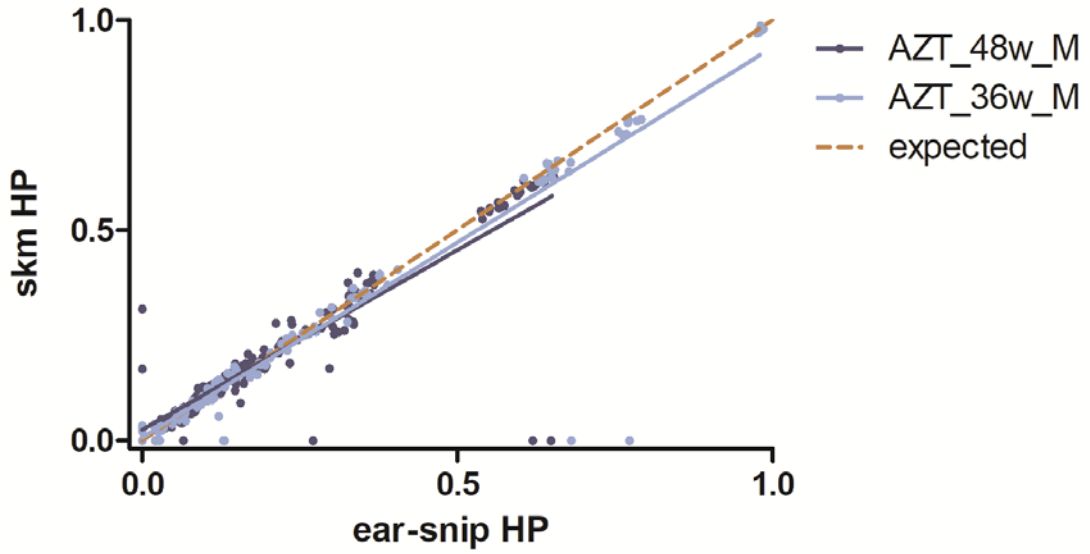

Figure 8.9. MtDNA heteroplasmy levels for ear snip variants in relation to skeletal muscle in WtN+ AZT-treated mice. MtDNA heteroplasmy shown for all variant types at 36-week and 48-week AZT time points, but excluded the 27-week toxicity time point. Every dot represents a variant. M is skeletal muscle. HP is heteroplasmy. Expected is a positive linear correlation line of slope=1.

As for the analyses on colon, I then used the regression residuals to assess the amount of drift of mtDNA variants in skeletal muscle compared to ear snip. Unlike in colon, there was no significant effect of either age or AZT treatment on the dispersion of variants in skeletal muscle (Figure 8.10A, Figure 8.10B).

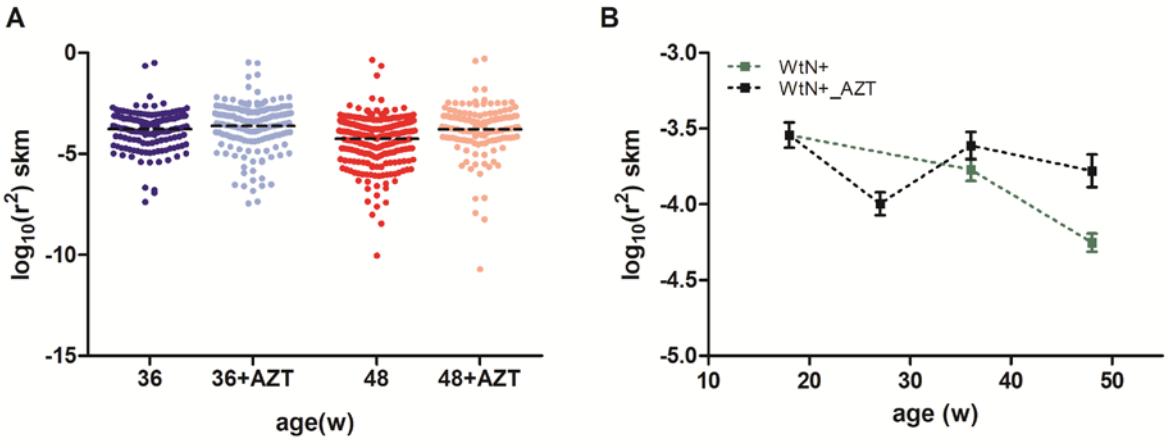

*Figure 8.10. Distribution of residuals in skeletal muscle in AZT-treated and untreated WtN+ mice. (**A**) Dispersion of residuals from baseline ear snip to skeletal muscle in both groups, 36 and 48 weeks old. (**B**) Residuals in skeletal muscle for all time points measured in AZT (black) and treatment naïve (green) mice. 27-week time point is included. Dots are mean ± SEM for each time point.*

8.4.4 Sequencing analysis of AZT-related toxicity

I then examined the mtDNA analysis performed in baseline ear snip for the subset of AZT-treated mice that were euthanised due to toxicity at 27 weeks old and compared to the other AZT-treated mice that did not get treatment-related toxicity. This was in order to determine whether the group exhibiting toxicity had a predisposition to more severe effects of AZT due to differences in baseline mtDNA mutations. This analysis showed that there was no difference in the mutation counts or loads (summed heteroplasmy) at baseline that would explain why one subset got AZT toxicity and the other did not (Figure 8.11).

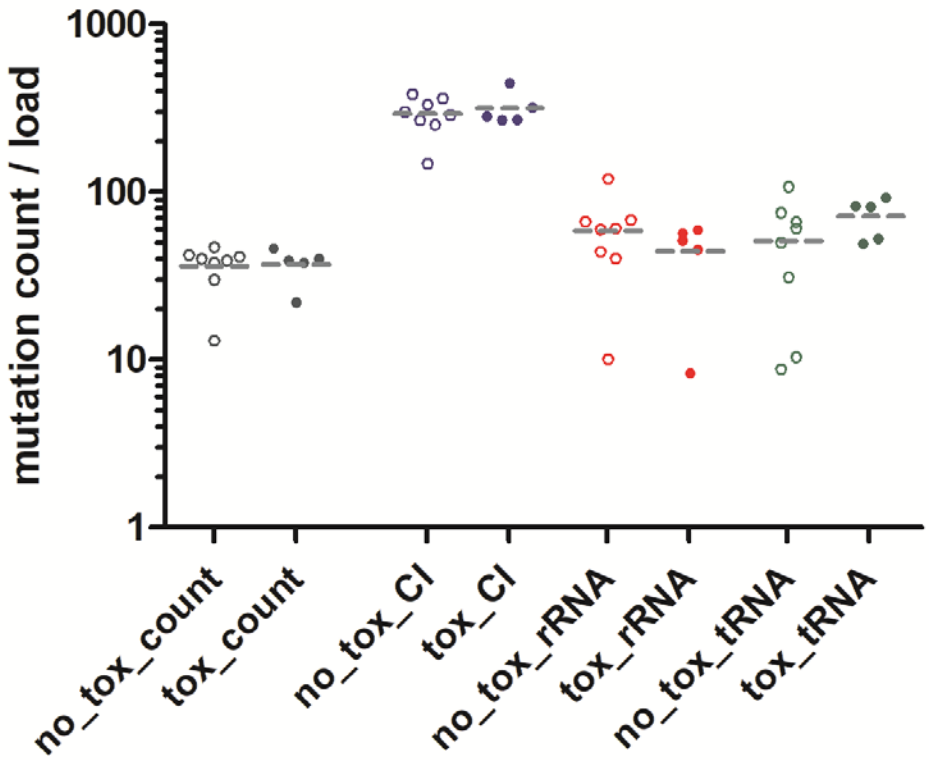

Figure 8.11. MtDNA mutation count and load for WtN+ AZT-treated mice with toxicity and without. Count is the number of total mtDNA variants with heteroplasmy 2%-98%. Load refers to total heteroplasmy load for each variant type. Every dot represents an individual mouse. Dotted line at mean. CI refers to the mtDNA non-synonymous complex I mutations. rRNA is the ribosomal RNA mtDNA variants. tRNA is the transfer RNA mtDNA variants. Tox is the subset of AZT mice that got toxicity. No_tox is the subset that did not get toxicity. Y axis is expressed as log_{10} values.

The same mtDNA analysis was performed in colon and skeletal muscle to compare the subset of AZT-treated mice that were euthanised due to toxicity at 27 weeks old to the other AZT-treated mice. As seen for the baseline results, this again showed that there was no difference in the mutation counts between the AZT-treated mice with toxicity and the ones without toxicity for both colon (Figure 8.12A) and skeletal muscle (Figure 8.12B).

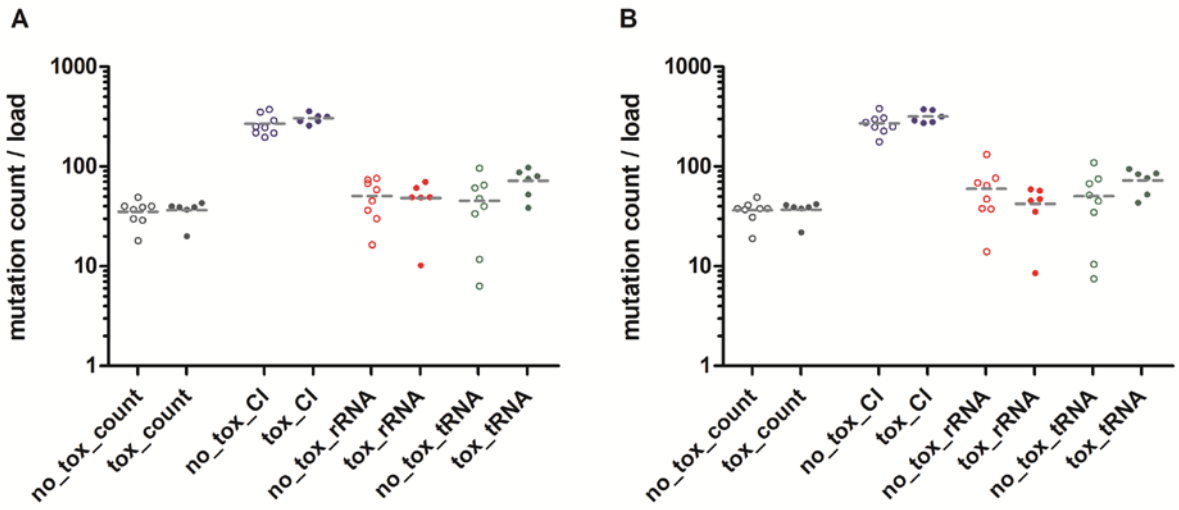

*Figure 8.12. MtDNA mutation count and load in colon and skeletal muscle of WtN+ AZT-treated mice with toxicity and without. Values are shown for colon (**A**) and skeletal muscle (**B**). Count is the number of total mtDNA variants with heteroplasmy 2%-98%. Load refers to total heteroplasmy load for each variant type. Every dot represents an individual mouse. Dotted line at mean. CI refers to the mtDNA non-synonymous complex I mutations. rRNA is the ribosomal RNA mtDNA variants. tRNA is the transfer RNA mtDNA variants. Tox is the subset of AZT mice that got toxicity. No_tox is the subset that did not get toxicity. Y axis is expressed as log_{10} values.*

8.4.5 Immunofluorescence for mitochondrial respiratory complexes activity

As detailed previously, WtN+ female mice were treated with AZT from week 20 to week 32 (shaded blue on plots), then returned to normal drinking water and culled at week 36 or 48. Some AZT-treated mice were also culled at week 27 due to anaemia. Complex I defects were much higher in AZT-treated mice at week 36, then decreased by week 48, though not back to the level of untreated mice (Figure 8.13A).

At 48 weeks, the difference between AZT-treated and untreated groups was significant for crypts with deficiency z-scores of z<-3 (p=0.001) and z<-4.5 (p=0.039), but not the severe deficiency of z<-6 (p=0.33) (Figure 8.13B).

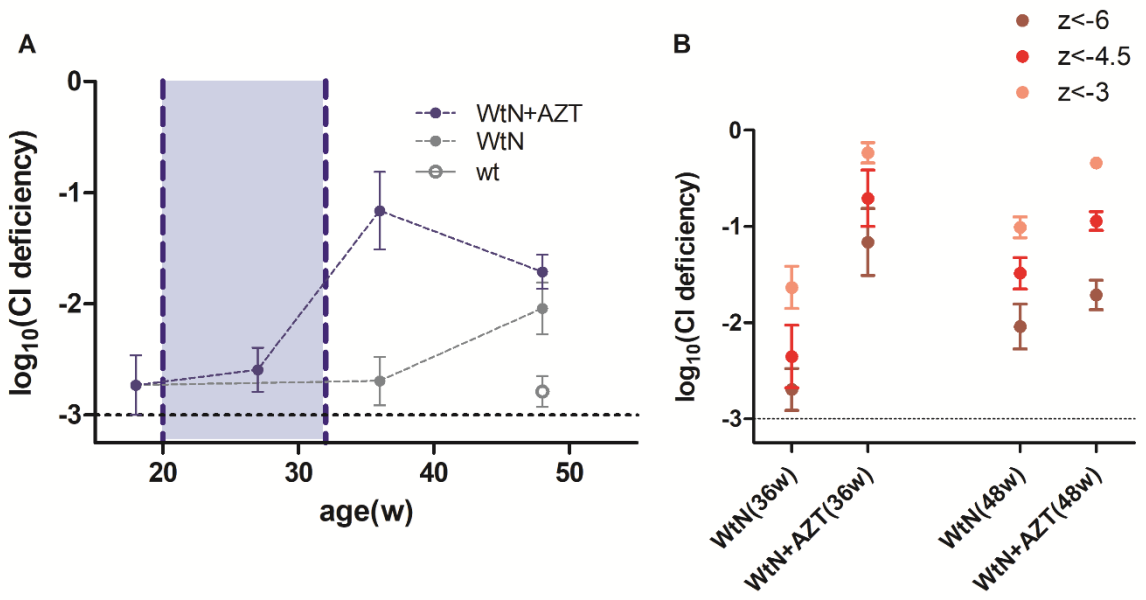

*Figure 8.13. Complex I deficiency in colonic crypts of different genotypes and AZT exposure. (**A**) CI deficiency increased dramatically in the AZT-treated mice compared to the untreated group. Wild-type values are represented in the last time point as a reference. Shaded blue is AZT treatment duration. 27-week AZT mice included as valid data point. (**B**) CI deficient crypts in treated and untreated at 36 and 48 weeks. Dots are mean ± SEM for each time point (**A**) and deficiency z-score (**B**). CI is complex I. Wt is wild-type. W is weeks. Z is z-score.*

The remaining complexes analysed in colon (complexes III, IV and V) did not show any significant deficiency (data not plotted).

The same immunofluorescence analysis was performed in skeletal muscle, but no significant complex I defects were observed in any of the AZT-exposed WtN+ mice, the untreated WtN+ or the wild-type mice (Figure 8.14).

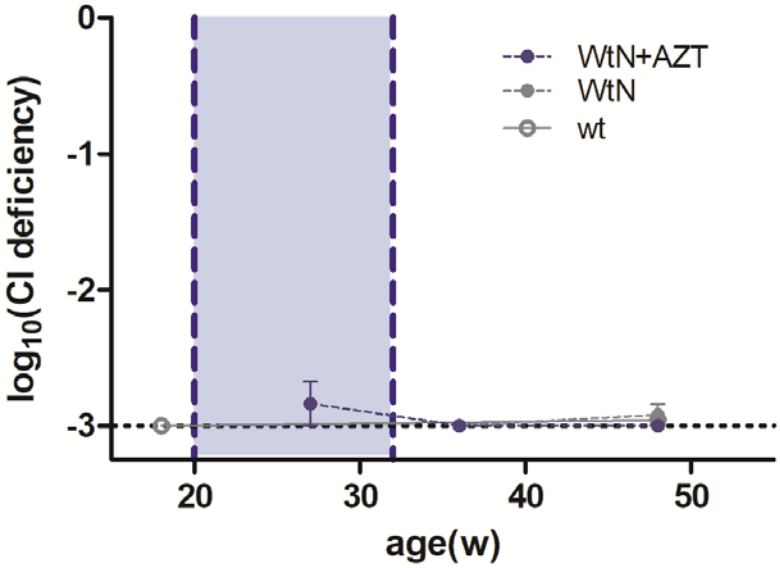

Figure 8.14. Complex I deficiency in skeletal muscle of different genotypes and AZT exposure. Shaded blue is AZT treatment duration. 27-week AZT mice included as valid data point. Dots are mean ± SEM for each time point. CI is complex I. Wt is wild-type. W is weeks.

The other complex analysed in quadruple immunofluorescence of skeletal muscle, complex IV, also did not show any significant deficiency (data not plotted).

8.4.6 Open field tests

Open field test data were obtained as previously described in Section 2.2.5, and results for the untreated ageing mouse cohort were already analysed in Section 5.4.2.

Analysis was performed for the AZT-treated and untreated female WtN+ mice at 35 and 47 weeks old, in all the open field parameters. Only the rearing of AZT mice at 47 weeks was significantly increased ($p=0.03$) compared to the WtN+ treatment naïve mice of the same time point (Figure 8.15B). The other measures of locomotor activity were not significantly different in the AZT groups.

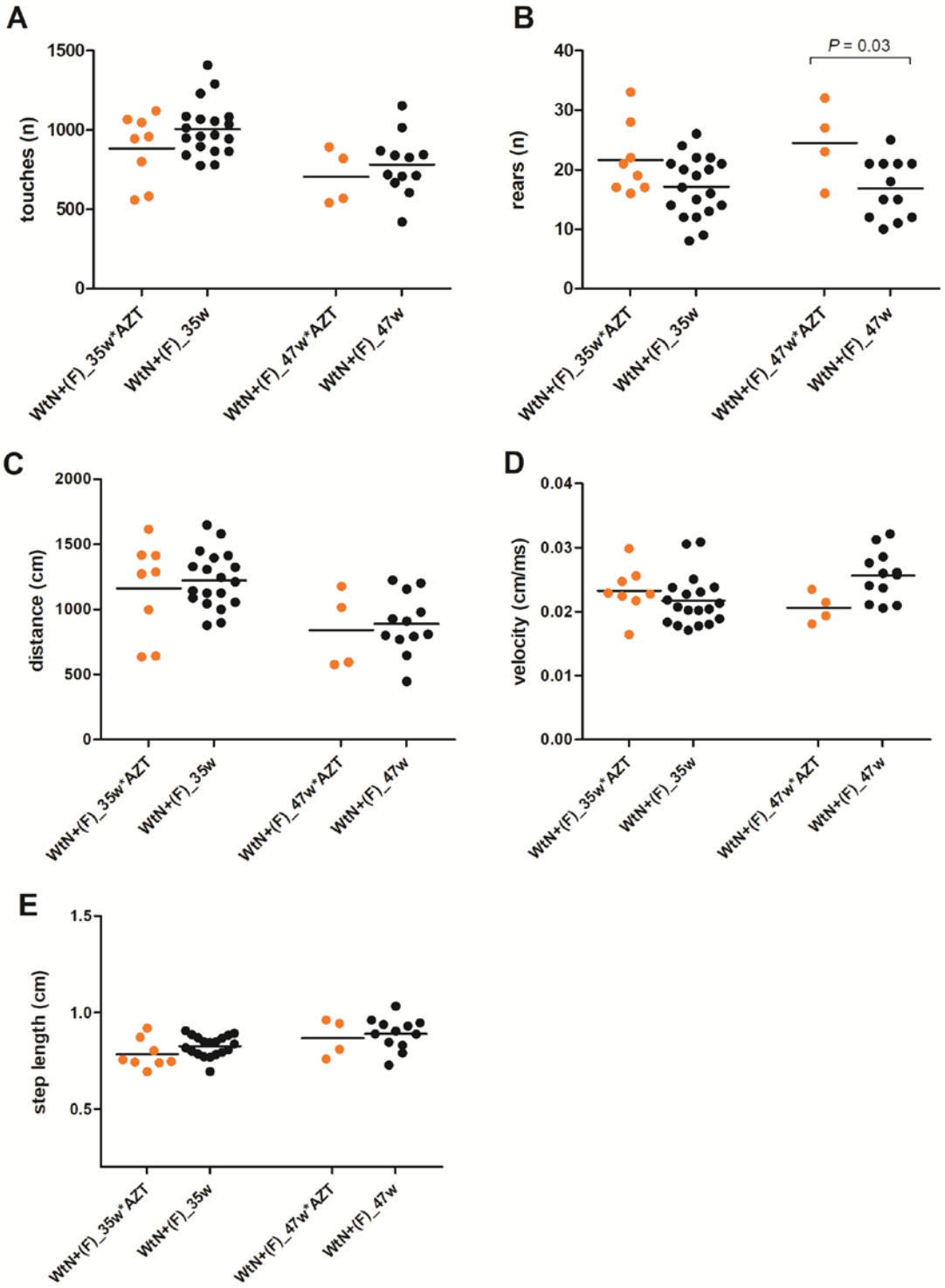

*Figure 8.15. Dot plot figures showing the open field test values for AZT-treated and untreated female WtN+ mice at 35 and 47 weeks old. Open field values measured were number of touches (**A**), number of rears (**B**), distance explored by the mice (**C**), the velocity they kept (**D**) and the step length (**E**). Each dot represents an individual animal. Line at mean. (n) is number. (cm) is centimetre. (cm/ms) is centimetre per millisecond. (F) is female. W is weeks. P is p-value for t-test.*

8.4.7 Metabolic treadmill tests

Metabolic parameters were measured as previously described in Section 2.2.6, and results for the untreated ageing mouse cohort were already analysed in Section 5.4.3.

Metabolic treadmill results were only taken at the 35-week time point for AZT-treated mice. At rest, metabolic treadmill parameters in 35-week old AZT-treated mice were significantly lower compared with untreated WtN+ mice, except for RER (Figure 8.16). Specifically, the AZT-treated group showed significant decreases in VO_2 ($p=0.0005$; Figure 8.16A), VCO_2 ($p=0.0005$; Figure 8.16B) and heat ($p=0.0002$; Figure 8.16D), but not in RER (Figure 8.16C), compared to the untreated WtN+ group.

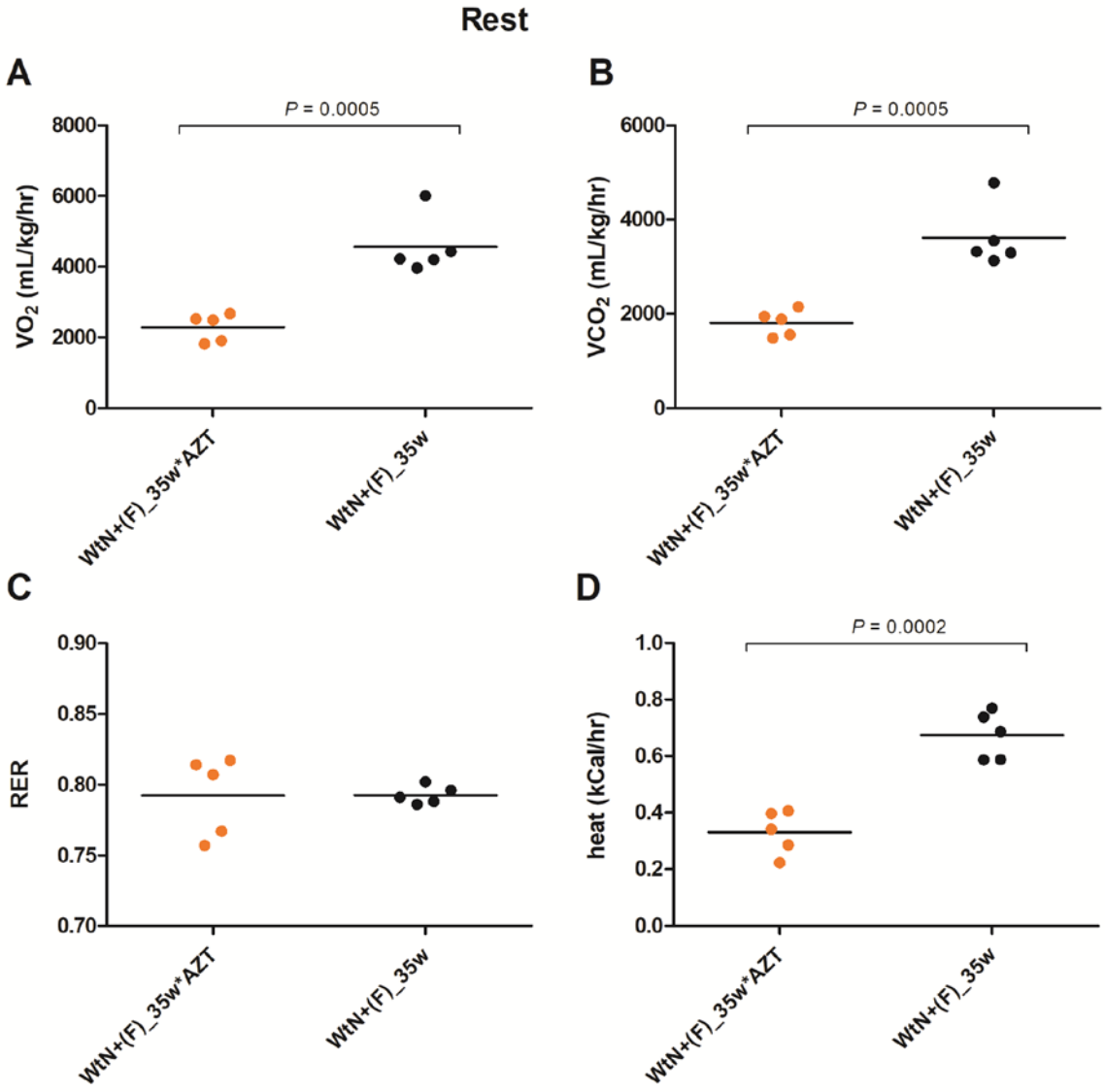

*Figure 8.16. Dot plots showing the metabolic treadmill values at rest for AZT-treated and untreated female WtN+ mice at 35 weeks old. Values were oxygen consumption (**A**), CO_2 produced (**B**), respiratory exchange ratio (RER, **C**) and heat produced (**D**). Each dot is the measurement of a single mouse. P is p-value for t-test. Line at mean. W is weeks.*

During exercise, there were no significant differences between AZT-treated and untreated WtN+ mice at 35 weeks on any parameter (Figure 8.17).

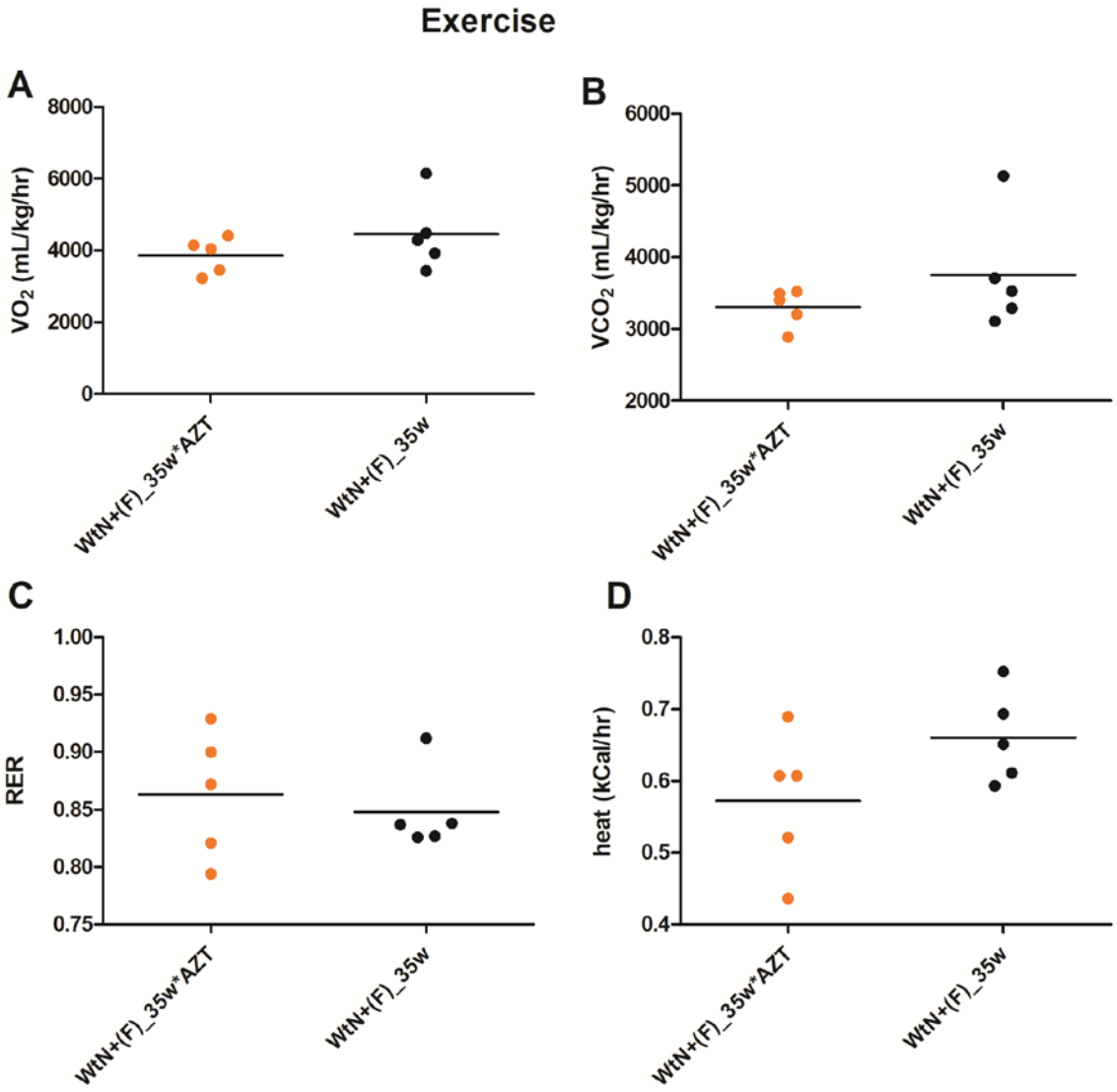

*Figure 8.17. Dot plots showing the metabolic treadmill values during exercise for AZT-treated and untreated female WtN+ mice at 35 weeks old. Values were oxygen consumption (**A**), CO_2 produced (**B**), respiratory exchange ratio (RER, **C**) and heat produced (**D**). Each dot is the measurement of a single mouse. Line at mean. W is weeks.*

8.4.8 Forelimb grip strength

Grip strength measurements were recorded as explained in Section 2.2.7. The three repeats measured were averaged and grip strength was adjusted for body weight. Results for the untreated ageing mouse cohort were already analysed in Section 5.4.6.

As observed for the untreated WtN+ female mice, the AZT-treated groups showed a significant decrease in grip strength between 35 and 47 weeks old (two-tailed unpaired t-test, p=0.02). Grip strength values were plotted to compare AZT-treated and untreated female WtN+ mice at 35 and 47 weeks old. A two-way ANOVA was performed for the female sex, to assess whether there was an interaction between age and AZT drug consumption on grip strength. The two-way ANOVA showed a strong association of grip strength with age (p=0.0002), but there was no effect of AZT (Figure 8.18). Therefore, grip strength decreased significantly with age, but not with AZT.

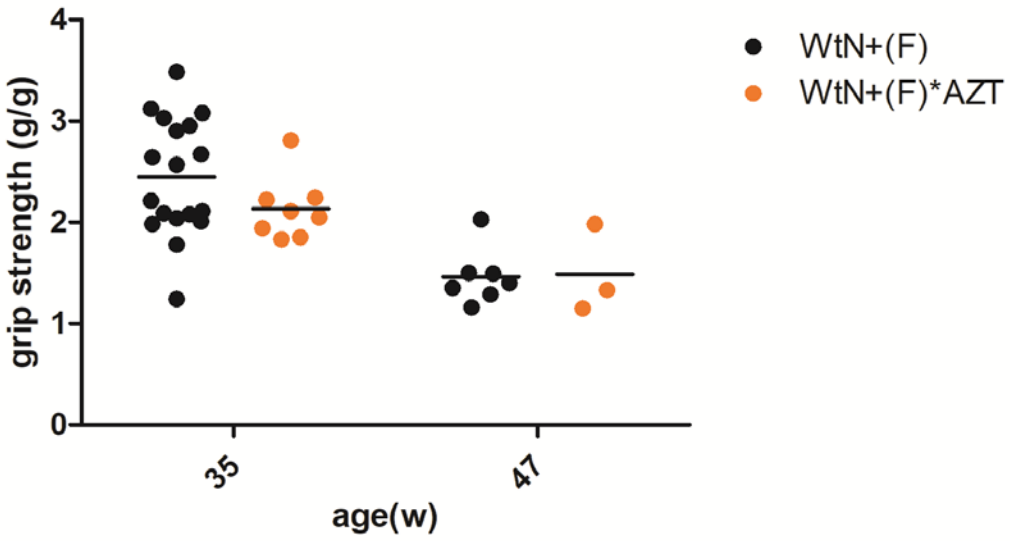

Figure 8.18. Dot plot showing the grip strength values for AZT-treated and untreated female WtN+ mice at 35 and 47 weeks old. Each dot is the mean of three grip strength measurements from a single mouse. (F) is female. (g/g) is the grip strength in grams adjusted for the mouse body weight in grams. (w) is weeks. Line at mean.

8.5 Discussion

Whilst the adverse effects observed, weight loss and anaemia, were expected as part of the ageing phenotype in this model, these were clearly potentiated in some mice by the AZT treatment. Anaemia has been linked with zidovudine use in HIV-infected humans (Richman *et al.*, 1987; Dainiak *et al.*, 1988; Fischl *et al.*, 1990; Falguera *et al.*, 1995; Semba *et al.*, 2002; Volberding *et al.*, 2004; Agarwal *et al.*, 2010; Dash *et al.*, 2015).

It was not clear why some mice experienced significant weight loss whereas others did not. I hypothesized that this may have been a 'double hit' of the mitochondrial defect and the treatment, however I was not able to demonstrate any differences in baseline, colon or skeletal muscle mtDNA mutations at euthanasia time point that predicted toxicity.

MtDNA CN results showed that there were no consistent patterns of mtDNA depletion with AZT treatment. The small changes observed were predicted by the fact that AZT is only a weak inhibitor of pol γ and as such, there was no expectation to observe large amounts of mtDNA depletion.

Sequencing of the mitochondrial genome of colon showed a selection against tRNA variants in the AZT WtN+ group, which was already found in Chapter 6 for untreated WtN+ mice, as opposed to no selection observed in skeletal muscle for these groups. The selection was no different in the presence or absence of AZT treatment. It should be specifically noted that no increase in number of mtDNA mutations was seen with AZT treatment, suggesting that AZT was not having a mutagenic effect in this experiment, at least within the limits of sensitivity of our MiSeq assay.

There was however, a progressive increase in residuals (i.e. drift of variants) over time in the colon of AZT-treated mice. This effect was much smaller without AZT treatment. This meant that AZT treatment resulted in a greater than expected divergence in mtDNA variant heteroplasmy between baseline ear snip and colon. These results altogether suggested that AZT may have modified clonal expansion of mtDNA mutations by accelerating drift of variant heteroplasmy, as hypothesised. These effects were not seen in skeletal muscle. As discussed previously, AZT is a relatively weak pol γ inhibitor and therefore did not cause significant mtDNA depletion in our model. This suggests that the accelerated drift of mtDNA heteroplasmy was

not caused by a molecular bottleneck effect (as occurs when the number of mtDNA molecules is profoundly reduced, for example during embryogenesis). Instead I hypothesise that the interfering effect of AZT on mtDNA replication (via pol γ and/or TK2) is nevertheless sufficient to increase the turnover of the mtDNA pool, leading to accelerated drift in mutation heteroplasmy.

The AZT-exposed 36-week WtN+ mice had a markedly worse complex I defect in colon than the untreated, and this difference persisted, although was reduced, in the 48-week AZT group. These findings could be due do the differences in washout durations. The 36-week group had a drug washout period of three weeks before the harvesting of the animal, which may not have allowed for complete recovery of mtDNA replication. The 48-week group had 15 weeks washout, which would certainly be expected to be long enough for complete recovery. The observation that CI defects remain significantly higher in previously AZT-exposed mice at 48 weeks compared with untreated mice despite the long period of drug washout is further strong evidence that clonal expansion may have been affected. This is in keeping with the predictions of *in silico* simulation models of clonal expansion, where after a finite period of NRTI exposure, the COX defect is predicted to continue to increase, even after the drug has been washed out (Payne *et al.*, 2011).

In terms of phenotyping results, no relevant differences were observed in the AZT cohort in the open field test. Similarly, grip strength was not associated with AZT treatment. In the metabolic treadmill test, AZT mice had significantly reduced metabolic values at rest but not during exercise. This suggests that the AZT-treated mice have adopted a more sedentary behaviour, perhaps due to either mitochondrial dysfunction or subclinical anaemia. However, the lack of effects of AZT treatment on metabolic parameters on exercise suggests that the AZT treatment did not lead to any severe phenotypic deficiencies.

8.6 Conclusion

This experiment gave some preliminary evidence that partial inhibition of mtDNA replication by an NRTI antiretroviral drug may increase clonal expansion of mtDNA mutations in the colon of our WtN+ mouse model as:

1. AZT treatment was associated with an increase in the drift of mtDNA mutations in colon;
2. AZT treatment resulted in an increase in CI-deficient colonic crypts (the end result of clonal expansion of mtDNA mutations), despite no evidence of mtDNA depletion and no increase in overall mtDNA mutation burden;
3. This effect appeared to exist even after washout of the drug, meaning it was not just a transient effect of current drug exposure.

Nevertheless, this effect was small and would need to be confirmed over a longer time course. Unfortunately, this was also limited by toxicity concerns.

This experiment also provided proof-of-concept that clonal expansion is a potentially modifiable process in our mouse model.

Chapter 9. General Discussion

9.1 Major findings

9.1.1 Mitochondrial DNA damage in human brain, HIV infection and antiretroviral treatment

The study of mtDNA damage in HIV infection in the setting of antiretroviral treatment and ageing was performed in frontal cortex homogenised samples. Age-associated mtDNA changes were observed as an increase in mtDNA point mutations and deletions and a decrease in mtDNA content. All of those changes were augmented in the HIV infected cohort in comparison to uninfected controls. Depletion of mtDNA has already been reported in ageing and neurodegenerative conditions such as Parkinson's disease (Grunewald *et al.*, 2015; Dolle *et al.*, 2016; Pyle *et al.*, 2016). These measures of molecular mtDNA damage (mtDNA point mutations, deletions and mtDNA content) were not associated with HIV disease progression markers, including lymphocyte counts and HIV RNA viral load, ART regimens or neurocognitive impairment measurements. These findings show an increase in 'brain ageing' in HIV-infected patients, which has been previously reported in brain imaging studies (Underwood *et al.*, 2017; van Zoest *et al.*, 2017), but not in a molecular study like this one.

To this author's knowledge, the sequencing approach used in this study was novel in that whole mitochondrial genome was sequenced and therefore all mtDNA variant types were analysed.

The age-associated decrease in mtDNA quantity and quality in PLWH compared to uninfected controls was observed to be augmented by the effects of HIV infection but not by ART. These findings contradict the myriad of *in vitro* and *in vivo* studies that have demonstrated associations between mtDNA depletion and ART, specifically certain older NRTIs which inhibit pol γ (Arnaudo *et al.*, 1991; Casademont *et al.*, 1996; Dalakas *et al.*, 2001; Lim and Copeland, 2001; Cote *et al.*, 2002; Walker *et al.*, 2004b; Buffet *et al.*, 2005; Haugaard *et al.*, 2005; Cherry *et al.*, 2006). The penetrance of ART in the CNS needs further investigation in order to determine if antiretroviral agents penetrate differently into the brain parenchyma, but comparison of ART levels in CSF and serum suggest that for many ART drugs, CNS levels are likely to be lower (Letendre *et al.*, 2008; Yilmaz *et al.*, 2012). It is therefore possible

that the level at which ART needs to be present in the CNS in order to cause mtDNA damage is not reached, meaning that the HIV effect predominates over any ART effect. As it seems to be HIV rather than ART that is driving the mtDNA defects, then full suppression of virus in the CNS (which is challenging due to the presence of CNS reservoirs) is probably a more important clinical consideration than the potential toxicities of ART drugs.

Viral proteins released in the cellular microenvironment could have a more highly deleterious effect in CNS cells than in other tissues. The fact that HIV infection on its own, without ART, produced the mtDNA changes observed is likely due to an HIV-mediated neurotoxicity associated with mitochondrial dysfunction. This could be explained by the fact that neurons contain large amounts of mitochondria, therefore mtDNA damage plausibly leads to neuronal dysfunction. These mtDNA changes could either be a direct effect or an indirect effect, that is, mtDNA damage could either be the cause or consequence of neuronal injury in HIV. Moreover, gliosis and neuronal loss are common phenomena in brains of patients with HAD and although severe forms of neurocognitive impairment are less prevalent now than in previous decades, mitochondrially-induced neurotoxicity could still have an impact in the conformation, health or even survival of CNS cell function.

No consistent relationship could be established in our findings of mtDNA damage and the neurocognitive impairment of the HIV cohort. Despite that the majority of HIV patients were on antiretroviral treatment, they were predominantly immunosuppressed with low CD4 counts. The fact that the HIV positive group showed advanced HIV (mean CD4 count 143 cells/μl) places some limitations on the generalisability of our findings to the whole HIV-infected population. More extensive studies should be conducted in larger sets of cases where HIV is consistently suppressed, however the availability of brain tissue from such patients is very limited. Moreover, a large number of factors are likely to contribute to NCI in people living with HIV, so it may be that the effects of mtDNA changes are masked by other factors, for example, depression and lifestyle factors (De Francesco *et al.*, 2019).

In addition, the clinical records provided to us from the biobanks reported that the majority of patients who were on ART at the time of last assessment had taken many different classes of antiretroviral regimens throughout their course of disease, sometimes in an on and off manner over many years. The nature of long-term and

such highly heterogeneous exposure to combination antiretroviral therapy makes it very difficult to assess the separate effects of individual classes of ART in mitochondrial molecular studies like the ones presented here.

Finding good animal or cellular models of the brain in which to study the impact of both HIV and ART simultaneously remains a challenge. Rodent studies of transgenic animals expressing *env*, *tat* or *pol* HIV genes cannot fully mimic HIV infection in human hosts (Saylor *et al.*, 2016). This human environment is difficult to replicate because it requires infectious and inflammatory molecular processes, the host immune response and the fact that the HIV genome integrates in different types of cells around the body. Monkey models have been used to study simian immunodeficiency virus (SIV) in order to mimic HIV pathogenesis, but to this author's knowledge, there are not any rodent studies that have looked at the combined effect of ART and HIV on brain (Gorantla *et al.*, 2012).

Limitations from the methodology used in the human brain study include that the DNA content obtained came from a homogenate of all the cell types found in the frontal grey matter of the brain. Therefore, results reported were expressed at the whole-tissue level. The poor morphological quality of fresh frozen brain tissue from the biobanks precluded any single cell studies. This likely reflects the post-mortem interval inherent in autopsy studies. If higher quality fresh frozen brain tissue had been available, laser microdissection of specific neurons could have been conducted, along with immunofluorescence for OXPHOS complex activity. This single cell assay would have given an indication of the mtDNA point mutation and deletion load in specific brain cell types. Another technique would have been fluorescence-activated cell sorting (FACS) to separate out astrocytes or glial cells in order to obtain a more homogeneous population for the study of mtDNA CN and the sequencing of mtDNA point mutations. If whole tissue was provided and there had been more time, other functional analyses could have been done including Western blotting for OXPHOS complex proteins. FFPE brain tissue from these biobanks could be studied as this should retain a higher quality tissue architecture. It may however be technically challenging to retrieve enough mtDNA to perform single-cell molecular studies on such tissue.

9.1.2 PolgA 'WtN+' mouse model of clonal expansion of mtDNA mutations in ageing

I generated a new mouse model with which to study the natural history of mitochondrial DNA mutations in ageing and disease. Specifically this model allowed us to study the critical biological process of clonal expansion of mitochondrial DNA mutations within cells – something which has not been previously possible.

This mouse was characterised at the cellular, molecular and organismal levels. The data generated supported the hypothesis that the phenotypic consequences of mitochondrial DNA mutations in ageing result from the clonal expansion of the mutations within cells, rather than the mutations *per se*. This hypothesis has been widely discussed in the literature but has never been able to be empirically proved.

The aim of the mouse cohort was to produce a good model of clonal expansion, which according to the results presented was successful.

Our novel WtN+ mouse model is unique and better in comparison to other current models, which are not optimal. The prototype model of mitochondrial ageing, the *PolgA* mouse, continuously produces very high levels of somatic mtDNA mutations which far exceed those seen in aged humans. This leads to a number of serious problems in its use as a model of human ageing, including: overly high mutation levels; the ageing phenotype being predominantly driven by very early mitochondrial dysfunction in stem cells, not by clonal expansion in somatic tissues; and since new mutations are constantly being produced, it is impossible to tell what is clonal expansion and what is mutagenesis (Trifunovic *et al.*, 2004; Kujoth *et al.*, 2005).

Another rodent model derived from the *PolgA* mouse, the $tRNA^{ALA}$ mouse, has a single trapped mtDNA germline mutation. This is much less representative of human ageing than a pool of multiple mtDNA mutations as I have generated in our study. Also, the mutation in the $tRNA^{ALA}$ mouse is present at a very high heteroplasmy level at baseline and appears to be selected against during life (Kauppila *et al.*, 2016).

During the breeding scheme for our WtN+ mice, the fertility difficulties that arose could suggest an early embryonic lethality. To further look into that, future work could investigate mtDNA mutations in embryos and oocytes of those mice although that was not part of the original study design.

Phenotypic investigations of the WtN+ model as presented in Chapter 5 showed that the model did not have a dramatic progeroid phenotype. This makes it difficult to make clear conclusions about the link between clonal expansion of mtDNA mutations and physical manifestations of the ageing process. However, a limitation for the phenotypic characterisation could be that the mice could have been aged for longer had there been more time, in order to show a more accentuated ageing phenotype. WtN+ aged mice were however weaker, with lower grip strength relative to their size, compared to wild-type mice. This is likely to indicate that there is some detrimental phenotypic effect of the mtDNA mutations on muscle function and/or body composition.

MtDNA copy number was higher in colon of the oldest WtN+ mice, which was likely to be a compensatory response to the increasing complex I deficiency.

Selection of mtDNA variants was stronger throughout successive generations of WtN+ mice (as described in Chapter 4) than during the lifetime of the experimental G3 WtN+ mice (as described in Chapter 6), suggesting the mechanism of germline purifying selection was more stringent than the one observed for somatic tissues, i.e., the extent to which the inherited mtDNA mutations were subject to selection during oogenesis/embryogenesis was stronger than any effect during the life of the mouse.

The WtN+ mice generated showed multiple mtDNA variants which were transmitted through the maternal germline. These were present at a wide range of heteroplasmy levels from 2% (the limit of the assay) to >50%. On the one hand, relatively high level heteroplasmies (around 50%) are ideal for studying clonal expansion as they will be expected to allow the largest shifts in heteroplasmy. However, as a model of mtDNA mutations in humans this is a potential limitation, as the mutations that ultimately clonally expand in single cells in ageing humans are likely to be initially present at very low heteroplasmy levels (Payne *et al.*, 2012). In a similar way, in our human brain sequencing data, somatic mtDNA mutations were generally present at low heteroplasmy levels (<10%). In our mouse model, very low-level heteroplasmic mutations (near 2%) were frequently lost during maternal transmission, such that it was the higher level heteroplasmies that tended to persist through successive generations. Clonal expansion of mtDNA mutations is thought to be a gradual process, which requires many cycles of mtDNA turnover. Over a typical human lifespan (~80 years) there is likely to be sufficient time for even very low level

heteroplasmic mtDNA mutations to clonally expand within individual cells. In contrast, in a mouse model of clonal expansion this needs to be achieved in a timespan that fits with the life expectancy of the laboratory mouse as well as other experimental constraints (<~2 years). In order for clonal expansion events to be observed within this shorter timescale likely requires baseline heteroplasmy levels to be higher. Therefore, although our mouse model did not perfectly recapitulate mtDNA mutations in normal human ageing, it nevertheless provides a useful model with which to study the clonal expansion of mtDNA mutations.

There were very small changes in skeletal muscle mtDNA mutations, as opposed to colon, confirming previous work in colonic crypts, which showed it to be the best tissue in which to study clonal expansion of mtDNA point mutations (Baines *et al.*, 2014).

Finally, the study of pooled individual mouse colonic crypts empirically proved the clonal expansion of complex I mutations. This approach shows that clonal expansion cannot be reliably inferred simply by looking for changes in heteroplasmy levels in tissue homogenates compared with baseline. At the whole tissue level, I saw no systematic increases in mutation heteroplasmy levels, and in some cases, slight negative selection. Instead, I showed that the increasing drift of heteroplasmy levels away from baseline with increasing age in colon is what provides evidence that clonal expansion could occur. This concept was then confirmed through the single crypt analyses.

One limitation of our work is that this is only a model for the clonal expansion of mtDNA point mutations and not for deletions. Deletions in our study were not generated, and I expect that they would not be tolerated to be transmitted through the maternal germline. Therefore, a model of the clonal expansion of mtDNA deletions would require another means of generating deletions in the mouse. A transgenic mouse model expressing mouse Twinkle with PEO patient mutations results in accumulation of mtDNA deletions but does not show a premature ageing phenotype possibly due to the short lifespan of mice not allowing phenotype expression (Tyynismaa *et al.*, 2005). Therefore, better mouse models to study mtDNA deletions are needed.

9.1.3 Antiretroviral drug exposure on WtN+ mice

The initial question was to investigate whether AZT produced *de novo* mtDNA mutations or lead to clonal expansion of existing mtDNA mutations. AZT was used to explore whether the rate of clonal expansion of mtDNA mutations in our novel WtN+ mouse model was able to be modified.

A subset of AZT-treated WtN+ mice reached a humane endpoint at 27 weeks, whereas other AZT-treated littermates remained well. If AZT was responsible for the toxicity observed in the 27-week WtN+ mice, there were no differences in underlying mtDNA mutations that appeared to have been responsible. Analysis in baseline tissue addressed the question of whether the mice that developed toxicity were predisposed by a high baseline mutation load, which did not seem to be the case. When the same analysis was performed for colon and skeletal muscle at the corresponding harvesting time points, no significant mtDNA variant differences were observed between mice with toxicity and mice without. Therefore, no clear explanation could be found for the rapid development of toxicity to the antiretroviral drug AZT in a subset of treated WtN+ mice.

The duration of AZT treatment that was used was limited by the onset of treatment toxicity that affected a subset of the WtN+ mice in this study. In order to see a change in clonal expansion, prolonged treatment would be needed as this change presumably requires many cycles of mtDNA replication to be able to take place. This experiment did nevertheless use a similar duration of AZT treatment than other previous rodent studies, which did not measure clonal expansion (Zhang *et al.*, 2014; Zhang *et al.*, 2015). However, ideally I would have given even longer treatment had I not had concerns about cumulative toxicity.

As was expected, changes in mtDNA CN with AZT treatment in WtN+ mice were small as AZT is only a mild inhibitor of polymerase γ. Future work could use more potent inhibitors of polymerase γ which induce significant depletion of mtDNA to see if this caused more profound effects on clonal expansion of mtDNA mutations.

The fact that no increase in mtDNA mutation number occurred during AZT treatment meant AZT did not act by increasing mutagenesis *de novo* but rather by clonal expansion. However, future analyses should study lower level variants, at less than 2% heteroplasmy, to fully exclude this effect.

In conclusion, sequencing results showed that AZT treatment: (1) did not modify the selection of mtDNA variants in WtN+ mice; (2) modified clonal expansion of mtDNA mutations in colon but not in skeletal muscle; and (3) did not increase mtDNA *de novo* mutations. These effects were achieved without inducing significant mtDNA depletion.

9.1.4 Next generation sequencing technology for studying mtDNA mutations

NGS is a powerful tool for studying heteroplasmic mtDNA point mutations and allowed us to study these mutations at great breadth (whole mtDNA genome) and great depth (to 2% heteroplasmy) in both the human and the mouse studies. There are however some limitations of NGS technologies for the study of mtDNA mutations.

Although read lengths for Illumina sequencing (including MiSeq) have improved in recent years, they remain relatively short (150-250bp reads). In our analyses of the transmission and clonal expansion of mtDNA point mutations I typically observed ~30-40 variants at >2% heteroplasmy per mouse. I have considered each variant as being independent, as the short read lengths mean that it is not possible to determine which variants sit on the same molecules of mtDNA. In fact, it is likely that some of the mtDNA mutations were clustered into clades. Future studies should investigate ways to reliably deep sequence long read lengths of mtDNA, preferably whole mtDNA genome in a single read. For example, Oxford Nanopore and Pacific Biosciences offer novel sequencing technologies with long read lengths.

NGS allowed our assays to cover all mtDNA variants across the whole mtDNA genome at a high read depth. However, very low level heteroplasmic variants (<2%) were excluded from our investigations in order to set a stringent filter below which mutations could be considered assay noise. Any threshold set in NGS deep sequencing analysis is somewhat subjective but considering only mtDNA mutations above 2% heteroplasmy, a conservative threshold, gave us high confidence that these mutations were in fact real. On the other hand, use of this threshold meant that I could not report changes in mutations present at very low heteroplasmy levels (<2%), which are nevertheless of potential importance when studying clonal expansion of mtDNA mutations. Future work could include looking at below 2% heteroplasmy level variants, but this may require more sophisticated NGS assays.

To overcome NGS limitations, a strand-specific unique molecular tagging technique was developed by the Loeb group (Schmitt *et al.*, 2012; Schmitt *et al.*, 2015). This method called duplex sequencing was created to reduce error by employing unique oligonucleotide barcodes to independently tag and sequence each strand of each duplex DNA molecule. The true mutations will be found in both strands and scored once, whereas sequencing errors will be found in only one strand and discarded. The authors claim this sensitive methodology can detect a single mutation present among $>10^{7}$ wild-type molecules and estimate its error rate to be $<4 \times 10^{-10}$ (Schmitt *et al.*, 2012; Schmitt *et al.*, 2015). Another similar technique that has been developed in order to avoid artefactual errors during deep sequencing was a high throughput assay for the accurate sequencing of the HIV-1 protease gene, called Primer ID (Jabara *et al.*, 2011). A block of degenerate nucleotides is attached to the cDNA primer to create distinct combinations or Primer IDs. The Primer ID is flanked by a three nucleotide barcode. When the Primer ID and the barcode are repetitively identified, a consensus sequence is formed (Jabara *et al.*, 2011). A unique molecular tagging approach similar to these methods was designed during this project (data not shown in this thesis), but due to time constraints I was not able to finalise optimising the sequencing protocol.

9.2 Final conclusion

The work in this thesis has provided a novel rodent model for the study of clonal expansion of mtDNA point mutations, the WtN+ mouse. Using molecular and immunohistochemical techniques, it was confirmed that mitotic tissues, particularly colon, are the best for the study of clonal expansion. Clonal expansion of complex I mutations in single colonic crypts was further confirmed using single cell work. Phenotypic descriptions of this WtN+ mouse showed an increase in weakness with age, which may be suggestive of premature frailty. However, the model did not show a dramatic premature ageing phenotype. In addition, our experiments with the NRTI zidovudine suggest that I am able to modify clonal expansion in this mouse.

Investigations conducted in human brain concluded that the mtDNA damage observed was driven by the effect of HIV infection itself, independently of ART. Nonetheless, these experiments supported the concept of an accelerated molecular ageing of the brain in people living with HIV.

Chapter 10. Appendices

10.1 Mouse monitoring sheets for clinical scoring

Mouse ID		RFID transponder **NA**			Notch			Cage				Harvest Date:		
Observation	Date	Weight (g)	Weight	Coat	Skin Tone	Behaviour	Posture and Mobility	Abdominal distension	Foot colour	Faeces	Total Score	RFID Temp	Notes
1													
2													
3													
4													
5													
6													
7													
8													
9													
10													
11													
12													
13													
14													
15													
16													
17													
18													
19													
20													
21													
22													
23													

Characteristic	Score	1. Normal	1. Mild	1. Moderate	3 - Substantial
1	Weight	No weight loss / gain	5-15% weight loss	15-20% weight loss	Over 20% weight loss
2	Coat- general	Normal	Slight lack of grooming	Starey	
3	Skin Tone	Normal	Tents, returns to normal in 1-2 seconds	Tents, persists	
4	Behaviour	Normal	Subdued but responsive. Animal shows normal behaviour patterns. Interacts with peers	Subdued- animal shows subdued behaviour. Little peer interaction. May show aggression.	Animal unresponsive to extraneous activity and provocation even when provoked.
5	Posture and mobility	Normal	Transient hunched posture, especially after dosing. Normal mobility	Hunched intermittently. Reduced mobility	Hunched persistently 'frozen'. No spontaneous mobility.
6	Abdominal distension	None	None	Abdominal distension up to the size expected in late pregnancy	Severe abdominal distension beyond that of late pregnancy affecting locomotor and / or breathing patterns.
7	Foot colour	Normal	Whitening of feet due to mild anaemia	Whitening of feet due to moderate anaemia	Feet are completely white due to severe anaemia
8	Faeces	Normal	No diarrhoea or transient diarrhoea	Intermittent or continuous diarrhoea (>72h). No dehydration.	Continuous diarrhoea (>72h) with faecal soiling of perineum and/or dehydration.

10.3 Study plan submission

Experimental Plan

PolgA (WtN derivative) and WT mice (male and female) will be aged and phenotyped. Of principle interest are age-associated mitochondrial dysfunction and tissue fibrosis, especially in skeletal muscle, bowel and liver. Approximately 1/3 of the mice will be killed at each of three time-points: 4 months, 8 months, and 12 months. The last time-point may be extended to 18 months depending on the speed of onset of the ageing phenotype in WtN mice. Mice will be weighed monthly (starting at 4 months), increased to weekly if clinical concern. Clinical phenotypic scoring will be performed monthly (starting at six months), increased to weekly if clinical concern. Behavioural testing: open field testing, grip strength and metabolic treadmill tests will be performed at 7 and 11 months. Blood samples: Blood (up to 0.2 ml) will be taken from mice restrained in an appropriate device every four months. Therapy: A group of WtN mice (n=16, female) will have AZT (zidovudine) treatment added to drinking water. This therapy is given to try and alter the rate of accumulation of mtDNA mutations and slow any ageing phenotype. To achieve a human equivalent dose requires 120mg/kg/d, as 24.7mg AZT per 30ml bottle of drinking water. Water bottles will be weighed to estimate drug intake per mouse per day (assumed to be 5mL). Animals will be dosed from six through to 10 months of age. Prior to commencing the experiment the palatability of the drug will be tested on a separate cage of mice and adjustments made to the drinking water if necessary (but previous published data suggest there is no effect). At the end of the experiment mice will be humanely killed by a schedule one method.

Adverse Effects Interventions

Phenotyping of young mice (<12 months) is not expected to cause any adverse effects. Older WtN mice (>12 months) may develop age related health issues e.g. reduced mobility, poor coats, however these features are expected to be mild in the WtN derivative of PolgA mice. The adverse effect will be recognised by clinical examination of animals and use of health score sheets. Animals showing more than moderate signs of conditions associated with aging would be humanely killed. The impact of the conditions may be reduced by provision of soft bedding and soaked diet. Clinical scores above moderate (10-14) would result in euthanasia. The rate of deterioration in these strains is variable therefore clinical score sheets will be used to

help assess these mice. Any genetically altered mouse that is showing signs of distress due to accelerated ageing will be killed on advice of the vet. Mice who lose >30% of body weight would be humanely killed irrespective of its clinical condition. Blood sampling: Animals could haemorrhage from the site of venepuncture, the likely incidence is <1%. The animal will be observed immediately after sampling, and checked again 5 minutes later. Adoption of appropriate methods of haemostasis will minimize the risk of this affect. If normal methods of haemostasis are not successful within a short period of time, the mice will be humanely killed. Therapy: We do not anticipate that administration of the AZT therapy will cause significant adverse effects. The effect, if any, on the ageing phenotype is expected to depend on whether the therapy alters the balance of mutant and wild-type mtDNA molecules. Whilst it is hoped that the therapy will slow the rate of onset of the ageing phenotype it is possible that it might accelerate it. However any effect on the rate of onset of ageing phenotype in older animals is expected to be much less than that attributable to the PolgA genotype. It would be rare that AZT therapy would cause toxic effects at the dose employed here (<5%). If adverse effects are observed at any time we will give appropriate supportive care e.g. fluids and/or soaked diet as necessary. Animals that exhibit a hunch posture, abnormal locomotion and ruffled fur coat, or diarrhoea would be humanely killed if they failed to respond to supportive care (warmth, fluids) within 48 hours. Mice who lose >25% of body weight would be humanely killed. Behavioural testing: Behavioural testing is not expected to cause any adverse effects other than mild stress during exposure to the apparatus.

10.4 Protocol Number 2 for Genetically Altered Animals

Protocol Title *

Phenotyping of genetically altered animals

PIL Holder Responsible *

Brendan Payne / Carla Roca

PIL Holder Email Address *

Start Date *

End Date (If Known) 31.8.2019

Number of animals *

86

Species and Strain(s) *

Mouse: PolgA^{mut} and WT (B6)

Current Cage Id(s) *

Severity *

Moderate

Experimental Plan *

Refer to the project licence protocol steps and list only the steps that these animals will go through

PolgA (Wt^{N} derivative) and WT mice will be aged and phenotyped. Of principle interest are age-associated mitochondrial dysfunction and tissue fibrosis, especially in skeletal muscle, bowel and liver. Approximately 1/3 of the mice will be killed at each of 3 time-points: 4 months, 8 months, and 12 months. The last time-point may be extended to 18 months depending on the speed of onset of the ageing phenotype in Wt^{N} mice.

WT mice will be weighed monthly (starting at 2 months), increased to weekly if clinical concern. GA mice will be weighed weekly, increased to twice weekly if clinical concern.

Clinical phenotypic scoring in WT mice will be performed monthly (starting at 6 months), increased to weekly if clinical concern. In GA mice scoring will be performed weekly, increased to twice weekly if clinic concern.

Behavioural testing: open field testing, grip strength and metabolic treadmill tests will be performed at 7 and 11 months.

Blood samples: Blood (up to 0.2 ml) will be taken from mice restrained in an appropriate device every 4 months.

Therapy: A group of Wt^N mice will have AZT (zidovudine) treatment added to drinking water. This treatment is given to try and alter the rate of accumulation of mtDNA mutations and slow any ageing phenotype. To achieve a human equivalent dose requires 120mg/kg/d, as 24.7mg AZT per 30ml bottle of drinking water. Water bottles will be weighed to estimate drug intake per mouse per day (assumed to be 5mL). Animals will be dosed from 20 through to 40 weeks of age. Prior to commencing the experiment the palatability of the drug will be tested on a separate cage of mice and adjustments made to the drinking water if necessary (but previous published data suggest there is no effect).

At the end of the experiment mice will be humanely killed by a schedule one method.

*Adverse Effects Interventions **

Detail adverse effects, interventions and state humane end points

Phenotyping of young mice (<12 months) is not expected to cause any adverse effects. Older Wt^N mice (>12 months) may develop age related health issues e.g. reduced mobility, poor coats, however these features are expected to be mild in the Wt^N derivative of PolgA mice. The adverse effect will be recognised by clinical examination of animals and use of health score sheets.

Animals showing more than moderate signs of conditions associated with aging would be humanely killed. The impact of the conditions may be reduced by provision of soft bedding and soaked diet. Clinical scores above moderate (10-14) would result

in euthanasia. The rate of deterioration in these strains is variable therefore clinical score sheets will be used to help assess these mice. Any GA mouse that is showing signs of distress due to accelerated ageing will be killed on advice of the vet. Mice who lose >30% of body weight would be humanely killed irrespective of its clinical condition.

Blood sampling: Animals could haemorrhage from the site of venepuncture, the likely incidence is <1%. The animal will be observed immediately after sampling, and checked again 5 minutes later. Adoption of appropriate methods of haemostasis will minimize the risk of this affect. If normal methods of haemostasis are not successful within a short period of time, the mice will be humanely killed.

Therapy: Our experience with this genotype shows that most mice tolerate AZT therapy without significant adverse effects beyond mild anaemia. However some animals have developed more rapid onset of weight loss. This is likely to be a combined effect of the PolgA genotype and the treatment. If adverse effects are observed at any time we will give appropriate supportive care e.g. fluids and/or soaked diet as necessary. Animals that exhibit a hunch posture, abnormal locomotion and ruffled fur coat, or diarrhoea would be humanely killed if they failed to respond to supportive care (warmth, fluids) within 48 hours. Mice who lose >30% of body weight would be humanely killed. Mice should be weighed and have clinical scoring twice weekly whilst on treatment. This should be increased to three times weekly if >5% weight loss. If >15% weight loss, treatment should be stopped and supportive care given.

Behavioural testing: Behavioural testing is not expected to cause any adverse effects other than mild stress during exposure to the apparatus.

Metabolic treadmill: May cause mild and short-lived stress.

Special requirements and/or instructions

Stocking densities should be kept consistent (4-6 mice per box).

Please note if you're not contactable animals may be humanely killed if it is deemed necessary.

10.5 Mouse harvesting sheets and instructions

Cage:	**Date:**
Mouse No:	**Storage Location:**
Harvest Number:	**Final Urine & Faeces location:**

Weighing and Measurements:

Remove any fat from tissue before weighing

Body weight	g
Liver	g
Spleen	g
Kidney R	g
Kidney L	g
Heart	g
Lung	g
Pancreas	g
Muscle	g
Fat	g
Brain	g
S. Intestine	cm
Colon	cm
Urogenitus	g
Testicle R	g
Testicle L	g

Equipment: Dissection kit, 21 Harvest tubes arranged in rack, 13 tissue cassettes, ruler, needle / syringe, Isopentane, Formalin, Liquid N_2.

Dissection Protocol

1. Spray the mouse with 70% EtOH, and cut open from the tail to the neck.
2. Aspirate blood from the heart and place it in ice (serum is collected from the supernatant after centrifugation at 8000rpm for 10mins).
3. **Weigh** each mouse tissue prior to dividing for fixing or freezing.
    a. Fixing 10% formalin
    b. Freezing in liquid N_2

Mouse Tissue

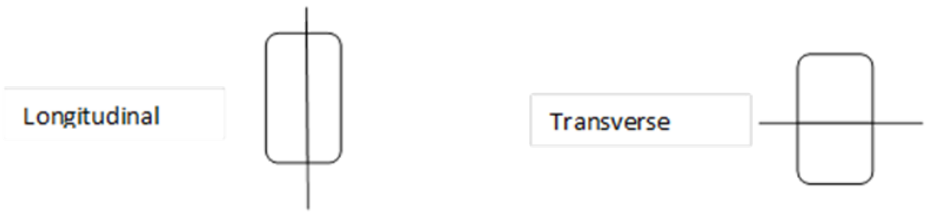

1. **Urogenitus (Bladder, prostate & urethra)** – Remove excess fat, lay flat on blue biopsy pad on tissue cassette. Unfurl the two seminal vesicles, and orient the bladder on the top & urethra at the bottom. Cover tissue with another biopsy pad, and fix whole urogenitus.
2. **Right Testis** – Cut longitudinal, half is fixed, half is frozen.
3. **Left Testis** – Cut transverse, half is fixed, half is frozen.
4. **Prostate**, half is fixed, half is frozen
5. **Right Kidney** – Cut longitudinal, half is fixed, half is frozen.
6. **Left Kidney** – Cut transverse, half is fixed, half is frozen.
7. **Skin** – Shave skin from back, use paper towel to cut 2 slivers. One is fixed, the other is frozen
8. **Brain** – Cut between hemispheres. Left hemisphere is fixed, the right hemisphere is frozen.
9. **Fat** – Scraped from the right side underneath the skin and is frozen (fat dissolves in formalin).
10. **Muscle** – Muscle is taken from the thigh. Take half of right thigh and half of left thigh and fix, the other half of rest and left thighs are frozen in isopentane first.
11. **Lung** – Left lung (2lobes) is fixed, the right lung is frozen.
12. **Heart** – Cut longitudinal, half is fixed and half is frozen in isopentane.
13. **Spleen** - Half the spleen goes into the tissue cassette with the Liver. The other half of the spleen gets frozen.
14. **Liver**– Triangular lobe of liver goes into tissue cassette. Cut a capsule off the bilobulated lobe and discard. Cut a sliver from the exposed capsule and place into tissue cassette. Cut a capsule off the large lobe and discard. Cut a sliver from the exposed capsule. Cut two squares from this sliver, one gets frozen for RNA, the other gets frozen for protein. The rest of the liver gets frozen.
15. **Pancreas** – This is located wrapped around the proximal SI next to the stomach. It is hard to distinguish from fat, however, if required, the pancreas sinks and fat floats in water. Half the pancreas is fixed, the other half is frozen.
16. **SI** – Measure the SI its contents are then collected. 2 ends of the SI are frozen. The rest is rolled up into a coil and fixed
17. **Colon** – The contents of the colon is collected. 2 ends of the colon are frozen. The rest is fixed.

18. **Caecum** – The contents of the caecum is collected.
19. **Stomach** – The contents of the stomach is emptied. The stomach is rolled up. A sliver is cut to be frozen. The rest is fixed.

10.6 Tests in the neuropsychological battery (provided by D. Moore)

Estimate of Premorbid Functioning

Wide Range Achievement Test (WRAT-3) – Reading Subtest (Wilkinson, 1993). The WRAT-3 reading subtest provides information on a subject's ability to recognize and name letters and their ability to pronounce words out of context. Subjects are instructed to individually read and pronounce a list of 42 words. Individuals who obtain less than five points on this section are then instructed to read the letters of the alphabet. This test is intended to measure word recognition, not speech or diction. (5 min.)

Verbal Fluency

Letter Fluency Tasks. (Borkowski, Benton, and Spreen, 1967). On the Letter Fluency Test the subject is asked to say as many words as possible that begin with the letters "F," "A," and "S," excluding proper names and different forms of the same word. For each letter, the subject is allowed one minute to generate words. Performance is measured by the total number of correct words generated. Perseverations (i.e., repetitions of a correct word) and intrusions (i.e., words not beginning with the designated letter) are also recorded, as well as variants (the same word with a different suffix (e.g., "big, bigger, biggest). (5 min.)

Speed of Information Processing

Trail Making Test A (Army Individual Test Battery, 1944; Reitan and Davison, 1974). This is a measure of psychomotor speed, attention and cognitive sequencing. Subjects are asked to connect quickly (in ascending order) a series of randomly arranged dots numbered from 1 to 25. (1 min.)

WAIS-III Digit Symbol (Wechsler, 1997). This is a test of psychomotor speed, concentration, and graphomotor abilities that requires the respondent to match symbols to numbers as quickly as possible, using a visual reference at the top of the page. (3 min.)

WAIS-III Symbol Search (Wechsler, 1997). This test requires psychomotor speed, attention, and concentration. Subjects are asked to scan two groups of symbols visually and determine if either of two target symbols matches any of five symbols appearing in an array to the right of the target symbols. The subject attempts to complete as many items as possible within a 120-second time limit. (3 min.)

Attention / Working Memory

WAIS-III Letter-Number Sequencing (Wechsler, 1997). The examiner reads a combination of scrambled numbers and letters that the subject is then asked to reproduce orally with the numbers first in ascending order, followed by the letters in alphabetical order. As the test progresses, items presented to the subject contain more numbers and letters. There are three items in each trial, and each trial has different combinations of numbers and letters. This test requires concentration, attention, and an ability to store and organize information in memory for a short duration. (5-10 min.)

Paced Auditory Serial Addition Task (PASAT) (Gronwall, 1977). In this test, a set of randomized digits is serially presented via tape recording (or computer generated voice in Spanish). Subjects are asked to add the current number to the number that preceded it and respond with the total. Thus, after each new digit is presented, a new total is achieved. The number of correct responses is scored. This also is an effective test of speed of information processing. (10 min.)

Learning and Recall (2 Domains)

Hopkins Verbal Learning Test - Revised (HVLT-R; Benedict, Schretlen, Groninger, and Brandt, 1998). The HVLT-R provides information on the ability to learn and immediately recall verbal information across trials, as well at the ability to recall and recognize this information after a delay. A list of 12 words (four words from each of three semantic categories) is presented to the subject over three trials. After each trial, the subject is asked to recall as many items as possible from the list in any desired order. A 20-minute delay follows the administration of the three trials, after which the subject is asked to recall the list. Subjects are then read a list of 24 words,

one at a time, and are asked if the word appeared in the original list. The items presented during the recognition phase contain the originally presented words, words in the same semantic class, and unrelated words. In order to minimize practice effects that may arise from repeated administrations in a longitudinal design as we are proposing here, six alternate forms of the test are available. There is no time limit on this test. (10-15 min.)

Brief Visuospatial Memory Test - Revised (Benedict, 1997). This test provides a measure of ability to learn and immediately recall visuospatial information. Delayed recall and recognition are also assessed. Subjects are presented with an 81/2" by 11" card containing six simple designs in a 2" by 3" matrix. The display is presented for 10 seconds, after which the subject is asked to reproduce as many of the designs as possible in their correct location on a blank sheet of paper. A total of three learning trials are administered. After a 25-minute delay, subjects are once again asked to reproduce the matrix. This is followed by a recognition trial in which subjects are shown 12 designs, one at a time, and asked if the design appeared in the original matrix. The recognition trial consists of the six original designs and six foils. A copy trial is administered in order to rule out poor performance due to graphomotor or visuospatial impairment. In the copy trial, subjects are given the display along with a blank sheet of paper and asked to copy the designs. There is no time limit for the recall, recognition or copy trials. (15-20 min.)

Abstraction / Executive Functioning

Trail Making Test B (Part A is considered under Speed of Information Processing) (Army Individual Test Battery, 1944; Reitan and Davison, 1974). This is a measure of psychomotor speed, attention, and cognitive sequencing. Part B requires subjects to connect a series of randomly arranged circles in a designated sequential order, based on alternating numbers and letters (i.e., 1 to A to 2 to B, etc.) In addition to the skills required in part A of this test, shifting cognitive sets is also required. (5-10 min.)

Wisconsin Card Sorting Test: Computer Version-2 (Research Edition: 64-item version) (Berg, 1948; Grant and Berg 1948; Heaton, Chelune, Talley, Kay, and Curtiss, 1993; Heaton and PAR Staff, 1993). This is a measure of executive function that requires planning, use of feedback, and shifting of cognitive sets. Subjects are

required to match a card that appears on the bottom part of the computer screen to one of four stimulus cards that are present on the upper part of the computer screen. The stimulus cards have four different designs on them -- the first has a red triangle, the second has two green stars, the third has three yellow crosses, the fourth has four blue circles. The cards that subjects are required to match to one of the four stimulus cards vary in color, geometric form, and number. Subjects receive feedback each time on correct or incorrect performances, and must use this feedback to alter their choices as the criteria for correct responses changes throughout the test. There is no time limit for this test. (15-30 min.)

Motor Skills

Grooved Pegboard (Kløve, 1963). This is a test of fine motor coordination and speed. In this test, subjects are required to place 25 small metal pegs into holes on a 3" x 3" metal board. All pegs are alike and have a ridge on one side, which corresponds to a notch in each hole on the board. First the dominant hand is tested, and subjects are asked to place the pegs in the holes as fast as they can. This is then repeated with the nondominant hand, and the total time for each hand is recorded (5 minutes).

Spanish-Language Tests

In order to assess Spanish-speaking subjects with a battery similar to the one administered to the English-speaking subjects, a number of tests have been selected that utilize similar paradigms but are more reflective of Hispanic culture and common Spanish language usage. Normative data from approximately 200 Spanish-speaking subjects are available for Dr. Artiola's instruments (Artiola et al., 1999), and additional norms have been developed for other tests in the battery by Drs. Heaton and Cherner in San Diego and are being published. When equivalent tests were not available, English-language tests and instructions were translated and adapted into Spanish by HNRC staff, using standard back-translation procedures. Individuals from five different Spanish-speaking regions (i.e. Mexico, Puerto-Rico, Cuba, Colombia, and Argentina) verified the translations. The WRAT-3 was not translated and was omitted from the Spanish-language battery.

Hopkins Verbal Learning Test-Revised. The majority of words in this list learning task were translated from the English, but some items had to be modified for appropriateness in Spanish (Cherner, Suarez, Lazzaretto, Artiola i Fortuny, Rivera-Mindt et al, 2006).

Letter Fluency (PMR). Similar to the Letter Fluency (Borkowski, Benton, and Spreen, 1967), but using the letters P, M, and R.

Self-assessment of Every-day functioning and Mood

Activities of Daily Living Questionnaire (ADL). The ADL is a brief self-administered questionnaire (modified for use at the HNRC from Lawton and Brody's Instrumental Activities of Daily Living scale) in which the participant reports the amount of assistance needed in accomplishing basic everyday tasks (e.g., shopping, cleaning, managing medications) under two conditions: when these tasks were accomplished at their best performance level and when these tasks are attempted at their current performance level. This measure allows the examiners to determine the extent to which changes in functioning may have occurred since optimal functioning and this information is useful in assisting clinicians in their determination of an AAN diagnosis. (10 minutes).

Beck Depression Inventory (BDI) (Beck, 1976). The BDI consists of 21 questions, each having 4 graded statements (labeled 0 to 3) ordered to show increasing symptoms of depression. The items of the BDI are clinically derived and there are numerous studies of reliability and validity. This measure is widely used in psychiatrically and medically ill populations and is a standard instrument for self-report symptoms of depressed mood (5-10 min.)

Patient's Assessment of Own Functioning Inventory (PAOFI) The PAOFI is a brief self-administered questionnaire in which the participant reports the frequency with which he/she experiences difficulties with memory, language and communication, use of his/her hands, sensory-perception, higher level cognitive and intellectual

functions, work and recreation. This instrument aids clinicians in their determination of a syndromic HIV-associated neurocognitive disorder (HAND) diagnosis. (10 minutes)

10.7 Antiretroviral drug regimens for HIV patients

PATID	CURRENT MEDARV					
6800278276	/					
7100056883	3TC	APV	D4T	DDI	NVP	ZDV
7100107766	3TC	ABC	EFV			
7100547672	ABC	APV	D4T	RTV		
7100616568	EFV	NVP				
7100626868	3TC	ABC	ZDV			
7100658283	/					
7101328666	ATV	FTC	RTV	TFV		
7102536771	EFV	FTC	TFV			
7200186777	/					
7200267172	ATV	RTV	FTC	TFV		
7200466870	3TC	RTV	SQV	TFV		
CA102	/					
CA125	/					
CA236	/					
CC163	3TC	ABC	KTA	NFV	RTV	TFV
CE129	/					
CE135	/					
CE144	/					
CG118	KTA	FTC	TFV			
CG157	/					
1004	NFV	ZDV	3TC			
1008	/					
1010	3TC	ATV	RTV	TFV		
1021	/					
1026	ATV	ABC	3TC	TFV		
1057	3TC	D4T	FTV	NVP		
1065	/					
1071	/					
1087	FTC					
1093	ATV	EFV	RTV	TFV		
1099	/					
1113	ATV	ABC	3TC	RTV		
1119	3TC					
1129	3TC	ABC	KTA	ZDV		
1141	ABC	DRV	RTV	T20	TFV	
1143	EFV	FTC	TFV			
1152	3TC	D4T	NVP	FTC	TFV	
1159	/					
2004	3TC	ABC	NVP			
2005	/					
2012	KTA	ZDV	3TC	ABC		
2035	/					
2066	ABC	APV	D4T			
2074	ABC	DDI	TFV			

2092	EFV	FTC	TFV							
4002	NVP	ZDV	3TC							
4028	/									
4049	/									
4067	KTA	TFV	ZDV	3TC						
4083	ATV	RTV	FTC	TFV						
4091	3TC	ABC	ATV	KTA	T20					
4109	FTV	RTV	FTC	TFV	SQV	ZDV	3TC			
4127	3TC	ZDV	3TC	EFV	KTA	NFV	RTV	EFV	FTC	TFV
4135	KTA	FTC	TFV	NVP	ZDV	3TC				
4139	ABC	3TC	KTA							
4144	EFV	FTC	TFV							
4149	DRV	RTV	RGV	TMC						
4175	EFV	FTC	TFV							
4179	DRV	RTV	FTC	TFV						
5007	DDI	EFV	KTA	NVP	TFZ	ZDV	3TC	ABC		
5008	DDI	RTV	TFV	FTV						
5016	/									
5055	DRV	RTV	FTC	TFV						
5057	3TC	ABC	ATV	DDI	KTA	RTV	TFV	ZDV		
5072	/									
6007	ABC	D4T	NFV							
6009	3TC	DLV	FTV	IDV	NFV	NVP	ZDV			
6037	3TC	ABC	D4T	FTV	IDV	KTA	RTV	ZDV		
6040	/									
6046	ZDV	3TC	ABC							
6050	/									
6052	3TC	ABC	D4T	EFV	IDV	KTA	NVP			
6065	/									
6068	/									
6073	/									
6078	/									
6081	ATV	FTC	RTV	TFV						
6083	FTC	NVP	TFV	FTC	TFV					
10001	3TC	D4T	KTA							
10011	/									
10016	/									
10025	3TC	IDV	ZDV							
10063	/									
10089	EFV	FTC	TFV							
10104	3TC	DDI	DLV	NFV	TFV					
10114	3TC	D4T	DDI	HU	KTA					
10133	/									
10147	ATV	RTV	FTC	TFV						
10251	RGV	FTC	TFV							
20033	APV	KTA	NVP							
30015	/									

List of antiretroviral drug regimens for HIV patients used for the study cohort in Chapter 3. PATID is patient ID. CURRENT MEDARV are the antiretroviral drugs that the patients were taking at the time of their last assessment. Drugs in orange are antiretroviral combination drugs, usually prescribed in combination of two or three simultaneous treatments.

PATID	PAST MEDARV																	
6800278276	3TC	ABC	ADV	APV	D4T	DDC	DDI	EFV	IDV	KTA	NVP	RTV	SQV	ZDV				
7100056883	ABC	D4T	DDC	EFV	HU	IDV	NFV	NVP	RTV	SQV								
7100107766	3TC	ABC	EFV	D4T	DDI	IDV	NFV	ZDV										
7100547672	3TC	ADV	DDC	DDI	EFV	HU	IDV	NFV	NVP	SQV								
7100616568	3TC	ABC	D4T	DDC	DDI	EFV	IDV	NFV	NVP	ZDV								
7100626868	D4T	DDI	EFV	IDV	NFV	RTV	SQV											
7100658283	D4T	DDI	NFV	RMN	3TC	ABC	NVP	KTA	TFV	ZDV	FTC	TFV						
7101328666	3TC	D4T	IDV	RTV	KTA	NVP	ATV	DDI	TFV	FTC								
7102536771	ZDV	3TC	KTA	EFV	FTC	TFV												
7200186777	/																	
7200267172	3TC	D4T	NFV	ABC	FTV	NVP	RTV	SQV	FTC	TFV								
7200466870	ABC	KTA	TFV	3TC	APV	D4T	DDC	DDI	EFV	IDV	NFV	NVP	RTV	SQV	ZDV			
CA102	/																	
CA125	3TC	ABC	D4T	DDC	DDI	DLV	EFV	IDV	NVP	RTV	SQV	ZDV						
CA236	D4T	DDI	IDV	3TC	ABC	KTA	RTV	TFV	ZDV									
CC163	3TC	ABC	APV	D4T	DDI	EFV	IDV	NFV	NVP	RTV	SQV	ZDV	KTA	TFV				
CE129	IDV	ZDV																
CE135	D4T	3TC	ABC	APV	DDI	EFV	FTV	KTA	NFV	TFV								
CE144	/																	
CG118	DDI	3TC	ZDV	KTA	RTV	TFV	FTC	FTC	TFV									
CG157	3TC	ATV	DDI	EFV	ABC	3TC	KTA	NFV	RTV	TFV	ZDV	3TC	ABC					
1004	3TC	ABC	APV	D4T	DDC	DDI	DLV	EFV	HU	IDV	NFV	NVP	RTV	SQV	ZDV			
1008	3TC	D4T	NFV	NVP	DDI	TFV												
1010	3TC	D4T	DDC	IDV	ZDV	ZDV	3TC	NVP	RTV	SQV	KTA	TFV						
1021	3TC	D4T	DLV															
1026	3TC	ABC	APV	EFV	IDV	ZDV	RTV	DDI	KTA	TFV	ATV							
1057	/																	
1065	/																	
1071	3TC	ABC	DDI	IDV	KTA	NFV	RTV	SQV	TFV	ZDV								
1087	TFV																	
1093	/																	
1099	/																	
1113	ATV	FTC	KTA	RTV	TFV	FTC	TFV	ABC	ABC	3TC	EFV	ZDV	3TC	ABC				
1119	/																	
1129	/																	
1141	/																	
1143	EFV	FTC	TFV															
1152	/																	
1159	/																	
2004	3TC	DDC	DDI	IDV	NVP	NFV	ZDV	ABC	TFV	KTA	RTV							
2005	DDI	KTA	RTV	TFV	D4T													
2012	3TC	D4T	DDI	FTV	NFV	NVP	SQV	ZDV	ABC	APV	ZDV	3TC	RTV	KTA	TFV	ZDV	3TC	ABC
2035	3TC	D4T	IDV	RTV														
2066	/																	
2074	3TC	D4T	IDV	NVP	RTV	ABC	KTA	NFV	RTV									

2092	3TC	ABC	NFV	RTV	SQV	ZDV	3TC	KTA	TFV												
4002	ABC	D4T	DDI	IDV	NVP	RTV	SQV	ZDV	ZDV	3TC											
4028	3TC	D4T	NVP																		
4049	APV	D4T	DDI	NVP																	
4067	/																				
4083	EFV	ZDV	3TC																		
4091	3TC	ABC	ATV	D4T	DDI	EFV	FTV	IDV	KTA	NFV	NVP	RTV	T20								
4109	/																				
4127	/																				
4135	/																				
4139	ABC	3TC	KTA																		
4144	/																				
4149	DRV	RTV																			
4175	EFV	FTC	TFV																		
4179	/																				
5007	/																				
5008	DDI	RTV	SQV	TFV																	
5016	ATV	ZDV	3TC	DDI	NFV	NVP	TFV	ZDV	ATV	EFV	RTV	T20									
5055	ATV	DDI	RTV																		
5057	/																				
5072	ABC	ATV	DDI	FPV	FTC	RTV	TFV	FTC	TFV	DRV											
6007	/																				
6009	/																				
6037	/																				
6040	/																				
6046	/																				
6050	/																				
6052	/																				
6065	ZDV	3TC	NVP																		
6068	/																				
6073	/																				
6078	/																				
6081	/																				
6083	/																				
10001	3TC	D4T	DDC	DDI	EFV	IDV	NFV	ZDV	ABC	APV	ZDV	3TC	KTA								
10011	3TC	ABC	D4T	DDI	EFV	HU	NVP	RTV	SQV	ZDV	ZDV	3TC	IDV	KTA	APV	FTC	T20	TFV	ZDV	3TC	ABC
10016	3TC	D4T																			
10025	/																				
10063	3TC	EFV	RTV	ZDV	ZDV	3TC	NFV														
10089	3TC	IDV	ZDV	EFV	KTA	ZDV	3TC	ABC													
10104	3TC	DDI	DLV	NFV	TFV																
10114	DDC	EFV	SQV	ZDV																	
10133	APV	ZDV	3TC	D4T	EFV	NFV	RTV														
10147	3TC	ABC	ATV	ZDV	3TC	D4T	EFV	KTA	NFV	RTV	SQV	DDI	TFV	FTC	TFV						
10251	3TC	DDC	EFV	FTC	TFV	ZDV	RGV														
20033	3TC	D4T	DDI	IDV	RTV	SQV	ZDV														
30015	3TC	ZDV	3TC	D4T	EFV	NVP	SQV	ZDV													

List of antiretroviral drug regimens for HIV patients used for the study cohort in Chapter 3. PATID is patient ID. PAST MEDARV are the antiretroviral drugs that the patients took at some point in the past. Drugs in orange are antiretroviral combination drugs, usually prescribed in combination of two or three simultaneous treatments.

Value	Label
3TC	3TC; lamivudine (Epivir)
ABC	ABC; abacavir (Ziagen)
ADV	ADV; adefovir dipivoxil (Preveon; Hepsera)
APV	APV; amprenavir (Agenerase)
ATR	ATR; efavirenz 600mg + emtricitabine 200mg + tenofivir DF 300mg (Atripla)
ATV	ATV; atazanavir (Reyataz)
CBV	CBV; zidovudine + lamivudine (Combivir)
COM	COM; emtricitabine 200mg + rilpivirine 25mg + tenofovir DF 300mg (Complera)
CPV	CPV; capravirine
D4T	d4T; stavudine (Zerit)
DDC	ddC; zalcitabine (Hivid)
DDI	ddI; didanosine (Videx)
DLV	DLV; delaviridine (Rescriptor)
DTG	DTG; dolutegravir (Tivicay)
EFV	EFV; efavirenz (Sustiva)
EMV	EMV; MKC-422, emivirine (Coactinon)
EPZ	EPZ; ziagen + epivir (Epzicom)
EVG	EVG; Elvitegravir
EVO	EVO; atazanavir 300mg + cobicistat 150mg (Evotaz)
FPV	FPV; fosamprenavir (Lexiva)
FTC	FTC; emtricitabine (Coviracil; Emtriva)
IDV	IDV; indinavir (Crixivan)
KTA	LPV/RTV; lopinavir/ritonavir (Kaletra)
MVC	MVC; maraviroc (Selzentry)
NFV	NFV; nelfinavir (Viracept)
NVP	NVP; nevirapine (Viramune)
PRE	PRE; darunavir 800mg + cobicistat 150mg (Prezcobix)
QUA	QUA; TRU + elvitegravir + cobicistat (Stribild formally Quad)
RGV	RGV; raltegravir (Isentress)
RPV	RPV; rilpivirine (Edurant)
RTV	RTV; ritonavir (Norvir)
FTV	SQV2 or FTV; saquinavir-sgc (Fortovase)
SQV	SQV; saquinavir (Invirase)
T20	T20; enfuvirtide; pentafuside (Fuzeon)
TFV	TFV, PMPA; tenofivir DF (Viread)
DRV	DRV; TMC-114, darunavir (Prezista)
TMC	TMC; TMC-125, etravirine (Intelence)
TMQ	TMQ; abacavir 600mg + dolutegravir 50mg + lamivudine 300mg (Triumeq)
TPV	TPV; tipranavir (Aptivus)
TRU	TRU; emtricitabine + tenofovir (Truvada)
TZV	TZV; AZT + 3TC + abacavir; zidovudine + lamivudine + abacavir (Trizivir)
VCV	VCV; vicriviroc
ZDV	ZDV; AZT, zidovudine (Retrovir)
ZTV	ZTV; AR-177 (Zintevir)

List of antiretroviral drug abbreviations. (Names in brackets refer to the drug trade name)

10.8 Coverage for deep sequencing of human mtDNA point variants in brain

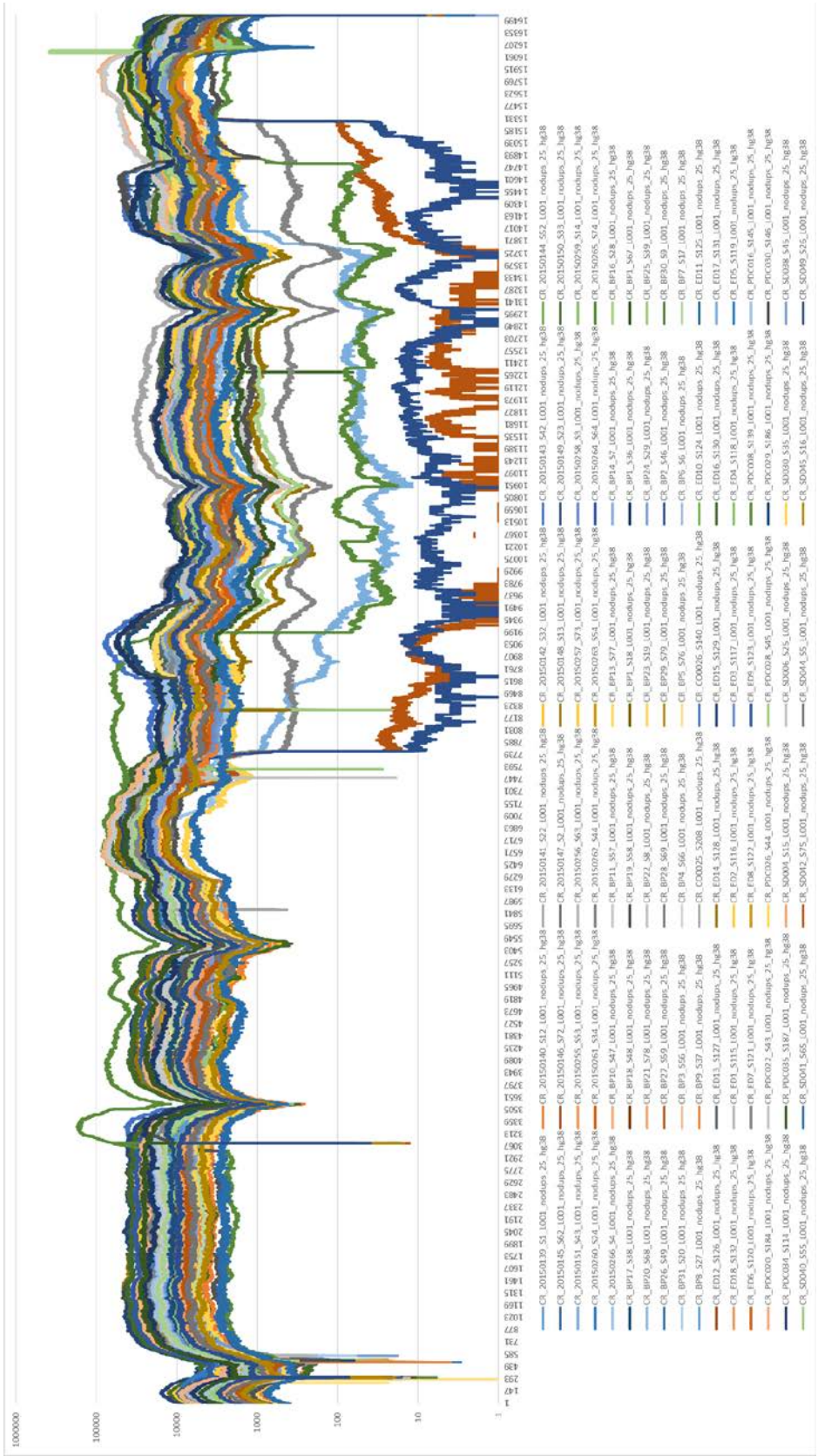

Coverage values from the Illumina MiSeq sequencing of human mtDNA point variants for HIV+ cases and HIV- uninfected controls. Coverage on the y axis is read depth log_{10} transformed. Values on the x axis represent the position of the human mitochondrial genome. Legend shows the samples sequenced. Samples with coverage dropout were excluded from analysis. This experiment covered the entire mitochondrial genome with two overlapping amplicons.

10.9 Coverage for deep sequencing of mouse mtDNA point variants in ear, colon and skeletal muscle

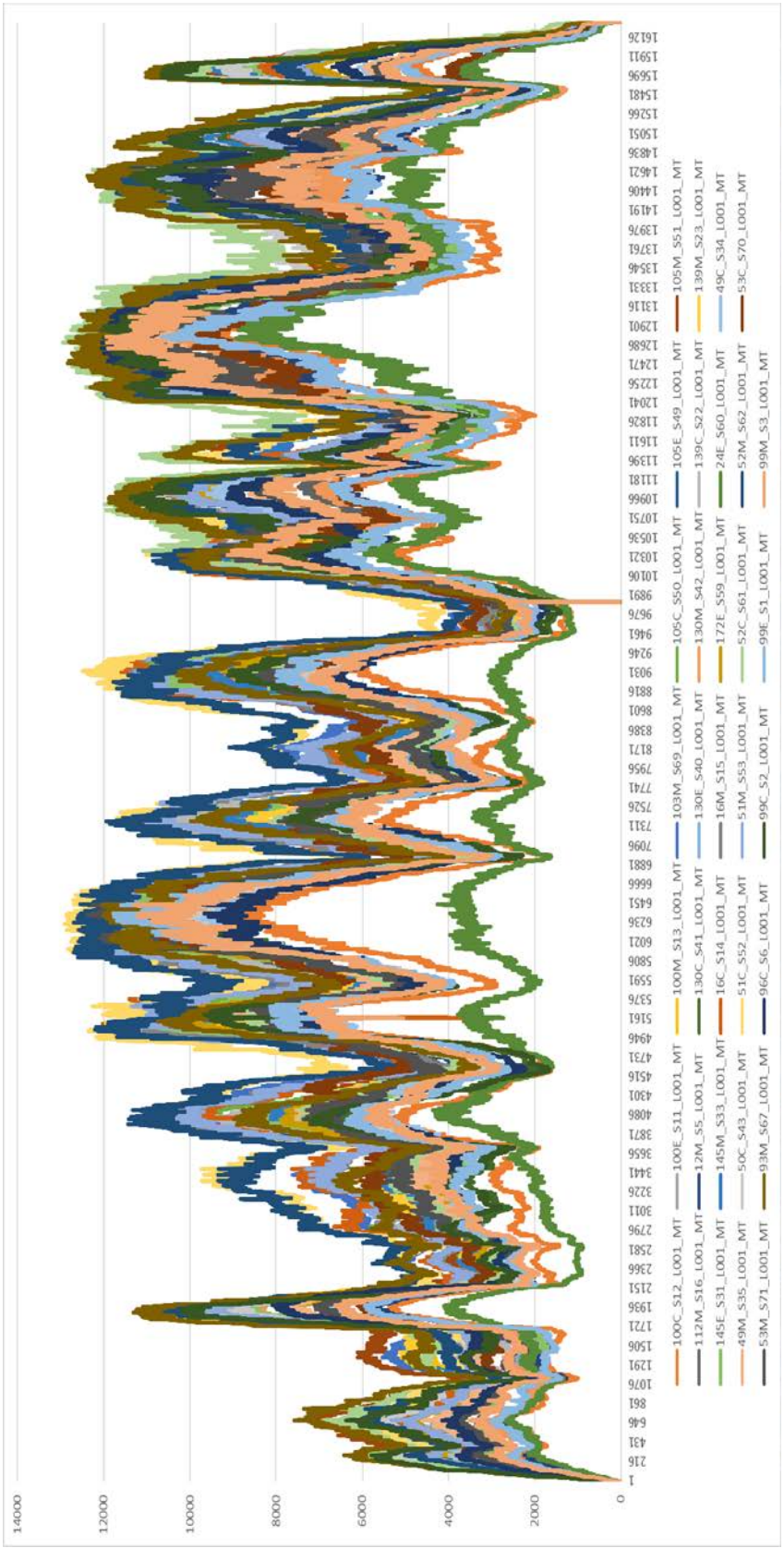

Coverage values from the Illumina MiSeq sequencing of mouse mtDNA point variants in ear, colon and skeletal muscle samples. Coverage on the y axis is read depth. Values on the x axis represent the position of the mouse mitochondrial genome. Legend shows the samples sequenced. This experiment covered the entire mitochondrial genome with two overlapping amplicons.

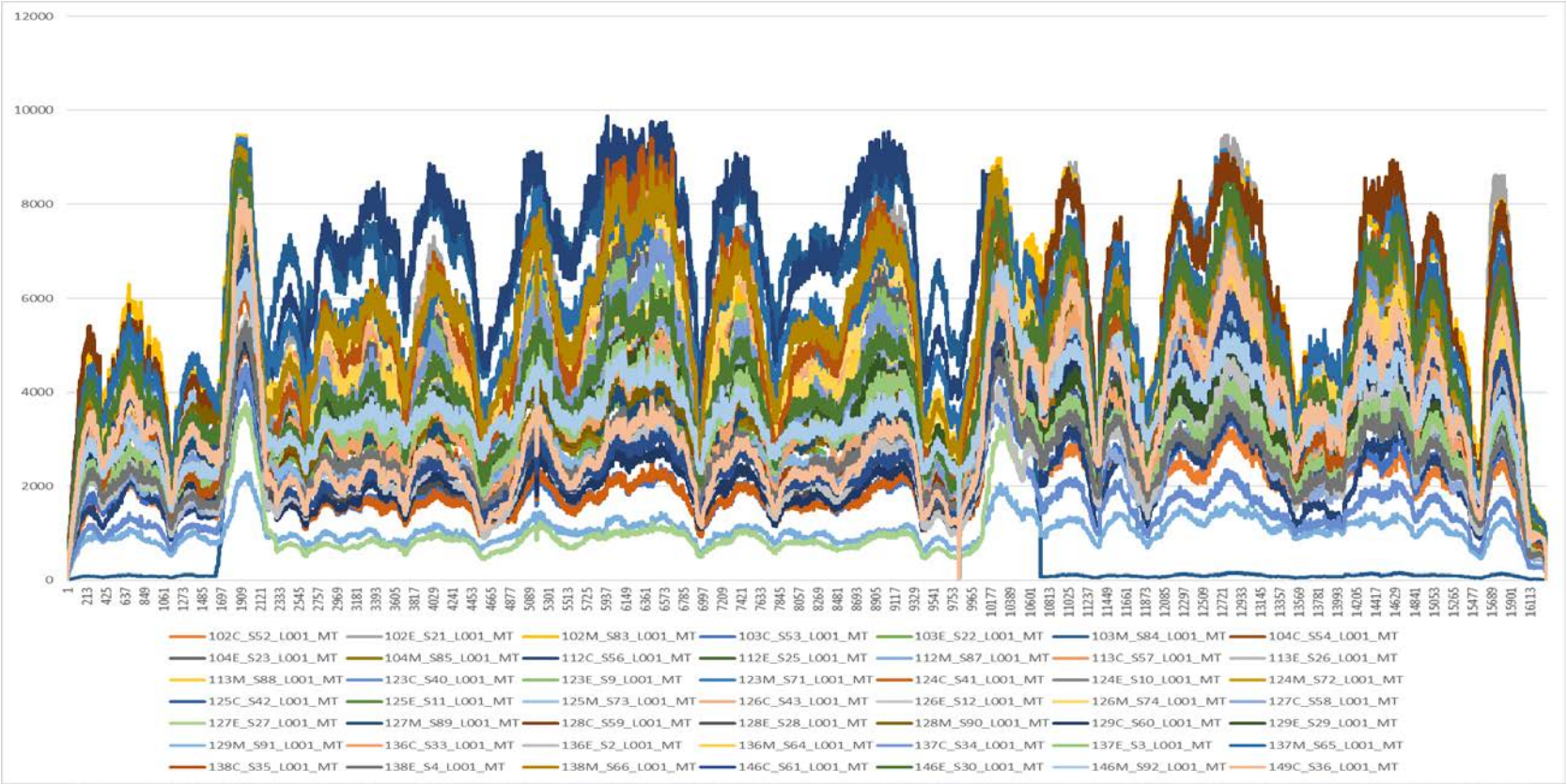

Coverage values from the Illumina MiSeq sequencing of mouse mtDNA point variants in ear, colon and skeletal muscle samples. Coverage on the y axis is read depth. Values on the x axis represent the position of the mouse mitochondrial genome. Legend shows the samples sequenced. This experiment covered the entire mitochondrial genome with two overlapping amplicons.

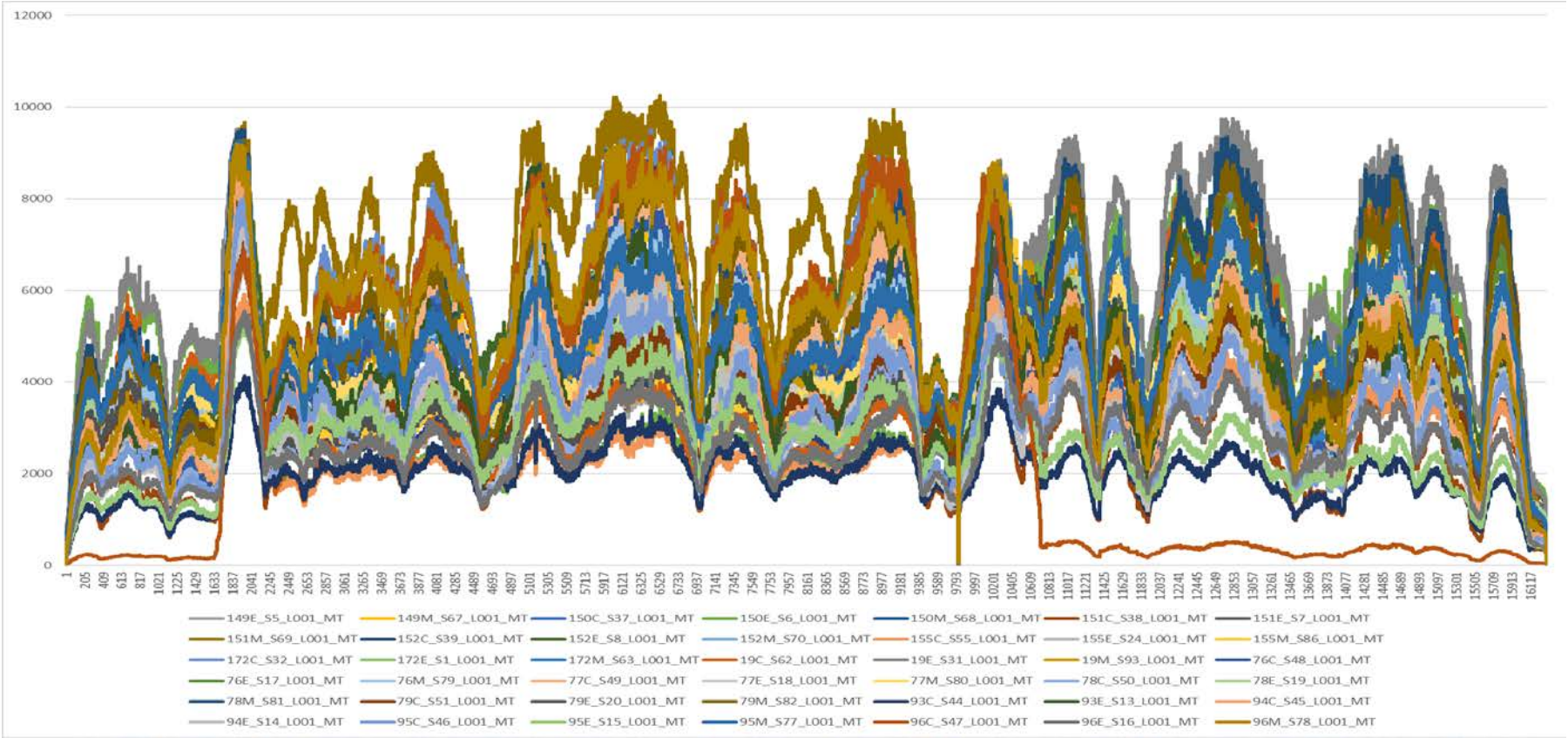

Coverage values from the Illumina MiSeq sequencing of mouse mtDNA point variants in ear, colon and skeletal muscle samples. Coverage on the y axis is read depth. Values on the x axis represent the position of the mouse mitochondrial genome. Legend shows the samples sequenced. This experiment covered the entire mitochondrial genome with two overlapping amplicons.

10.10 Coverage for deep sequencing of mouse mtDNA point variants in single colon crypts

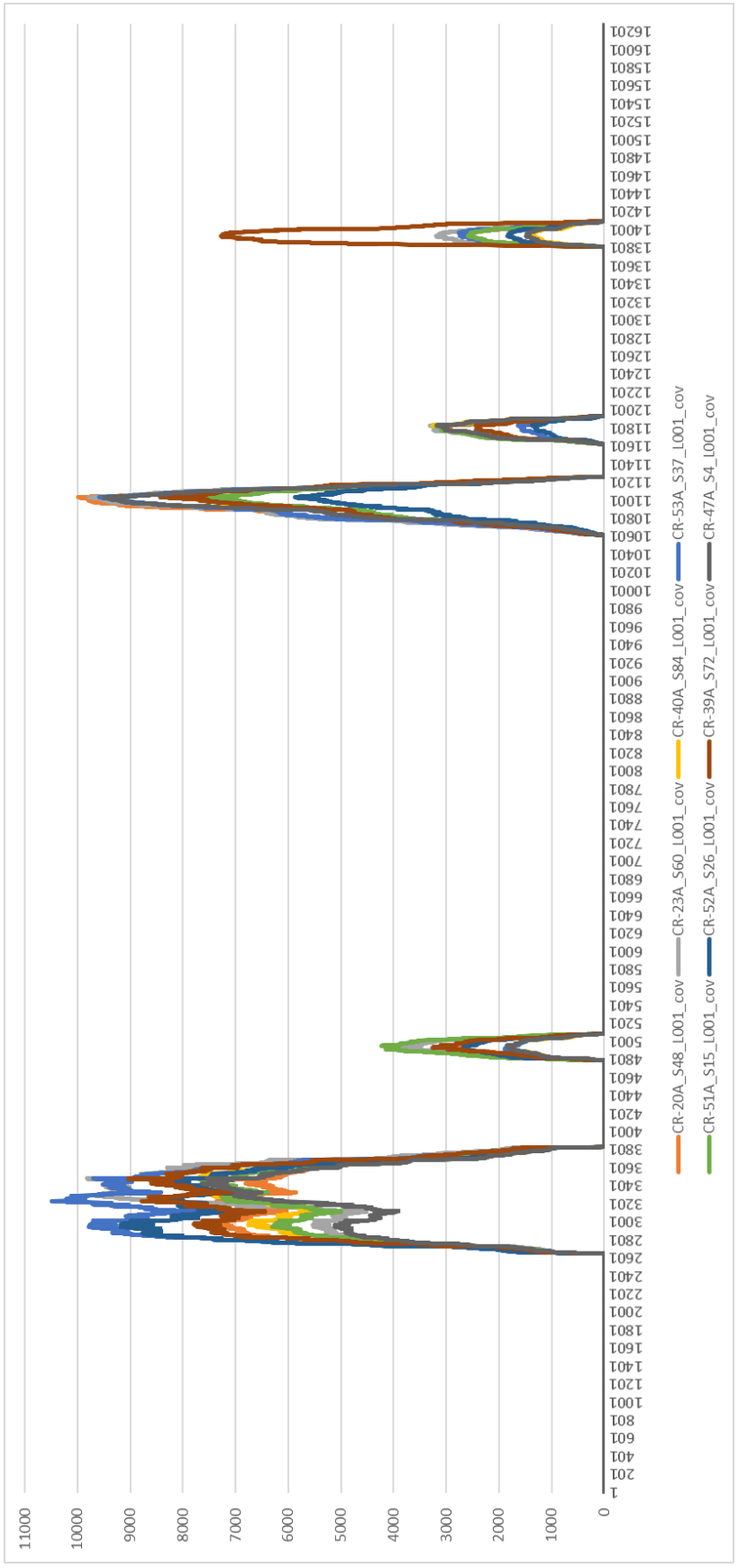

Coverage values from the Illumina MiSeq sequencing of mouse mtDNA six fragments of single mouse colon crypts. Coverage on the y axis is read depth. Values on the x axis represent the position of the mouse mitochondrial genome. Legend shows the eight samples sequenced. This experiment used six amplicons of ~600 or ~300bp.

Chapter 11. References

Abbas, W., Tariq, M., Iqbal, M., Kumar, A. and Herbein, G. (2015) 'Eradication of HIV-1 from the macrophage reservoir: an uncertain goal?', *Viruses*, 7(4), pp. 1578-98.

Agarwal, D., Chakravarty, J., Chaube, L., Rai, M., Agrawal, N.R. and Sundar, S. (2010) 'High incidence of zidovudine induced anaemia in HIV infected patients in eastern India', *Indian J Med Res*, 132, pp. 386-9.

Ahmed, S.T., Alston, C.L., Hopton, S., He, L., Hargreaves, I.P., Falkous, G., Olahova, M., McFarland, R., Turnbull, D.M., Rocha, M.C. and Taylor, R.W. (2017) 'Using a quantitative quadruple immunofluorescent assay to diagnose isolated mitochondrial Complex I deficiency', *Sci Rep*, 7(1), p. 15676.

Akman, H.O., Dorado, B., Lopez, L.C., Garcia-Cazorla, A., Vila, M.R., Tanabe, L.M., Dauer, W.T., Bonilla, E., Tanji, K. and Hirano, M. (2008) 'Thymidine kinase 2 (H126N) knockin mice show the essential role of balanced deoxynucleotide pools for mitochondrial DNA maintenance', *Hum Mol Genet*, 17(16), pp. 2433-40.

Albright, A.V., Shieh, J.T., Itoh, T., Lee, B., Pleasure, D., O'Connor, M.J., Doms, R.W. and Gonzalez-Scarano, F. (1999) 'Microglia express CCR5, CXCR4, and CCR3, but of these, CCR5 is the principal coreceptor for human immunodeficiency virus type 1 dementia isolates', *J Virol*, 73(1), pp. 205-13.

Alston, C.L., Davison, J.E., Meloni, F., van der Westhuizen, F.H., He, L., Hornig-Do, H.T., Peet, A.C., Gissen, P., Goffrini, P., Ferrero, I., Wassmer, E., McFarland, R. and Taylor, R.W. (2012) 'Recessive germline SDHA and SDHB mutations causing leukodystrophy and isolated mitochondrial complex II deficiency', *J Med Genet*, 49(9), pp. 569-77.

An, S.F., Groves, M., Gray, F. and Scaravilli, F. (1999) 'Early entry and widespread cellular involvement of HIV-1 DNA in brains of HIV-1 positive asymptomatic individuals', *J Neuropathol Exp Neurol*, 58(11), pp. 1156-62.

Anderson, S., Bankier, A.T., Barrell, B.G., de Bruijn, M.H., Coulson, A.R., Drouin, J., Eperon, I.C., Nierlich, D.P., Roe, B.A., Sanger, F., Schreier, P.H., Smith, A.J., Staden, R. and Young, I.G. (1981) 'Sequence and organization of the human mitochondrial genome', *Nature*, 290(5806), pp. 457-65.

Antinori, A., Arendt, G., Becker, J.T., Brew, B.J., Byrd, D.A., Cherner, M., Clifford, D.B., Cinque, P., Epstein, L.G., Goodkin, K., Gisslen, M., Grant, I., Heaton, R.K., Joseph, J., Marder, K., Marra, C.M., McArthur, J.C., Nunn, M., Price, R.W., Pulliam,

L., Robertson, K.R., Sacktor, N., Valcour, V. and Wojna, V.E. (2007) 'Updated research nosology for HIV-associated neurocognitive disorders', *Neurology*, 69(18), pp. 1789-99.
Arnaudo, E., Dalakas, M., Shanske, S., Moraes, C.T., DiMauro, S. and Schon, E.A. (1991) 'Depletion of muscle mitochondrial DNA in AIDS patients with zidovudine-induced myopathy', *Lancet*, 337(8740), pp. 508-10.
Arnberg, A., van Bruggen, E.F. and Borst, P. (1971) 'The presence of DNA molecules with a displacement loop in standard mitochondrial DNA preparations', *Biochim Biophys Acta*, 246(2), pp. 353-7.
Arner, E.S. and Eriksson, S. (1995) 'Mammalian deoxyribonucleoside kinases', *Pharmacol Ther*, 67(2), pp. 155-86.
Asin-Cayuela, J., Schwend, T., Farge, G. and Gustafsson, C.M. (2005) 'The human mitochondrial transcription termination factor (mTERF) is fully active in vitro in the non-phosphorylated form', *J Biol Chem*, 280(27), pp. 25499-505.
Avdoshina, V., Fields, J.A., Castellano, P., Dedoni, S., Palchik, G., Trejo, M., Adame, A., Rockenstein, E., Eugenin, E., Masliah, E. and Mocchetti, I. (2016) 'The HIV Protein gp120 Alters Mitochondrial Dynamics in Neurons', *Neurotox Res*, 29(4), pp. 583-93.
Baines, H.L., Stewart, J.B., Stamp, C., Zupanic, A., Kirkwood, T.B., Larsson, N.G., Turnbull, D.M. and Greaves, L.C. (2014) 'Similar patterns of clonally expanded somatic mtDNA mutations in the colon of heterozygous mtDNA mutator mice and ageing humans', *Mech Ageing Dev*, 139, pp. 22-30.
Baker, L.M., Paul, R.H., Heaps-Woodruff, J.M., Chang, J.Y., Ortega, M., Margolin, Z., Usher, C., Basco, B., Cooley, S. and Ances, B.M. (2015) 'The Effect of Central Nervous System Penetration Effectiveness of Highly Active Antiretroviral Therapy on Neuropsychological Performance and Neuroimaging in HIV Infected Individuals', *J Neuroimmune Pharmacol*, 10(3), pp. 487-92.
Balcarek, K., Venhoff, N., Deveaud, C., Beauvoit, B., Bonnet, J., Kirschner, J., Venhoff, A.C., Lebrecht, D. and Walker, U.A. (2010) 'Role of pyrimidine depletion in the mitochondrial cardiotoxicity of nucleoside analogue reverse transcriptase inhibitors', *J Acquir Immune Defic Syndr*, 55(5), pp. 550-7.
Bansal, A.K., Mactutus, C.F., Nath, A., Maragos, W., Hauser, K.F. and Booze, R.M. (2000) 'Neurotoxicity of HIV-1 proteins gp120 and Tat in the rat striatum', *Brain Res*, 879(1-2), pp. 42-9.

Bartley, P.B., Westacott, L., Boots, R.J., Lawson, M., Potter, J.M., Hyland, V.J. and Woods, M.L., 2nd (2001) 'Large hepatic mitochondrial DNA deletions associated with L-lactic acidosis and highly active antiretroviral therapy', *AIDS*, 15(3), pp. 419-20.
Bender, A., Krishnan, K.J., Morris, C.M., Taylor, G.A., Reeve, A.K., Perry, R.H., Jaros, E., Hersheson, J.S., Betts, J., Klopstock, T., Taylor, R.W. and Turnbull, D.M. (2006) 'High levels of mitochondrial DNA deletions in substantia nigra neurons in aging and Parkinson disease', *Nat Genet*, 38(5), pp. 515-7.
Bibb, M.J., Van Etten, R.A., Wright, C.T., Walberg, M.W. and Clayton, D.A. (1981) 'Sequence and gene organization of mouse mitochondrial DNA', *Cell*, 26(2 Pt 2), pp. 167-80.
Birkus, G., Hitchcock, M.J.M. and Cihlar, T. (2002) 'Assessment of Mitochondrial Toxicity in Human Cells Treated with Tenofovir: Comparison with Other Nucleoside Reverse Transcriptase Inhibitors', *Antimicrobial Agents and Chemotherapy*, 46(3), pp. 716-723.
Bishop, J.B., Tani, Y., Witt, K., Johnson, J.A., Peddada, S., Dunnick, J. and Nyska, A. (2004) 'Mitochondrial damage revealed by morphometric and semiquantitative analysis of mouse pup cardiomyocytes following in utero and postnatal exposure to zidovudine and lamivudine', *Toxicol Sci*, 81(2), pp. 512-7.
Blackstone, K., Moore, D.J., Franklin, D.R., Clifford, D.B., Collier, A.C., Marra, C.M., Gelman, B.B., McArthur, J.C., Morgello, S., Simpson, D.M., Ellis, R.J., Atkinson, J.H., Grant, I. and Heaton, R.K. (2012) 'Defining neurocognitive impairment in HIV: deficit scores versus clinical ratings', *Clin Neuropsychol*, 26(6), pp. 894-908.
Bogenhagen, D. and Clayton, D.A. (1977) 'Mouse L cell mitochondrial DNA molecules are selected randomly for replication throughout the cell cycle', *Cell*, 11(4), pp. 719-27.
Brown, M.D., Voljavec, A.S., Lott, M.T., Torroni, A., Yang, C.C. and Wallace, D.C. (1992) 'Mitochondrial DNA complex I and III mutations associated with Leber's hereditary optic neuropathy', *Genetics*, 130(1), pp. 163-73.
Brown, T.T. and Qaqish, R.B. (2006) 'Antiretroviral therapy and the prevalence of osteopenia and osteoporosis: a meta-analytic review', *AIDS*, 20(17), pp. 2165-74.
Brown, W.M., George, M., Jr. and Wilson, A.C. (1979) 'Rapid evolution of animal mitochondrial DNA', *Proc Natl Acad Sci U S A*, 76(4), pp. 1967-71.
Bua, E., Johnson, J., Herbst, A., Delong, B., McKenzie, D., Salamat, S. and Aiken, J.M. (2006) 'Mitochondrial DNA-deletion mutations accumulate intracellularly to

detrimental levels in aged human skeletal muscle fibers', *Am J Hum Genet*, 79(3), pp. 469-80.
Buffet, M., Schwarzinger, M., Amellal, B., Gourlain, K., Bui, P., Prevot, M., Deleuze, J., Morini, J.P., Gorin, I., Calvez, V. and Dupin, N. (2005) 'Mitochondrial DNA depletion in adipose tissue of HIV-infected patients with peripheral lipoatrophy', *J Clin Virol*, 33(1), pp. 60-4.
Burdo, T.H., Lackner, A. and Williams, K.C. (2013) 'Monocyte/macrophages and their role in HIV neuropathogenesis', *Immunol Rev*, 254(1), pp. 102-13.
Calvo, S.E. and Mootha, V.K. (2010) 'The mitochondrial proteome and human disease', *Annu Rev Genomics Hum Genet*, 11, pp. 25-44.
Cao, L., Shitara, H., Horii, T., Nagao, Y., Imai, H., Abe, K., Hara, T., Hayashi, J. and Yonekawa, H. (2007) 'The mitochondrial bottleneck occurs without reduction of mtDNA content in female mouse germ cells', *Nat Genet*, 39(3), pp. 386-90.
Carelli, V., Rugolo, M., Sgarbi, G., Ghelli, A., Zanna, C., Baracca, A., Lenaz, G., Napoli, E., Martinuzzi, A. and Solaini, G. (2004) 'Bioenergetics shapes cellular death pathways in Leber's hereditary optic neuropathy: a model of mitochondrial neurodegeneration', *Biochim Biophys Acta*, 1658(1-2), pp. 172-9.
Casademont, J., Barrientos, A., Grau, J.M., Pedrol, E., Estivill, X., Urbano-Marquez, A. and Nunes, V. (1996) 'The effect of zidovudine on skeletal muscle mtDNA in HIV-1 infected patients with mild or no muscle dysfunction', *Brain*, 119 (Pt 4), pp. 1357-64.
Castellano, P., Prevedel, L. and Eugenin, E.A. (2017) 'HIV-infected macrophages and microglia that survive acute infection become viral reservoirs by a mechanism involving Bim', *Sci Rep*, 7(1), p. 12866.
Castellano, P., Prevedel, L., Valdebenito, S. and Eugenin, E.A. (2019) 'HIV infection and latency induce a unique metabolic signature in human macrophages', *Sci Rep*, 9(1), p. 3941.
Cenker, J.J., Stultz, R.D. and McDonald, D. (2017) 'Brain Microglial Cells Are Highly Susceptible to HIV-1 Infection and Spread', *AIDS Res Hum Retroviruses*, 33(11), pp. 1155-1165.
Chan, S.S., Santos, J.H., Meyer, J.N., Mandavilli, B.S., Cook, D.L., Jr., McCash, C.L., Kissling, G.E., Nyska, A., Foley, J.F., van Houten, B., Copeland, W.C., Walker, V.E., Witt, K.L. and Bishop, J.B. (2007) 'Mitochondrial toxicity in hearts of CD-1 mice following perinatal exposure to AZT, 3TC, or AZT/3TC in combination', *Environ Mol Mutagen*, 48(3-4), pp. 190-200.

Chen, T., He, J., Shen, L., Fang, H., Nie, H., Jin, T., Wei, X., Xin, Y., Jiang, Y., Li, H., Chen, G., Lu, J. and Bai, Y. (2011) 'The mitochondrial DNA 4,977-bp deletion and its implication in copy number alteration in colorectal cancer', *BMC Med Genet*, 12, p. 8.
Cherry, C.L., Nolan, D., James, I.R., McKinnon, E.J., Mallal, S.A., Gahan, M.E., Lal, L., McArthur, J.C. and Wesselingh, S.L. (2006) 'Tissue-specific associations between mitochondrial DNA levels and current treatment status in HIV-infected individuals', *J Acquir Immune Defic Syndr*, 42(4), pp. 435-40.
Chinnery, P.F. and Hudson, G. (2013) 'Mitochondrial genetics', *Br Med Bull*, 106, pp. 135-59.
Chinnery, P.F. and Samuels, D.C. (1999) 'Relaxed replication of mtDNA: A model with implications for the expression of disease', *Am J Hum Genet*, 64(4), pp. 1158-65.
Clay Montier, L.L., Deng, J.J. and Bai, Y. (2009) 'Number matters: control of mammalian mitochondrial DNA copy number', *J Genet Genomics*, 36(3), pp. 125-31.
Clayton, D.A. (1982) 'Replication of animal mitochondrial DNA', *Cell*, 28(4), pp. 693-705.
Clifford, D.B. (2017) 'HIV-associated neurocognitive disorder', *Curr Opin Infect Dis*, 30(1), pp. 117-122.
Clifford, D.B. and Ances, B.M. (2013) 'HIV-associated neurocognitive disorder', *Lancet Infect Dis*, 13(11), pp. 976-86.
Cole, J.H., Caan, M.W.A., Underwood, J., De Francesco, D., van Zoest, R.A., Wit, F., Mutsaerts, H., Leech, R., Geurtsen, G.J., Portegies, P., Majoie, C., Schim van der Loeff, M.F., Sabin, C.A., Reiss, P., Winston, A., Sharp, D.J. and Comorbidity in Relations to, A.C. (2018) 'No Evidence for Accelerated Aging-Related Brain Pathology in Treated Human Immunodeficiency Virus: Longitudinal Neuroimaging Results From the Comorbidity in Relation to AIDS (COBRA) Project', *Clin Infect Dis*, 66(12), pp. 1899-1909.
Coleman, C.M. and Wu, L. (2009) 'HIV interactions with monocytes and dendritic cells: viral latency and reservoirs', *Retrovirology*, 6, p. 51.
Cooper, A., Garcia, M., Petrovas, C., Yamamoto, T., Koup, R.A. and Nabel, G.J. (2013) 'HIV-1 causes CD4 cell death through DNA-dependent protein kinase during viral integration', *Nature*, 498(7454), pp. 376-9.
Cooper, D.L. and Lovett, S.T. (2011) 'Toxicity and tolerance mechanisms for azidothymidine, a replication gap-promoting agent, in Escherichia coli', *DNA Repair (Amst)*, 10(3), pp. 260-70.

Corral-Debrinski, M., Horton, T., Lott, M.T., Shoffner, J.M., Beal, M.F. and Wallace, D.C. (1992) 'Mitochondrial DNA deletions in human brain: regional variability and increase with advanced age', *Nat Genet*, 2(4), pp. 324-9.
Cote, H.C., Brumme, Z.L., Craib, K.J., Alexander, C.S., Wynhoven, B., Ting, L., Wong, H., Harris, M., Harrigan, P.R., O'Shaughnessy, M.V. and Montaner, J.S. (2002) 'Changes in mitochondrial DNA as a marker of nucleoside toxicity in HIV-infected patients', *N Engl J Med*, 346(11), pp. 811-20.
Coxhead, J., Kurzawa-Akanbi, M., Hussain, R., Pyle, A., Chinnery, P. and Hudson, G. (2016) 'Somatic mtDNA variation is an important component of Parkinson's disease', *Neurobiol Aging*, 38, pp. 217 e1-6.
Cree, L.M., Samuels, D.C., de Sousa Lopes, S.C., Rajasimha, H.K., Wonnapinij, P., Mann, J.R., Dahl, H.H. and Chinnery, P.F. (2008) 'A reduction of mitochondrial DNA molecules during embryogenesis explains the rapid segregation of genotypes', *Nat Genet*, 40(2), pp. 249-54.
Currier, J.S., Taylor, A., Boyd, F., Dezii, C.M., Kawabata, H., Burtcel, B., Maa, J.F. and Hodder, S. (2003) 'Coronary heart disease in HIV-infected individuals', *J Acquir Immune Defic Syndr*, 33(4), pp. 506-12.
Daems, W.T. and Wisse, E. (1966) 'Shape and attachment of the cristae mitochondriales in mouse hepatic cell mitochondria', *J Ultrastruct Res*, 16(1), pp. 123-40.
Dai, D.F., Chen, T., Wanagat, J., Laflamme, M., Marcinek, D.J., Emond, M.J., Ngo, C.P., Prolla, T.A. and Rabinovitch, P.S. (2010) 'Age-dependent cardiomyopathy in mitochondrial mutator mice is attenuated by overexpression of catalase targeted to mitochondria', *Aging Cell*, 9(4), pp. 536-44.
Dai, Y., Kiselak, T., Clark, J., Clore, E., Zheng, K., Cheng, A., Kujoth, G.C., Prolla, T.A., Maratos-Flier, E. and Simon, D.K. (2013) 'Behavioral and metabolic characterization of heterozygous and homozygous POLG mutator mice', *Mitochondrion*, 13(4), pp. 282-91.
Dainiak, N., Worthington, M., Riordan, M.A., Kreczko, S. and Goldman, L. (1988) '3'-Azido-3'-deoxythymidine (AZT) inhibits proliferation in vitro of human haematopoietic progenitor cells', *Br J Haematol*, 69(3), pp. 299-304.
Dalakas, M.C. (2001) 'Peripheral neuropathy and antiretroviral drugs', *J Peripher Nerv Syst*, 6(1), pp. 14-20.

Dalakas, M.C., Illa, I., Pezeshkpour, G.H., Laukaitis, J.P., Cohen, B. and Griffin, J.L. (1990) 'Mitochondrial myopathy caused by long-term zidovudine therapy', *N Engl J Med*, 322(16), pp. 1098-105.
Dalakas, M.C., Semino-Mora, C. and Leon-Monzon, M. (2001) 'Mitochondrial alterations with mitochondrial DNA depletion in the nerves of AIDS patients with peripheral neuropathy induced by 2'3'-dideoxycytidine (ddC)', *Lab Invest*, 81(11), pp. 1537-44.
Dash, K.R., Meher, L.K., Hui, P.K., Behera, S.K. and Nayak, S.N. (2015) 'High Incidence of Zidovudine Induced Anaemia in HIV Infected Patients in Southern Odisha', *Indian J Hematol Blood Transfus*, 31(2), pp. 247-50.
Dawson, V.L., Dawson, T.M., Uhl, G.R. and Snyder, S.H. (1993) 'Human immunodeficiency virus type 1 coat protein neurotoxicity mediated by nitric oxide in primary cortical cultures', *Proc Natl Acad Sci U S A*, 90(8), pp. 3256-9.
De Francesco, D., Underwood, J., Bagkeris, E., Boffito, M., Post, F.A., Mallon, P., Vera, J.H., Williams, I., Anderson, J., Johnson, M., Sabin, C.A., Winston, A., Pharmacokinetic and Clinical Observations in People over Fifty, s. (2019) 'Depression, lifestyle factors and cognitive function in people living with HIV and comparable HIV-negative controls', *HIV Med*, 20(4), pp. 274-285.
De Francesco, D., Wit, F.W., Cole, J.H., Kootstra, N.A., Winston, A., Sabin, C.A., Underwood, J., van Zoest, R.A., Schouten, J., Kooij, K.W., Prins, M., Guaraldi, G., Caan, M.W.A., Burger, D., Franceschi, C., Libert, C., Burkle, A., Reiss, P. and collaboration, C.O.i.R.t.A. (2018) 'The 'COmorBidity in Relation to AIDS' (COBRA) cohort: Design, methods and participant characteristics', *PLoS One*, 13(3), p. e0191791.
de Grey, A.D. (1997) 'A proposed refinement of the mitochondrial free radical theory of aging', *Bioessays*, 19(2), pp. 161-6.
de Moura, M.B., dos Santos, L.S. and Van Houten, B. (2010) 'Mitochondrial dysfunction in neurodegenerative diseases and cancer', *Environ Mol Mutagen*, 51(5), pp. 391-405.
Deeks, S.G. (2011) 'HIV infection, inflammation, immunosenescence, and aging', *Annu Rev Med*, 62, pp. 141-55.
Desquilbet, L., Jacobson, L.P., Fried, L.P., Phair, J.P., Jamieson, B.D., Holloway, M., Margolick, J.B. and Multicenter, A.C.S. (2007) 'HIV-1 infection is associated with an earlier occurrence of a phenotype related to frailty', *J Gerontol A Biol Sci Med Sci*, 62(11), pp. 1279-86.

Dickinson, M.E., Flenniken, A.M., Ji, X., Teboul, L., Wong, M.D., White, J.K., Meehan, T.F., Weninger, W.J., Westerberg, H., Adissu, H., Baker, C.N., Bower, L., Brown, J.M., Caddle, L.B., Chiani, F., Clary, D., Cleak, J., Daly, M.J., Denegre, J.M., Doe, B., Dolan, M.E., Edie, S.M., Fuchs, H., Gailus-Durner, V., Galli, A., Gambadoro, A., Gallegos, J., Guo, S., Horner, N.R., Hsu, C.W., Johnson, S.J., Kalaga, S., Keith, L.C., Lanoue, L., Lawson, T.N., Lek, M., Mark, M., Marschall, S., Mason, J., McElwee, M.L., Newbigging, S., Nutter, L.M., Peterson, K.A., Ramirez-Solis, R., Rowland, D.J., Ryder, E., Samocha, K.E., Seavitt, J.R., Selloum, M., Szoke-Kovacs, Z., Tamura, M., Trainor, A.G., Tudose, I., Wakana, S., Warren, J., Wendling, O., West, D.B., Wong, L., Yoshiki, A., International Mouse Phenotyping, C., Jackson, L., Infrastructure Nationale Phenomin, I.C.d.l.S., Charles River, L., Harwell, M.R.C., Toronto Centre for, P., Wellcome Trust Sanger, I., Center, R.B., MacArthur, D.G., Tocchini-Valentini, G.P., Gao, X., Flicek, P., Bradley, A., Skarnes, W.C., Justice, M.J., Parkinson, H.E., Moore, M., Wells, S., Braun, R.E., Svenson, K.L., de Angelis, M.H., Herault, Y., Mohun, T., Mallon, A.M., Henkelman, R.M., Brown, S.D., Adams, D.J., Lloyd, K.C., McKerlie, C., Beaudet, A.L., Bucan, M. and Murray, S.A. (2016) 'High-throughput discovery of novel developmental phenotypes', *Nature*, 537(7621), pp. 508-514.

Dieterich, D.T. (2006) 'Disease management--constructing optimal NRTI-based combinations: past, present, and future', *MedGenMed*, 8(1), p. 16.

Doitsh, G., Galloway, N.L., Geng, X., Yang, Z., Monroe, K.M., Zepeda, O., Hunt, P.W., Hatano, H., Sowinski, S., Munoz-Arias, I. and Greene, W.C. (2014) 'Cell death by pyroptosis drives CD4 T-cell depletion in HIV-1 infection', *Nature*, 505(7484), pp. 509-14.

Doitsh, G. and Greene, W.C. (2016) 'Dissecting How CD4 T Cells Are Lost During HIV Infection', *Cell Host Microbe*, 19(3), pp. 280-91.

Dokianakis, E. and Ladoukakis, E.D. (2014) 'Different degree of paternal mtDNA leakage between male and female progeny in interspecific Drosophila crosses', *Ecol Evol*, 4(13), pp. 2633-41.

Dolce, V., Fiermonte, G., Runswick, M.J., Palmieri, F. and Walker, J.E. (2001) 'The human mitochondrial deoxynucleotide carrier and its role in the toxicity of nucleoside antivirals', *Proc Natl Acad Sci U S A*, 98(5), pp. 2284-8.

Dolle, C., Flones, I., Nido, G.S., Miletic, H., Osuagwu, N., Kristoffersen, S., Lilleng, P.K., Larsen, J.P., Tysnes, O.B., Haugarvoll, K., Bindoff, L.A. and Tzoulis, C. (2016)

'Defective mitochondrial DNA homeostasis in the substantia nigra in Parkinson disease', *Nat Commun*, 7, p. 13548.
Elson, J.L., Samuels, D.C., Turnbull, D.M. and Chinnery, P.F. (2001) 'Random intracellular drift explains the clonal expansion of mitochondrial DNA mutations with age', *Am J Hum Genet*, 68(3), pp. 802-6.
Erlandson, K.M., Allshouse, A.A., Jankowski, C.M., MaWhinney, S., Kohrt, W.M. and Campbell, T.B. (2013) 'Functional impairment is associated with low bone and muscle mass among persons aging with HIV infection', *J Acquir Immune Defic Syndr*, 63(2), pp. 209-15.
Falguera, M., Perez-Mur, J., Puig, T. and Cao, G. (1995) 'Study of the role of vitamin B12 and folinic acid supplementation in preventing hematologic toxicity of zidovudine', *Eur J Haematol*, 55(2), pp. 97-102.
Fan, W., Waymire, K.G., Narula, N., Li, P., Rocher, C., Coskun, P.E., Vannan, M.A., Narula, J., Macgregor, G.R. and Wallace, D.C. (2008) 'A mouse model of mitochondrial disease reveals germline selection against severe mtDNA mutations', *Science*, 319(5865), pp. 958-62.
Fields, J.A., Serger, E., Campos, S., Divakaruni, A.S., Kim, C., Smith, K., Trejo, M., Adame, A., Spencer, B., Rockenstein, E., Murphy, A.N., Ellis, R.J., Letendre, S., Grant, I. and Masliah, E. (2016) 'HIV alters neuronal mitochondrial fission/fusion in the brain during HIV-associated neurocognitive disorders', *Neurobiol Dis*, 86, pp. 154-69.
Fischl, M., Galpin, J.E., Levine, J.D., Groopman, J.E., Henry, D.H., Kennedy, P., Miles, S., Robbins, W., Starrett, B., Zalusky, R. and et al. (1990) 'Recombinant human erythropoietin for patients with AIDS treated with zidovudine', *N Engl J Med*, 322(21), pp. 1488-93.
Furtado, M.R., Callaway, D.S., Phair, J.P., Kunstman, K.J., Stanton, J.L., Macken, C.A., Perelson, A.S. and Wolinsky, S.M. (1999) 'Persistence of HIV-1 transcription in peripheral-blood mononuclear cells in patients receiving potent antiretroviral therapy', *N Engl J Med*, 340(21), pp. 1614-22.
Garg, H. and Joshi, A. (2017) 'Host and Viral Factors in HIV-Mediated Bystander Apoptosis', *Viruses*, 9(8).
Garg, H., Mohl, J. and Joshi, A. (2012) 'HIV-1 induced bystander apoptosis', *Viruses*, 4(11), pp. 3020-43.

Gendron, S.P., Mallet, J.D., Bastien, N. and Rochette, P.J. (2012) 'Mitochondrial DNA common deletion in the human eye: a relation with corneal aging', *Mech Ageing Dev*, 133(2-3), pp. 68-74.
Ghorpade, A., Xia, M.Q., Hyman, B.T., Persidsky, Y., Nukuna, A., Bock, P., Che, M., Limoges, J., Gendelman, H.E. and Mackay, C.R. (1998) 'Role of the beta-chemokine receptors CCR3 and CCR5 in human immunodeficiency virus type 1 infection of monocytes and microglia', *J Virol*, 72(4), pp. 3351-61.
Gorantla, S., Poluektova, L. and Gendelman, H.E. (2012) 'Rodent models for HIV-associated neurocognitive disorders', *Trends Neurosci*, 35(3), pp. 197-208.
Gorman, G.S., Schaefer, A.M., Ng, Y., Gomez, N., Blakely, E.L., Alston, C.L., Feeney, C., Horvath, R., Yu-Wai-Man, P., Chinnery, P.F., Taylor, R.W., Turnbull, D.M. and McFarland, R. (2015) 'Prevalence of nuclear and mitochondrial DNA mutations related to adult mitochondrial disease', *Ann Neurol*, 77(5), pp. 753-9.
Greaves, L.C., Elson, J.L., Nooteboom, M., Grady, J.P., Taylor, G.A., Taylor, R.W., Mathers, J.C., Kirkwood, T.B. and Turnbull, D.M. (2012) 'Comparison of mitochondrial mutation spectra in ageing human colonic epithelium and disease: absence of evidence for purifying selection in somatic mitochondrial DNA point mutations', *PLoS Genet*, 8(11), p. e1003082.
Greaves, L.C., Nooteboom, M., Elson, J.L., Tuppen, H.A., Taylor, G.A., Commane, D.M., Arasaradnam, R.P., Khrapko, K., Taylor, R.W., Kirkwood, T.B., Mathers, J.C. and Turnbull, D.M. (2014) 'Clonal expansion of early to mid-life mitochondrial DNA point mutations drives mitochondrial dysfunction during human ageing', *PLoS Genet*, 10(9), p. e1004620.
Greber, B.J., Bieri, P., Leibundgut, M., Leitner, A., Aebersold, R., Boehringer, D. and Ban, N. (2015) 'Ribosome. The complete structure of the 55S mammalian mitochondrial ribosome', *Science*, 348(6232), pp. 303-8.
Groot, F., Welsch, S. and Sattentau, Q.J. (2008) 'Efficient HIV-1 transmission from macrophages to T cells across transient virological synapses', *Blood*, 111(9), pp. 4660-3.
Gross, N.J., Getz, G.S. and Rabinowitz, M. (1969) 'Apparent turnover of mitochondrial deoxyribonucleic acid and mitochondrial phospholipids in the tissues of the rat', *J Biol Chem*, 244(6), pp. 1552-62.
Group, I.S.S., Lundgren, J.D., Babiker, A.G., Gordin, F., Emery, S., Grund, B., Sharma, S., Avihingsanon, A., Cooper, D.A., Fatkenheuer, G., Llibre, J.M., Molina, J.M., Munderi, P., Schechter, M., Wood, R., Klingman, K.L., Collins, S., Lane, H.C.,

Phillips, A.N. and Neaton, J.D. (2015) 'Initiation of Antiretroviral Therapy in Early Asymptomatic HIV Infection', *N Engl J Med*, 373(9), pp. 795-807.
Grunewald, A., Rygiel, K.A., Hepplewhite, P.D., Morris, C.M., Picard, M. and Turnbull, D.M. (2015) 'Mitochondrial DNA depletion in respiratory chain-deficient Parkinson disease neurons', *Ann Neurol*.
Guo, X., Popadin, K.Y., Markuzon, N., Orlov, Y.L., Kraytsberg, Y., Krishnan, K.J., Zsurka, G., Turnbull, D.M., Kunz, W.S. and Khrapko, K. (2010) 'Repeats, longevity and the sources of mtDNA deletions: evidence from 'deletional spectra'', *Trends Genet*, 26(8), pp. 340-3.
Guo, Y., Li, C.I., Sheng, Q., Winther, J.F., Cai, Q., Boice, J.D. and Shyr, Y. (2013) 'Very low-level heteroplasmy mtDNA variations are inherited in humans', *J Genet Genomics*, 40(12), pp. 607-15.
Gyllensten, U., Wharton, D., Josefsson, A. and Wilson, A.C. (1991) 'Paternal inheritance of mitochondrial DNA in mice', *Nature*, 352(6332), pp. 255-7.
Harman, D. (1956) 'Aging: a theory based on free radical and radiation chemistry', *J Gerontol*, 11(3), pp. 298-300.
Harman, D. (1972) 'The biologic clock: the mitochondria?', *J Am Geriatr Soc*, 20(4), pp. 145-7.
Haugaard, S.B., Andersen, O., Pedersen, S.B., Dela, F., Richelsen, B., Nielsen, J.O., Madsbad, S. and Iversen, J. (2005) 'Depleted skeletal muscle mitochondrial DNA, hyperlactatemia, and decreased oxidative capacity in HIV-infected patients on highly active antiretroviral therapy', *J Med Virol*, 77(1), pp. 29-38.
He, Y., Wu, J., Dressman, D.C., Iacobuzio-Donahue, C., Markowitz, S.D., Velculescu, V.E., Diaz, L.A., Jr., Kinzler, K.W., Vogelstein, B. and Papadopoulos, N. (2010) 'Heteroplasmic mitochondrial DNA mutations in normal and tumour cells', *Nature*, 464(7288), pp. 610-4.
Heaton, R.K., Clifford, D.B., Franklin, D.R., Jr., Woods, S.P., Ake, C., Vaida, F., Ellis, R.J., Letendre, S.L., Marcotte, T.D., Atkinson, J.H., Rivera-Mindt, M., Vigil, O.R., Taylor, M.J., Collier, A.C., Marra, C.M., Gelman, B.B., McArthur, J.C., Morgello, S., Simpson, D.M., McCutchan, J.A., Abramson, I., Gamst, A., Fennema-Notestine, C., Jernigan, T.L., Wong, J., Grant, I. and Group, C. (2010) 'HIV-associated neurocognitive disorders persist in the era of potent antiretroviral therapy: CHARTER Study', *Neurology*, 75(23), pp. 2087-96.
Heaton, R.K., Franklin, D.R., Jr., Deutsch, R., Letendre, S., Ellis, R.J., Casaletto, K., Marquine, M.J., Woods, S.P., Vaida, F., Atkinson, J.H., Marcotte, T.D., McCutchan,

J.A., Collier, A.C., Marra, C.M., Clifford, D.B., Gelman, B.B., Sacktor, N., Morgello, S., Simpson, D.M., Abramson, I., Gamst, A.C., Fennema-Notestine, C., Smith, D.M., Grant, I. and Group, C. (2015) 'Neurocognitive change in the era of HIV combination antiretroviral therapy: the longitudinal CHARTER study', *Clin Infect Dis*, 60(3), pp. 473-80.

Helbert, M., Fletcher, T., Peddle, B., Harris, J.R. and Pinching, A.J. (1988) 'Zidovudine-associated myopathy', *Lancet*, 2(8612), pp. 689-90.

Herskowitz, A., Willoughby, S.B., Baughman, K.L., Schulman, S.P. and Bartlett, J.D. (1992) 'Cardiomyopathy associated with antiretroviral therapy in patients with HIV infection: a report of six cases', *Ann Intern Med*, 116(4), pp. 311-3.

Hillen, H.S., Temiakov, D. and Cramer, P. (2018) 'Structural basis of mitochondrial transcription', *Nat Struct Mol Biol*, 25(9), pp. 754-765.

Holm, G.H. and Gabuzda, D. (2005) 'Distinct mechanisms of CD4+ and CD8+ T-cell activation and bystander apoptosis induced by human immunodeficiency virus type 1 virions', *J Virol*, 79(10), pp. 6299-311.

Holt, I.J., Harding, A.E. and Morgan-Hughes, J.A. (1988) 'Deletions of muscle mitochondrial DNA in patients with mitochondrial myopathies', *Nature*, 331(6158), pp. 717-9.

Holt, I.J., Lorimer, H.E. and Jacobs, H.T. (2000) 'Coupled leading- and lagging-strand synthesis of mammalian mitochondrial DNA', *Cell*, 100(5), pp. 515-24.

Hudson, G. and Chinnery, P.F. (2006) 'Mitochondrial DNA polymerase-gamma and human disease', *Hum Mol Genet*, 15 Spec No 2, pp. R244-52.

Igarashi, T., Brown, C.R., Endo, Y., Buckler-White, A., Plishka, R., Bischofberger, N., Hirsch, V. and Martin, M.A. (2001) 'Macrophage are the principal reservoir and sustain high virus loads in rhesus macaques after the depletion of CD4+ T cells by a highly pathogenic simian immunodeficiency virus/HIV type 1 chimera (SHIV): Implications for HIV-1 infections of humans', *Proc Natl Acad Sci U S A*, 98(2), pp. 658-63.

Issekutz, B.J., Birkhead, N.C. and Rodahl, K. (1962) 'Use of respiratory quotients in assessment of aerobic work capacity', *Journal of Applied Physiology*, 17(1), pp. 47-50.

Itsara, L.S., Kennedy, S.R., Fox, E.J., Yu, S., Hewitt, J.J., Sanchez-Contreras, M., Cardozo-Pelaez, F. and Pallanck, L.J. (2014) 'Oxidative stress is not a major contributor to somatic mitochondrial DNA mutations', *PLoS Genet*, 10(2), p. e1003974.

Jabara, C.B., Jones, C.D., Roach, J., Anderson, J.A. and Swanstrom, R. (2011) 'Accurate sampling and deep sequencing of the HIV-1 protease gene using a Primer ID', *Proc Natl Acad Sci U S A*, 108(50), pp. 20166-71.
Jana, A. and Pahan, K. (2004) 'Human immunodeficiency virus type 1 gp120 induces apoptosis in human primary neurons through redox-regulated activation of neutral sphingomyelinase', *J Neurosci*, 24(43), pp. 9531-40.
Janssen, R.J., Nijtmans, L.G., van den Heuvel, L.P. and Smeitink, J.A. (2006) 'Mitochondrial complex I: structure, function and pathology', *J Inherit Metab Dis*, 29(4), pp. 499-515.
Jitratkosol, M.H., Sattha, B., Maan, E.J., Gadawski, I., Harrigan, P.R., Forbes, J.C., Alimenti, A., van Schalkwyk, J., Money, D.M., Cote, H.C., Therapy, C.E.T.G.o.H. and Aging (2012) 'Blood mitochondrial DNA mutations in HIV-infected women and their infants exposed to HAART during pregnancy', *AIDS*, 26(6), pp. 675-83.
Johnson, A.A., Ray, A.S., Hanes, J., Suo, Z., Colacino, J.M., Anderson, K.S. and Johnson, K.A. (2001) 'Toxicity of antiviral nucleoside analogs and the human mitochondrial DNA polymerase', *J Biol Chem*, 276(44), pp. 40847-57.
Johnson, M.A., Turnbull, D.M., Dick, D.J. and Sherratt, H.S. (1983) 'A partial deficiency of cytochrome c oxidase in chronic progressive external ophthalmoplegia', *J Neurol Sci*, 60(1), pp. 31-53.
Joseph, S.B., Arrildt, K.T., Sturdevant, C.B. and Swanstrom, R. (2015) 'HIV-1 target cells in the CNS', *J Neurovirol*, 21(3), pp. 276-89.
Kaguni, L.S. (2004) 'DNA polymerase gamma, the mitochondrial replicase', *Annu Rev Biochem*, 73, pp. 293-320.
Kakuda, T.N. (2000) 'Pharmacology of nucleoside and nucleotide reverse transcriptase inhibitor-induced mitochondrial toxicity', *Clin Ther*, 22(6), pp. 685-708.
Kallianpur, A.R. and Hulgan, T. (2009) 'Pharmacogenetics of nucleoside reverse-transcriptase inhibitor-associated peripheral neuropathy', *Pharmacogenomics*, 10(4), pp. 623-37.
Katada, S., Mito, T., Ogasawara, E., Hayashi, J. and Nakada, K. (2013) 'Mitochondrial DNA with a large-scale deletion causes two distinct mitochondrial disease phenotypes in mice', *G3 (Bethesda)*, 3(9), pp. 1545-52.
Kauppila, J.H., Baines, H.L., Bratic, A., Simard, M.L., Freyer, C., Mourier, A., Stamp, C., Filograna, R., Larsson, N.G., Greaves, L.C. and Stewart, J.B. (2016) 'A Phenotype-Driven Approach to Generate Mouse Models with Pathogenic mtDNA Mutations Causing Mitochondrial Disease', *Cell Rep*, 16(11), pp. 2980-90.

Kazachkova, N., Ramos, A., Santos, C. and Lima, M. (2013) 'Mitochondrial DNA damage patterns and aging: revising the evidences for humans and mice', *Aging Dis*, 4(6), pp. 337-50.
Kennedy, S.R., Salk, J.J., Schmitt, M.W. and Loeb, L.A. (2013) 'Ultra-sensitive sequencing reveals an age-related increase in somatic mitochondrial mutations that are inconsistent with oxidative damage', *PLoS Genet*, 9(9), p. e1003794.
Koboldt, D.C., Zhang, Q., Larson, D.E., Shen, D., McLellan, M.D., Lin, L., Miller, C.A., Mardis, E.R., Ding, L. and Wilson, R.K. (2012) 'VarScan 2: somatic mutation and copy number alteration discovery in cancer by exome sequencing', *Genome Res*, 22(3), pp. 568-76.
Koczor, C., Kohler, J. and Lewis, W. (2010) 'Transgenic mouse models of mitochondrial toxicity associated with HIV/AIDS and antiretrovirals', *Methods*, 51(4), pp. 399-404.
Kollberg, G., Darin, N., Benan, K., Moslemi, A.R., Lindal, S., Tulinius, M., Oldfors, A. and Holme, E. (2009) 'A novel homozygous RRM2B missense mutation in association with severe mtDNA depletion', *Neuromuscul Disord*, 19(2), pp. 147-50.
Kondo, R., Matsuura, E.T. and Chigusa, S.I. (1992) 'Further observation of paternal transmission of Drosophila mitochondrial DNA by PCR selective amplification method', *Genet Res*, 59(2), pp. 81-4.
Koneru, R., Olive, M.F. and Tyor, W.R. (2014) 'Combined antiretroviral therapy reduces brain viral load and pathological features of HIV encephalitis in a mouse model', *J Neurovirol*, 20(1), pp. 9-17.
Koppensteiner, H., Brack-Werner, R. and Schindler, M. (2012) 'Macrophages and their relevance in Human Immunodeficiency Virus Type I infection', *Retrovirology*, 9, p. 82.
Krebs, H.A. and Johnson, W.A. (1937) 'Metabolism of ketonic acids in animal tissues', *Biochem J*, 31(4), pp. 645-60.
Krishnan, K.J., Reeve, A.K., Samuels, D.C., Chinnery, P.F., Blackwood, J.K., Taylor, R.W., Wanrooij, S., Spelbrink, J.N., Lightowlers, R.N. and Turnbull, D.M. (2008) 'What causes mitochondrial DNA deletions in human cells?', *Nat Genet*, 40(3), pp. 275-9.
Kujoth, G.C., Hiona, A., Pugh, T.D., Someya, S., Panzer, K., Wohlgemuth, S.E., Hofer, T., Seo, A.Y., Sullivan, R., Jobling, W.A., Morrow, J.D., Van Remmen, H., Sedivy, J.M., Yamasoba, T., Tanokura, M., Weindruch, R., Leeuwenburgh, C. and

Prolla, T.A. (2005) 'Mitochondrial DNA mutations, oxidative stress, and apoptosis in mammalian aging', *Science*, 309(5733), pp. 481-4.
Kukat, C., Wurm, C.A., Spahr, H., Falkenberg, M., Larsson, N.G. and Jakobs, S. (2011) 'Super-resolution microscopy reveals that mammalian mitochondrial nucleoids have a uniform size and frequently contain a single copy of mtDNA', *Proc Natl Acad Sci U S A*, 108(33), pp. 13534-9.
Kunkel, T.A. and Loeb, L.A. (1981) 'Fidelity of mammalian DNA polymerases', *Science*, 213(4509), pp. 765-7.
Lee, H.C., Pang, C.Y., Hsu, H.S. and Wei, Y.H. (1994) 'Differential accumulations of 4,977 bp deletion in mitochondrial DNA of various tissues in human ageing', *Biochim Biophys Acta*, 1226(1), pp. 37-43.
Lehmann, H.C., Chen, W., Borzan, J., Mankowski, J.L. and Hoke, A. (2011) 'Mitochondrial dysfunction in distal axons contributes to human immunodeficiency virus sensory neuropathy', *Ann Neurol*, 69(1), pp. 100-10.
Letendre, S., Marquie-Beck, J., Capparelli, E., Best, B., Clifford, D., Collier, A.C., Gelman, B.B., McArthur, J.C., McCutchan, J.A., Morgello, S., Simpson, D., Grant, I., Ellis, R.J. and Group, C. (2008) 'Validation of the CNS Penetration-Effectiveness rank for quantifying antiretroviral penetration into the central nervous system', *Arch Neurol*, 65(1), pp. 65-70.
Lewis, W. (2003) 'Defective mitochondrial DNA replication and NRTIs: pathophysiological implications in AIDS cardiomyopathy', *Am J Physiol Heart Circ Physiol*, 284(1), pp. H1-9.
Lewis, W. and Dalakas, M.C. (1995) 'Mitochondrial toxicity of antiviral drugs', *Nat Med*, 1(5), pp. 417-22.
Lewis, W., Day, B.J. and Copeland, W.C. (2003) 'Mitochondrial toxicity of NRTI antiviral drugs: an integrated cellular perspective', *Nat Rev Drug Discov*, 2(10), pp. 812-22.
Lewis, W., Gonzalez, B., Chomyn, A. and Papoian, T. (1992) 'Zidovudine induces molecular, biochemical, and ultrastructural changes in rat skeletal muscle mitochondria', *J Clin Invest*, 89(4), pp. 1354-60.
Li, H. and Durbin, R. (2009) 'Fast and accurate short read alignment with Burrows-Wheeler transform', *Bioinformatics*, 25(14), pp. 1754-60.
Li, H., Handsaker, B., Wysoker, A., Fennell, T., Ruan, J., Homer, N., Marth, G., Abecasis, G., Durbin, R. and Genome Project Data Processing, S. (2009) 'The Sequence Alignment/Map format and SAMtools', *Bioinformatics*, 25(16), pp. 2078-9.

Li, M., Foli, Y., Liu, Z., Wang, G., Hu, Y., Lu, Q., Selvaraj, S., Lam, W. and Paintsil, E. (2017) 'High frequency of mitochondrial DNA mutations in HIV-infected treatment-experienced individuals', *HIV Med*, 18(1), pp. 45-55.
Li, M., Schonberg, A., Schaefer, M., Schroeder, R., Nasidze, I. and Stoneking, M. (2010) 'Detecting heteroplasmy from high-throughput sequencing of complete human mitochondrial DNA genomes', *Am J Hum Genet*, 87(2), pp. 237-49.
Lightowlers, R.N. and Chrzanowska-Lightowlers, Z.M. (2010) 'Terminating human mitochondrial protein synthesis: a shift in our thinking', *RNA Biol*, 7(3), pp. 282-6.
Lim, S.E. and Copeland, W.C. (2001) 'Differential incorporation and removal of antiviral deoxynucleotides by human DNA polymerase gamma', *J Biol Chem*, 276(26), pp. 23616-23.
Linnane, A.W., Marzuki, S., Ozawa, T. and Tanaka, M. (1989) 'Mitochondrial DNA mutations as an important contributor to ageing and degenerative diseases', *Lancet*, 1(8639), pp. 642-5.
Liu, A. (2010) 'Laser capture microdissection in the tissue biorepository', *J Biomol Tech*, 21(3), pp. 120-5.
Liu, K., Sun, Y., Liu, D., Yin, J., Qiao, L., Shi, Y., Dong, Y., Li, N., Zhang, F. and Chen, D. (2013) 'Mitochondrial toxicity studied with the PBMC of children from the Chinese national pediatric highly active antiretroviral therapy cohort', *PLoS One*, 8(2), p. e57223.
Luo, S., Valencia, C.A., Zhang, J., Lee, N.C., Slone, J., Gui, B., Wang, X., Li, Z., Dell, S., Brown, J., Chen, S.M., Chien, Y.H., Hwu, W.L., Fan, P.C., Wong, L.J., Atwal, P.S. and Huang, T. (2018) 'Biparental Inheritance of Mitochondrial DNA in Humans', *Proc Natl Acad Sci U S A*, 115(51), pp. 13039-13044.
Mabrouk, O.S., Dripps, I.J., Ramani, S., Chang, C., Han, J.L., Rice, K.C. and Jutkiewicz, E.M. (2014) 'Automated touch screen device for recording complex rodent behaviors', *J Neurosci Methods*, 233, pp. 129-36.
Mai, N., Chrzanowska-Lightowlers, Z.M. and Lightowlers, R.N. (2017) 'The process of mammalian mitochondrial protein synthesis', *Cell Tissue Res*, 367(1), pp. 5-20.
Malim, M.H. and Bieniasz, P.D. (2012) 'HIV Restriction Factors and Mechanisms of Evasion', *Cold Spring Harb Perspect Med*, 2(5), p. a006940.
Man, S.M., Karki, R. and Kanneganti, T.D. (2017) 'Molecular mechanisms and functions of pyroptosis, inflammatory caspases and inflammasomes in infectious diseases', *Immunol Rev*, 277(1), pp. 61-75.
Margulis, L. (1971) 'Symbiosis and evolution', *Sci Am*, 225(2), pp. 48-57.

Martin-Hernandez, E., Garcia-Silva, M.T., Quijada-Fraile, P., Rodriguez-Garcia, M.E., Rivera, H., Hernandez-Lain, A., Coca-Robinot, D., Fernandez-Toral, J., Arenas, J., Martin, M.A. and Martinez-Azorin, F. (2017) 'Myopathic mtDNA Depletion Syndrome Due to Mutation in TK2 Gene', *Pediatr Dev Pathol*, 20(5), pp. 416-420.
Martin, A.M., Hammond, E., Nolan, D., Pace, C., Den Boer, M., Taylor, L., Moore, H., Martinez, O.P., Christiansen, F.T. and Mallal, S. (2003) 'Accumulation of mitochondrial DNA mutations in human immunodeficiency virus-infected patients treated with nucleoside-analogue reverse-transcriptase inhibitors', *Am J Hum Genet*, 72(3), pp. 549-60.
Masanes, F., Barrientos, A., Cebrian, M., Pedrol, E., Miro, O., Casademont, J. and Grau, J.M. (1998) 'Clinical, histological and molecular reversibility of zidovudine myopathy', *J Neurol Sci*, 159(2), pp. 226-8.
Mathiesen, C. and Hagerhall, C. (2002) 'Transmembrane topology of the NuoL, M and N subunits of NADH:quinone oxidoreductase and their homologues among membrane-bound hydrogenases and bona fide antiporters', *Biochim Biophys Acta*, 1556(2-3), pp. 121-32.
McComsey, G., Bai, R.K., Maa, J.F., Seekins, D. and Wong, L.J. (2005a) 'Extensive investigations of mitochondrial DNA genome in treated HIV-infected subjects: beyond mitochondrial DNA depletion', *J Acquir Immune Defic Syndr*, 39(2), pp. 181-8.
McComsey, G.A., Paulsen, D.M., Lonergan, J.T., Hessenthaler, S.M., Hoppel, C.L., Williams, V.C., Fisher, R.L., Cherry, C.L., White-Owen, C., Thompson, K.A., Ross, S.T., Hernandez, J.E. and Ross, L.L. (2005b) 'Improvements in lipoatrophy, mitochondrial DNA levels and fat apoptosis after replacing stavudine with abacavir or zidovudine', *AIDS*, 19(1), pp. 15-23.
McGuire, J.L., Gill, A.J., Douglas, S.D., Kolson, D.L. and group, C.H.A.-R.T.E.R. (2015) 'Central and peripheral markers of neurodegeneration and monocyte activation in HIV-associated neurocognitive disorders', *J Neurovirol*, 21(4), pp. 439-48.
Mimaki, M., Wang, X., McKenzie, M., Thorburn, D.R. and Ryan, M.T. (2012) 'Understanding mitochondrial complex I assembly in health and disease', *Biochim Biophys Acta*, 1817(6), pp. 851-62.
Miura, T., Goto, M., Hosoya, N., Odawara, T., Kitamura, Y., Nakamura, T. and Iwamoto, A. (2003) 'Depletion of mitochondrial DNA in HIV-1-infected patients and its amelioration by antiretroviral therapy', *J Med Virol*, 70(4), pp. 497-505.

Monroe, K.M., Yang, Z., Johnson, J.R., Geng, X., Doitsh, G., Krogan, N.J. and Greene, W.C. (2014) 'IFI16 DNA sensor is required for death of lymphoid CD4 T cells abortively infected with HIV', *Science*, 343(6169), pp. 428-32.
Moraes, C.T., DiMauro, S., Zeviani, M., Lombes, A., Shanske, S., Miranda, A.F., Nakase, H., Bonilla, E., Werneck, L.C., Servidei, S. and et al. (1989) 'Mitochondrial DNA deletions in progressive external ophthalmoplegia and Kearns-Sayre syndrome', *N Engl J Med*, 320(20), pp. 1293-9.
Mott, J.L., Zhang, D., Stevens, M., Chang, S., Denniger, G. and Zassenhaus, H.P. (2001) 'Oxidative stress is not an obligate mediator of disease provoked by mitochondrial DNA mutations', *Mutat Res*, 474(1-2), pp. 35-45.
Moyle, G.J. and Sadler, M. (1998) 'Peripheral neuropathy with nucleoside antiretrovirals: risk factors, incidence and management', *Drug Saf*, 19(6), pp. 481-94.
Muller-Hocker, J., Pongratz, D. and Hubner, G. (1983) 'Focal deficiency of cytochrome-c-oxidase in skeletal muscle of patients with progressive external ophthalmoplegia. Cytochemical-fine-structural study', *Virchows Arch A Pathol Anat Histopathol*, 402(1), pp. 61-71.
Murphy, M.P. (2009) 'How mitochondria produce reactive oxygen species', *Biochem J*, 417(1), pp. 1-13.
Nissen, S.K., Hojen, J.F., Andersen, K.L., Kofod-Olsen, E., Berg, R.K., Paludan, S.R., Ostergaard, L., Jakobsen, M.R., Tolstrup, M. and Mogensen, T.H. (2014) 'Innate DNA sensing is impaired in HIV patients and IFI16 expression correlates with chronic immune activation', *Clin Exp Immunol*, 177(1), pp. 295-309.
Nomura, R., Sato, T., Sato, Y., Medin, J.A., Kushimoto, S. and Yanagisawa, T. (2017) 'Azidothymidine-triphosphate impairs mitochondrial dynamics by disrupting the quality control system', *Redox Biol*, 13, pp. 407-417.
Nunes, M.D., Dolezal, M. and Schlotterer, C. (2013) 'Extensive paternal mtDNA leakage in natural populations of Drosophila melanogaster', *Mol Ecol*, 22(8), pp. 2106-17.
Ortiz, M., Poloni, E.S., Furrer, H., Kovari, H., Martinez, R., Arnedo, M., Elzi, L., Bernasconi, E., Vernazza, P., Hirschel, B., Cavassini, M., Ledergerber, B., Gunthard, H.F., Telenti, A., Tarr, P.E. and Swiss, H.I.V.C.S. (2011) 'No longitudinal mitochondrial DNA sequence changes in HIV-infected individuals with and without lipoatrophy', *J Infect Dis*, 203(5), pp. 620-4.
Palade, G.E. (1953) 'An electron microscope study of the mitochondrial structure', *J Histochem Cytochem*, 1(4), pp. 188-211.

Payne, B.A. and Chinnery, P.F. (2015) 'Mitochondrial dysfunction in aging: Much progress but many unresolved questions', *Biochim Biophys Acta*, 1847(11), pp. 1347-53.
Payne, B.A., Wilson, I.J., Hateley, C.A., Horvath, R., Santibanez-Koref, M., Samuels, D.C., Price, D.A. and Chinnery, P.F. (2011) 'Mitochondrial aging is accelerated by anti-retroviral therapy through the clonal expansion of mtDNA mutations', *Nat Genet*, 43(8), pp. 806-10.
Payne, B.A.I., Wilson, I.J., Yu-Wai-Man, P., Coxhead, J., Deehan, D., Horvath, R., Taylor, R.W., Samuels, D.C., Santibanez-Koref, M. and Chinnery, P.F. (2012) 'Universal heteroplasmy of human mitochondrial DNA', *Human Molecular Genetics*, 22(2), pp. 384-390.
Perales-Clemente, E., Fernandez-Vizarra, E., Acin-Perez, R., Movilla, N., Bayona-Bafaluy, M.P., Moreno-Loshuertos, R., Perez-Martos, A., Fernandez-Silva, P. and Enriquez, J.A. (2010) 'Five entry points of the mitochondrially encoded subunits in mammalian complex I assembly', *Mol Cell Biol*, 30(12), pp. 3038-47.
Peters, B.S., Winer, J., Landon, D.N., Stotter, A. and Pinching, A.J. (1993) 'Mitochondrial myopathy associated with chronic zidovudine therapy in AIDS', *Q J Med*, 86(1), pp. 5-15.
Petrosino, J.M., Heiss, V.J., Maurya, S.K., Kalyanasundaram, A., Periasamy, M., LaFountain, R.A., Wilson, J.M., Simonetti, O.P. and Ziouzenkova, O. (2016) 'Graded Maximal Exercise Testing to Assess Mouse Cardio-Metabolic Phenotypes', *PLoS One*, 11(2), p. e0148010.
Phillips, A.F., Millet, A.R., Tigano, M., Dubois, S.M., Crimmins, H., Babin, L., Charpentier, M., Piganeau, M., Brunet, E. and Sfeir, A. (2017) 'Single-Molecule Analysis of mtDNA Replication Uncovers the Basis of the Common Deletion', *Mol Cell*, 65(3), pp. 527-538 e6.
Pinto, M. and Moraes, C.T. (2015) 'Mechanisms linking mtDNA damage and aging', *Free Radic Biol Med*, 85, pp. 250-8.
Posse, V., Shahzad, S., Falkenberg, M., Hallberg, B.M. and Gustafsson, C.M. (2015) 'TEFM is a potent stimulator of mitochondrial transcription elongation in vitro', *Nucleic Acids Res*, 43(5), pp. 2615-24.
Poulton, J., Hirano, M., Spinazzola, A., Arenas Hernandez, M., Jardel, C., Lombes, A., Czermin, B., Horvath, R., Taanman, J.W., Rotig, A., Zeviani, M. and Fratter, C. (2009) 'Collated mutations in mitochondrial DNA (mtDNA) depletion syndrome

(excluding the mitochondrial gamma polymerase, POLG1)', *Biochim Biophys Acta*, 1792(12), pp. 1109-12.
Prakash, A. and Doublie, S. (2015) 'Base Excision Repair in the Mitochondria', *J Cell Biochem*, 116(8), pp. 1490-9.
Pyle, A., Anugrha, H., Kurzawa-Akanbi, M., Yarnall, A., Burn, D. and Hudson, G. (2016) 'Reduced mitochondrial DNA copy number is a biomarker of Parkinson's disease', *Neurobiol Aging*, 38, pp. 216 e7-216 e10.
Pyle, A., Brennan, R., Kurzawa-Akanbi, M., Yarnall, A., Thouin, A., Mollenhauer, B., Burn, D., Chinnery, P.F. and Hudson, G. (2015a) 'Reduced cerebrospinal fluid mitochondrial DNA is a biomarker for early-stage Parkinson's disease', *Ann Neurol*, 78(6), pp. 1000-4.
Pyle, A., Burn, D.J., Gordon, C., Swan, C., Chinnery, P.F. and Baudouin, S.V. (2010) 'Fall in circulating mononuclear cell mitochondrial DNA content in human sepsis', *Intensive Care Med*, 36(6), pp. 956-62.
Pyle, A., Hudson, G., Wilson, I.J., Coxhead, J., Smertenko, T., Herbert, M., Santibanez-Koref, M. and Chinnery, P.F. (2015b) 'Extreme-Depth Re-sequencing of Mitochondrial DNA Finds No Evidence of Paternal Transmission in Humans', *PLoS Genet*, 11(5), p. e1005040.
Richman, D.D., Fischl, M.A., Grieco, M.H., Gottlieb, M.S., Volberding, P.A., Laskin, O.L., Leedom, J.M., Groopman, J.E., Mildvan, D., Hirsch, M.S. and et al. (1987) 'The toxicity of azidothymidine (AZT) in the treatment of patients with AIDS and AIDS-related complex. A double-blind, placebo-controlled trial', *N Engl J Med*, 317(4), pp. 192-7.
Rocha, M.C., Grady, J.P., Grunewald, A., Vincent, A., Dobson, P.F., Taylor, R.W., Turnbull, D.M. and Rygiel, K.A. (2015) 'A novel immunofluorescent assay to investigate oxidative phosphorylation deficiency in mitochondrial myopathy: understanding mechanisms and improving diagnosis', *Sci Rep*, 5, p. 15037.
Ross, J.M., Stewart, J.B., Hagstrom, E., Brene, S., Mourier, A., Coppotelli, G., Freyer, C., Lagouge, M., Hoffer, B.J., Olson, L. and Larsson, N.G. (2013) 'Germline mitochondrial DNA mutations aggravate ageing and can impair brain development', *Nature*, 501(7467), pp. 412-5.
Rozzi, S.J., Avdoshina, V., Fields, J.A. and Mocchetti, I. (2018) 'Human immunodeficiency virus Tat impairs mitochondrial fission in neurons', *Cell Death Discov*, 4, p. 8.

Rylova, S.N., Albertioni, F., Flygh, G. and Eriksson, S. (2005) 'Activity profiles of deoxynucleoside kinases and 5'-nucleotidases in cultured adipocytes and myoblastic cells: insights into mitochondrial toxicity of nucleoside analogs', *Biochem Pharmacol*, 69(6), pp. 951-60.
Safdar, A., Annis, S., Kraytsberg, Y., Laverack, C., Saleem, A., Popadin, K., Woods, D.C., Tilly, J.L. and Khrapko, K. (2016) 'Amelioration of premature aging in mtDNA mutator mouse by exercise: the interplay of oxidative stress, PGC-1alpha, p53, and DNA damage. A hypothesis', *Curr Opin Genet Dev*, 38, pp. 127-132.
Safdar, A., Bourgeois, J.M., Ogborn, D.I., Little, J.P., Hettinga, B.P., Akhtar, M., Thompson, J.E., Melov, S., Mocellin, N.J., Kujoth, G.C., Prolla, T.A. and Tarnopolsky, M.A. (2011) 'Endurance exercise rescues progeroid aging and induces systemic mitochondrial rejuvenation in mtDNA mutator mice', *Proc Natl Acad Sci U S A*, 108(10), pp. 4135-40.
Sagan, L. (1967) 'On the origin of mitosing cells', *J Theor Biol*, 14(3), pp. 255-74.
Samuels, D.C. (2004) 'Mitochondrial DNA repeats constrain the life span of mammals', *Trends Genet*, 20(5), pp. 226-9.
Samuels, D.C., Schon, E.A. and Chinnery, P.F. (2004) 'Two direct repeats cause most human mtDNA deletions', *Trends Genet*, 20(9), pp. 393-8.
Samuels, R., Bayerri, C.R., Sayer, J.A., Price, D.A. and Payne, B.A.I. (2017) 'Tenofovir disoproxil fumarate-associated renal tubular dysfunction: noninvasive assessment of mitochondrial injury', *AIDS*, 31(9), pp. 1297-1301.
Saylor, D., Dickens, A.M., Sacktor, N., Haughey, N., Slusher, B., Pletnikov, M., Mankowski, J.L., Brown, A., Volsky, D.J. and McArthur, J.C. (2016) 'HIV-associated neurocognitive disorder--pathogenesis and prospects for treatment', *Nat Rev Neurol*, 12(4), pp. 234-48.
Schaefer, A.M., McFarland, R., Blakely, E.L., He, L., Whittaker, R.G., Taylor, R.W., Chinnery, P.F. and Turnbull, D.M. (2008) 'Prevalence of mitochondrial DNA disease in adults', *Ann Neurol*, 63(1), pp. 35-9.
Schindelin, J., Arganda-Carreras, I., Frise, E., Kaynig, V., Longair, M., Pietzsch, T., Preibisch, S., Rueden, C., Saalfeld, S., Schmid, B., Tinevez, J.Y., White, D.J., Hartenstein, V., Eliceiri, K., Tomancak, P. and Cardona, A. (2012) 'Fiji: an open-source platform for biological-image analysis', *Nat Methods*, 9(7), pp. 676-82.
Schmitt, M.W., Fox, E.J., Prindle, M.J., Reid-Bayliss, K.S., True, L.D., Radich, J.P. and Loeb, L.A. (2015) 'Sequencing small genomic targets with high efficiency and extreme accuracy', *Nat Methods*, 12(5), pp. 423-5.

Schmitt, M.W., Kennedy, S.R., Salk, J.J., Fox, E.J., Hiatt, J.B. and Loeb, L.A. (2012) 'Detection of ultra-rare mutations by next-generation sequencing', *Proc Natl Acad Sci U S A*, 109(36), pp. 14508-13.
Schnell, G., Joseph, S., Spudich, S., Price, R.W. and Swanstrom, R. (2011) 'HIV-1 replication in the central nervous system occurs in two distinct cell types', *PLoS Pathog*, 7(10), p. e1002286.
Schon, E.A., Rizzuto, R., Moraes, C.T., Nakase, H., Zeviani, M. and DiMauro, S. (1989) 'A direct repeat is a hotspot for large-scale deletion of human mitochondrial DNA', *Science*, 244(4902), pp. 346-9.
Schwartz, M. and Vissing, J. (2002) 'Paternal inheritance of mitochondrial DNA', *N Engl J Med*, 347(8), pp. 576-80.
Sciacco, M., Bonilla, E., Schon, E.A., DiMauro, S. and Moraes, C.T. (1994) 'Distribution of wild-type and common deletion forms of mtDNA in normal and respiration-deficient muscle fibers from patients with mitochondrial myopathy', *Hum Mol Genet*, 3(1), pp. 13-9.
Semba, R.D., Shah, N., Klein, R.S., Mayer, K.H., Schuman, P., Vlahov, D. and Human Immunodeficiency Virus Epidemiology Research Study, G. (2002) 'Prevalence and cumulative incidence of and risk factors for anemia in a multicenter cohort study of human immunodeficiency virus-infected and -uninfected women', *Clin Infect Dis*, 34(2), pp. 260-6.
Sherengul, W., Kondo, R. and Matsuura, E.T. (2006) 'Analysis of paternal transmission of mitochondrial DNA in Drosophila', *Genes Genet Syst*, 81(6), pp. 399-404.
Sherry, S.T., Ward, M.H., Kholodov, M., Baker, J., Phan, L., Smigielski, E.M. and Sirotkin, K. (2001) 'dbSNP: the NCBI database of genetic variation', *Nucleic Acids Res*, 29(1), pp. 308-11.
Shikuma, C.M., Hu, N., Milne, C., Yost, F., Waslien, C., Shimizu, S. and Shiramizu, B. (2001) 'Mitochondrial DNA decrease in subcutaneous adipose tissue of HIV-infected individuals with peripheral lipoatrophy', *AIDS*, 15(14), pp. 1801-9.
Shoffner, J.M., Lott, M.T., Voljavec, A.S., Soueidan, S.A., Costigan, D.A. and Wallace, D.C. (1989) 'Spontaneous Kearns-Sayre/chronic external ophthalmoplegia plus syndrome associated with a mitochondrial DNA deletion: a slip-replication model and metabolic therapy', *Proc Natl Acad Sci U S A*, 86(20), pp. 7952-6.

Short, K.R., Bigelow, M.L., Kahl, J., Singh, R., Coenen-Schimke, J., Raghavakaimal, S. and Nair, K.S. (2005) 'Decline in skeletal muscle mitochondrial function with aging in humans', *Proc Natl Acad Sci U S A*, 102(15), pp. 5618-23.
Sicheritz-Ponten, T., Kurland, C.G. and Andersson, S.G. (1998) 'A phylogenetic analysis of the cytochrome b and cytochrome c oxidase I genes supports an origin of mitochondria from within the Rickettsiaceae', *Biochim Biophys Acta*, 1365(3), pp. 545-51.
Spinelli, J.B. and Haigis, M.C. (2018) 'The multifaceted contributions of mitochondria to cellular metabolism', *Nat Cell Biol*, 20(7), pp. 745-754.
Stehling, O. and Lill, R. (2013) 'The role of mitochondria in cellular iron-sulfur protein biogenesis: mechanisms, connected processes, and diseases', *Cold Spring Harb Perspect Biol*, 5(8), p. a011312.
Stewart, J.B., Freyer, C., Elson, J.L., Wredenberg, A., Cansu, Z., Trifunovic, A. and Larsson, N.G. (2008) 'Strong purifying selection in transmission of mammalian mitochondrial DNA', *PLoS Biol*, 6(1), p. e10.
Stewart, J.B. and Larsson, N.G. (2014) 'Keeping mtDNA in shape between generations', *PLoS Genet*, 10(10), p. e1004670.
Takeshita, H., Yamamoto, K., Nozato, S., Inagaki, T., Tsuchimochi, H., Shirai, M., Yamamoto, R., Imaizumi, Y., Hongyo, K., Yokoyama, S., Takeda, M., Oguro, R., Takami, Y., Itoh, N., Takeya, Y., Sugimoto, K., Fukada, S.I. and Rakugi, H. (2017) 'Modified forelimb grip strength test detects aging-associated physiological decline in skeletal muscle function in male mice', *Sci Rep*, 7, p. 42323.
Tanhauser, S.M. and Laipis, P.J. (1995) 'Multiple deletions are detectable in mitochondrial DNA of aging mice', *J Biol Chem*, 270(42), pp. 24769-75.
Taylor, R.W., Barron, M.J., Borthwick, G.M., Gospel, A., Chinnery, P.F., Samuels, D.C., Taylor, G.A., Plusa, S.M., Needham, S.J., Greaves, L.C., Kirkwood, T.B. and Turnbull, D.M. (2003) 'Mitochondrial DNA mutations in human colonic crypt stem cells', *J Clin Invest*, 112(9), pp. 1351-60.
Tengan, C.H., Gabbai, A.A., Shanske, S., Zeviani, M. and Moraes, C.T. (1997) 'Oxidative phosphorylation dysfunction does not increase the rate of accumulation of age-related mtDNA deletions in skeletal muscle', *Mutat Res*, 379(1), pp. 1-11.
Teodorof-Diedrich, C. and Spector, S.A. (2018) 'Human Immunodeficiency Virus Type 1 gp120 and Tat Induce Mitochondrial Fragmentation and Incomplete Mitophagy in Human Neurons', *J Virol*, 92(22).

Trifunovic, A., Hansson, A., Wredenberg, A., Rovio, A.T., Dufour, E., Khvorostov, I., Spelbrink, J.N., Wibom, R., Jacobs, H.T. and Larsson, N.G. (2005) 'Somatic mtDNA mutations cause aging phenotypes without affecting reactive oxygen species production', *Proc Natl Acad Sci U S A*, 102(50), pp. 17993-8.
Trifunovic, A. and Larsson, N.G. (2008) 'Mitochondrial dysfunction as a cause of ageing', *J Intern Med*, 263(2), pp. 167-78.
Trifunovic, A., Wredenberg, A., Falkenberg, M., Spelbrink, J.N., Rovio, A.T., Bruder, C.E., Bohlooly, Y.M., Gidlof, S., Oldfors, A., Wibom, R., Tornell, J., Jacobs, H.T. and Larsson, N.G. (2004) 'Premature ageing in mice expressing defective mitochondrial DNA polymerase', *Nature*, 429(6990), pp. 417-23.
Tsukihara, T., Aoyama, H., Yamashita, E., Tomizaki, T., Yamaguchi, H., Shinzawa-Itoh, K., Nakashima, R., Yaono, R. and Yoshikawa, S. (1996) 'The whole structure of the 13-subunit oxidized cytochrome c oxidase at 2.8 A', *Science*, 272(5265), pp. 1136-44.
Tuppen, H.A., Blakely, E.L., Turnbull, D.M. and Taylor, R.W. (2010) 'Mitochondrial DNA mutations and human disease', *Biochim Biophys Acta*, 1797(2), pp. 113-28.
Tyynismaa, H., Mjosund, K.P., Wanrooij, S., Lappalainen, I., Ylikallio, E., Jalanko, A., Spelbrink, J.N., Paetau, A. and Suomalainen, A. (2005) 'Mutant mitochondrial helicase Twinkle causes multiple mtDNA deletions and a late-onset mitochondrial disease in mice', *Proc Natl Acad Sci U S A*, 102(49), pp. 17687-92.
Ugalde, C., Hinttala, R., Timal, S., Smeets, R., Rodenburg, R.J., Uusimaa, J., van Heuvel, L.P., Nijtmans, L.G., Majamaa, K. and Smeitink, J.A. (2007) 'Mutated ND2 impairs mitochondrial complex I assembly and leads to Leigh syndrome', *Mol Genet Metab*, 90(1), pp. 10-4.
Underwood, J., Cole, J.H., Caan, M., De Francesco, D., Leech, R., van Zoest, R.A., Su, T., Geurtsen, G.J., Schmand, B.A., Portegies, P., Prins, M., Wit, F., Sabin, C.A., Majoie, C., Reiss, P., Winston, A., Sharp, D.J. and Comorbidity in Relation to, A.C. (2017) 'Gray and White Matter Abnormalities in Treated Human Immunodeficiency Virus Disease and Their Relationship to Cognitive Function', *Clin Infect Dis*, 65(3), pp. 422-432.
Underwood, J. and Winston, A. (2016) 'Guidelines for Evaluation and Management of Cognitive Disorders in HIV-Positive Individuals', *Curr HIV/AIDS Rep*, 13(5), pp. 235-40.

Valcour, V., Shikuma, C., Shiramizu, B., Watters, M., Poff, P., Selnes, O., Holck, P., Grove, J. and Sacktor, N. (2004) 'Higher frequency of dementia in older HIV-1 individuals: the Hawaii Aging with HIV-1 Cohort', *Neurology*, 63(5), pp. 822-7.
van Zoest, R.A., Underwood, J., De Francesco, D., Sabin, C.A., Cole, J.H., Wit, F.W., Caan, M.W.A., Kootstra, N.A., Fuchs, D., Zetterberg, H., Majoie, C., Portegies, P., Winston, A., Sharp, D.J., Gisslen, M., Reiss, P. and Comorbidity in Relation to, A.C. (2017) 'Structural Brain Abnormalities in Successfully Treated HIV Infection: Associations With Disease and Cerebrospinal Fluid Biomarkers', *J Infect Dis*, 217(1), pp. 69-81.
Var, S.R., Day, T.R., Vitomirov, A., Smith, D.M., Soontornniyomkij, V., Moore, D.J., Achim, C.L., Mehta, S.R. and Perez-Santiago, J. (2016) 'Mitochondrial injury and cognitive function in HIV infection and methamphetamine use', *AIDS*, 30(6), pp. 839-48.
Vermulst, M., Bielas, J.H., Kujoth, G.C., Ladiges, W.C., Rabinovitch, P.S., Prolla, T.A. and Loeb, L.A. (2007) 'Mitochondrial point mutations do not limit the natural lifespan of mice', *Nat Genet*, 39(4), pp. 540-3.
Vermulst, M., Wanagat, J., Kujoth, G.C., Bielas, J.H., Rabinovitch, P.S., Prolla, T.A. and Loeb, L.A. (2008) 'DNA deletions and clonal mutations drive premature aging in mitochondrial mutator mice', *Nat Genet*, 40(4), pp. 392-4.
Volberding, P.A., Levine, A.M., Dieterich, D., Mildvan, D., Mitsuyasu, R., Saag, M. and Anemia in, H.I.V.W.G. (2004) 'Anemia in HIV infection: clinical impact and evidence-based management strategies', *Clin Infect Dis*, 38(10), pp. 1454-63.
Wai, T., Teoli, D. and Shoubridge, E.A. (2008) 'The mitochondrial DNA genetic bottleneck results from replication of a subpopulation of genomes', *Nat Genet*, 40(12), pp. 1484-8.
Walker, D.M., Poirier, M.C., Campen, M.J., Cook, D.L., Jr., Divi, R.L., Nagashima, K., Lund, A.K., Cossey, P.Y., Hahn, F.F. and Walker, V.E. (2004a) 'Persistence of mitochondrial toxicity in hearts of female B6C3F1 mice exposed in utero to 3'-azido-3'-deoxythymidine', *Cardiovasc Toxicol*, 4(2), pp. 133-53.
Walker, U.A., Bauerle, J., Laguno, M., Murillas, J., Mauss, S., Schmutz, G., Setzer, B., Miquel, R., Gatell, J.M. and Mallolas, J. (2004b) 'Depletion of mitochondrial DNA in liver under antiretroviral therapy with didanosine, stavudine, or zalcitabine', *Hepatology*, 39(2), pp. 311-7.
Wallace, D.C. (1992) 'Diseases of the mitochondrial DNA', *Annu Rev Biochem*, 61, pp. 1175-212.

Wallace, D.C. (2015) 'Mitochondrial DNA Variation in Human Radiation and Disease', *Cell*, 163(1), pp. 33-8.
Wallace, D.C., Singh, G., Lott, M.T., Hodge, J.A., Schurr, T.G., Lezza, A.M., Elsas, L.J., 2nd and Nikoskelainen, E.K. (1988) 'Mitochondrial DNA mutation associated with Leber's hereditary optic neuropathy', *Science*, 242(4884), pp. 1427-30.
West, A.P. and Shadel, G.S. (2017) 'Mitochondrial DNA in innate immune responses and inflammatory pathology', *Nat Rev Immunol*, 17(6), pp. 363-375.
West, A.P., Shadel, G.S. and Ghosh, S. (2011) 'Mitochondria in innate immune responses', *Nat Rev Immunol*, 11(6), pp. 389-402.
Williams, S.L., Huang, J., Edwards, Y.J., Ulloa, R.H., Dillon, L.M., Prolla, T.A., Vance, J.M., Moraes, C.T. and Zuchner, S. (2010) 'The mtDNA mutation spectrum of the progeroid Polg mutator mouse includes abundant control region multimers', *Cell Metab*, 12(6), pp. 675-82.
Xu, H., Luo, X., Qian, J., Pang, X., Song, J., Qian, G., Chen, J. and Chen, S. (2012) 'FastUniq: a fast de novo duplicates removal tool for paired short reads', *PLoS One*, 7(12), p. e52249.
Ye, J., Coulouris, G., Zaretskaya, I., Cutcutache, I., Rozen, S. and Madden, T.L. (2012) 'Primer-BLAST: a tool to design target-specific primers for polymerase chain reaction', *BMC Bioinformatics*, 13, p. 134.
Yilmaz, A., Price, R.W. and Gisslen, M. (2012) 'Antiretroviral drug treatment of CNS HIV-1 infection', *J Antimicrob Chemother*, 67(2), pp. 299-311.
Youle, R.J. and van der Bliek, A.M. (2012) 'Mitochondrial fission, fusion, and stress', *Science*, 337(6098), pp. 1062-5.
Yu-Wai-Man, P., Turnbull, D.M. and Chinnery, P.F. (2002) 'Leber hereditary optic neuropathy', *J Med Genet*, 39(3), pp. 162-9.
Zerbino, D.R., Achuthan, P., Akanni, W., Amode, M.R., Barrell, D., Bhai, J., Billis, K., Cummins, C., Gall, A., Giron, C.G., Gil, L., Gordon, L., Haggerty, L., Haskell, E., Hourlier, T., Izuogu, O.G., Janacek, S.H., Juettemann, T., To, J.K., Laird, M.R., Lavidas, I., Liu, Z., Loveland, J.E., Maurel, T., McLaren, W., Moore, B., Mudge, J., Murphy, D.N., Newman, V., Nuhn, M., Ogeh, D., Ong, C.K., Parker, A., Patricio, M., Riat, H.S., Schuilenburg, H., Sheppard, D., Sparrow, H., Taylor, K., Thormann, A., Vullo, A., Walts, B., Zadissa, A., Frankish, A., Hunt, S.E., Kostadima, M., Langridge, N., Martin, F.J., Muffato, M., Perry, E., Ruffier, M., Staines, D.M., Trevanion, S.J., Aken, B.L., Cunningham, F., Yates, A. and Flicek, P. (2018) 'Ensembl 2018', *Nucleic Acids Res*, 46(D1), pp. D754-D761.

Zeviani, M., Moraes, C.T., DiMauro, S., Nakase, H., Bonilla, E., Schon, E.A. and Rowland, L.P. (1988) 'Deletions of mitochondrial DNA in Kearns-Sayre syndrome', *Neurology*, 38(9), pp. 1339-46.

Zhang, D., Mott, J.L., Farrar, P., Ryerse, J.S., Chang, S.W., Stevens, M., Denniger, G. and Zassenhaus, H.P. (2003) 'Mitochondrial DNA mutations activate the mitochondrial apoptotic pathway and cause dilated cardiomyopathy', *Cardiovasc Res*, 57(1), pp. 147-57.

Zhang, S.B., Maguire, D., Zhang, M., Zhang, Z., Zhang, A., Yin, L., Zhang, L., Huang, L., Vidyasagar, S., Swarts, S. and Okunieff, P. (2013) 'The murine common deletion: mitochondrial DNA 3,860-bp deletion after irradiation', *Radiat Res*, 180(4), pp. 407-13.

Zhang, Y., Song, F., Gao, Z., Ding, W., Qiao, L., Yang, S., Chen, X., Jin, R. and Chen, D. (2014) 'Long-term exposure of mice to nucleoside analogues disrupts mitochondrial DNA maintenance in cortical neurons', *PLoS One*, 9(1), p. e85637.

Zhang, Y., Wang, B., Liang, Q., Qiao, L., Xu, B., Zhang, H., Yang, S., Chen, J., Guo, H., Wu, J. and Chen, D. (2015) 'Mitochondrial DNA D-loop AG/TC transition mutation in cortical neurons of mice after long-term exposure to nucleoside analogues', *J Neurovirol*, 21(5), pp. 500-7.

Zhao, X., Li, N., Guo, W., Hu, X., Liu, Z., Gong, G., Wang, A., Feng, J. and Wu, C. (2004) 'Further evidence for paternal inheritance of mitochondrial DNA in the sheep (Ovis aries)', *Heredity (Edinb)*, 93(4), pp. 399-403.

Zhu, J., Vinothkumar, K.R. and Hirst, J. (2016) 'Structure of mammalian respiratory complex I', *Nature*, 536(7616), pp. 354-358.